University of Canterbury

Doctoral Thesis

Estimation of the time-varying elastance of the left and right ventricles

Author:
David Stevenson

Supervisor:
Dr. Geoffrey Chase

A thesis submitted in partial fulfilment for the degree of Doctor of Philosophy

in

Bioengineering,
Department of Mechanical Engineering

September 2013

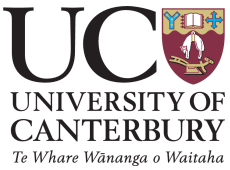

Soli Deo gloria — Glory to God alone

Abstract

The intensive care unit treats the most critically ill patients in the hospital, and as such the clinical staff in the intensive care unit have to deal with complex, time-sensitive and life-critical situations. Commonly, patients present with multiple organ dysfunctions, require breathing and cardiovascular support, which make diagnosis and treatment even more challenging. As a result, clinical staff are faced with processing large quantities of often confusing information, and have to rely on experience and trial and error. This occurs despite the wealth of cardiovascular metrics that are available to the clinician.

Computer models of the cardiovascular system can help enormously in an intensive care setting, as they can take the monitored data, and aggregate it in such a way as to present a clear and understandable picture of the cardiovascular system. With additional help that such systems can provide, diagnosis can be more accurate and arrived at faster, alone with better optimised treatment that can start sooner, all of which results in decreased mortality, length of stay and cost.

This thesis presents a model of the cardiovascular system, which mimics a specific patient's cardiovascular state, based on only metrics that are commonly measured in an intensive care setting. This intentional limitation gives rise to additional complexities and challenges in identifying the model, but do not stand in the way of achieving a model that can represent and track all the important cardiovascular dynamics of a specific patient. One important complication that comes from limiting the data set is need for an estimation for the ventricular time-varying elastance waveform. This waveform is central to the dynamics of the cardiovascular model and is far too invasive to measure in an intensive care setting.

This thesis thus goes on to present a method in which the value-normalised ventricular time-varying elastance is estimated from only metrics which are commonly available in an intensive care setting. Both the left and the right ventricular time-varying elastance are estimated with good accuracy, capturing both the shape and timing through the progress of pulmonary embolism and septic shock. For pulmonary embolism, with the

algorithm built from septic shock data, a time-varying elastance waveform with median error of 1.26% and 2.52% results for the left and right ventricles respectively. For septic shock, with the algorithm built from pulmonary embolism data, a time-varying elastance waveform with median error of 2.54% and 2.90% results for the left and right ventricles respectively. These results give confidence that the method will generalise to a wider set of cardiovascular dysfunctions.

Furthermore, once the ventricular time-varying elastance is known, or estimated to a adequate degree of accuracy, the time-varying elastance can be used in its own right to access valuable information about the state of the cardiovascular system. Due to the centrality and energetic nature of the time-varying elastance waveform, much of the state of the cardiovascular system can be found within the waveform itself. In this manner this thesis presents three important metrics which can help a clinician distinguish between, and track the progress of, the cardiovascular dysfunctions of pulmonary embolism and septic shock, from estimations based of the monitored pressure waveforms. With these three metrics, a clinician can increase or decrease their probabilistic measure of pulmonary embolism and septic shock.

Acknowledgements

There are many people I would like to thank for their help and support throughout the completion of my thesis.

Geoff Chase, my supervisor. Thank you for the support and guidance you have offered me, as well as your direction and academic wisdom that enabled me to finish this thesis. Thank you for the many and varied opportunities during this period of research, including the conferences I attended and the support to write several journal papers.

Geoff Shaw, and **Thomas Desaive**, my co-supervisors. Thank you for the support and knowledge that you gave to this research. Thank you Geoff, for the medical and clinical insight and guidance, this was invaluable to the research. Thomas, thank you for hosting my time in Liege and for the guidance and support in journal publications.

To my lovely wife, **Emma**, thank you for supporting me throughout the trials of research, studying abroad in Belgium, and your help with navigating the final write up. You have been a blessing to me in so many unnamed ways.

Thank you to **my immediate and extended family**, for your support, encouragement, understanding and always taking an interest in my work. Also a special thank you for the help with the final proof reading.

Finally, to **Jesus Christ**, my saviour, "through whom all things were made" – John 1:3, and "in Him all things hold together" – Colossians 1:17. It is truly an honour to study God's creation with the highest level of academic rigour that is required for a doctoral thesis. Also to all my **brothers and sisters in Christ**, thank you for your support, both in my faith and studies.

Contents

List of Figures

List of Tables

Nomenclature

Acronyms

AL	Afterload
AP	Arterial pressure
CO	Cardiac output
CT	Computer tomography
CVP	Central venous pressure
CVS	Cardiovascular system
DVT	deep venous thrombus
ECG	Electrocardiogram
ED	End-diastole
EDP	End-diastolic pressure
EDPVR	End-diastolic pressure-volume relation
EDV	End-diastolic volume
ES	End-systole
ESPVR	End-systolic pressure-volume relation
ESV	End-systolic volume
GEDV	Global end-diastolic volume

HR	Heart rate
ICU	Intensive Care Unit
LSV	Left stroke volume
LVEDV	Left ventricle end-diastolic volume
MAP	Mean arterial pressure
PAC	Pulmonary artery catheter
PAC	Pulmonary artery catheter
PAP	Pulmonary artery pressure
PE	Pulmonary embolism
PE	Pulmonary embolism
PP	Pulse pressure
PV	Pressure-volume
PVA	Pressure-volume area
RMSE	Root mean square error
RSV	Right stroke volume
RV	Right ventricle
RVEDV	Right ventricle end-diastolic volume
SE	Start of ejection
SF	Start of filling
SIRS	Systemic inflammatory response syndrome
SV	Stroke volume
TVE	Time-varying elastance
V/Q	Ventilation-perfusion scintigraphy

VTE	venous thromboembolism

Roman Symbols

C	Compliance
E	Elastance
I	Inertia
P	Pressure
Q	Flow rate
R	Resistance
T	Period
t	Time
V	Volume

Greek Symbols

$\mathcal{H}$	Half rectifier
ϕ_{shear}	The shear transform function

Other Symbols

$\mathcal{S}$	Shear transform
CO_2	Carbon Dioxide
$\bar{X}$	The mean value of X
$DMPG$	Driver maximum positive gradient
DN	Dicrotic notch
$E(t)$	Time-varying elastance — general concept
$e(t)$	Time-varying elastance, value normalised

LS	Left shoulder
MN	Minimum point
MNG	Maximum negative gradient
MPG	Maximum positive gradient
MX	Maximum
O_2	Oxygen
RS	Right shoulder

Subscripts

ao	Aorta
approx	The approximated value
av	Aortic valve
ed	End-diastole
end	The final value of a data set
est	The estimated value
es	End-systole
fm	Five chamber model
lvf	Left ventricle free wall
lv	Left ventricle
max	Maximum value
measured	Value from the measured data
min	Minimum value
modelled	Value from the model's output
mt	Mitral valve

pa	Pulmonary artery
pcd	Pericardial difference
peri	Pericardium
pul	Pulmonary
pu	Pulmonary vein
pv	Pulmonary valve
rvf	Right ventricle free wall
rv	Right ventricle
sm	Systemic model
spt	Ventricular septum
sum	Summation of parameters
sys	Systemic
tc	Tricuspid valve
th	Thoracic
true	The true value
vc	Vena cava
v	Ventricle
a	Arterial

Chapter 1

Introduction

Cardiac disturbances are difficult to diagnose and treat, especially in an Intensive Care Unit (ICU), which can lead to poor management (Hall and Guyton, 2011; Grenvik et al., 1989). Inadequate diagnosis is common, and plays a significant role in increased length of stay and death (Angus et al., 2001; Kearon, 2003; Pineda et al., 2001), despite access to many different cardiac measurements and metrics. Currently, internal haemodynamic measurements are possible only at the arterial or venous locations where catheters are placed. This limited set of data can severely restrict clinical diagnostic capability. In addition, they return pressure or flow rate waveforms that provide a wealth of information, but not in a form that easily matches the mental models of clinical staff. Thus, the use of these catheters is not necessarily associated with improved outcomes (Frazier and Skinner, 2008; Chatterjee, 2009; Cooper and Doig, 1996). Overall, a lot of data currently available to ICU clinicians that could have significant clinical value is under utilised.

Using computer modelling techniques, this limited set of data can be expanded to estimate a much greater set of clinically and physiologically relevant data to enable more accurate diagnosis. For example, acute cardiovascular dysfunctions, like pulmonary embolism (PE) and septic shock, severely alter cardiovascular system (CVS) haemodynamics around the heart. These changes can be seen by catheter measurements as a change in the balance of preload and afterload around the heart, resulting in an altered cardiac energetic state (Weber and Janicki, 1979; Ross, 1976). Detailed cardiac energetics are too invasive to measure in an ICU setting. However, if the relevant energetics could

be captured from a nearby catheter with the use of a physiologically relevant computer model, then the clinical potential of such measurements could be realised. To date, no such method achieves this aim.

1.1 Cardiovascular disease

The prevalence and cost of cardiovascular disease is an enormous problem, and one that is not new. In every year since 1900, except 1918, cardiovascular disease was the leading cause of death in the United States (Roger et al., 2012). In 2008, it was the biggest cause of death worldwide, with more than 17 million casualties (Mendis et al., 2011), of which an estimated three million could have been prevented. Similarly in 2008, cardiovascular disease was the underlying cause of just under one third of all deaths in the United States, and contributed to over half of all deaths. Currently, it is estimated that nearly 83 million American adults, more than a third of the population, have one or more types of cardiovascular disease (Roger et al., 2012).

It is also apparent that cardiovascular disease can effect all age groups. Although age is still an important risk factor in developing cardiovascular disease, the prevalence of cardiac dysfunction is showing a worrying trend in youth populations (McGill et al., 2008). In particular, an estimated nearly six thousand paediatric out-of-hospital cardiac arrests occur annually in the United States alone (Roger et al., 2011).

Aside from the human cost and social ramifications of cardiovascular disease, the economic cost is also significant. It is estimated that the total direct and indirect cost of cardiovascular disease in the United States in 2008 was a massive $297 billion (up $11 billion from the previous year), which is the highest of any diagnostic group (Roger et al., 2011, 2012). This value is expected to reach $818 billion by 2030 (Heidenreich et al., 2011). This cost is a heavy burden on the economy, as well as on hospital resources, with nearly 7.5 million inpatient cardiovascular operations and procedures performed in 2009 in the United States alone (Roger et al., 2012).

Overall, it is clear that cardiovascular disease is a serious human and economic problem, growing in epidemic proportions worldwide. Even small advances in diagnosing and treating cardiovascular disease would see significant benefits in reduced mortality and financial savings. However, due to many factors, including the complexity of

the cardiovascular system, diagnosis and optimal treatment is often very difficult. In particular, severe sepsis and septic shock, which have high occurrence rates, significant mortality and costs (Karlsson et al., 2007), continue to be difficult to manage in an ICU, and reflect the overall issues of occurrence and cost of cardiovascular disease in general within this hospital environment.

1.1.1 Septic shock

Severe sepsis and septic shock are a major problem in intensive care units today, and have been for some time (Dombrovskiy et al., 2007). Like cardiovascular disease in general, they have high rates of occurrence, significant mortality and high cost (Karlsson et al., 2007), both in adult and paediatric populations (Watson et al., 2003).

Despite many attempts to estimate its burden, actual rates of sepsis are not well defined (Artero et al., 2012). A study taken from 1993 to 2000 showed an increasing trend from 7–10 % of ICU admissions with severe sepsis or septic shock (Annane et al., 2003). An Italian study showed 6 % (Salvo et al., 1995), and an international multi-centre study found approximately 7 % (Artero et al., 2012). The highest rate of 11 % (Angus et al., 2001) is potentially overstated (Martin et al., 2003). The cost of severe sepsis and septic shock is likewise hard to estimate, but is thought to be around USD $50,000 per patient.

Septic shock mortality can be estimated at around 50 %. However, its impact is much higher as even those who survive will likely have a significant reduction in quality of life (Martin et al., 2003).

In general, the precursor to septic shock is sepsis. Sepsis itself is a syndrome, and is very difficult to diagnose and treat. More specifically, there are no real-time measurements of sepsis nor of the loss of vaso-motor control indicative of septic shock. Thus, clinicians must rely on cruder measurements and clinical experience.

1.1.2 Pulmonary Embolism

Despite advances in prevention, diagnostics and treatment, pulmonary embolism (PE) still remains one of the major challenges in care of the critically ill (Bahloul et al., 2010). Intensive care patients are at very high risk of any form of venous thromboembolism.

Combined with the often non-specific nature of the visible effects of PE, it becomes clear why PE is another leading cause of in-hospital morbidity and mortality (Tapson, 2008; Kasper et al., 1997; Konstantinides et al., 1997). Mortality rates vary widely, from 8.1 % in stable patients to 65 % in post-cardiopulmonary resuscitation (Goldhaber et al., 1999; Kasper et al., 1997; Douketis, 2001). It is also a widespread problem with an incidence rate of 1 per 2000 person-years (Naess et al., 2007). Hence, it is another high cost, frequently occurring cardiovascular dysfunction for which proper diagnosis and optimal treatment are difficult.

1.1.3 Diagnosis and Treatment

The treatment of cardiovascular disease is not a simple task. This issue is due to many factors including the complexity of the cardiovascular system and the patient-specific nature of the cardiac related problems. Both diagnosis and treatment can thus be problematic. In particular, there is no direct measurement of thromboembolism or blocking of blood flow that is currently available in real-time. Thus, clinicians often have to rely on experience and intuition, using cruder surrogates, to make a diagnosis or to recognise PE as it emerges. This situation leads to increased clinical errors and suboptimal patient outcomes.

Hence, overall, diagnosis of many cardiovascular dysfunctions are non trivial. The complexity of the cardiovascular system, interactions and complex reflex responses result in conditions that can be difficult to reliably and accurately diagnose in a timely fashion. This issue is further complicated by patient-specific differences and responses to conditions and treatments. Finally, the measurements available are not entirely physiologically relevant to clinical or specific dysfunction. The resulting situation for a clinician is often that of intuition plus trial and error, leading to suboptimal and variable diagnosis and treatment.

1.2 Current practice

The ICU provides care for patients who are the most critically ill in the hospital. Thus, the clinical staff are often faced with hard decisions in stressful and time-sensitive

situations. There are many procedures and methods to enable staff to make good decisions in specific situations or treatments. However, much of the time these methods are optimised for population outcomes, which can result in patient-specific details being neglected. The result is more consistent care, but not necessarily more optimal care.

In addition, all patients have their own unique expressions of a cardiovascular disease or dysfunction, as well as unique responses to treatment. This variability and resultant uncertainty leaves the clinician with a vast array of scenarios and data to mentally process including the patient's history, their current cardiovascular state, their current response to treatment, and the results of the vast quantity of invasive and non-invasive clinical studies. The result is often an array of sometimes conflicting possible treatments paths. With this issue in mind, it is no surprise that clinical management and patient outcomes vary between medical centres (Kennedy et al., 2010; Wennberg, 2002), and that clinical error rates are common (Abramson et al., 1980; Donchin et al., 1995; Morris, 2001; Suresh et al., 2004)

For much of the treatment in the ICU, haemodynamic monitoring is a first port of call. However, for any monitoring to improve outcome, the information gained must then direct or influence treatment, and only in beneficial ways. For this reason, the use of the pulmonary artery catheter (PAC) is declining worldwide due to the lack of improved patient outcomes (Wiener and Welch, 2007). Many variables are still monitored as part of standard practice, resulting in a wealth of patient-specific haemodynamic information, much of which is not fully utilised in treatment decisions (Pinsky, 2003; Greenberg et al., 2009). Too much information can lead to confusing and apparent contradictory diagnostic and treatment paths, and may be no better than an incomplete understanding due to too little information. This problem can be seen through the apparent lack of improved patient outcomes from the monitoring of stroke volume and cardiovascular output using a PAC (Mutoh et al., 2007; Pinsky, 2007; Greenberg et al., 2009) despite their importance to the state of cardiovascular health.

To fully utilise the information gained by haemodynamic monitoring, this information must be aggregated into a simpler, yet more complete picture of the cardiovascular system. Without this clearer picture the wealth of relevant clinical information in monitored variables is far too large, and the interaction too complex for the clinician to

form a clear, concise understanding of the patient-specific cardiovascular state upon which to base treatment decisions. Historically, this type of outcome has been best achieved through the use of computer models (Le Compte et al., 2009; Chase et al., 2008; Evans et al., 2011). Such models can incorporate complex interactions, and distil the large quantity of monitored information into manageable and understandable information that can be standardised, yet remain patient-specific. To be clinically applicable, such models should be able to accurately predict cardiovascular health markers, track pathologically important haemodynamic trends, indicate the effectiveness of treatment over time, be cost effective and easy to implement, provide real-time information, and improve current clinical methods and outcomes.

1.3 Time-varying elastance

For many of the cardiovascular models developed in the literature, an important input function is the time-varying elastance (TVE) waveform. This waveform describes the energetic input to the contracting ventricles and, as such, drives the pumping action of the models. Furthermore, due to the centrality of the time-varying elastance and the energetic implications, the waveform is useful in its own right. However, the time-varying elastance is impractical to measure in a clinical setting. Thus, it has not reached clinical practice to the extent it is seen in animal research and clinical textbooks.

There have been several attempts to estimate TVE (Guarini et al., 1998; Swamy et al., 2009; Shishido et al., 2000; Senzaki et al., 1996; Brinke et al., 2010). However, none have estimated it for its own sake. Most studies present a method using the TVE to estimate a specific clinical parameter, most commonly end-systolic elastance (Shishido et al., 2000; Brinke et al., 2010; Senzaki et al., 1996) and ejection fraction (Swamy et al., 2009). However, their validation is based on these metrics, which in turn capture cardiovascular state at a specific instant, and not on the resulting TVE waveform.

1.4 Goals for this research

The overall goal of this research is to further the clinical applicability of a relatively minimal cardiovascular system model (Starfinger, 2008). This model can be fitted to

capture the behaviour of a specific patient and thus give accurate information to the clinician about the patient's cardiovascular state. For this outcome to be clinically relevant, it must be possible for the model to be identified to simulate a specific patient and to do that in a real-time fashion. It also must be done through the use of only measurements that are typically available in the ICU, so as to not add additional cost or risk to the patient.

These criteria require a validated and accurate model, and a method to convert the limited measured data that is available in the ICU into the required parameters for the model to match a specific patient. Along with this requirement is the necessity for an accurate representation of the time-varying elastance (TVE) waveform, as this waveform is a central input to the model and is too invasive to measure directly. Therefore, the estimation of the TVE is critical to the success of the model as a clinical tool, and thus the TVE waveform is the main focus of this research.

1.5 Preface

In Chapter 2 this thesis will cover the background material necessary to fully understand the concepts, models and physiology mentioned in this research. This background includes the physiology and anatomy of the heart and circulation system, as well as the clinically relevant metrics and concepts that are discussed in later chapters. This chapter also covers the major cardiac dysfunctions relevant to this research, their pathologies, current diagnostic methods and typical treatment paths.

Chapter 3 will introduce and define the lumped cardiovascular system model, giving a basic demonstration of its derivation, guiding principles and background philosophy and direction, including a full definition of the model. The simulation of the model will also be discussed along with the assumptions and limitations of the model. The process of identifying the model is then shown in Chapter 4, where the iterative process is outlined. Also discussed is the sensitivity of the model to the time-varying elastance input waveform.

Chapter 5 then introduces the time-varying elastance in much more detail, outlining the evolution of this concept from its inception in the 1960s to its current usage and

implications today, including the relevant literature. The three major uses of the time-varying elastance are covered, namely the maximal elastance, total mechanical energy formulation from the pressure-volume diagram and the time-varying elastance as an input to lumped parameter cardiovascular models.

With this background in place, Chapters 6 and 7 outline and discuss the method by which the time-varying elastance can be accurately estimated using only measurements that are typically available in an ICU setting. This process involves the automation of the processing of the input waveforms to obtain the required data, and is shown in Chapter 6. This is followed by the method of estimating the time-varying elastance from the processed data, and is discussed in Chapter 7.

Chapter 8 follows this estimation with the clinical relevance of the time-varying elastance apart from the cardiovascular model. Three correlations are proposed that can give further insight into the cardiovascular state, in a similar way to the full cardiovascular model, without the computation cost involved in identifying and simulating the full model.

Finally, Chapter 9 gives an overall summary and conclusions of this research, with future work that could be done next around this topic, discussed in Chapter 10.

Chapter 2

Cardiovascular Physiology and Background

This chapter introduces the anatomy and physiology behind the cardiac and circulation systems. It provides the background information for which the later chapters assume a working knowledge.

2.1 Anatomy of the heart

The heart primarily consists of two separate pumps, the left heart which pumps oxygenated blood to the body's periphery, and the right heart which pumps blood to the lung to be re-oxygenated. Each side of the heart contains a main pump, the ventricle, and a much weaker upstream pump, the atrium. The left and right ventricle share a common wall, called the interventricular septum, and thus are in direct contact and interact in terms of pressure and volume. The entire heart is enclosed by the pericardium, a stiff membrane that constrains the total volume of the heart. Figure 2.1 shows a representation of the heart and connection vessels.

2.1.1 Heart chambers

There are four active chambers in the heart that contribute to the pumping of blood. These are the left and right atria, and the left and right ventricles. All four interact on

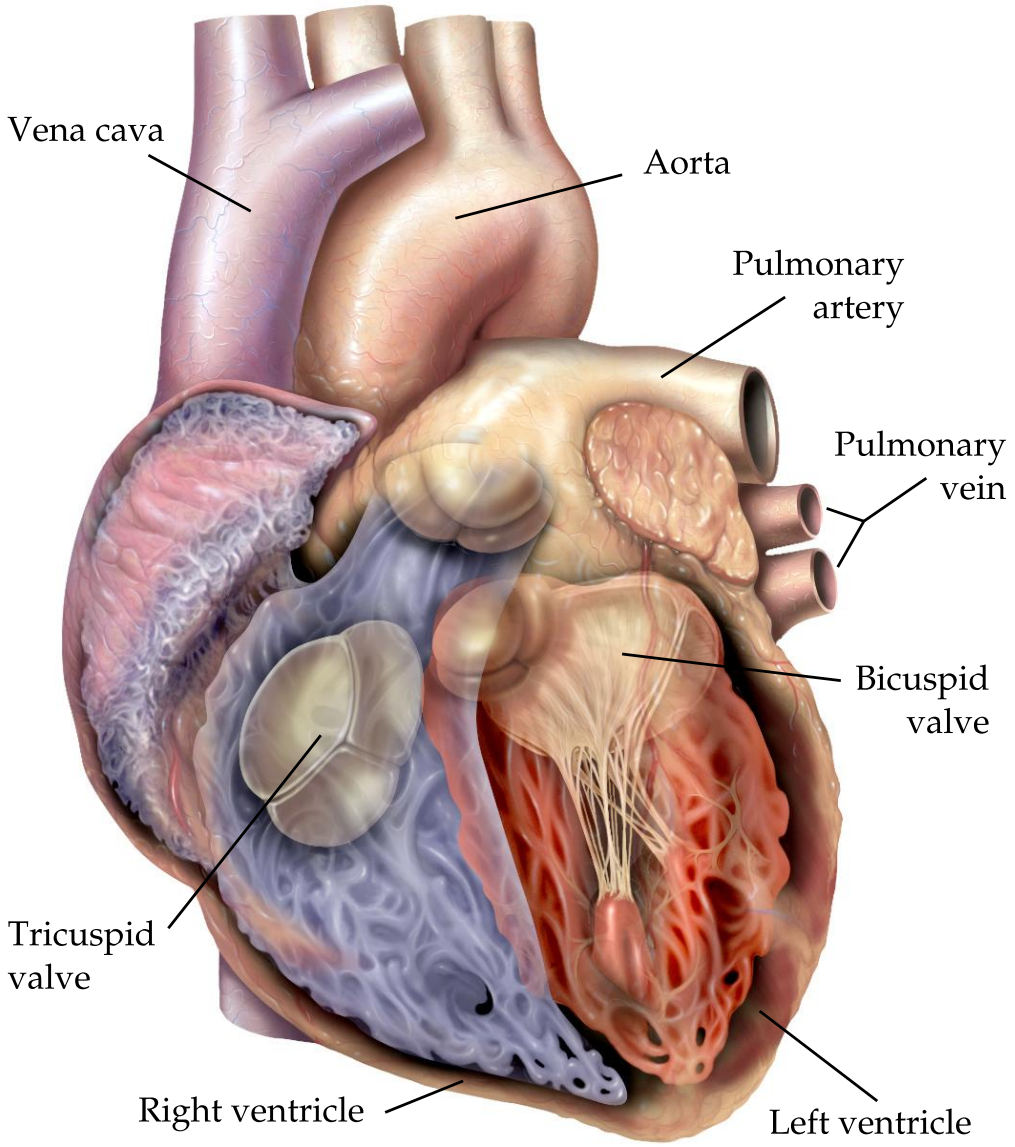

FIGURE 2.1: A diagram of the heart. Patrick J. Lynch. Adapted under Creative Commons Attribution 2.5 License.

each side to create a full cardiac cycle. These chambers are shown in Figure 2.2.

The left atrium receives blood from the lungs, and through the bicuspid valve, delivers it to the left ventricle to be pumped through the systemic circulation. The left ventricle operates at high pressure against significant resistance. Hence it has strong, thick walls and a circular lumen.

The right atrium takes blood from the superior and inferior venae cavae and the

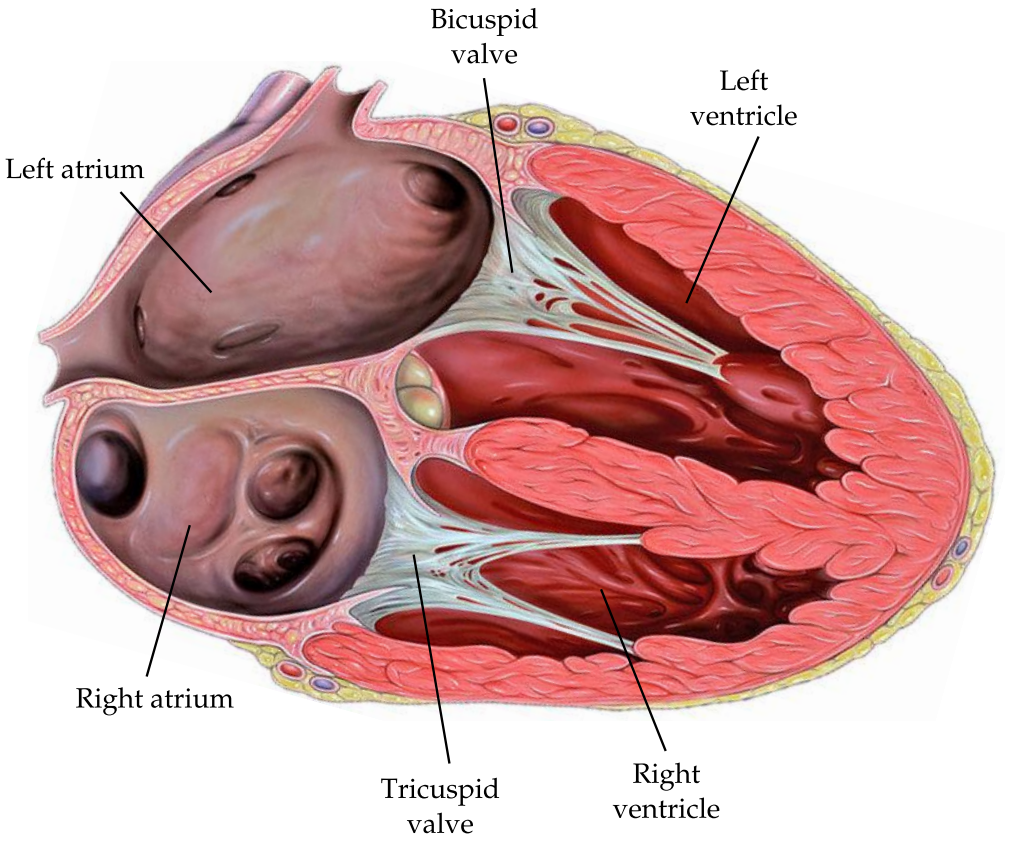

FIGURE 2.2: An illustration of a sectioned heart. Patrick J. Lynch. Adapted under Creative Commons Attribution 2.5 License.

coronary sinus, and delivers it to the right ventricle, through the tricuspid valve. The right ventricle, operating at a much lower pressure than the left ventricle, then pushes this blood into the pulmonary circulation through the pulmonary valve. The right ventricle has thinner walls, and a less circular lumen.

The left and right ventricles are connected by the interventricular septum, and are thus dynamically linked. This interaction can be important in certain disease states or dysfunction. Section 2.1.3 has a full description.

2.1.2 Cardiac muscle

The walls of the heart consist of three layers: the epicardium, myocardium and endocardium. The epicardium is the thin, outermost layer and houses the major coronary blood vessels that supply the myocardium. The myocardium is composed of cardiac

muscle tissue and makes up the greater part of the heart wall's thickness. The endocardium is a smooth inner layer of the heart that helps to reduce surface friction of the muscle.

There are three types of muscle that make up the heart: atrial muscle, ventricular muscle and conductive muscle fibres. There is much in common between cardiac and skeletal muscle. However, cardiac muscle is specialised in a number of ways. The atrial and ventricular muscles are similar to one another and contract in a similar way to skeletal muscle, whereas the conductive muscles fibres do not contract much, as their primary purpose is conduction.

Cardiac muscle contraction differs slightly from skeletal muscle in two main ways. Specifically, it has longer action potential and exhibits a plateau after the initial spike. This prolonged action potential and plateau are caused in part by the addition of slow calcium channels (Tortora and Derrickson, 2011). Both types of muscles have the fast sodium channels which remain open for a very short time allowing sodium ions to enter the muscle. The slow calcium channels are slower to open and remain open for longer, allowing both calcium and sodium to flow into the cardiac muscle maintaining a prolonged depolarisation. A second cause of the difference between skeletal and cardiac muscle is the permeability to potassium, which, in cardiac muscle, drastically reduces during the polarisation. This reduction decreases the loss of positively charged potassium ions, helping to maintain an elevated voltage for longer than skeletal muscle. At the close of the slow calcium channels, the permeability returns to normal, reducing the voltage to its resting level. Finally, cardiac muscle (both atrial and ventricular) also has a much slower action potential velocity, clocking in at around 0.3–0.5 $\mathrm{m\,s^{-1}}$, nearly 10 times slower than skeletal muscle.

2.1.3 Ventricular interaction

The left and right ventricles share a common boundary muscle, called the interventricular septum. Hence, the dynamics of the two ventricles are closely linked. This interaction is significant in a healthy heart, but can play a much greater role with certain types of dysfunction, especially those that cause the pericardium to contract. Thus, the status of the septum is important clinically. In particular, the septum is generally pushed into the right ventricle, as shown in Figure 2.3, due to the much higher pressure

in the left ventricle. This action reduces right ventricle volume and thus the amount of blood that can be re-oxygenated, with detrimental follow-on effect to other organs.

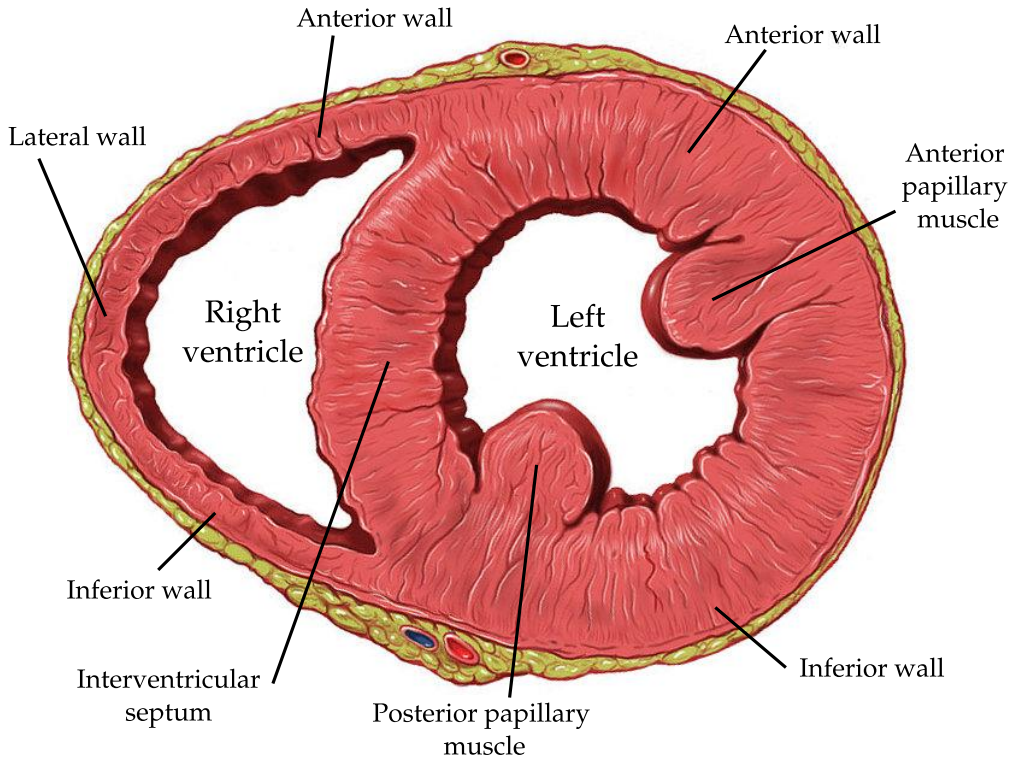

FIGURE 2.3: A sectioned view of healthy left and right ventricles, showing their shared muscle wall, relative sizes and wall thickness Patrick J. Lynch. Adapted under Creative Commons Attribution 2.5 License.

2.1.4 Pericardium

The pericardium is a tough double-layered membrane that surrounds the heart and the root of the great vessels (aorta, pulmonary artery and vena cava). The two membranes are separated by pericardial fluid, which helps to cushion the heart. Due to the stiff nature of the pericardium, it helps to prevent over filling and distension of the cardiac muscle. Hence, it prevents damaging dilation of the heart and acts as a reaction wall when blood is ejected. The pericardium also helps to reduce the friction of the heart as it moves against the surrounding tissues.

2.2 Circulation

The circulation is the key mechanism for which the heart exists. The circulation, in turn, serves the purpose of supplying the body with oxygen and nutrients, along with other transport operations. It is the need for such transport that drives the function of the circulation, its components, and ultimately, the heart itself.

There are three major parts to the circulation system: the arterial system, the venous system and the capillary system. The arterial system transports the oxygenated blood from the heart to the tissues at high pressure and high velocity, via arterioles and ever-smaller branches of blood vessels, terminating with the capillaries. The capillaries are where exchange of oxygen, nutrients and waste products mainly occur. The venous system then returns blood to the heart at lower pressure and velocity.

2.2.1 Arterial system

The arterial system carries blood from the heart to the body's organs, and comprises three main forms: 1) elastic arteries, 2) muscular arteries, and 3) arterioles. As the blood leaves the heart, it enters an elastic artery (the aorta for the left side, and pulmonary artery for the right). These elastic arteries easily change volume in response to a change of pressure, and thus have high compliance. Due to this high compliance, elastic energy can be stored. This is then released to aid in propelling the blood through the circulation system after the heart has finished its main pumping action. Hence, the elastic arteries act as a pressure reservoir, and to elongate the pumping action over a longer period into a more continuous waveform.

There are two major arteries that leave the heart, the aorta and the pulmonary artery. The aorta takes oxygenated blood from the left side of the heart and supplies the body. The pulmonary artery takes the de-oxygenated blood from the right side of the heart and supplies it to the lungs to be re-oxygenated. These two arteries have significant and important flow; they see the blood first after the heart, and can readily have catheters placed for measurement.

After the elastic arteries have branched a few times, the blood moves into the muscular arteries. These arteries are medium-sized with proportionally thicker walls than elastic

arteries and a consequent lower compliance, but are capable of actively dilating and contracting to enable efficient blood flow and to help maintain blood pressure. These vessels repeatedly branch, eventually distributing blood to the arterioles.

The arterioles are very small, but proportionally strong and thick walled vessels that connect the arteries to the capillaries, and also regulate blood flow and pressure. Arterioles range in size from 300 µm down to 15 µm. In contrast, muscular arteries range from 4 mm to 0.5 mm and elastic arteries can be as large as 25 mm in diameter (Martini et al., 2011).

2.2.2 Capillary system

Capillaries are the smallest blood vessels with diameters ranging from 5–10 µm, which goes below the diameter of a single red blood cell (8 µm), and a wall thickness of only a single layer of endothelial cells. The capillaries are the means by which substances are diffused into and out of tissue, thus supplying nutrients and removing waste. This exchange is made possible by the vast number (around 20 billion) of short capillary vessels, distributed around the body to reach every tissue cell according to its nutrient requirements.

2.2.3 Venous system

After the blood has travelled through the capillaries it then moves into the venous system, starting with the venules. These are small, thin walled vessels, that, due to their porous walls and proximity to the tissue, contribute significantly to the exchange of nutrients and waste as well as to white blood cell emigration. As the veins get further from the capillaries, the walls get thicker and more muscular, and diffusion with the interstitial fluid stops. The venules, like the elastic arteries, have a high compliance and thus can serve as a reservoir for large quantities of blood.

After the venules, the blood moves into the veins. The veins are thinned walled in comparison to the arteries, but are otherwise of a similar structure. Their thin walls reflect the significantly lower blood pressure in the venous system than the arterial system. The main purpose of the veins is to return the blood to the heart, which is

helped by the skeletal muscles in the lower limbs and several valves to prevent the back flow of blood.

2.2.4 Blood distribution

The veins and venules contain the largest proportion of blood, and act as a blood reservoir. This reservoir can shrink and expand as needed to provide more or less blood for active circulation. If more blood is needed for the skeletal muscles, the veins and venules will contract (venoconstriction) pushing a greater percentage of blood around the circulation system. Conversely, the veins and venules dilate to reduce the flow and pressure of blood. Figure 2.4 shows a typical distribution of blood in a healthy cardiovascular system at rest (Tortora and Derrickson, 2011).

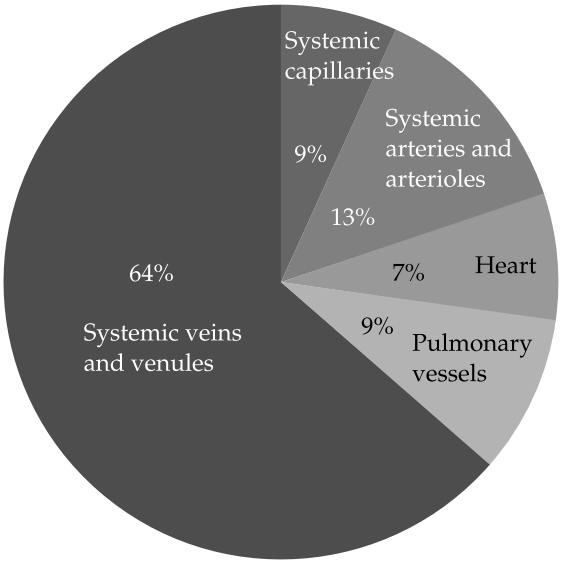

FIGURE 2.4: The relative distribution of blood in the circulation system of an average, healthy, young adult at rest (Tortora and Derrickson, 2011).

2.2.5 Blood pressure and flow

The total blood flow at any given time is called the cardiac output (CO), and is the product of the heart rate and stroke volume of each heartbeat. Typical values for male and female humans is $5.6\,\mathrm{L\,min^{-1}}$ and $4.9\,\mathrm{L\,min^{-1}}$ respectively (Hall and Guyton, 2011). Ultimately, the flow is a function of the vascular resistance and the pressure differential

across the systemic arteries, both of which are controlled by the body in various ways. Cardiac output is regulated to ensure exchange of oxygen to tissues at a rate relative to demand, which thus influences total blood flow and circulatory resistance or "tone" (Hall and Guyton, 2011).

Blood pressure is a function of cardiac output, total blood volume and vascular resistance, and in a relaxed young adult is approximately 110 mmHg (systolic) over 70 mmHg (diastolic). These values drop down to about 35 mmHg in the capillaries, where the pulse fluctuations cease, and again to about 16 mmHg at the venules. This overall level of blood pressure is represented in Figure 2.5.

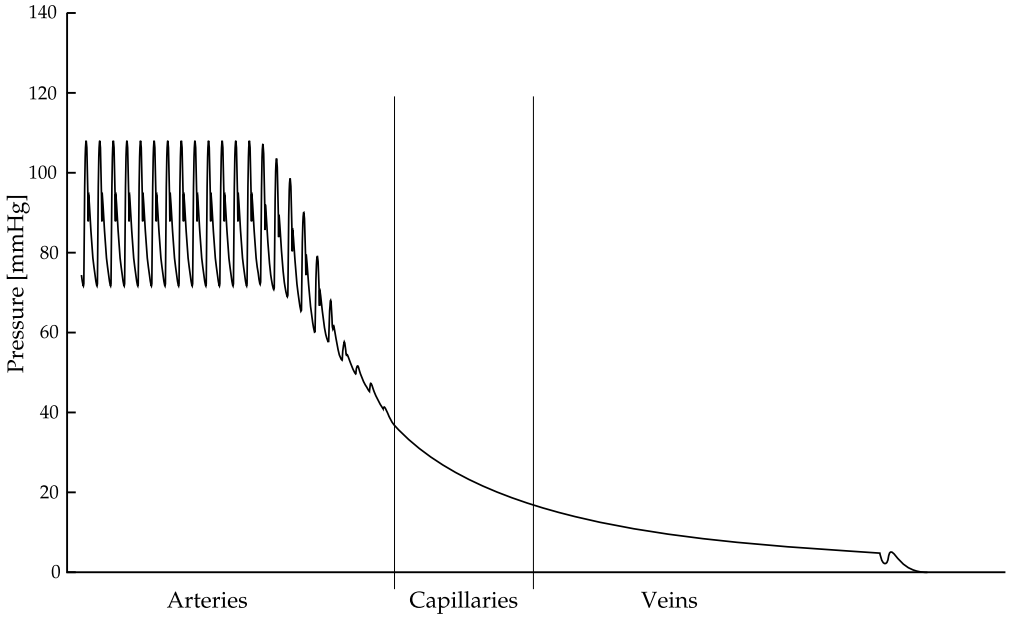

FIGURE 2.5: A representation of the pressure of the left side of the circulation system, starting from the aortic artery, through the capillaries and ending where the vena cava joins the heart. This chart is diagrammatic, and was adapted from Tortora and Derrickson (2011).

The vascular resistance is primarily a function of the lumen size, which is the internal diameter of the vessel. The lumen size is controlled by the muscle fibres surrounding the vessels. Hence, resistance, and thus resulting pressures, can be actively controlled.

More specifically, the whole system is controlled by negative feedback loops through several different channels, neural feedback, hormonal feedback and autoregulation. Neural feedback uses receptors located around the circulation system to give feedback to the cardiovascular centre, at the base of the skull, which in turn responds to adjust the

pressure and flow. Baroreceptors respond to changes in pressure, while chemoreceptors respond to changes in O_2, CO_2 and pH. Both these types of receptors have their most important locations in the aorta and carotid sinus. Hormonal regulation works on the release of certain types or hormones such as renin, epinephrine and norepinephrine among others, which work on the heart and vessels to adjust their performance and/or properties. Autoregulation, in contrast, is the ability of the tissue itself to adjust the blood flow and pressure to suit its current needs (Tortora and Derrickson, 2011; Hall and Guyton, 2011).

2.3 Mechanical properties of the heart

To date, the cardiac pressure-volume (PV) loop is one of the richest sources of information about the heart. The diagram itself is simply a trace of the ventricle pressure against the ventricle volume over a single cardiac cycle. From this diagram, many different metrics can be seen or created, and many more arise from examining the change in PV loops over time (Burkhoff et al., 2005; Suga, 1990a; Sagawa et al., 1988; Moscato et al., 2007; Pacher et al., 2008). Figure 2.6 shows a typical (idealised) PV loop.

Three important metrics are shown in Figure 2.6, stroke volume (SV), end-systolic pressure-volume relation (ESPVR) and end-diastolic pressure-volume relation (EDPVR). The stroke volume is simply the difference in the volume of the ventricle over one heart beat — the end-diastolic volume (EDV) minus the end-systolic volume (ESV). The ESPVR and EDPVR are relationships that help define filling and ejection of the heart.

ESPVR, as the name suggests, is the relationship between pressure and volume at the point of end-systole. This relationship was initially proposed to be linear (Weisfeldt et al., 1976; Sagawa et al., 1977). However, more recent studies have shown that ESPVR can be approximated as linear only within limits (Burkhoff et al., 1987; Krosl and Abel, 1998; Noda et al., 1993). This relationship represents the pressure and volume interaction of the maximally activated myocardium, and therefore provides a boundary for the PV loop at the end of systole. The most important feature of this relationship is the end-systolic elastance, E_{es}, which is the slope of this line. For more details on ESPVR and its clinical significance, see Section 2.3.4.

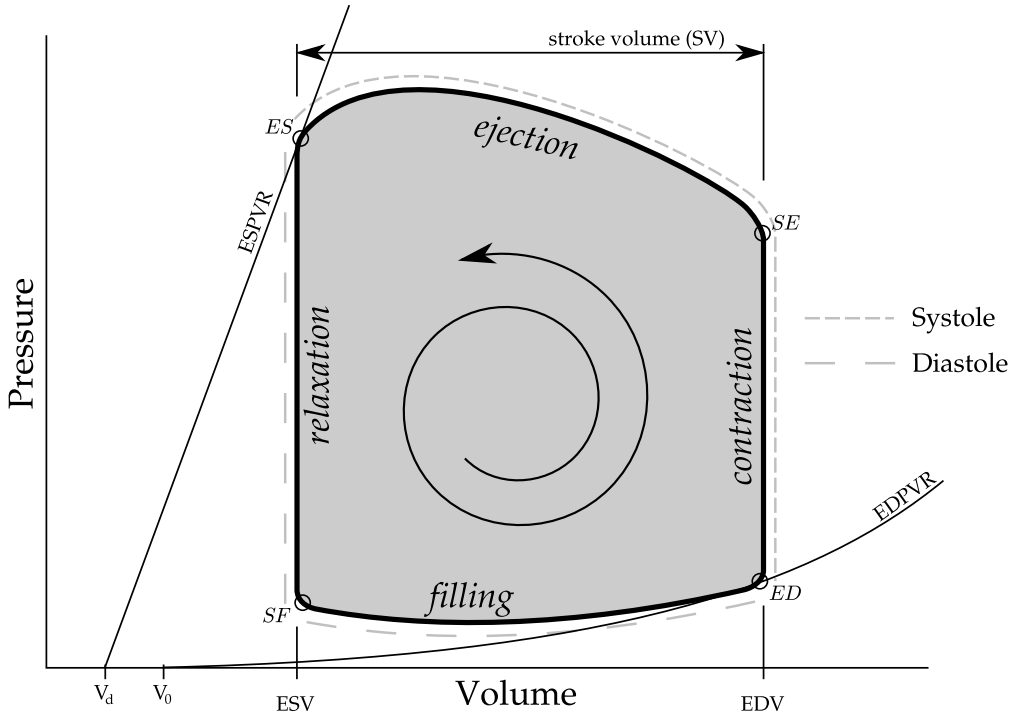

FIGURE 2.6: A typical pressure-volume (PV) loop for one cardiac cycle. The parts of the cycle are shown, along with the end-systolic pressure-volume relation (ESPVR) and the end-diastolic pressure-volume relation (EDPVR). Points are defined as: start of filling (SF), end-diastole (ED), start of ejection (SE) and end-systole (ES).

EDPVR, in contrast to ESPVR, is distinctly non-linear, and confines the lower end of the PV loop. This curve represents the pressure and volume relationship of the totally relaxed myocardium, and therefore acts as a boundary for the PV loop at the end of diastole. In particular, EDPVR is related to the preload as EDPVR gives a relationship between diastolic volume and filling pressure (Klotz et al., 2007; Jacob and Kissling, 1989; Sagawa, 1981).

Theoretically, ESPVR intercepts the volume axis at V_d, while EDPVR intercepts at V_0. However, in practice these two points, V_d and V_0, are usually taken as the same, and referred to as the dead space volume. EDPVR is fundamental to aspects of heart failure, such as ventricle remodelling and the effect of surgical, pharmacological and device-based treatment strategies on reverse remodelling (Klotz et al., 2007; Kass et al., 1995; Klotz et al., 2005; Pouleur et al., 1993; Royse and Royse, 2005).

2.3.1 Cardiac cycle

The cardiac cycle consists of four segments, distinct in their cardiac function, as shown in Figure 2.6. The start of the cycle is typically depicted as starting with the filling of the ventricles (SF), a point partway through diastole. This filling segment occupies the lower beam of the PV diagram — from SF to end-diastole (ED) — and ends as the ventricles start to contract, and the valve upstream of the ventricle closes. The next phase is the iso-volumetric contraction — from ED to the start of ejection (SE) — in which the pressure of the ventricle rises as the ventricle myocardium starts to depolarise. As the pressure in the ventricle rises above the arterial pressure, the downstream valve opens (point SE), and the ejection phase starts. The ejection phase sees volume in the ventricle decrease along with a rise and fall in pressure as the ventricle myocardium starts and finishes contracting. The final phase, iso-volumetric relaxation, occurs when both valves are closed, and consists of the repolarisation of the myocardium, from the end of systole (ES) to SF).

2.3.2 Preload

Preload can, most consistently, be defined as representing all the factors that contribute to the passive ventricular wall stress (or tension) at the end of diastole (Norton, 2001). More practically, it can be thought of as the stretch of the ventricular myocardium just prior to any ventricular contraction (Klabunde, 2011). The most direct factors that effect preload are the end-diastolic chamber radius, the end-diastolic filling pressure and the myocardial wall thickness. In turn, the end-diastolic chamber radius is a function of the end-diastolic filling pressure and the compliance of the ventricle, while the end-diastolic filling pressure is a function of total blood volume, atrial contraction, venous compliance, and venous return among others. However, in clinical practice, preload is often measured as right ventricle end-diastolic pressure, via central venous pressure (CVP), for the right heart, and pulmonary artery occlusion pressure for the left heart (Nahouraii and Rowell, 2010).

Preload has a significant and crucial effect on the output of the heart, namely stroke volume and cardiac output. Cardiac muscle under greater stretch prior to contraction (greater preload), contracts with greater force. This effect is called the Frank-Starling

mechanism, described in Section 2.3.5. A change in preload can be seen in the PV loop diagram of Figure 2.7, as an increase in stroke volume (EDV is increased more than ESV) and end-diastolic volume, while afterload and contractility remain unchanged.

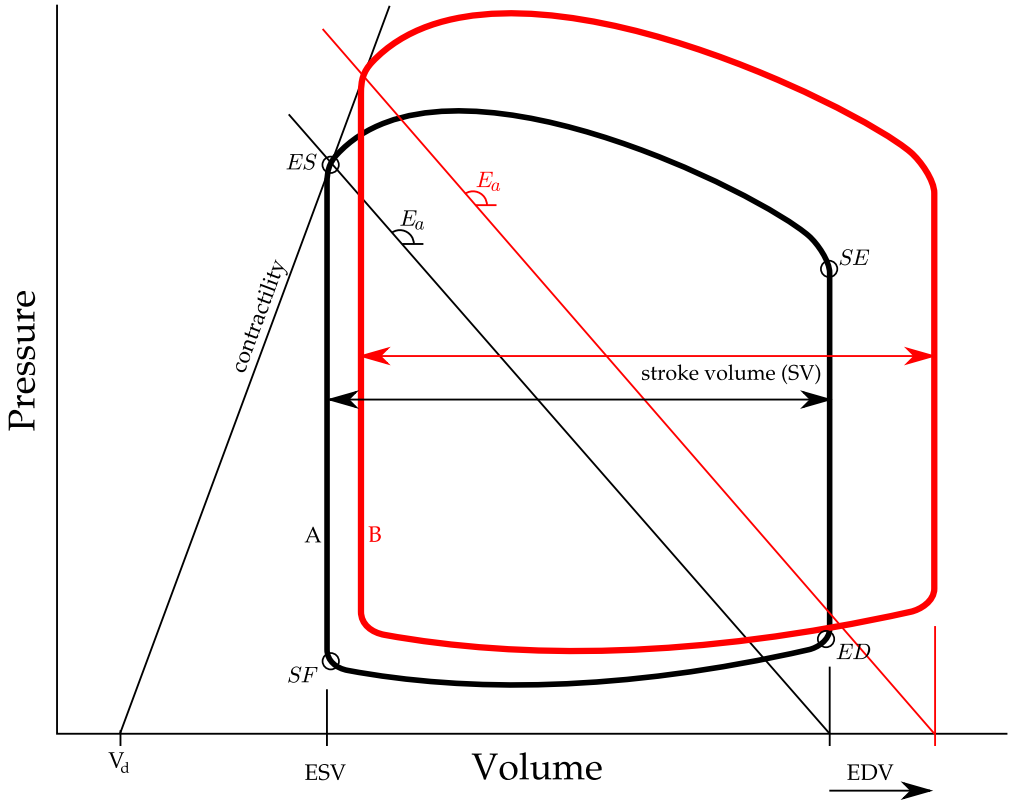

FIGURE 2.7: An illustration of changing preload, increasing from loop A to loop B. Stroke volume and EDV increase, while contractility (slope of ESPVR) and afterload (E_a) remain constant. Points are defined as: start of filling (SF), end-diastole (ED), start of ejection (SE) and end-systole (ES).

2.3.3 Afterload

Afterload is best described as representing all the factors that contribute to the total myocardial wall stress (or tension) during systolic ejection, ED to ES, (Norton, 2001). This load can be thought of as the load against which the heart pumps blood, and usually, in a healthy heart, is imposed by the arterial system resistance. In a clinical setting afterload is assessed through various metrics. These include mean arterial pressure (MAP), systemic resistance, arterial impedance, and myocardial peak wall stress (Burkhoff, 2002).

MAP provides a pressure at which the heart must pump blood. However, this metric is a function of both ventricle and arterial properties, and thus does not uniquely characterise afterload (Burkhoff, 2002). Systemic resistance, or total peripheral resistance, is a commonly used index of preload (Lang et al., 1986), and is equivalent to $\frac{P_{ao}-P_{sys}}{SV}$, and is independent of the properties of the ventricle. Systemic resistance is thus, theoretically, a better index of afterload than MAP (Burkhoff, 2002) although it does not take into account the pulsatile nature of the flow (Weber et al., 1982; O'Rourke, 1982; Nichols and Pepine, 1982). Note that P_{ao} is pressure in the aorta, P_{sys} is systemic vessels and SV is stroke volume. Hence, systemic resistance is merely the ratio of the forcing pressure on the systemic side and the stroke volume.

Arterial impedance can also be used to quantify afterload and is based on an analysis of the relationship between pulsatile flow and pressure waves in the arterial system (Wigfull, 2005; Milnor, 1975; Lang et al., 1986). It uses Fourier analysis, in which flow and pressure waves are decomposed into their harmonic components and the ratio between the magnitudes of pressure and flow waves. Thus, impedance essentially provides a measure of resistance at different driving frequencies (Burkhoff, 2002).

Peak wall stress relates to the amount of force and work the muscle itself does during contraction, and can therefore be used as a measure of afterload. However, like MAP, this metric is not solely a property of the arterial system, but includes ventricular properties. Hence, it is not an exact metric.

Another metric can be found from the PV loop: the effective arterial elastance (E_a). E_a is closely related to the systemic resistance as its definition is the ratio of the pressure differential across the systemic circulation and the stroke volume. In particular, E_a is the gradient of the line connecting the point of end-systole and the volume intercept of end-diastolic volume, as shown in Figure 2.8.

2.3.4 Contractility

Contractility is the measure of the strength of the cardiac muscle. Ventricular contractility is not identical to, but closely resembles and reflects, the myocardial contractility. The myocardial contractility is changed when certain low level cellular functions are altered, such as (Burkhoff, 2002):

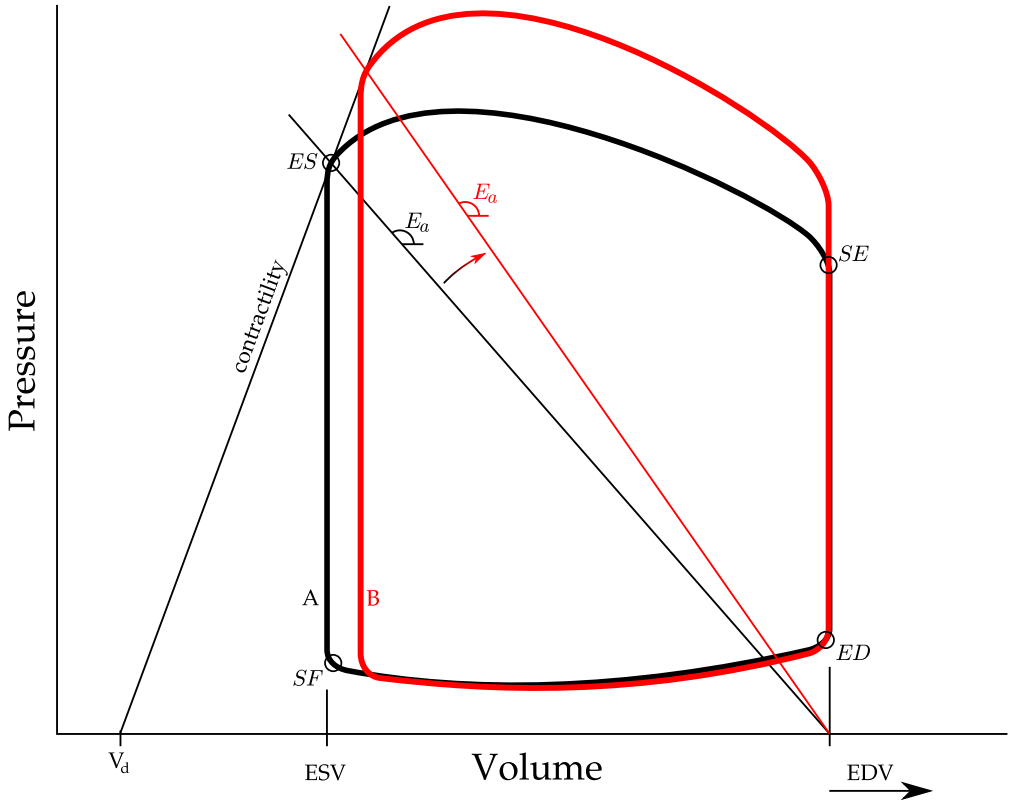

FIGURE 2.8: An illustration of changing afterload, increasing from loop A to loop B. Points are defined as: start of filling (SF), end-diastole (ED), start of ejection (SE) and end-systole (ES).

- the amount of calcium released to the myofilaments
- the affinity of the myofilaments for calcium
- the number of participating myofilaments

The ventricular contractility has been shown to be closely related to ESPVR, (Sagawa et al., 1977; Noda et al., 1993; Shoucri, 2006). In addition, neither V_d nor EDPVR change significantly with altered contractility. Hence, E_{es} can be used as an index of contractility. Drugs that alter this relationship are known as inotropic agents (Hall and Guyton, 2011; Tortora and Derrickson, 2011). The effect of such agents is shown in Figure 2.9.

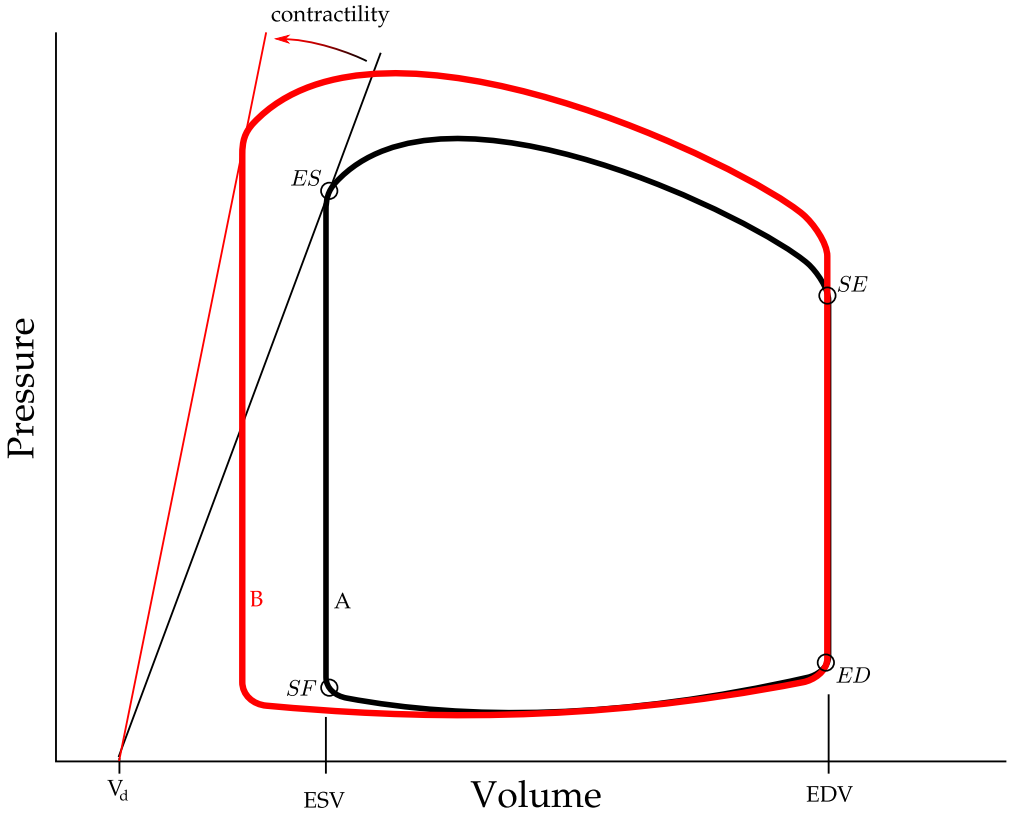

FIGURE 2.9: Contractility as measured off a PV loop, increasing with, in this case, an increased stroke volume and pulse pressure. Contractility is the slope of the line joining V_d and the point of end-ejection. Points are defined as: start of filling (SF), end-diastole (ED), start of ejection (SE) and end-systole (ES).

2.3.5 Frank-Starling Mechanism

In the 19th century, Otto Frank discovered that peak ventricular pressure increases as the end-diastolic volume increases (Frank, 1895). Starling followed this result by showing that there is a non-linear relationship between end-diastolic volume and cardiac output (Starling, 1918). These two observations have now become known as the Frank-Starling Law, derived in part from the relationship between cardiac output and the end-diastolic pressure (EDP) shown in Figure 2.10, which states that cardiac performance increases as preload is increased. More specifically, as the end-diastolic pressure (or filling pressure) increases, cardiac output increases. This can be seen in Figure 2.7, as increased filling pressure pushes the point ED to the right along the line of EDPVR while a constant contractility holds back the point SF. This combined effect increases stroke volume and thus cardiac output. The Frank-Starling relationship exists

within physiological ranges, as there are practical limits to the filling pressures and cardiac output that can be reached, especially in a non-healthy heart.

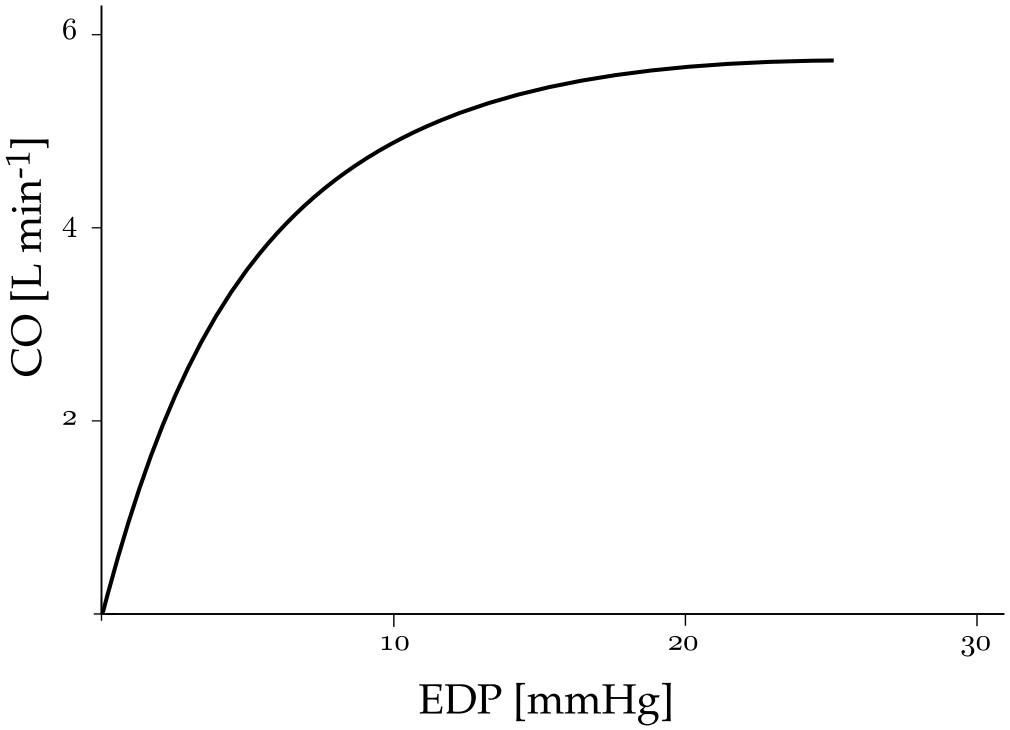

FIGURE 2.10: The relationship between cardiac output (CO) and end-diastolic pressure (EDP), which is the basis of the Frank-Starling law, source (Burkhoff, 2002).

Although the preload is a significant factor contributing to cardiac output, it is not the only one. Others include ventricular contractility and afterload, which in turn influence the Frank-Starling curves.

2.3.6 Cardiac work

The heart converts energy into work, as it pumps blood from the low pressure veins to the high pressure arteries. This total work can be seen as the total area enclosed by the pressure-volume loop, as in Figure 2.6. This definition of work is analogous to any mechanical pump or engine.

2.4 Electrical function of the heart

The contraction of the myocardium is controlled primarily by the sinoatrial node. Within the sinoatrial node, autorhythmic fibres generate action potentials without external stimulus, thus providing the continued spontaneous source of myocardium excitation. This excitation leaves the sinoatrial node and propagates through both atria, causing them to contract simultaneously. The action potential then reaches the atrioventricular node. From here, the conduction path follows the bundle of His, into the left and right bundle branches, then through the Purkinje fibres, finally reaching the myocardium. This propagation path is shown in Figure 2.11.

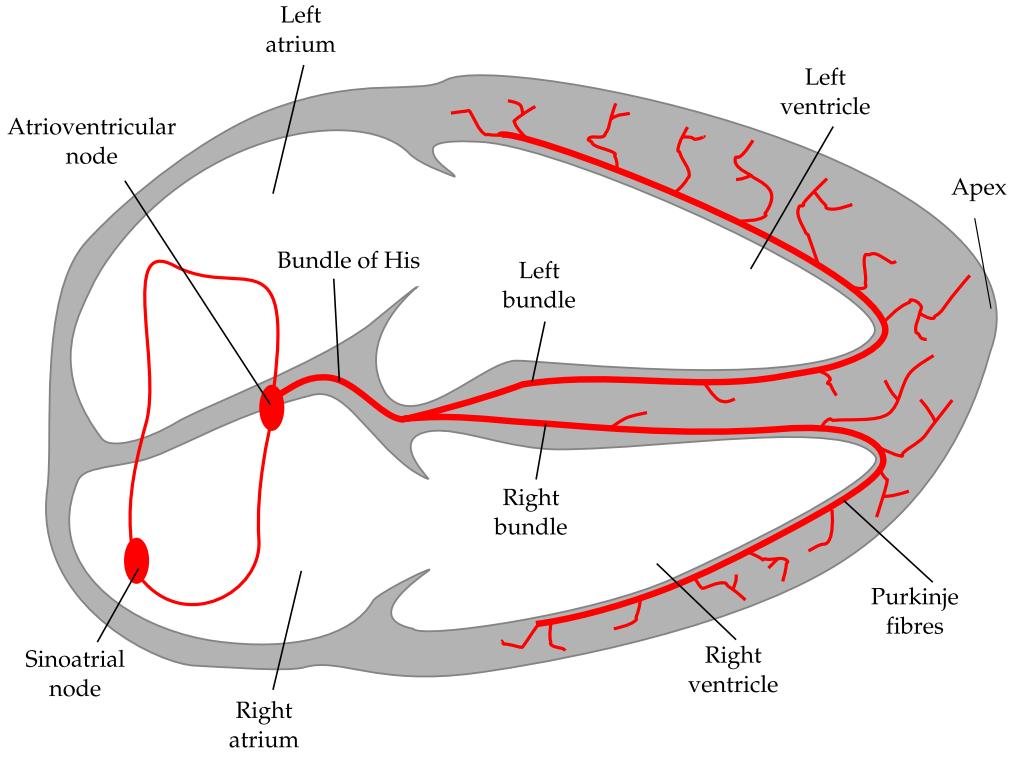

FIGURE 2.11: The propagation channels of the electrical activation of the heart muscle.

The conduction path allows the heart to contract in such a way as to efficiently pump blood. The atria contract first, ejecting the last of their blood, pre-loading the downstream ventricles. The atrioventricular node slows the propagation of the action potential, delaying the contraction of the ventricles. When the ventricles do contract, the contraction starts from the apex, and propagates towards the exit valves, squeezing out blood.

2.4.1 Electrocardiogram

An electrocardiogram (ECG) is the recording of the electrical activation of the heart, and is measured by placing electrodes on different parts of the torso. The difference between any two electrodes is one ECG trace.

A typical ECG trace has three distinct sections, the P wave, the QRS complex and the T wave. These are shown on a schematic ECG trace in Figure 2.12. In normal cardiac function, an action potential originating in the sinoatrial node, travels to the atrioventricular node, causing the atria to depolarise which shows as the P wave on the ECG. After the atrioventricular node, the action potential depolarises the interventricular septum, followed by the rest of the ventricle's contractile fibres, resulting in the QRS complex on the ECG. As the ventricles relax, the repolarisation shows on the ECG as the T wave.

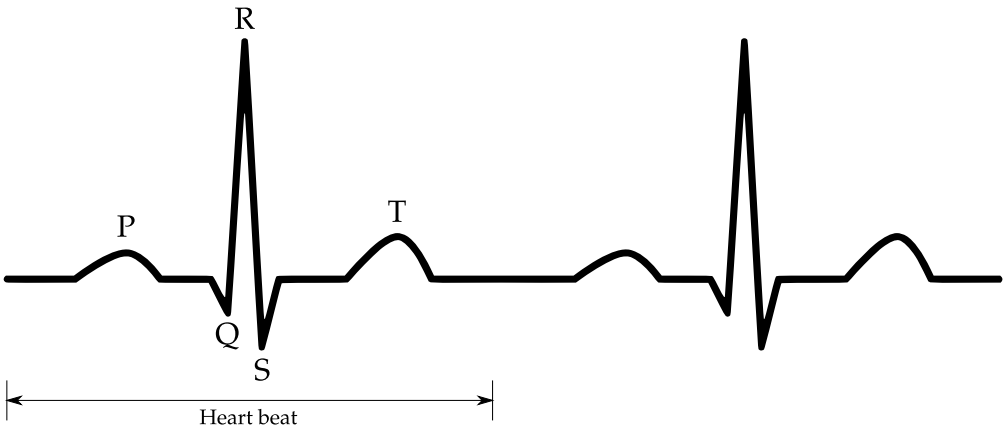

FIGURE 2.12: A idealised illustration of a typical healthy ECG trace, showing the P, R, Q, S and T points of the trace.

2.5 Cardiac Dysfunction

As described in Section 1.1, cardiac dysfunction is an enormous burden on society and the economy. Literally thousands of analyses and studies have been published for improving the diagnosis and treatment of many forms of cardiovascular disease. In this research, two cardiac dysfunctions have been singled out for investigation: pulmonary embolism and septic shock. These two dysfunctions have been chosen for their high

prevalence in the ICU and the challenges they present to the ICU clinician in diagnosis and treatment (Dombrovskiy et al., 2007; Bahloul et al., 2010).

2.5.1 Pulmonary Embolism

Pulmonary embolism (PE) is a cardiovascular emergency, and can lead to life-threatening, but potentially reversible right ventricle failure. However, immediate diagnosis and treatment is highly effective in reducing negative outcomes. Hence, the early diagnosis of pulmonary embolism is critical (Torbicki et al., 2008). Over-treatment is also dangerous as it exposes the patient without PE to unjustified risk of major bleeding (Pineda et al., 2001). Unfortunately, PE is not easy to diagnose, as clinical presentation is atypical (Al Otair et al., 2009). In an ICU, most patients require sedation and mechanical ventilation, and therefore, the clinical manifestations expected from PE often cannot be observed directly or immediately (Bahloul et al., 2010).

2.5.1.1 Physiology and clinical presentation of PE

Pulmonary embolism is the occlusion of the pulmonary bed, and most commonly originates from deep venous thrombosis (DVT) of the legs (Tapson, 2008). PE ranges in severity from asymptomatic, incidentally discovered emboli, to immediate death from massive embolism. Pulmonary embolism becomes significant when more than 20–50 % of the pulmonary bed is occluded (McIntyre and Sasahara, 1971), and the consequences are mostly haemodynamic (Wood, 2002). Emboli can increase pulmonary vascular resistance to a level which cannot be matched by the right ventricle. Alternatively, systemic hypotension induced by PE, can lead to shock and acute right ventricle failure. Left ventricular failure can also occur as a result of compromised cardiac output from the rightward bulging interventricular septum (Jardin et al., 1997). Even if right ventricular failure is initially survived, subsequent haemodynamic instability may be caused by recurrent emboli, or a weakened right ventricular function, or other pre-existing cardiovascular dysfunction. (Torbicki et al., 2008). Annually, more than 300,000 people in the United States die from acute PE (Tapson, 2007), and the diagnosis is often not made until autopsy (Tapson, 2008; Investigators, 1997).

Both PE and DVT are clinical manifestations of venous thromboembolism (VTE), and represent the spectrum of the one disease, VTE. In most cases, pulmonary embolism is a consequence of DVT (Torbicki et al., 2008). For patients presenting with pulmonary embolism, around 79 % have evidence of DVT, and for those that do not, it is likely that the whole thrombus has already detached and embolized (Sandler and Martin, 1989; Moser et al., 1994; Sevitt and Gallagher, 1961). Conversely, about half of the patients presenting with DVT will have some form of pulmonary embolism as well (Tapson, 2008).

2.5.1.2 Diagnosis

Due to the non-specific nature of the clinical presentation of pulmonary embolism, a range of tests and diagnostic strategies exists. The first and most important of these assesses the probability of pulmonary embolism, based on the symptoms and signs that are prevalent in PE. These symptoms and signs include breathing difficulties, chest pain, low blood oxygen saturation, tachypnea and tachycardia (Torbicki et al., 2008), palpitations, and pulmonary hypertension (Tapson, 2008).

Due to complications of sedation and mechanical ventilation, suspicion of pulmonary embolism can be formed from un-explicated hypoxaemia and/or shock, and arterial hypotension (Bahloul et al., 2010). Many systems exist that aim to indicate a probability of pulmonary embolism based on clinical symptoms (Kearon, 2003; Wells et al., 2000; Wicki et al., 2001; Wells et al., 1998; Perrier et al., 2000). However, none of these methods allow the exclusion or confirmation of PE, but merely increase the index of its suspicion (Torbicki et al., 2008). There are many further tests ranging in cost and level of invasiveness, including ventilation-perfusion lung scan, D-dimer blood tests, helical (or spiral) computed tomography (CT), echocardiography, and pulmonary angiography (Kearon, 2003; Torbicki et al., 2008). However, these are limited by lack of sensitivity and specificity, along with cost, time and expertise to perform and interpret.

Despite the limitations of clinical assessment, it still remains a critical first step in the diagnosis of PE. Although most signs and symptoms have a poor combination of sensitivity and specificity, when multiple variables are combined, it is possible to achieve a good index of the probability of PE (Torbicki et al., 2008). Implicit clinical judgement has also been shown to be valuable (Musset et al., 2002; Perrier et al., 2000,

1999), but is problematic in its lack of standardisation and teachability. The two most used standardised rule sets for clinical assessment of PE are the Canadian Rule (Wells et al., 2000), and the revised Geneva Rule (Le Gal et al., 2006).

A D-dimer test can refer to a number of similar blood assays that can effectively rule out a PE diagnosis (Stein et al., 2004; Di Nisio et al., 2007). D-dimer levels are elevated in plasma in the presence of an acute blood clot, and therefore a normal D-dimer result means that acute PE or DVT is very unlikely (Torbicki et al., 2008). These tests range from highly to moderately sensitive (Kearon, 2003).

Ventilation-perfusion scintigraphy (V/Q) scan is a safe and well understood scan that can, for a normal result, eliminate the diagnosis of PE (Torbicki et al., 2008; Kruip et al., 2003; Ten Wolde et al., 2004; Anderson, 2007). However, a V/Q scan is non-specific, with only about one third of patients with V/Q scan defects actually having PE (Kearon, 2003; Groot et al., 1999; Miron et al., 1999). Hence, a V/Q scan has high sensitivity and low specificity.

Helical computed tomography (CT), also known as spiral CT, is another widely used clinical tool with good specificity and moderate sensitivity (Kearon, 2003). Traditional computed tomography is not suitable for diagnoses of PE due to the long exposure times that would be required. Helical CT can be completed during a breath hold, or about 20 seconds. From two sets of studies, the sensitivity and specificity has been shown to be around 70 % and 88 % respectively (Perrier et al., 2001; Monye and Pattynama, 2001; Van Strijen et al., 2005).

Pulmonary angiography has historically been the standard for diagnosing PE (Kearon, 2003). However, it must be used with caution as it has side effects such as a small chance or mortality (Kearon, 2003; Stein et al., 1992), as well as increasing the risk of bleeding complications in some situations (Agnelli et al., 2002; Wan et al., 2004). It is also technically demanding and costly. Furthermore, CT technology has improved to the point where it can provide similar results in a non-invasive manner (Torbicki et al., 2008).

Echocardiography is another test for diagnosing PE, and is particularly helpful in emergency management situations (Torbicki et al., 2008). The main use of echocardiography is for patients with shock or hypotension, and is used to rule out PE in the absence of

right ventricle (RV) overload or dysfunction. Echocardiography can visualise the right heart haemodynamic changes (Goldhaber, 2002) along with a measure of RV volume (Puchalski et al., 2007), which therefore means it can directly assess PE. However, it is time consuming and costly and does not operate in real time.

The diagnosis of PE involves a nuanced approach that takes into account a variety of variables and tests, using them to asses the probability of PE (Roy et al., 2006). Better tests exist, but these are not readily assessed in real time. Hence, an implicit diagnosis or noting of symptoms is required. What is necessary is an automated, higher resolution measurement or diagnostic tool.

2.5.1.3 Treatment

With early diagnosis, treatment of PE is highly effective (Bahloul et al., 2010). The initial treatment is aimed at the life-saving restoration of flow through the occluded arteries, in combination with the prevention of early recurrences which can be fatal (Torbicki et al., 2008). Haemodynamic and respiratory support are often necessary, especially with patients presenting with shock or hypotension. Long term treatment usually involves anticoagulation agents to prevent further recurrence (Tapson, 2008).

2.5.2 Septic Shock

Septic shock is an advanced stage of systemic inflammatory response syndrome (SIRS) in the presence of an infection and organ failure (Annane et al., 2005). Septic shock is a major cause of mortality and cost (Remick, 2007; Artero et al., 2012; Angus et al., 2001), and continues to be a significant challenge to clinicians (Nduka and Parrillo, 2009; Dellinger et al., 2008).

2.5.2.1 Physiology and clinical presentation

Septic shock is a serious and life threatening disorder, that originates with a dysfunctional immune system response to an infection and affects many aspects of the patient's physiology, importantly the cardiovascular system, and if left untreated, ultimately leads to organ failure. Septic shock is thus a range or syndrome of related disorders

from systemic inflammatory response syndrome, sepsis, severe sepsis, septic shock and finally refractory septic shock. This range is shown and defined in Table 2.1.

TABLE 2.1: The range of systemic inflammatory response syndromes, summarised from Annane et al. (2005).

Dysfunction	description
Systemic inflammatory response syndrome	Two or more of: abnormal body temperature, elevated heart rate, elevated respiratory rate or low arterial CO_2 tension, abnormal white blood cell count.
Sepsis	Systemic inflammation response syndrome with documented infection.
Severe sepsis	Sepsis and at least one sign of organ hypoperfusion or organ dysfunction, such as acute lung injury or cardiac dysfunction.
Septic shock	Severe sepsis and one of: low systemic mean blood pressure after fluids have been administered, the need for vasopressors to maintain mean blood pressure.

Sepsis is the systemic maladaptive response of the body to an invasion by pathogenic micro-organisms to normally sterile tissue (Nduka and Parrillo, 2009), and can be defined in more clinical terms as an infection with evidence of systemic inflammation, consisting of two or more of the following: increased or decreased temperature or leukocyte count, tachycardia and rapid breathing. Shock is a state of widespread and profound reduction of effective tissue perfusion, which can lead to reversible or irreversible cellular damage (Nduka and Parrillo, 2009). Finally, septic shock is sepsis with hypotension that persists after resuscitation with intravenous fluid (Annane et al., 2005).

Sepsis occurs when the immune and neuroendocrine system fails to tightly control the local inflammatory response in the presence of infection leading to systemic inflammation and anything from sepsis to septic shock. The final condition is a result of a complex set of interactions between the host and any number of pathogens, involving an over reaction from the host leading to organ dysfunction or failure. It is often characterised by dysfunction involving all aspects of the immune system (Nduka and Parrillo, 2009).

The initial cause of sepsis comes primarily (80 %) from infections of the chest, abdomen, genitourinary system and primary blood stream (Annane et al., 2003; Martin et al., 2003; Alberti et al., 2002). The cardiovascular dysfunction resulting from septic shock has been studied extensively over the last five decades (Calvin et al., 1981; Parker et al., 1990; Munt et al., 1998; Poelaert et al., 1997). The results of these studies suggest that cardiac performance during septic shock includes reduced left and right ventricular ejection fractions, increased end-diastolic and end-systolic volumes of both ventricles with normal stroke volume, while heart rate and cardiac output are elevated and systemic vascular resistance is reduced.

2.5.2.2 Diagnosis

Due the complications of confirming — in a timely manner — both infection and organ failure caused by infection, diagnosis can be difficult. To confirm a diagnosis of septic shock there must be a recognised infection and an established causal link between that infection and organ failure and shock (Annane et al., 2005). The infection may be clinically obvious or otherwise discovered from recovery of pathogens from blood or tissue culture. However, such cultures can take time to produce and are not usually sensitive enough to rule out infection (Annane et al., 2005). Organ failure and the link to infection can also be problematic to confirm, especially as organ failure scores often ignore pre-existing organ function (Moreno et al., 2002). For cardiovascular failure, it is important to differentiate between cardiac and circulatory dysfunction and is often best characterised by echocardiography (Vieillard-Baron et al., 2003), which is resource intensive, not real-time, and costly.

Shock is widely recognised in practice by the need for vasopressors to maintain arterial pressure, (Bone et al., 1992). There are often indicators, such as low central venous oxygen saturation (Rivers et al., 2001), visualisation of altered micro-circulation (Spronk et al., 2002; De Backer et al., 2002), and impaired cardiovascular variability (Annane et al., 1999). Hence, it can be diagnosed symptomatically, but only after it is advanced.

Due to the complications of confirming both infection and organ failure caused by infection in a timely manner, diagnosis of septic shock can be difficult to diagnose with certainty. To be confident of a septic shock diagnosis, a documented infection must be present along with organ failure with no other relevant acute illness. Therefore, as

with many diagnostic methods, a probabilistic scale is used, with the likelihood of a septic shock diagnosis reducing as the likelihood of infection decreases and other acute illnesses are present. However, these diagnostics lack sensitivity and specificity, and importantly, cannot be assessed in real-time or continuously.

2.5.2.3 Treatment

The main treatment strategies include immediate control of infection and haemodynamic status, as well as support for failing organs, and restoration of immune, neuroendocrine and haemostasis responses (Annane et al., 2005). Infection is primarily controlled by appropriate antibodies. Management of shock and organ dysfunction can be more involved, usually starting with fluid resuscitation and continuous monitoring of central venous oxygen saturation, cardiac output among other cardiovascular metrics (Annane et al., 2005). Anticoagulant therapies have also been shown to be an important tool for treating septic shock (Rapaport et al., 1964; Corrigan et al., 1968). High-volume haemofiltration can also be effective (Cole et al., 2001; Cornejo et al., 2006; Bouman, 2007; Rogiers, 2005), although it was first proposed as a renal replacement therapy (Kramer et al., 1977). The ability to assess the impact of therapy, in real-time, would greatly enhance the ability to treat patients effectively.

Chapter 3

Cardiovascular System Model

Throughout this research a lumped parameter model of the cardiovascular system is used to describe cardiovascular and circulatory dynamics. This chapter describes the model, as previously developed (Smith, 2004; Smith et al., 2004, 2005, 2006; Starfinger et al., 2008a).

3.1 Introduction

Models are extremely useful constructions that can provide great insight into the specific details of systems that cannot otherwise be known in a practical manner. The cardiovascular system has many dynamics that would be clinically useful for monitoring, diagnostics and treatment selection. However, many of them are too invasive to measure directly. Hence, a cardiovascular model that can accurately capture these properties and dynamics could have broad and significant use within a clinical environment.

The cardiovascular model presented in this chapter has been previously published (Smith, 2004; Smith et al., 2004, 2005, 2006; Starfinger et al., 2008a), and describes the important properties and dynamics of the cardiovascular system under healthy and a variety of pathological, physiological and clinical conditions (Revie et al., 2011a; Smith et al., 2007, 2006; Starfinger et al., 2008a,b).

3.1.1 The model

The model presented in this chapter is a lumped parameter model, and thus is a compromise between accuracy and complexity. In this manner, a six chamber model is presented that can represent the important dynamics without additional complexity. An eight chamber version of this same model has also been published (e.g. Starfinger et al., 2008a). However, it has yet to be shown that the added complexity of the additional two chambers is beneficial in a clinical setting and is therefore not presented in the research here.

The lumped nature of the model implies that the parameters and components of the model relate metaphorically, rather than directly, to specific anatomy and physiology. As such, each of the six chambers in the model represent the combination of a set of general anatomical or physiological compartments. Another compromise is the addition or exclusion of inertial effects, which, if included, moves the model from a system of six differential equations to ten, adding significant computational expense to solve the system, for, sometimes, minimal gain (Smith et al., 2003).

3.1.1.1 The six chambers

There are six distinct chambers in this model, each representing a portion of the circulation with elastic properties. These compartments are, the left ventricle, the aorta, the vena cava, the right ventricle, the pulmonary artery and the pulmonary vein. Four of these chambers are passive and linear in their relationship between pressure and volume. These passive chambers are, the aorta, the vena cava and the pulmonary artery and vein. Due to the nature of the model each of these chambers represent the summed effect of all the vessels within their respective section between the heart and the capillaries.

The left and right ventricles are active chambers in the relationship between pressure and volume, and, as such, have an elastance that varies with time in accordance with the activation of the cardiac muscle. This time-varying elastance creates a non-linear pressure-volume (PV) relationship. Therefore, active, non-linear PV relationship is the basis of the rhythm and energetics of the model, and characterises each of the left and

right ventricles as a pump. They are thus the primary elements driving circulatory dynamics, as expected.

Due to the proximity of the ventricle chambers to each other, their activation is not independent, but also not identical. This interaction is captured in the model by coupling the two ventricles through the inter-ventricular septum and surrounding pericardium. This enables the relationship between pressure and volume in each of the ventricles to be partially independent and partially influenced by the other.

Since the heart and surrounding large vessels reside within the thoracic cavity, the pressures in these vessels and compartments are also influenced by the thoracic pressure. Including this thoracic pressure in the model enables the model to capture the effects of respiration, whether natural or mechanical, and can play a significant role especially in a critical care situation where both respiratory and cardiac support are required.

3.1.1.2 Inter-chamber properties

Between the chambers, there exist other properties to account for the remaining model dynamics. These dynamics include pressure drops, inertial effects and valves. There are four main circulatory valves, which appear at either side of the ventricles: the aortic, tricuspid, pulmonary and mitral valves. These valves open on a positive pressure gradient, and close on backward flow. Each valve causes a pressure drop and is thus modelled alongside a resistance. Inertial effects can also be included here as the flow and volume of blood is at its largest. Note that the model presented in this chapter is presented with and without inertia, as the addition of inertia greatly increases the computation cost of simulation.

There are two other important pressure drops represented in the model, occurring across the pulmonary and systemic portions of the circulation. These pressure drops are modelled as the summed resistance over the entire left (systemic) and right (pulmonary) sides of the circulation. Therefore, they include all the resistance to flow through the artery, capillaries and veins on their respective side.

3.1.1.3 The atria

The model presented here does not include a separate elastic chamber for the left and right atria. These compartments are lumped into the pulmonary vein and vena cava respectively. Work is ongoing to add these chambers to the model (Pironet et al., 2012; Pironet, 2011). However, the major dynamics of the cardiovascular system can be captured with the current model (Smith, 2004).

3.2 Electrical analogy and equations

Electrical analogies can be helpful to create and solve models that are outside the electrical domain, such as cardiovascular models (Olansen et al., 2000; Ottesen et al., 2004; Smith, 2004). This is done by recognising the analogous metrics and components between the two systems, and thus the equations of electrical origin which can be used.

There are four basic electronic properties used in the analogy between electronics and fluid dynamics. These are voltage, current, resistance and charge, and each have direct equivalence in fluid dynamics. Voltage is equivalent to fluid pressure, current to fluid flow, resistance is the same in both situations, and charge is equivalent to fluid volume. Table 3.1 shows these relationships along with the symbols typically used in each discipline. In this and following chapters, symbols will be in reference to the fluid dynamic concepts per Table 3.1, except where explicitly stated.

TABLE 3.1: The analogous metrics between the electrical domain and fluid dynamics along with their typical symbols, and units in each system.

Electrical	Fluid dynamics
Voltage, V [V]	Pressure, P [mmHg]
Current, I [A]	Flow rate, Q [$\mathrm{ml\,s^{-1}}$]
Resistance, R [Ω]	Resistance, R [$\mathrm{mmHg\,s\,ml^{-1}}$]
Inductance, L [H]	Inertia, I [$\mathrm{mmHg\,s^2\,ml^{-1}}$]
Charge, Q [C]	Volume, V [ml]
Capacitance, C [F]	Compliance, C [$\mathrm{ml\,mmHg^{-1}}$]

There are three main electrical circuit components with analogous fluid dynamic properties. These components are: the resistor, representing the resistance of a pipe or vessel to the flow of fluid; the inductor, representing the inertia of the fluid; and the capacitor, which represents the ability of a compartment to hold and release a volume of fluid. These components and their equivalents are shown with their respective symbols and base units in Table 3.2.

TABLE 3.2: The analogous components between the electrical domain and fluid dynamics along with their typical symbols.

Electrical	Fluid dynamics metaphor
Resistor (—/\/\/\/\—)	Vessel resistance
Inductor (—∩∩∩—)	Fluid inertia
Capacitor (—||—)	Vessel compliance

From the analogy in Tables 3.1–3.2, many fluid dynamic systems can be modelled as electrical circuits and solved using the established circuit theory and equations. There are three equations used, Ohm's law, and the relationship between current and voltage for both capacitor and an inductor. Ohm's law provides an equation to relate fluid pressure to resistance and flow, and is defined:

$$P = Q \times R \tag{3.1}$$

The equation governing a capacitor, and therefore vessel compliance is defined:

$$Q = C \cdot \frac{dP}{dt} \tag{3.2}$$

From Equation (3.2), the relationship between pressure, volume and elastance (units of $\mathrm{mmHg\,ml^{-1}}$) can be derived:

$$Q = \frac{1}{E} \cdot \frac{dP}{dt} \tag{3.3}$$

$$\Rightarrow \quad \frac{dP}{dt} = E \cdot Q \tag{3.4}$$

$$\Rightarrow \quad P = E \cdot \int Q dt \tag{3.5}$$

$$\Rightarrow \quad P = E \cdot V \tag{3.6}$$

Finally, the equation governing an inductor, and therefore fluid inertia is defined:

$$P = L \cdot \frac{dQ}{dt} \tag{3.7}$$

Variables are as defined in Tables 3.1–3.2.

3.3 Model background

3.3.1 Windkessel model

The Windkessel model was first described by the German physiologist by Frank (1899), and since then has been used in numerous physiological models to simulate the elasticity of a compartment. The term Windkessel loosely translates from German as "air chamber". The original model was based on a hydraulic circuit consisting of a water pump connected to a chamber of air. As water is pumped into the chamber, the water compresses the air at the same time as pushing water out of the chamber and back to the pump. The compressibility of the air simulates the compliance of the chamber. This type of model is most commonly used to simulate blood in a vessel that exhibits elasticity of its walls, typically referred to by its inverse value, compliance $= 1/$elastance.

There are many different ways to formulate a Windkessel model, from a simple two-element model to higher order models, both in parallel and in series. The CVS model presented in the chapter is largely based on a chain of three-element series models, one of which is shown as an electrical analogy in Figure 3.1, where the capacitor represents compliance (C), the resistance (R) represents resistance to blood flow back to the pump, and the inductance (I) represents the inertia of the blood.

3.4 Schematic model derivation

The general principle behind a lumped parameter model is to achieve a description of the necessary system properties and dynamics with the minimal amount of complexity, lumping any excess complexity into single parameters or units. In this manner the

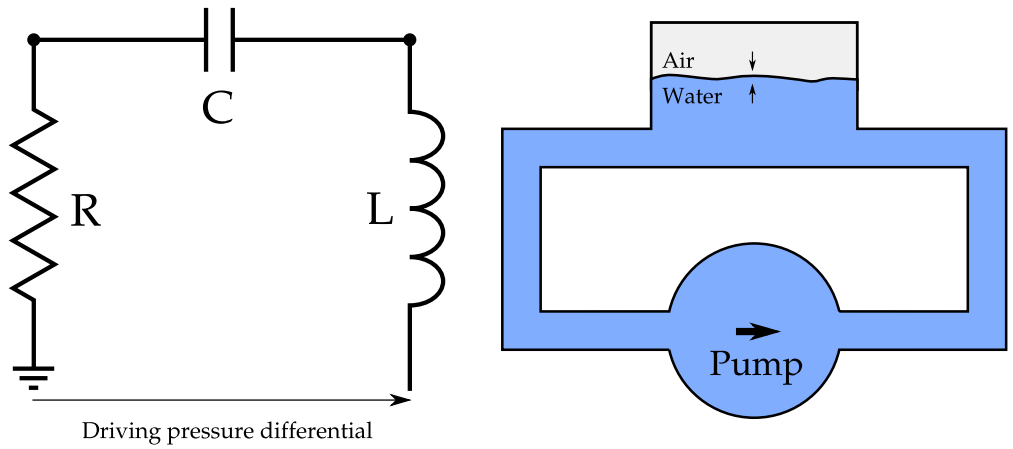

FIGURE 3.1: A Windkessel model and a three-element series electrical representation. This is the basic compartment or element model from which the overall CVS model is derived.

circulation can be traced through its complete cycle, forming a closed loop fluid dynamic system. Each significant section (by volume) of the circulation is represented as an elastic chamber (Windkessel model) which is allowed to vary in pressure and volume with a constant chamber stiffness.

Each passage of flow will encounter resistance, and the portions that have highest mass and volume will also exhibit the greatest inertia. Ignoring the valves in the veins, there are four main valves in the normal human circulation which are located either side of the ventricles. Finally, the pumping of the heart is modelled in the elastic chambers, representing the ventricles, by allowing these chambers to vary in elastance over time, to capture the heart's active, electro-mechanical activation. Hence, this time-varying elastance is the core mechanism by which the model is pressurised and driven, and can thus be thought of as the driver function. The full schematic representation is shown in Figure 3.2, along with an analogous electrical circuit.

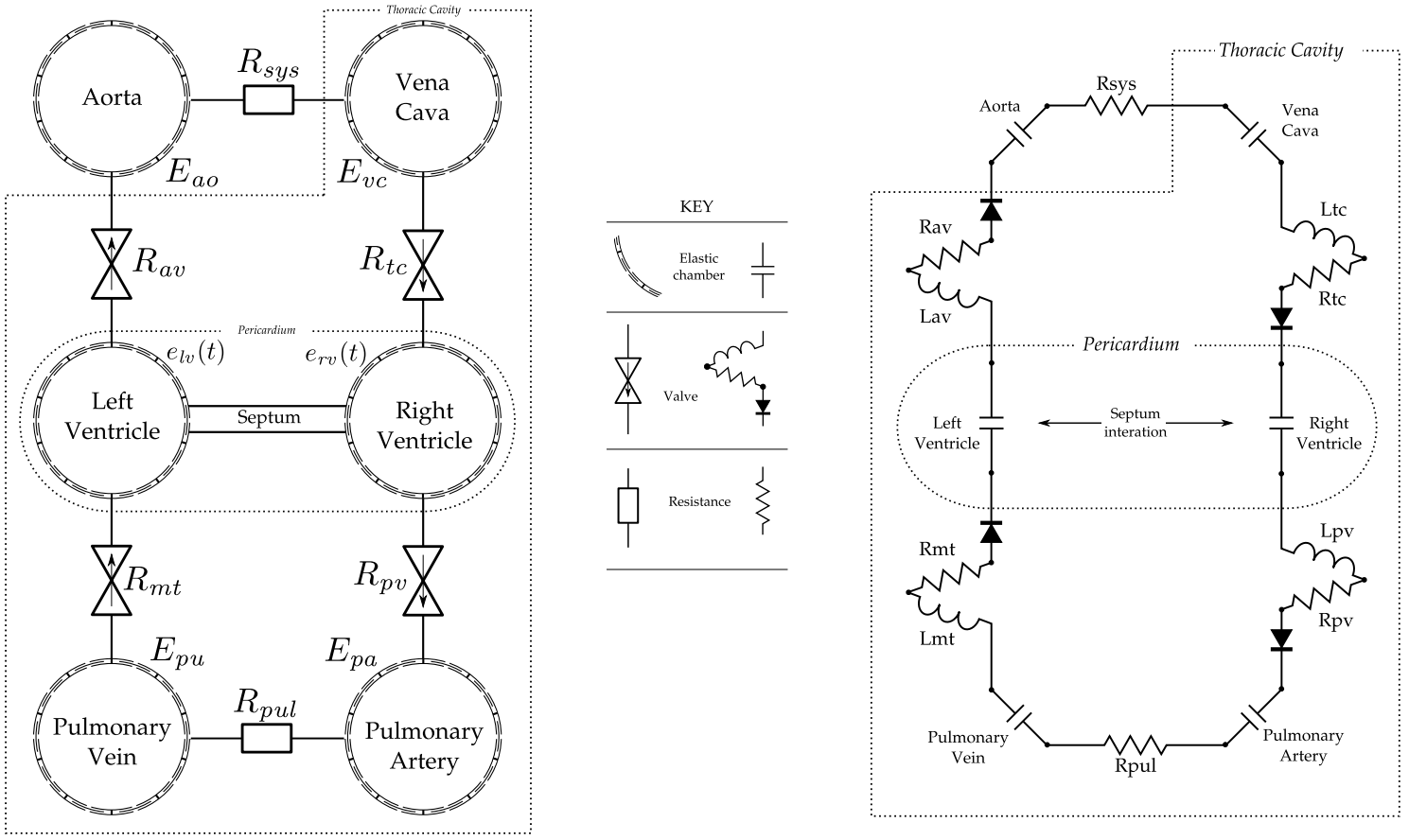

FIGURE 3.2: The schematic model and its electrical circuit equivalent. Note that for simplicity the ventricle interaction through the septum is not fully described in the electrical equivalence.

3.5 Equation derivation

The model is derived by creating a series of equations based on electrical circuit theory for the components of the system. This process starts with a mass balance across each elastic chamber. A general elastic chamber is shown in Figure 3.3.

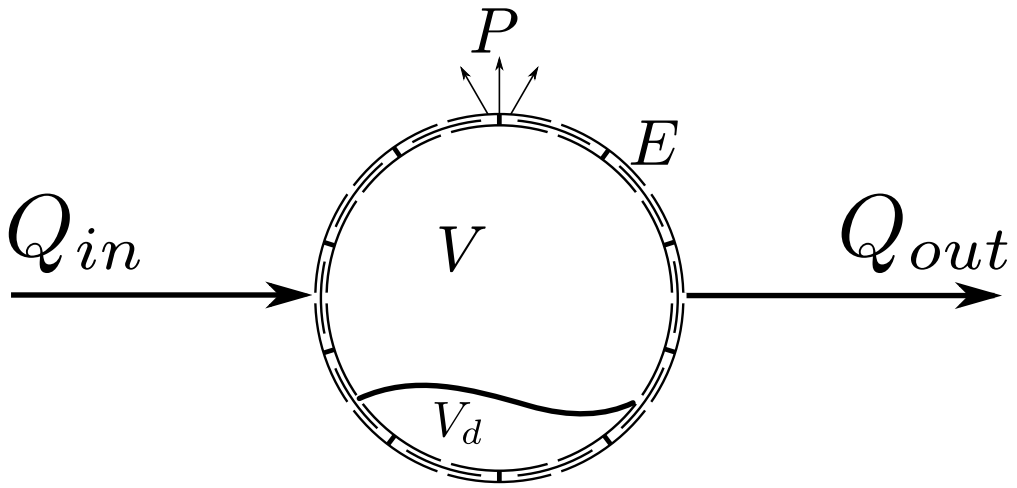

FIGURE 3.3: A single elastic chamber shown in isolation. P is pressure, E the elastance, V the volume, V_d the unstressed volume and Q is the flow.

Figure 3.3 yields an equation for the change in volume of a chamber:

$$\frac{dV}{dt} = Q_{in} - Q_{out} \tag{3.8}$$

Each flow rate in the set of equations generalised by Equation (3.8) can be derived as a function of the adjacent chamber volumes and other parameters by looking at the section between two chambers. These sections come in two forms: a valve, incorporating resistance and inertia; and a sole resistance, for peripheral sections where no valves exist and inertia is low. There are also two derivations possible, one accounting for inertia, the other neglecting inertia in favour of the resulting simpler set of equations that are faster to solve. These two derivations are shown in Sections 3.5.1 and 3.5.2 respectively.

3.5.1 The valves

There are four sections that have valves, representing the four valves found in the heart: the aortic valve, the tricuspid valve, the pulmonary valve, and the mitral value. Each of these valves can be represented by a resistor, inductor and diode, shown in Figure 3.4. As the diode is only meant to represent a fluid dynamic construction of no back flow, the physical details of an electrical diode, such as forward and reverse bias, are ignored.

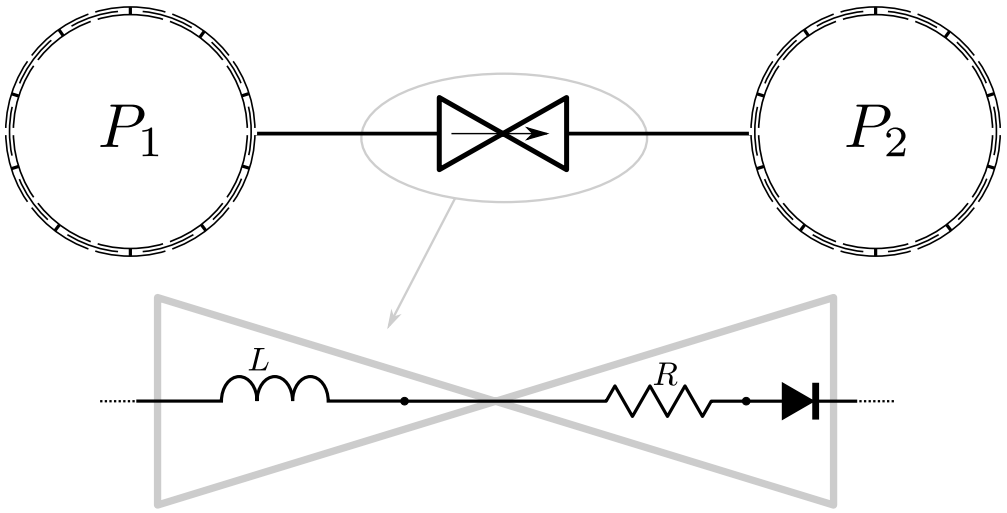

FIGURE 3.4: The representation of a valve between two chambers. The valve is modelled as a diode, with resistance and inertial effects.

Using electrical equations for the voltage, or pressure difference across this section, $P_2 - P_1$, a differential equation in Q can be derived from Equations (3.1) and (3.7):

$$P_2 - P_1 = Q \cdot R + \dot{Q} \cdot L \tag{3.9}$$

$$\Rightarrow \dot{Q} = \frac{P_2 - P_1 - Q \cdot R}{L} \tag{3.10}$$

To account for the diode/valve, a Heaviside function is introduced to zero all negative flow. The Heaviside is defined:

$$H(f) = \begin{cases} 0 & \text{if } f \leq 0 \\ 1 & \text{if } f = 0 \end{cases} \tag{3.11}$$

Thus the diode is implemented as $\mathcal{H}(f)$, and is defined:

$$\mathcal{H}(f) = H(f) \cdot f \tag{3.12}$$

3.5.2 Peripheral flow

The model also has inter-chamber flow through the systemic and pulmonary circulation with no valves and negligible inertia. This situation is shown in Figure 3.5. This case results in the following equations:

$$P_2 - P_1 = Q \cdot R \tag{3.13}$$

$$\Rightarrow Q = \frac{P_2 - P_1}{R} \tag{3.14}$$

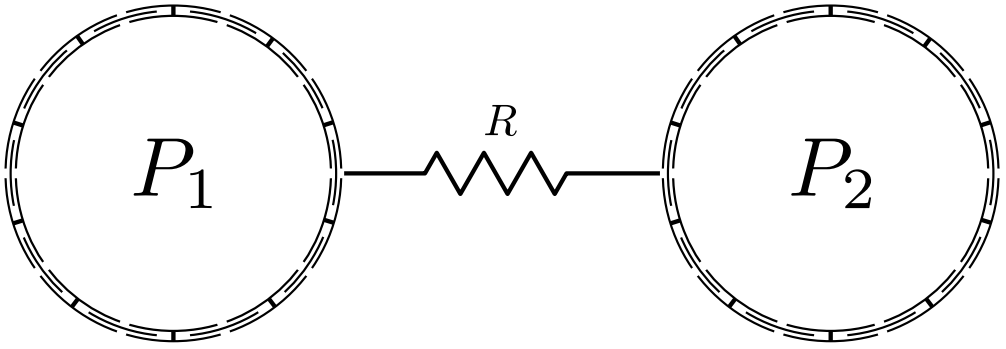

FIGURE 3.5: Flow between elastic chambers with only resistance.

3.5.3 Pressure and volume

At this point, there are six equations relating the change in a chamber's volume to its pressure and surrounding parameters of resistance and inductance. For the four passive chambers of the model in Figure 3.2, the pressure can be found as a function of volume through the electrical equations of a capacitor outlined with Equations (3.3)–(3.6), resulting in:

$$P = E \cdot V \tag{3.15}$$

It is now necessary to formulate the pressure, as a function of volume, for the driven chambers representing the two ventricles.

3.5.4 Ventricle pressure and volume

The relationship between pressure and volume in the ventricles is more complicated than Equation (3.15), as these chambers are actively pressurising and de-pressurising over time, and thus the pressure-volume relationship is non-linear. A common method for describing this relationship is to allow the elastance in the model components for the ventricular chambers to vary with time, thus giving the name time-varying elastance (Beyar et al., 1987; Burkhoff and Tyberg, 1993; Chung et al., 1997; Santamore and Burkhoff, 1991).

From Figure 3.6, it can be seen that limits for the elastance in the ventricular chambers are defined by the two relationships of ESPVR and EDPVR as the upper and lower bounds respectively. These two elastance relationships are described in Section 2.3. To use these limits, descriptive equations are required and these equations are defined for the linear ESPVR:

$$P_{es} = E_{es}\left(V_{es} - V_d\right) \tag{3.16}$$

For the non-linear EDPVR they are defined:

$$P_{ed} = P_0\left(e^{\lambda(V_{ed}-V_0)} - 1\right) \tag{3.17}$$

where the subscripts *es* and *ed* represent end-systole and end-diastole respectively, and the parameters P_0, λ and V_0 represent the gradient, curvature and volume at zero pressure respectively for EDPVR.

To define the complete relationship for pressure and volume in the ventricles the time-varying elastance is normalised to vary between 0 (at end-diastole) and 1 (at end-systole), and given the symbolic notation of $e(t)$. This normalised curve can then be used as a weighted sum to provide the pressure-volume relationship outside the already defined points of end-diastole and end-systole. Ventricular pressure is thus defined as:

$$P = e\left(t\right) \cdot P_{es} + \left(1 - e\left(t\right)\right) \cdot P_{ed} \tag{3.18}$$

Since the volume is now allowed to vary beyond that at end-diastole and end-systole, and noting that the ventricles reside within the pericardium, the full pressure-volume

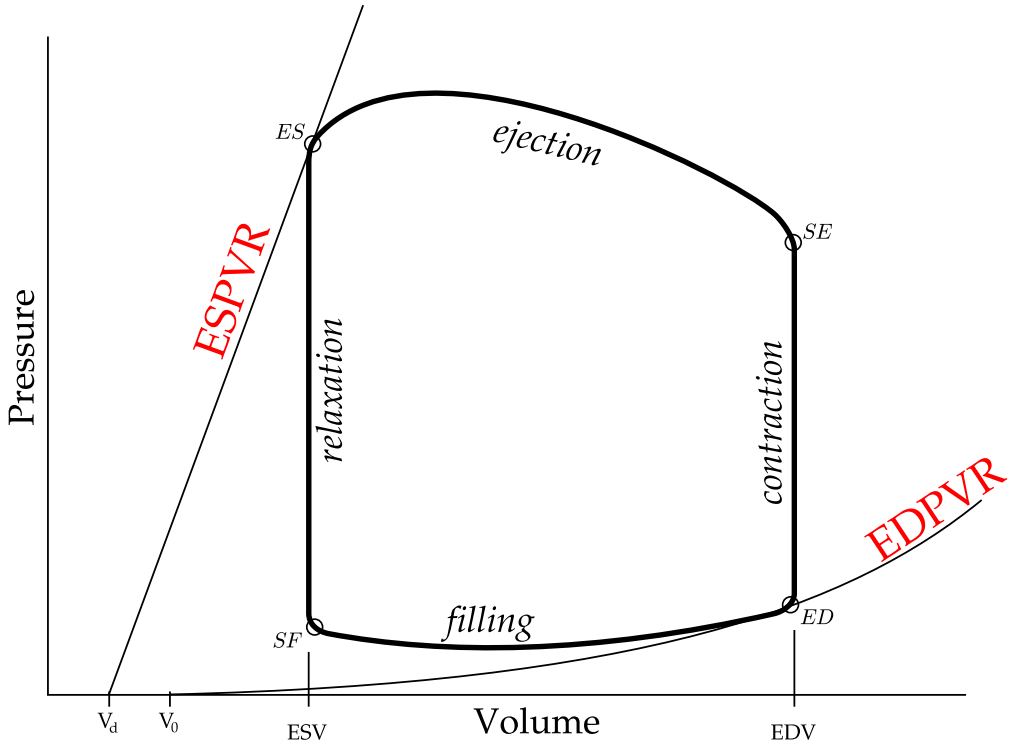

FIGURE 3.6: The pressure-volume loop, as defined in Figure 2.6, showing ESPVR and EDPVR as defined in Equations (3.16) and (3.17).

relationship for the ventricles becomes:

$$P = e(t) \cdot E_{es}(V - V_d) + (1 - e(t)) \cdot \left(P_0\left(e^{\lambda(V-V_0)} - 1\right)\right) + P_{peri} \tag{3.19}$$

where the pericardium pressure, P_{peri}, is described as the pressure across the pericardium *pcd*, plus the thoracic pressure, defined:

$$P_{peri} = P_{pcd} + P_{th} \tag{3.20}$$

In practice the contribution of EDPVR from Equation (3.17) to the pressure-volume relationship of Equation (3.19) is small, leading to a simplification described by setting $P_0 = 0$, resulting in the following equation for the pressure-volume relationship:

$$P = e(t) \cdot E_{es}(V - V_d) + P_{peri} \tag{3.21}$$

This equation closely resembles the general equation for a passive chamber in Equation (3.15), with an additional pressure, which under certain conditions can be assumed to be negligible. Although the full unsimplified ventricular pressure-volume relationship is used in the simulation of the model, the simplified version is used in this research as a means to calculate and estimate the time-varying elastance $e(t)$.

At this point in the derivation, six differential equations have been defined for the volume of each elastic chamber in the model. However, unlike the four passive chambers, the volumes and pressures in the driven chambers do not stand in isolation, but rather interact with one another, requiring more complexity to the driven chamber pressure-volume equations.

3.5.5 Ventricular interaction

The two ventricles of the heart share a common muscle boundary called the interventricular septum. The ventricles also reside within the pericardium. This shared wall and surrounding membrane gives rise to shared dynamics and interaction between the two ventricles. These shared dynamics play an important role in the overall dynamics of the cardiovascular system (Weber et al., 1982; Fogel et al., 1998), and account for differences between the two ventricles in terms of pressure and volume that otherwise could not be captured. This aspect is especially important in abnormal pathologies, such as an overloaded right ventricle with pulmonary hypertension, which results in impaired left ventricle filling due to ventricular interaction (Gan et al., 2006). In such cases, the right ventricle extends into the normally larger left ventricle, skewing the balance of pressure and volume normally seen between these chambers. Hence, the model must be able to capture this dynamic, and does so via this model mechanism.

Figure 3.7 shows two depictions of the two ventricles and their interaction in volume and pressure. For ease of modelling, the concept of a 'free wall volume' is defined as the volume contained by the boundary of the wall. This free wall volume is distinct from a normal volume as shown in Figure 3.7, as well as creating imaginary volumes such as the volume of the septum V_{spt}.

Given the concept of a free wall compartment, designated by appending f to an existing subscript, the ventricular volumes can be defined in relation to the free wall volumes

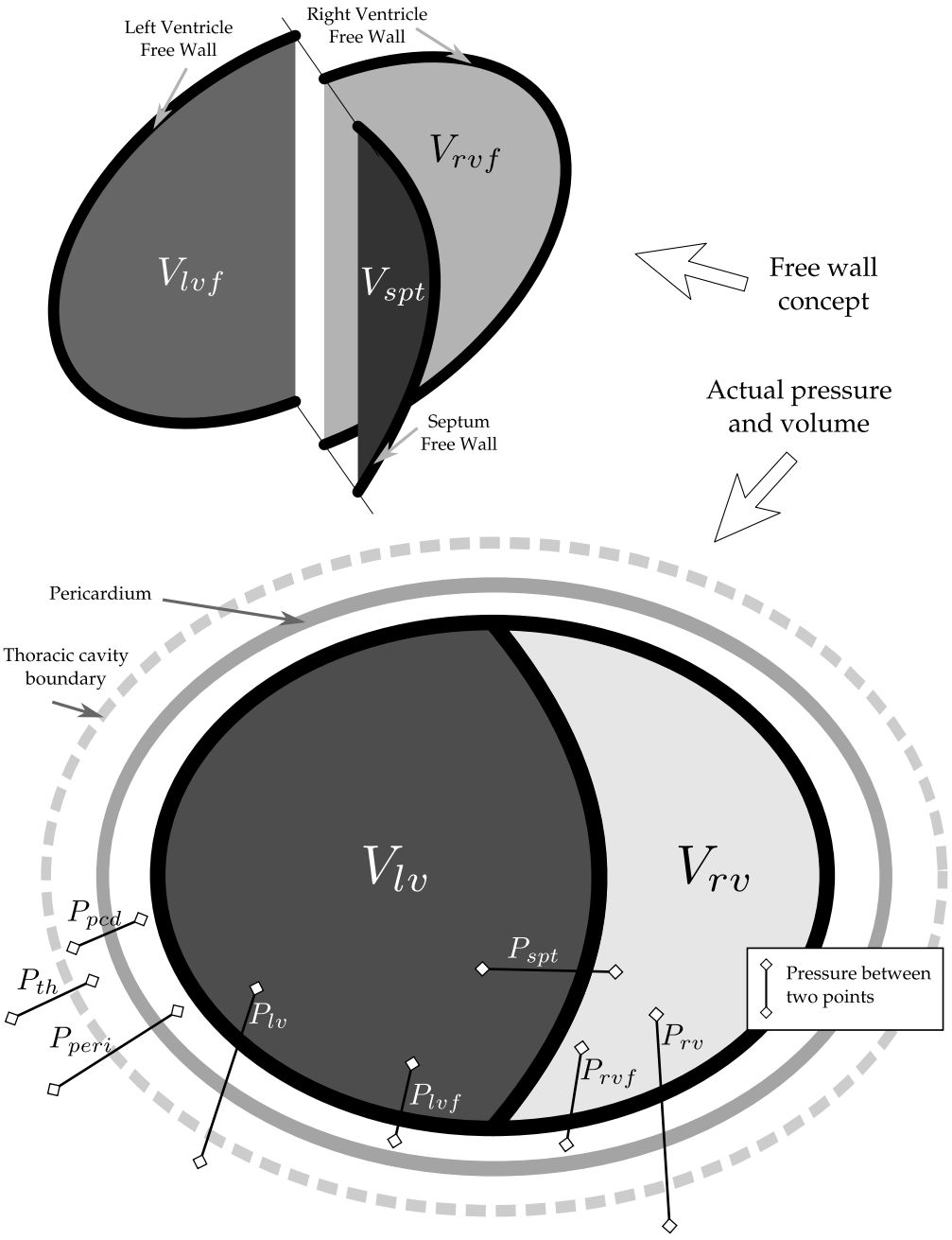

FIGURE 3.7: The free wall concept, top graphic, showing the left and right free wall volumes along with the septum free wall volume. The actual pressure and volume of the ventricles and surroundings are shown in the lower graphic.

and the septum volume:

$$V_{lv} = V_{lvf} + V_{spt} \tag{3.22}$$

$$V_{rv} = V_{rvf} - V_{spt} \tag{3.23}$$

and the septum pressure is defined:

$$P_{spt} = P_{lv} - P_{rv} = P_{lvf} - P_{rvf} \tag{3.24}$$

The sign convention used here references the tendency for the left ventricle to extend into the right ventricle, which holds in most cases barring few and specific pathologies.

The pressure-volume relationship of the septum is modelled in the same way as the free-wall construction of the ventricles, as in Equation (3.18). Applying Equation (3.19) to P_{lvf} and P_{rvf} and Equation (3.18) to P_{spt}, Equation (3.24) can be rewritten as:

$$\begin{aligned} e_{spt}(t) \cdot E_{es,spt}\left(V_{spt} - V_{d,spt}\right) + \left(1 - e_{spt}(t)\right) \cdot \left(P_{0,spt}\left(e^{\lambda\left(V_{spt} - V_{0,spt}\right)} - 1\right)\right) = \\ e_{lv}(t) \cdot E_{es,lvf}\left(V_{lvf} - V_{d,lvf}\right) + \left(1 - e_{lvf}(t)\right) \cdot \left(P_{0,lvf}\left(e^{\lambda\left(V_{lvf} - V_{0,lvf}\right)} - 1\right)\right) - \\ e_{rv}(t) \cdot E_{es,rvf}\left(V_{rvf} - V_{d,rvf}\right) + \left(1 - e_{rvf}(t)\right) \cdot \left(P_{0,rvf}\left(e^{\lambda\left(V_{rvf} - V_{0,rvf}\right)} - 1\right)\right) \end{aligned} \tag{3.25}$$

Equation (3.25) can be numerically solved via zero-finding solutions. However, such numerical methods are slow and a closed form approximation for V_{spt} from Equation (3.25) has been derived (Hann et al., 2005), and is shown in Section 3.6.

Finally, the time-varying elastance of the septum is assumed to be the average of the time-varying elastance for the left and right ventricles, defined:

$$e_{spt}(t) = \frac{e_{lv}(t) + e_{rv}(t)}{2} \tag{3.26}$$

3.6 The full model equations

The six differential equations that the overall model is built around, as derived in the previous section, and using Newton's notation where $\dot{x} \equiv \frac{dx}{dt}$, are thus defined:

$$\dot{V}_{lv}(t) = Q_{mt}(t) - Q_{av}(t) \tag{3.27}$$

$$\dot{V}_{ao}(t) = Q_{av}(t) - Q_{sys}(t) \tag{3.28}$$

$$\dot{V}_{vc}(t) = Q_{sys}(t) - Q_{tc}(t) \tag{3.29}$$

$$\dot{V}_{rv}(t) = Q_{tc}(t) - Q_{pv}(t) \tag{3.30}$$

$$\dot{V}_{pa}(t) = Q_{pv}(t) - Q_{pul}(t) \tag{3.31}$$

$$\dot{V}_{pu}(t) = Q_{pul}(t) - Q_{mt}(t) \tag{3.32}$$

where, the flow rates are described by:

$$Q_{pul}(t) = \frac{P_{pa}(t) - P_{pu}(t)}{R_{pul}} \tag{3.33}$$

$$Q_{sys}(t) = \frac{P_{ao}(t) - P_{vc}(t)}{R_{sys}} \tag{3.34}$$

$$\dot{Q}_{tc}(t) = \mathcal{H}\left(\frac{P_{vc}(t) - P_{rv}(t) - Q_{tc}(t) \cdot R_{tc}}{L_{tc}}\right) \tag{3.35}$$

$$\dot{Q}_{pv}(t) = \mathcal{H}\left(\frac{P_{rv}(t) - P_{pa}(t) - Q_{vc}(t) \cdot R_{pv}}{L_{pv}}\right) \tag{3.36}$$

$$\dot{Q}_{mt}(t) = \mathcal{H}\left(\frac{P_{pu}(t) - P_{lv}(t) - Q_{mt}(t) \cdot R_{mt}}{L_{mt}}\right) \tag{3.37}$$

$$\dot{Q}_{av}(t) = \mathcal{H}\left(\frac{P_{lv}(t) - P_{ao}(t) - Q_{av}(t) \cdot R_{av}}{L_{av}}\right) \tag{3.38}$$

and where $\mathcal{H}(f)$ implements the effect of a valve, zeroing all negative values, as defined in Equation (3.12).

If initial effects are neglected, the equations for flow through the valves become closed form equations, resulting in four less differential equations. These inertia-less flow

equations are defined:

$$Q_{pul}(t) = \frac{P_{pa}(t) - P_{pu}(t)}{R_{pul}} \tag{3.39}$$

$$Q_{tc}(t) = \mathcal{H}\left(\frac{P_{vc}(t) - P_{rv}(t)}{R_{tc}}\right) \tag{3.40}$$

$$Q_{pv}(t) = \mathcal{H}\left(\frac{P_{rv}(t) - P_{pa}(t)}{R_{pv}}\right) \tag{3.41}$$

$$Q_{sys}(t) = \frac{P_{ao}(t) - P_{vc}(t)}{R_{sys}} \tag{3.42}$$

$$Q_{mt}(t) = \mathcal{H}\left(\frac{P_{pu}(t) - P_{lv}(t)}{R_{mt}}\right) \tag{3.43}$$

$$Q_{av}(t) = \mathcal{H}\left(\frac{P_{lv}(t) - P_{ao}(t)}{R_{av}}\right) \tag{3.44}$$

The pressure in the four passive chambers: the aorta, the vena cava, the pulmonary artery and the pulmonary vein, are defined assuming a linear relationship between pressure and volume as described in Section 3.5.3. Note that three of the four passive chambers comprising the pulmonary artery, the pulmonary vein, and the vena cava, reside within the thoracic cavity and therefore have an addition external pressure applied to them, the thoracic pressure, P_{th}, yielding:

$$P_{pa}(t) = E_{pa} \cdot V_{pa}(t) + P_{th} \tag{3.45}$$

$$P_{pu}(t) = E_{pu} \cdot V_{pu}(t) + P_{th} \tag{3.46}$$

$$P_{vc}(t) = E_{vc} \cdot V_{vc}(t) + P_{th} \tag{3.47}$$

$$P_{ao}(t) = E_{ao} \cdot V_{ao}(t) \tag{3.48}$$

The two driven chambers are defined slightly differently, as described in Section 3.5.5.

$$P_{lv}(t) = P_{lvf}(t) + P_{pcd}(t) + P_{th} \tag{3.49}$$

$$P_{rv}(t) = P_{rvf}(t) + P_{pcd}(t) + P_{th} \tag{3.50}$$

$$\tag{3.51}$$

where

$$P_{lvf}(t) = e_{lv}(t) \cdot E_{es,lv} \cdot \left(V_{lvf}(t) - V_{d,lvf}\right) + (1 - e_{lv}(t)) \cdot P_{0,lvf} \cdot \left(e^{\lambda_{lvf}\left(V_{lvf}(t) - V_{0,lvf}\right)} - 1\right) \quad (3.52)$$

and

$$P_{rvf}(t) = e_{rv}(t) \cdot E_{es,rv} \cdot \left(V_{rvf}(t) - V_{d,rvf}\right) + (1 - e_{rv}(t)) \cdot P_{0,rvf} \cdot \left(e^{\lambda_{rvf}\left(V_{rvf}(t) - V_{0,rvf}\right)} - 1\right) \quad (3.53)$$

and

$$P_{pcd}(t) = P_{0,pcd} \cdot \left(e^{\lambda_{pcd} \cdot \left(V_{pcd}(t) - V_{0,pcd}\right)} - 1\right) \quad (3.54)$$

The free wall ventricle volumes are defined:

$$V_{lvf}(t) = V_{lv}(t) - V_{spt}(t) \quad (3.55)$$

$$V_{rvf}(t) = V_{rv}(t) + V_{spt}(t) \quad (3.56)$$

and when summed, the ventricles make the volume of the pericardium, defined:

$$V_{pcd}(t) = V_{lv}(t) + V_{rv}(t) \quad (3.57)$$

The volume of the septum is defined as a closed-form approximation to Equation (3.25), as derived (Hann et al., 2005):

$$V_{spt} = \frac{a}{b} \quad (3.58)$$

where a and b are defined:

$$\begin{aligned} a = {} & e_{spt}(t) \cdot E_{es,spt} \cdot V_{d,spt} \\ & + e_{lv}(t) \cdot E_{es,lvf} \cdot \left(V_{lv} - V_{d,lvf}\right) \\ & - e_{rv}(t) \cdot E_{es,rvf} \cdot \left(V_{rv} - V_{d,rvf}\right) \\ & - \left(1 - e_{spt}(t)\right) \cdot P_{0,spt} \cdot \left(b_{spt} \cdot e^{-\lambda_{spt} \cdot V_{0,spt}} - 1\right) \\ & + \left(1 - e_{lv}(t)\right) \cdot P_{0,lvf} \cdot \left(b_{lvf} \cdot e^{\lambda_{lvf} \cdot \left(V_{lv} - V_{0,lvf}\right)} - 1\right) \\ & - \left(1 - e_{rv}(t)\right) \cdot P_{0,rvf} \cdot \left(b_{rvf} \cdot e^{\lambda_{rvf} \cdot \left(V_{rv} - V_{0,rvf}\right)} - 1\right) \end{aligned} \tag{3.59}$$

$$\begin{aligned} b = {} & e_{spt}(t) \cdot E_{es,spt} \\ & - e_{lv}(t) \cdot E_{es,lvf} - e_{rv} \cdot E_{es,rvf} \\ & + \left(1 - e_{spt}(t)\right) \cdot P_{0,spt} \cdot a_{spt} \cdot e^{-\lambda_{spt} \cdot V_{0,spt}} \\ & - \left(1 - e_{lv}(t)\right) \cdot P_{0,lvf} \cdot a_{lvf} \cdot e^{\lambda_{lvf} \cdot \left(V_{lv} - V_{0,lvf}\right)} \\ & + \left(1 - e_{rv}(t)\right) \cdot P_{0,rvf} \cdot a_{rvf} \cdot e^{\lambda_{rvf} \cdot \left(V_{rv} - V_{0,rvf}\right)} \end{aligned} \tag{3.60}$$

and the parameters a_{spt}, a_{lvf}, a_{rvf}, b_{spt}, b_{lvf}, b_{rvf} are defined:

$$x_1 = V_{spt,old} + \Delta V_{spt} \tag{3.61}$$

$$x_2 = V_{spt,old} - \Delta V_{spt} \tag{3.62}$$

$$a_i = \frac{e^{\lambda_i \cdot x_2} - e^{\lambda_i \cdot x_1}}{x_2 - x_1}, i = spt, lvf \text{ and } rvf \tag{3.63}$$

$$b_i = e^{\lambda_i \cdot x_1} - \left(e^{\lambda_i \cdot x_2} - \frac{e^{\lambda_i \cdot x_1}}{x_2 - x_1} \cdot x_1\right), i = spt, lvf \text{ and } rvf \tag{3.64}$$

where $V_{spt,old}$ is the septum volume of the previous time-step and $\Delta V_{spt} = 0.1$ml.

The set of equations defined in Equations (3.27)–(3.64) form a complete system that represents all the major dynamics and properties of the cardiovascular system. Table 3.3 lists all the input parameters to the model along with approximate healthy values, while Table 3.4 list the outputs of the model.

TABLE 3.3: Model input parameters for the six-chamber cardiovascular model along with units and healthy values.

Input	Name	Units	Value
R_{pul}	Pulmonary vascular resistance	$\mathrm{mmHg\,s\,ml^{-1}}$	0.018
R_{sys}	Systemic vascular resistance	$\mathrm{mmHg\,s\,ml^{-1}}$	1.0889
R_{tc}	Tricuspid valve resistance	$\mathrm{mmHg\,s\,ml^{-1}}$	0.0237
R_{pv}	Pulmonary valve resistance	$\mathrm{mmHg\,s\,ml^{-1}}$	0.0055
R_{mt}	Mitral valve resistance	$\mathrm{mmHg\,s\,ml^{-1}}$	0.0158
R_{av}	Aortic valve resistance	$\mathrm{mmHg\,s\,ml^{-1}}$	0.018
L_{tc}	Tricuspid valve blood inertia	$\mathrm{mmHg\,s^2\,ml^{-1}}$	8.0093×10^{-5}
L_{pv}	Pulmonary valve blood inertia	$\mathrm{mmHg\,s^2\,ml^{-1}}$	1.4868×10^{-4}
L_{mt}	Mitral valve blood inertia	$\mathrm{mmHg\,s^2\,ml^{-1}}$	7.6968×10^{-5}
L_{av}	Aortic valve blood inertia	$\mathrm{mmHg\,s^2\,ml^{-1}}$	1.2189×10^{-4}
E_{pa}	Pulmonary artery elastance	$\mathrm{mmHg\,ml^{-1}}$	0.369
E_{pu}	Pulmonary vein elastance	$\mathrm{mmHg\,ml^{-1}}$	0.0073
E_{vc}	Vena cava elastance	$\mathrm{mmHg\,ml^{-1}}$	0.0059
E_{ao}	Aortic elastance	$\mathrm{mmHg\,ml^{-1}}$	0.6913
P_{th}	Thoracic pressure	mmHg	-4
$E_{es,lv}$	Left ventricle end-systolic elastance	$\mathrm{mmHg\,ml^{-1}}$	2.8798
$V_{d,lvf}$	Unstressed left ventricle volume	ml	0
$V_{0,lvf}$	Zero-pressure left ventricle volume	ml	0
$P_{0,lvf}$	Zero-volume left ventricle pressure	mmHg	0.1203
λ_{lvf}	Left ventricle lambda	$\mathrm{ml^{-1}}$	0.033
$E_{es,rv}$	Right ventricle end-systolic elastance	$\mathrm{mmHg\,ml^{-1}}$	0.5850
$V_{d,rvf}$	Unstressed right ventricle volume	ml	0
$V_{0,rvf}$	Zero-pressure right ventricle volume	ml	0
$P_{0,rvf}$	Zero-volume right ventricle pressure	mmHg	0.2157
λ_{rvf}	Right ventricle lambda	$\mathrm{ml^{-1}}$	0.023

Table 3.3 — *(continued)*

Input	Name	Units	Value
$E_{es,spt}$	Septum end-systolic elastance	$\mathrm{mmHg\,ml^{-1}}$	48.0754
$V_{d,spt}$	Unstressed septum volume	ml	2
$V_{0,spt}$	Zero-pressure septum volume	ml	2
$P_{0,spt}$	Zero-volume septum pressure	mmHg	1.1101
λ_{spt}	Septum lambda	$\mathrm{ml^{-1}}$	0.435
$P_{0,pcd}$	Zero-volume pericardium pressure	mmHg	0.5003
$V_{0,pcd}$	Zero-pressure pericardium volume	ml	200
λ_{pcd}	Pericardium lambda	$\mathrm{ml^{-1}}$	0.03

3.7 Simulation

The solution to the CVS model is found by solving the system of differential equations listed in Equations (3.27)–(3.32) and, if inertia is not neglected, additionally Equations (3.35)–(3.38). In this research, the routine `ODE45` from the software package MATLAB® (The MathWorks, Natick, USA) is used to numerically solve for the state variables defined:

$$x = [V_{lv}, V_{ao}, V_{vc}, V_{rv}, V_{pa}, V_{pu}, Q_{tc}, Q_{pv}, Q_{mt}, Q_{av}] \tag{3.65}$$

or, if inertia is neglected, the state variables defined:

$$x = [V_{lv}, V_{ao}, V_{vc}, V_{rv}, V_{pa}, V_{pu}] \tag{3.66}$$

Apart from these parameters the simulation needs some extra information. The first is an initial state, which is a vector corresponding to Equation (3.65) or Equation (3.66).

TABLE 3.4: The outputs of the model along with their respective numerical units.

Output	Name	Units
V_{lv}	Left ventricle volume	ml
V_{ao}	Aortic volume	ml
V_{vc}	Vena cava volume	ml
V_{rv}	Right ventricle volume	ml
V_{pa}	Pulmonary artery volume	ml
V_{pu}	Pulmonary vein volume	ml
Q_{pul}	Pulmonary vascular flow	$\mathrm{ml\,s^{-1}}$
Q_{sys}	Systemic vascular flow	$\mathrm{ml\,s^{-1}}$
Q_{tc}	Tricuspid valve flow	$\mathrm{ml\,s^{-1}}$
Q_{pv}	Pulmonary valve flow	$\mathrm{ml\,s^{-1}}$
Q_{mt}	Mitral valve flow	$\mathrm{ml\,s^{-1}}$
Q_{av}	Aortic valve flow	$\mathrm{ml\,s^{-1}}$
P_{lv}	Left ventricle pressure	mmHg
P_{ao}	Aortic pressure	mmHg
P_{vc}	Vena cava pressure	mmHg
P_{rv}	Right ventricle pressure	mmHg
P_{pa}	Pulmonary artery pressure	mmHg
P_{pu}	Pulmonary vein pressure	mmHg
V_{spt}	Inter-ventricular septum volume	ml
P_{pcd}	Pericardium pressure	mmHg

A maximum step-size was also enforced at 0.001 s to keep the solver stable. However, this limitation can be relaxed substantially if the time-varying elastance is smooth, as discussed later in Section 3.7.1.

Once the solver is set up, the model is simulated over a time span of 20 heartbeats to ensure it has reached an oscillatory, steady state solution. For the given solution, the last three heartbeats are isolated and used as the steady state solution.

After a steady state solution has been reached for the state variables, the remaining outputs of the model can be calculated. This calculation is done using Equations (3.33)–(3.64).

3.7.1 Parameters

To simulate this model, all parameters must be defined, which includes the left and right driver functions, or time-varying elastance. This definition of the driver function has been done in several ways in the past. The most accurate method of creating a function for the time-varying elastance is to measure it directly. Direct measurement is done by re-arranging Equation (3.19), such that:

$$e(t) = \frac{P + P_{peri} - P_{ed}}{E_{es}(V - V_d) - P_{ed}} \tag{3.67}$$

where P_{ed} is the lower bound, as defined Equation (3.17) and repeated here:

$$P_{ed} = P_0 \left(e^{\lambda(V - V_0)} - 1 \right) \tag{3.68}$$

In most cases, including this research, where the ventricle pressure and volume are measured, measurements are done with an open chest and thus $P_{peri} = 0$ by definition. It can also be assumed that P_{ed} is small in comparison to E_{es} and therefore neglected. These assumptions are discussed further in Section 3.8. This approach leaves the time-varying elastance defined as a function of the ventricle pressure and volume:

$$e(t) = \frac{P}{E_{es} \cdot V} \tag{3.69}$$

where

$$E_{es} = max \left(\frac{P}{V} \right) \tag{3.70}$$

However, this approach in Equations (3.67)–(3.70) requires the invasive measurement of pressure and volume in the left and right ventricles, which ultimately goes against the overall ethic of the model's clinical application, which is to avoid further invasiveness. There have been several approaches to address this problem and these are discussed in Chapter 4.

These approaches, although removing the need for invasive measurement of the ventricles, also removed much of the patient-specific energetic information present in the time-varying elastance. Hence, a patient-specific approach has been developed and published (Stevenson et al., 2012a,b), and is presented in Chapters 6 and 7. This

patient-specific approach creates an estimation for the time-varying elastance as defined in Equation (3.69).

3.7.2 Simulation example

An example simulation using healthy porcine data is given in Figure 3.8. This simulation was done using a measured time-varying elastance and a thoracic pressure of zero, $P_{th} = 0$. The goal is to show the basic simulation and resulting model outputs.

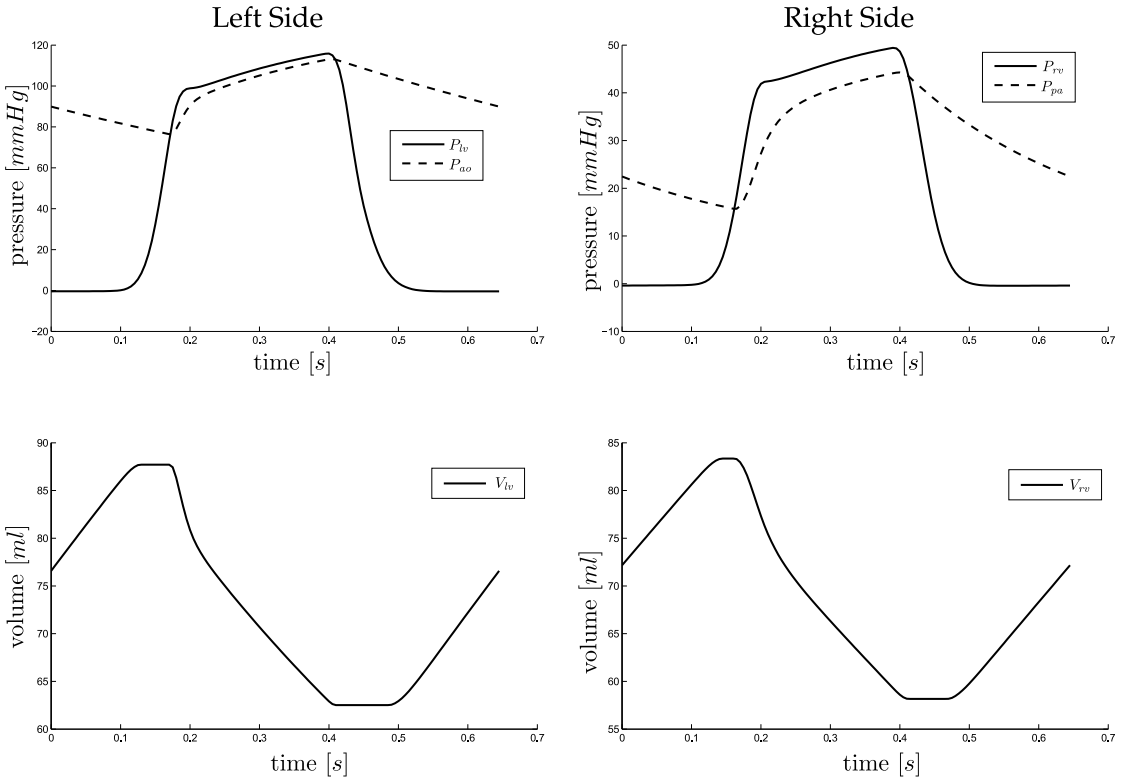

FIGURE 3.8: A single heart beat from a simulation of the model. The parameters were chosen to resemble a healthy porcine subject, with a measured time-varying elastance. Pressure in the ventricle and downstream vessel are shown for each side of the heart, including the ventricle volume.

3.8 Discussion

The model presented in this chapter is a lumped parameter model. As such, it does not relate exactly to physiology. Assumptions and simplifications were made to achieve a balance of complexity and accuracy.

3.8.1 Simplifications

Perhaps the biggest simplification is the representation of large sections of the circulation through discrete model chambers. These chambers appear, and are named, in the model as a single section, but physiologically and anatomically represent a much wider context. For example the aortic chamber represents the entire series of elastic arteries of the systemic circulation. Therefore, the associated model parameters are averages or averaged representations of this large section of the circulation.

Another simplification in this model is the lack of distinct chambers representing the atria. In general, the atria have only a small influence on the cardiovascular trends, and as such, the additional complexity required was considered unjustified. However, the effects of the atria are partially present in the current model, as they are lumped into the pulmonary vein and vena cava chambers. Work is ongoing in formulating the atria as separate identifiable chambers (Pironet et al., 2012; Pironet, 2011).

3.8.2 Assumptions

At a fluid dynamics level, there are a few assumptions made in the derivation of the model. To make the transition from fluid dynamics to electrical circuits, fluid flow was modelled assuming a Poiseuille profile. A Poiseuille flow profile represents an incompressible, Newtonian, laminar, fully developed flow through a rigid vessel of constant circular cross-section. To assume Poiseuille flow implies assumptions about the nature of blood and its containing vessels:

- Blood can be treated as incompressible (White, 1991).
- Blood is assumed to behave as a Newtonian fluid with constant viscosity (Fung, 1993). This cannot be said for flow in the capillaries but is reasonable in the larger vessels.
- Blood vessels are assumed to be rigid with a constant cross-sectional area. This is consistent with a Windkessel model where the combination of a rigid pipe and an elastic chamber capture the fluid dynamics and vessel compliance (Tsitlik et al., 1992; Melchior et al., 1992).

- Laminar, uni-directional, axi-symmetric flow is assumed throughout the circulation. Some turbulence will occur in places around the circulation, especially in proximity to the valves and bifurcations. However, this is assumed to be of negligible significance to the overall flow profile.
- The flow is assumed to be fully developed, and thus the velocity profile is constant along the length of the vessel (Fung, 1993).

These assumptions allow the formulation of a fluid dynamic system as a simple electrical circuit (Beyar et al., 1987; Burkhoff and Tyberg, 1993; Chung et al., 1997; Olansen et al., 2000; Smith et al., 2004), as shown in Section 3.2. However, these assumptions are all simplifications and approximations of the real situation and thus, to varying degrees, add error into the model. This is inherent to the nature of a minimally complex model, and thus cannot be avoided. Rather, error is minimised by making only justifiable and reasonable assumptions.

One of the more significant assumptions is that the flow is fully developed. Due to the pulsatile nature of blood flow in the larger vessels of the circulation, this is obviously false in these regions. Inertial effects, if included in the simulation with Equations (3.35)–(3.38), can compensate for this approximation. However, the effect of inertia can generally be regarded as insignificant, which is typically the case in many models.

The main parameters of the model, namely, elastance (E), resistance (R), and inductance (L) are assumed to be constant except for the ventricular elastances which vary in time. This assumption is a simplification of the real physiology. However, it does not introduce much error compared to measurement errors, and vastly reduces the complexity and computational cost for solving the model. Hence, the assumption of constant parameter values is common among lumped parameter models (Beyar et al., 1987; Olansen et al., 2000; Ursino, 1999; Wang et al., 2003).

As already mentioned, the effects of inertia are small. Therefore, the benefit of adding a time-dependency to the inertial parameters makes little sense. This set of parameters is also based mostly on the properties of the blood, whose changes are too slow to be captured by a single simulation of the model.

The parameter of resistance comes in two forms, valve resistance (R_{av}, R_{tc}, R_{pv} and R_{mt}), and peripheral resistance (R_{sys} and R_{pul}). Valve resistance has been suggested to be the most useful clinical index of valve function, as it represents more closely the functional impairment of the valve, than other indices such as valve area (Antonini-Canterin et al., 1999). Valve resistance has also been shown to be less dependant on flow (Antonini-Canterin et al., 1999; Ford et al., 1994; Casale et al., 1992; Blitz and Herrmann, 1996; Bermejo et al., 1996; Ford et al., 1990), although these findings have been questioned (Blais et al., 2001; Mascherbauer et al., 2004). Valve resistance is also easily combined with other haemodynamic calculations (Ford et al., 1994). Peripheral resistance can reasonably be assumed to be constant, as the flow and pressure through the capillaries is relatively steady over a single heartbeat.

The third constant parameter, elastance, must also be divided between venous and arterial elastance. For the venous system, the elastance has been shown to be constant over physiological ranges of venous pressure (Batzel and Bachar, 2010). Assuming arterial elastance to be constant is the largest simplification of all the parameters, as the aorta, in some capacity, actively pushes blood in a similar, though much weaker, manner to the ventricles, and it is widely accepted that the arterial elastance is non-linear with respect to pressure (Batzel and Bachar, 2010; Li et al., 1990; Westerhof et al., 2009). However, the effect of modelling this variable and patient- and condition-specific non-linearity has been shown to be of no measurable advantage in different Windkessel models (Fogliardi et al., 1996). Therefore, a constant arterial elastance can be justified.

3.8.3 Limitations

The lumped parameter nature of the model gives rise to some limitations on the accuracy and detail of the physiological dynamics that the model can capture. For example, the dicrotic notch in the aortic pressure waveform is not captured by the model, due to the lack of reflected pressure waveforms in the model. However, the model does capture all the major dynamics of the cardiovascular system that are important in managing and controlling cardiac dysfunction in a clinical setting.

The valves are modelled based on an 'open on pressure, close on flow' formulation, and inherently do not allow flow in the reverse direction. Therefore dysfunctions such as mitral (Paeme et al., 2011) and aortic regurgitation, which are the insufficient valvular

functions allowing some back flow, cannot be captured without modification to the model.

Other limitations arise from the assumptions made in the derivation of the model as discussed in Section 3.8.2.

3.9 Summary

This chapter has presented a lumped parameter cardiovascular model that is capable of representing the important properties and dynamics of the cardiovascular system in a healthy state as well as a range of pathological conditions. The model is a compromise between physiological accuracy and computational expense, and has been shown in two configurations, one accounting for inertia, the other neglecting inertial effects.

The model contains six elastic chambers representing portions of the circulatory system, two of which act as pumps. Resistances, inertial effects and valves are all included to capture the important dynamics of the cardiovascular system. Inter-ventricular coupling is also captured through the interaction of the two ventricular chambers, as well as the pressure effects from the respiratory system.

This model is the basis for the work done in the remaining chapters of this research.

Chapter 4

CVS Model Identification

Before the CVS model can be of clinical use, the model parameters must be identified to a specific patient's cardiovascular state using physiologically and clinically relevant model parameter values. This process, of parameter identification that matches the outputs of the model to measurements that are commonly available in a clinical setting, is presented in this chapter.

4.1 Introduction

This chapter presents a method for the identification of the parameters of the six-chamber model presented in Chapter 3, and shown here for clarity in Figure 4.1. This process results in a model whose outputs match a set of measured clinical data, and accurately represents the dynamics of the cardiovascular system from which the measurements were taken. Therefore, the identified model has potential for patient-specific diagnostic and treatment processes in a clinical environment.

To be useful in a clinical setting, the identification process must use only measurements that are generally available in the ICU. It should also be able to provide real-time feedback as well as additional and useful cardiovascular information that can be readily understood and used by clinical staff. Thus, the identified model should aggregate the measured data into a clear, physiological picture.

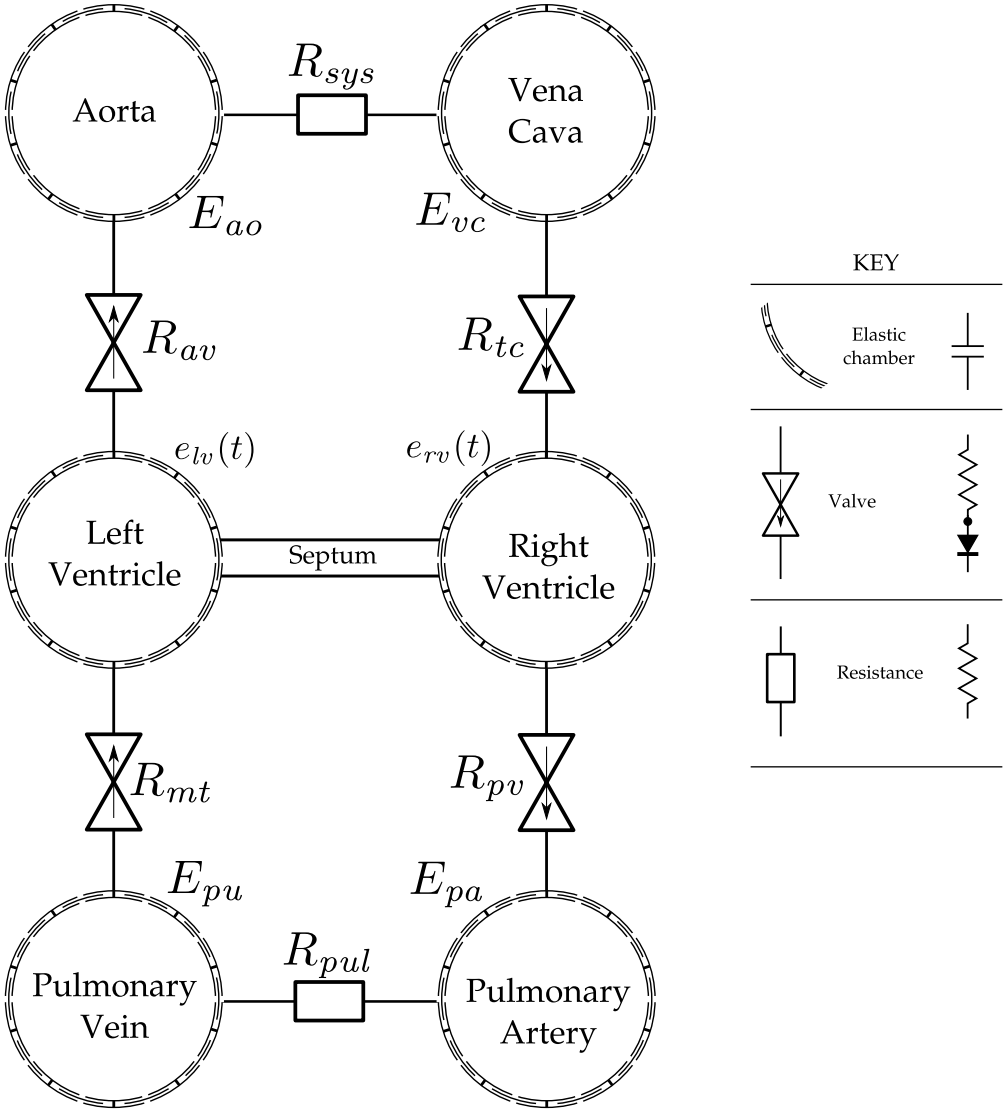

FIGURE 4.1: The full six-chamber model of the cardiovascular system as outlined in Chapter 3.

The identification algorithm presented in this chapter was based on a previously developed integral-based method (Starfinger, 2008; Starfinger et al., 2008b,a, 2007), and presented in more detail by Revie et al. (2011b). The previous method relied on knowledge of the left and right ventricular pressure and volume waveforms, limiting the real-time clinical usage of the model. The method presented here removes the dependency on ventricular waveforms, and thus uses only measurements commonly available in the ICU. These changes clear the way for the model's use in clinical applications. The measurements used include the aortic, pulmonary artery and central venous pressures, stroke volume, cardiac output, global end-diastolic volume, heart

rate and the timing of the mitral and tricuspid valve closures.

4.2 Pre-requisites

4.2.1 Identification Assumptions

As with the model itself, assumptions must be made to identify the model given the limited set of data that can be used in the identification process. This choice is an intentional limitation. However, because of how they are chosen, none of these assumptions are of great significance.

4.2.1.1 Steady state

The measured data is assumed to be at steady state. This choice allows for the further assumption that the left and right stroke volumes are equal. Assuming stroke volume equality is physiologically reasonable, because the heart generally maintains a balance of ejected blood as described by the Frank Starling mechanism.

4.2.1.2 Inertia is negligible

For simplicity, inertia in the model is neglected. This choice has very little impact on the output of the model (Smith et al., 2004), and significantly decreases the complexity of the model and the computational cost of simulation. Thus, it reduces the number of parameters to identify, and the computational cost of identification.

4.2.1.3 Valve timing

It is assumed that at the time the ventricle inlet valves close, the ventricle pressure is equal to the pressure directly upstream. This choice translates into:

$$P_{lv}(t_{mt}) \equiv P_{pu}\left(t_{mt}\right) \tag{4.1}$$

$$P_{rv}(t_{tc}) \equiv P_{vc}\left(t_{tc}\right) \tag{4.2}$$

This assumption makes sense for this model because the model neglects both atria (Smith et al., 2004; Starfinger et al., 2007). Hence, the pulmonary vein effectively connects directly to the ventricle, and, similarly, for the right side. Since inertia has been neglected, the valves close on a negative pressure gradient, as opposed to backward flow when inertia is included. Therefore, the mitral valve will close when the left ventricle pressure first increases above the pulmonary vein, which occurs momentarily after $P_{lv} = P_{pu}$ in the model.

4.2.1.4 Change in contractilities are proportional

To identify the contractilities of the left and right ventricles with the standard set of measurements in the ICU environment, some assumptions need to be made to give the required additional information. It is thus assumed that any inotropic effect acts equally to change cardiac contractility on both sides of the heart, resulting in the ratio of contractilities staying constant over time. This assumption enables the identification of the separate left and right ventricle contractilities in an ICU setting.

4.2.1.5 GEDV $\propto$ LVEDV + RVEDV

It is assumed that the global end-diastolic volume (GEDV) is proportional to the sum of the ventricle end-diastolic volumes. The GEDV that is measured in the ICU setting, which is usually found from thermodilution, would include the volume of the atria as well. However, this volume is minimal, as most of the atrial volume will have been ejected into the ventricles by the time of end-systole. Therefore, the major contributors to GEDV are the left ventricle end-diastolic volume (LVEDV) and the right ventricle end-diastolic volume (RVEDV) (Sakka et al., 2000), and thus the assumption made is reasonable for the way this value is used.

4.2.1.6 Valve resistances

It is assumed that the resistance of the valves does not change over short periods of time, which is physiologically reasonable. This assumption allows the identification of the model to run over several beats and eliminates spurious, non-clinically relevant variables.

4.2.1.7 Unidentified parameters

There are several parameters of the full model that have assumed values and are not identified. These variables include:

- $V_{0,lv} = V_{0,rv} = V_{0,ao} = V_{0,pa} = V_{0,vc} = V_{0,pa} = 0$
- $V_{d,lvf} = V_{d,rvf} = 23$ for swine (Desaive et al., 2008), and 0 for humans
- $P_{0,lvf} = P_{0,rvf} = 0$

The reason these parameters are left at the assumed values defined, is the lack of specific information from a typical ICU setting. This choice also results in the model focusing more on the physiologically and clinically important model parameters, ensuring they are identified in an accurate and robust manner relative to these assumptions.

4.2.2 Measured data in the ICU

As stated, the measurements on which the identification of the model is based, are restricted to those that can be readily accessed in a typical ICU setting. The measurements required include: arterial pressure (AP), central venous pressure (CVP), pulmonary artery pressure (PAP), heart rate (HR) mitral valve timing (t_{mt}), cardiac output (CO) and global end-diastolic volume (GEDV).

4.2.2.1 Arterial pressure

The actual measurement required by the model is aortic pressure (P_{ao}). However, the exact pressure is not usually available in the ICU. Instead, aortic pressure can be found from radial arterial pressure, which is normally available through one of several known methods (Westerhof et al., 2008; O'Rourke, 2004; Hope et al., 2004; Cloud et al., 2003; Pauca et al., 2001; Chen et al., 1997).

4.2.2.2 Pulmonary artery pressure

Pulmonary artery pressure, P_{pa}, as measured with a pulmonary artery catheter (PAC), is decreasingly common in a general ICU bed. However, it can be measured and is still

common practice in some ICUs. This is more common in specialised ICUs such as the cardiac ICU.

4.2.2.3 Central venous pressure (CVP)

Central venous pressure (CVP) is commonly available in the ICU as standard practice through a central line catheter. This pressure is then equivalent to the modelled vena cava pressure (P_{vc}).

4.2.2.4 Cardiac output and GEDV

Both cardiac output and global end-diastolic volume can be measured through thermodilution techniques (Michard et al., 2003; Sakka et al., 2000; Stetz et al., 1982; Ganz et al., 1971), which are commonly used in an ICU setting.

4.2.2.5 Heart rate

Electrocardiogram (ECG) is also a matter of standard practice in the ICU, and easily provides the heart rate and period, along with an estimate of the timing of the mitral and tricuspid valve closures.

4.3 Identification process

The identification process uses two key conceptual methods. First, the model is reduced in size and complexity to a point where individual parameters can be identified. These simplified models are then put back together to estimate the remaining parameters. This method greatly increases the robustness of the identification process. Second, each parameter is identified using a proportional feedback control approach to match a specific output measurement.

The whole process is inherently iterative. Initial values are established. Each sub-model is then run, updating the respective parameters. The ventricular contractility is then updated, after which the sub-models are put back together and the full six-chamber

model is run, to update the remaining two elastance parameters. In each successive update the parameters get closer to their true value. After all parameter values have settled, an identified solution is said to have been found.

4.3.1 Simplified models

The six-chamber model described in Chapter 3 is divided into two sub-models, one for the systemic circulation, the other for the pulmonary circulation. Each sub-model can stand on its own, but can also feed parameters to the other side during the iterative identification process. Each simplified model gets run in two steps. Each step identifies a subset of the parameters of that model. More detail about each of the models can be found in Sections 4.4.2 and 4.4.3. Both sub-models, systemic and pulmonary, are shown in Figure 4.2 in the context of the full six-chamber model, showing how the six-chamber model is broken up, and the communication between the two sub-models.

4.3.2 Proportional gain identification

Proportional gain is a robust and fast way to identify a parameter given that two assumptions apply. First, the parameter in question must be either directly or inversely proportional to a unique known measurement. This measurement becomes the surrogate error metric for the parameter, and thus must be related to its respective parameter. Second, each output metric can be used as a surrogate error by only one parameter.

Once a parameter has been linked with its own measurement, the ratio of the measured value to the modelled value (or its inverse) can be used to correct the current parameter value. In other words, the parameter is multiplied by a number proportional to its surrogate error. This approach is defined:

$$P_{n+1} = \frac{A}{B} \cdot P_n \tag{4.3}$$

where P_n is a parameter at iteration n, and the ratio of A to B is the ratio of the measured to modelled output metric or its inverse, depending on the relationship between the measured metric and the parameter. As A and B converge, $P_{n+1} \to P_n$.

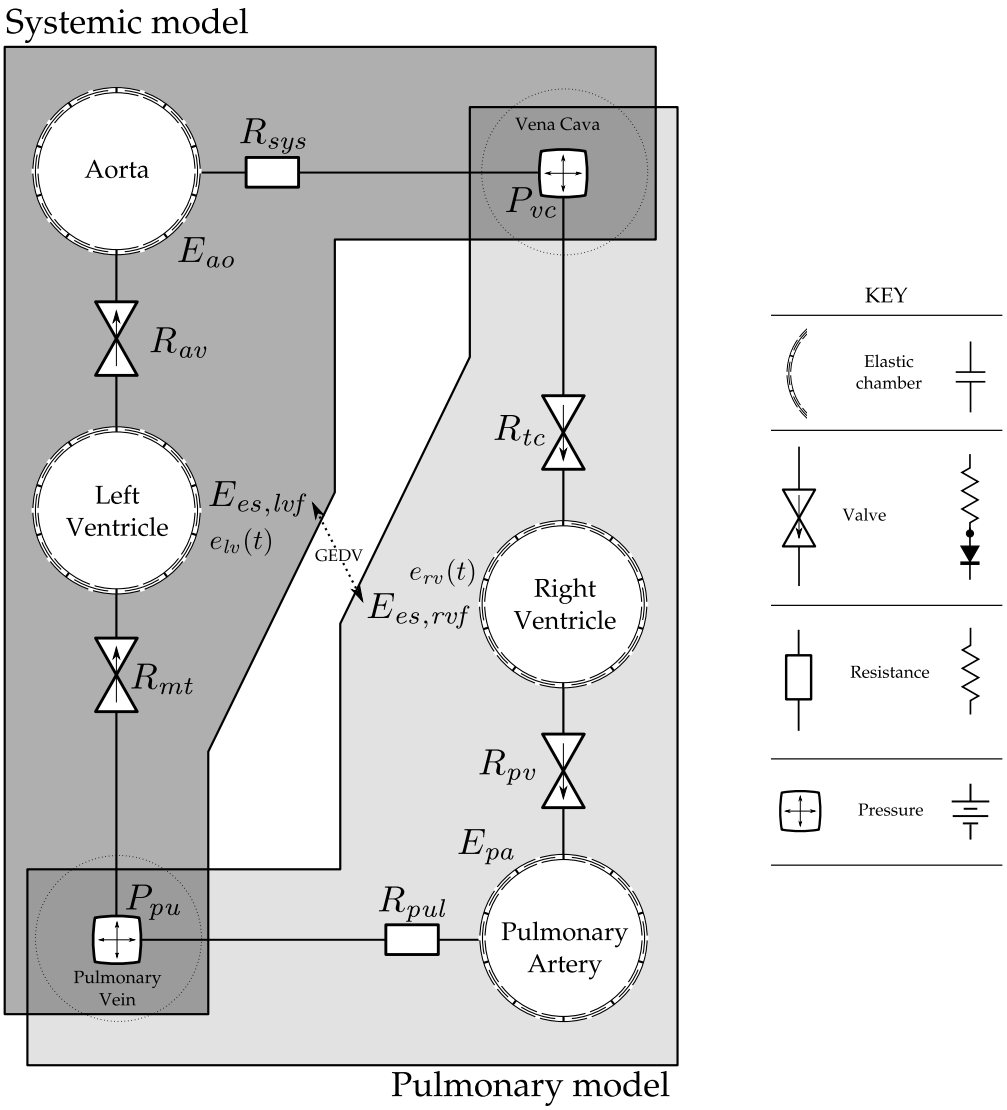

FIGURE 4.2: The model in pictorial form, split into two sub-models, the systemic and pulmonary models. Each sub-model has external bounds which overlap, namely the vena cava pressure (P_{vc}), and the pulmonary vein pressure (P_{pu}). These overlapping chambers are no longer elastic, and thus the two respective pressures are constant with respect to time. The two contractilities, $E_{es,lvf}$ and $E_{es,rvf}$ are also used to couple the models together. The parameters to be identified are shown, including the left and right time-varying elastances.

4.4 The identification

4.4.1 Pre-requisites

The process of identifying the model involves running the model, or simplified models, and using the output of that simulation to correct the parameters it was simulated

with. This approach means an initial simulation must be run with initial values for the parameters and input functions. Aside from parameters with assumed values, as defined in Section 4.2.1, the default parameter values are listed in Table 4.1.

The time-varying elastance (TVE) for the left, $e_{lv}(t)$, and right, $e_{rv}(t)$, ventricles must also be defined, as both simplified models require this input function. Due to the centrality of these functions to model output, it is critical that the time-varying elastance be known accurately. Every step of the identification process, except for the contractility, uses a model simulation involving one or both of these ventricular time-varying elastances. Therefore, any error in these functions will affect the whole process in a complex and undefined manner. This issue is discussed further in Section 4.5.

In particular, this need for accurate time-varying elastances was part of the motivation behind the development of algorithms that would accurately estimate the left and right time-varying elastances from available ICU metrics (Stevenson et al., 2012a,b). These algorithms are presented in Chapters 6 and 7.

TABLE 4.1: The parameters of the six-chamber model along with their initial values, surrogate errors and the sub-model in which they are used.

Parameter	Initial value	Surrogate error	Sub model
R_{mt}	0.05	left stroke volume	systemic (set 1)
R_{sys}	2.5	mean P_{ao}	systemic (set 1)
E_{ao}	2.5	P_{ao} pulse pressure	systemic (set 1)
R_{av}	0.04	$\max\left(\frac{d}{dt}\left(P_{ao}\right)\right)$	systemic (set 2)
R_{tc}	0.04	right stroke volume	pulmonary (set 1)
R_{pul}	0.4	mean P_{pa}	pulmonary (set 1)
E_{pa}	2.1	P_{pa} pulse pressure	pulmonary (set 1)
R_{pv}	0.03	$\max\left(\frac{d}{dt}\left(P_{pa}\right)\right)$	pulmonary (set 2)
$E_{es,lvf}$	2	–	ventricle
$E_{es,rvf}$	0.8	–	ventricle
P_{vc}	5	–	pulmonary & systemic
P_{pu}	5	–	pulmonary & systemic

4.4.2 Systemic sub-model identification

The systemic model is a little less than half of the full model, taking the systemic side of the circulation between the pulmonary vein and the vena cava. However, the two end points, the pulmonary vein and the vena cava, are no longer elastic chambers, but have constant pressures with respect to time. Thus, they become pseudo parameters for the sub-models. P_{pu} is identified by the systemic model, while P_{vc} is identified by the pulmonary model. Therefore, the systemic model is now a two-chamber model.

The first step in the identification process is to simulate this two-chamber systemic model with the required parameters from Table 4.1. The results of the simulation include, by definition, the surrogate errors associated with the model parameters. Thus, the sub-model parameters can be adjusted accordingly.

There are three points of iteration. First, the systemic ID set 1 is solved, followed by the systemic ID set 2. Since the parameters that are updated in set 2 affect the values of those updated in set 1, the whole process is repeated until all parameters are changed by less than 0.5 %. This process is illustrated in Figure 4.3

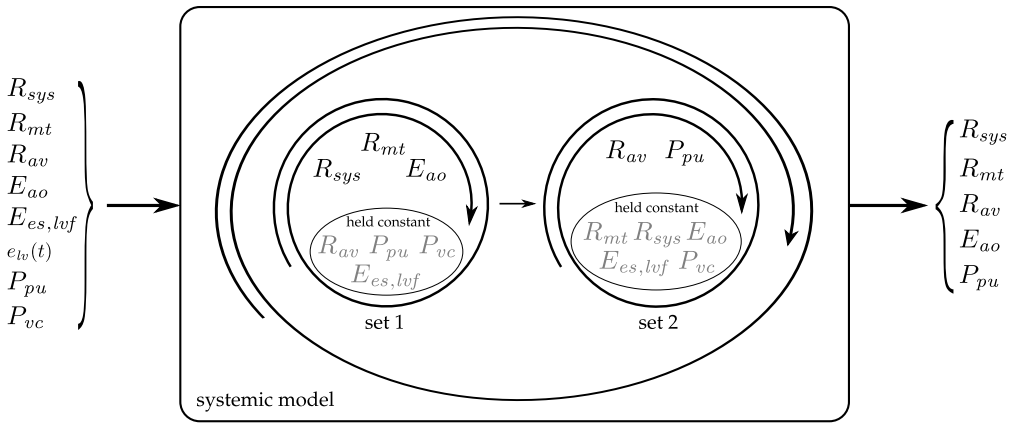

FIGURE 4.3: The identification of the systemic model with three points of iteration. The model is given seven parameter values and the time-varying elastance of the left ventricle, and returns five modified, and converged, parameter values.

4.4.2.1 Systemic ID iteration set 1: R_{mt}, R_{sys}, and E_{ao}

The first set of iterations focuses on the three sub-model parameters, R_{mt}, R_{sys}, and E_{ao}. All three are simultaneously adjusted after each simulation, while keeping all other

parameters constant. Once these values have converged to within 0.5 % this iteration set is said to have converged and the identification process moves on to the systemic ID set 2.

These three parameters were controlled at the end of each iteration by the following proportional control, defined:

$$R_{mt\,n+1} = \frac{SV_{lv,\,modelled}}{SV_{measured}} \cdot R_{mt\,n} \tag{4.4}$$

$$R_{sys\,n+1} = \frac{P_{ao,\,measured}}{P_{ao,\,modelled}} \cdot R_{sys\,n} \tag{4.5}$$

$$E_{ao\,n+1} = \frac{PP_{ao,\,measured}}{PP_{ao,\,modelled}} \cdot E_{ao\,n} \tag{4.6}$$

4.4.2.2 Systemic ID iteration set 2: R_{av}, and P_{pu}

The next step in the identification process is to find values for R_{av}, and P_{pu}. Both parameters depend on correct values from the previous iteration set, and thus are identified separately. The pulmonary vein pressure is assumed equal to the left ventricular pressure at the time the mitral valve closes. This assumption is reasonable given that when the mitral valve closes, isolating the ventricle from the pulmonary vein, the flow rate is zero and thus there should be no pressure drop across the valve. This point in time is defined:

$$P_{pu} = P_{lv}(t_{mt}) \tag{4.7}$$

As the pulmonary vein pressure is found as a function of the left ventricle pressure, it can be seen that the value of R_{mt} is required, as ultimately, the left ventricle pressure is a function of R_{mt} (see Section 3.6).

R_{av} must also be separated from the initial set, as its identification requires the correct stroke volume to be present. The adjustment to R_{av} is thus defined:

$$R_{av\,n+1} = \frac{\max\left(\frac{d}{dt}\left(P_{ao,\,modelled}\right)\right)}{\max\left(\frac{d}{dt}\left(P_{ao,\,meassured}\right)\right)} \cdot R_{av\,n} \tag{4.8}$$

4.4.3 Pulmonary sub-model identification

The pulmonary sub-model is the pulmonary equivalent of the systemic model, taking the other 'half' of the full model. In the same fashion as the systemic model, the two overlapping chambers — the vena cava and pulmonary vein — have constant pressures with respect to time. P_{vc} becomes a pseudo-parameter in the pulmonary model, while P_{pu} is taken as already identified by the systemic model, and thus held constant.

In an analogous process to the systemic model, the pulmonary model is broken into two parts to identify two different sets of parameters, and a similar iteration process takes place, as shown in Figure 4.4.

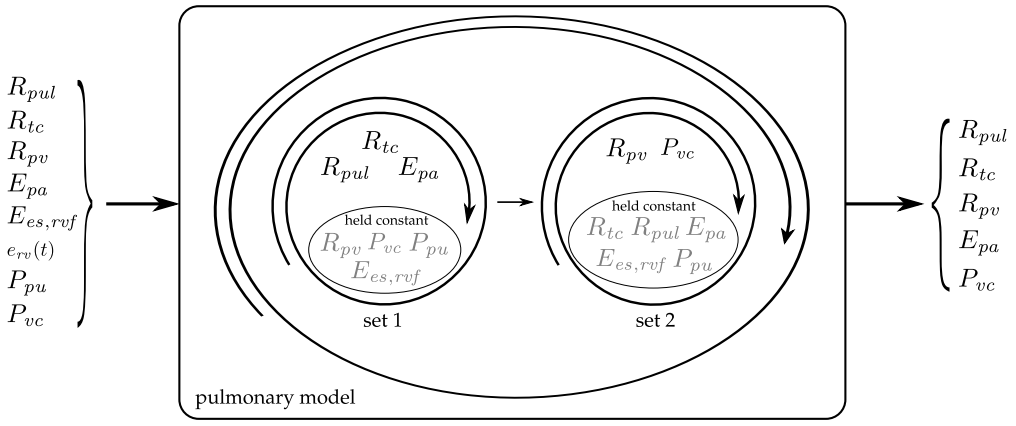

FIGURE 4.4: The identification of the pulmonary model with three points of iteration. The model is given seven parameter values and the time-varying elastance of the right ventricle, and returns five modified, and converged, parameter values.

4.4.3.1 Pulmonary ID iteration set 1: R_{tc}, R_{pul} and E_{pa}

In an equivalent manner to the systemic ID iteration set 1, two resistances and an elastance are identified simultaneously by the following proportional control, defined:

$$R_{tc_{n+1}} = \frac{SV_{rv,\,modelled}}{SV_{measured}} \cdot R_{tc_n} \tag{4.9}$$

$$R_{pul_{n+1}} = \frac{P_{pa,\,measured}}{P_{pa,\,modelled}} \cdot R_{pul_n} \tag{4.10}$$

$$E_{pa_{n+1}} = \frac{PP_{pa,\,measured}}{PP_{pa,\,modelled}} \cdot E_{pa_n} \tag{4.11}$$

4.4.3.2 Pulmonary ID iteration set 2: R_{pv} and P_{vc}

Once iteration set 1 has converged, the remaining resistance R_{pv} and pseudo-parameter P_{vc} can be found. Similar to the pulmonary vein pressure, the vena cava pressure is assumed to be equal to the right ventricle pressure at the time the tricuspid valve closes. Hence, it is defined:

$$P_{vc} = P_{rv}\left(t_{tc}\right) \tag{4.12}$$

The pulmonary valve resistance proportional control is then defined:

$$R_{vc_{n+1}} = \frac{\max\left(\frac{d}{dt}\left(P_{pa,\,modelled}\right)\right)}{\max\left(\frac{d}{dt}\left(P_{pa,\,meassured}\right)\right)} \cdot R_{vc_n} \tag{4.13}$$

4.4.4 Ventricle contractility

Ventricular contractility was identified in two steps. First, the sum of the left and right ventricular contractility, $E_{es,\,sum}$, was identified using GEDV as a surrogate error metric. GEDV can be measured through a thermodilution test, and modelled as the sum of the maximum volumes of the left and right ventricles. The proportional control is thus defined:

$$E_{es,\,sum_{n+1}} = \frac{GEDV_{modelled}}{GEDV_{measured}} \cdot E_{es,\,sum_n} \tag{4.14}$$

Second, the individual contractilities were split from the sum using a ratio of elastances that stays constant for each subject. This assumption requires that inotropic effects act equally on both sides of the heart. The ratio of contractilities is found through a correlation with the ratio of afterloads and modelled vena cava pressure (Anrep, 1912; Knowlton and Starling, 1912; Sarnoff and Mitchell, 1961), and is defined:

$$C_E = \frac{\overline{P_{ao}} - P_{vc}}{\overline{P_{ao}} - \overline{P_{pa}}} = \frac{E_{es,\,lvf}}{E_{es,\,lvf} + E_{es,\,rvf}} = \text{constant} \tag{4.15}$$

where a bar represents the mean.

The value of C_E is assumed to stay constant for each subject and is thus calculated as an average over a range of data for each subject, neglecting physiological outliers, $C_E < 0.6$, ensuring that the left ventricle has a greater contractility than the right

(Hosepud and Greenberg, 2007; Konstam et al., 1985). Using the subjects C_E, the left and right contractilities can be calculated from $E_{es,sum}$ as defined:

$$E_{es,lvf} = C_E \cdot E_{es,sum} \tag{4.16}$$

$$E_{es,rvf} = E_{es,sum} - E_{es,lvf} \tag{4.17}$$

Once the contractilities are updated, the identification can start from the beginning with the newly found values, potentially producing different maximum values for the left and right ventricular volumes, resulting in a different modelled GEDV. Thus, the iterative process continues until GEDV stabilises.

The six-chamber model includes more detailed ventricular interaction through the modelling of the ventricular septum, as shown in Figures 4.1 and 4.5. The systemic and pulmonary sub-models can also include this interaction, by the inclusion of non-zero values for V_{spt} and P_{pcd}. With identified values for the left and right ventricular contractility, values for V_{spt} and P_{pcd} can also be updated, as described by Equations (3.54) and (3.58).

4.4.5 Venous chambers

After the systemic and pulmonary sub-models have been identified and the ventricle contractility has been found, the only remaining parameters to the full six-chamber model are the elastance of the vena cava, E_{vc}, and pulmonary vein, E_{pu}, chambers. These two elastances, E_{vc} and E_{pu}, are identified using a five-chamber model, under the same proportional control method as the rest of the parameters. This five-chamber model is the full six-chamber model with the pulmonary vein pressure held constant at the value identified with the simplified models, and is shown in Figure 4.5.

E_{vc} is identified by matching the vena cava pressure output of the five-chamber model to that which was identified in the systemic model. Thus, P_{vc} becomes a surrogate error metric for E_{vc}. This proportional control is defined:

$$E_{vc_{n+1}} = \frac{P_{vc_{sm}}}{\text{mean}\left(P_{vc_{fm}}\right)} \cdot E_{vc_n} \tag{4.18}$$

where *sm* donates the systemic model and *fm*, the five chamber model.

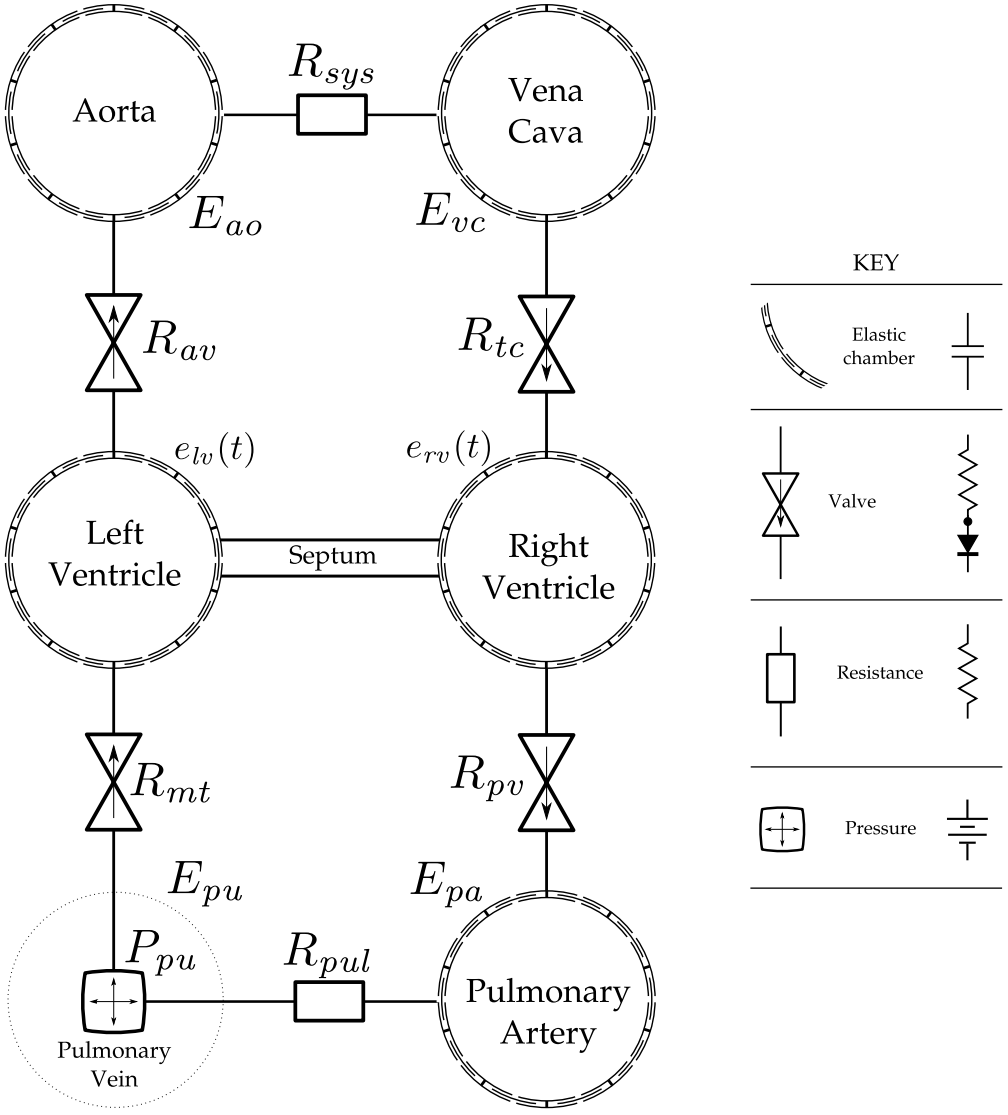

FIGURE 4.5: The modified version of the model that is used to identify the venous chamber elastances. This model is identical to the full six-chamber except for one aspect, the pulmonary vein pressure is held constant, turning the six-chamber model into a five chamber model.

This process is iterated until E_{vc} converges, after which the value of E_{pu} can be directly calculated. This approach is a result of a dependence of the pulmonary volume, V_{pu} on E_{vc}. Specifically, after E_{vc} has settled to the correct value, E_{pu} can be calculated from the constant pulmonary vein pressure and the pulmonary vein volume, using the relationship defined:

$$E_{pu} = \frac{P_{pu_{sm}}}{\text{mean}\left(V_{pu_{fm}}\right)} \tag{4.19}$$

4.4.6 Valve Resistance

Inter-beat variability in measured data can be a major problem in identification algorithms. This variability is a significant problem with this algorithm for the valve resistances, which are highly sensitive to small changes in the measured data. To reduce the sensitivity, the model was identified over a range of different measured beats, and, for each set, the valve resistances were stored and averaged. The whole identification process is then re-run, leaving out the identification of the now known and averaged resistances values.

Furthermore, the equations for P_{pu} and P_{vc} as functions of their respective ventricle pressures were replaced with proportional control, thus removing the dependence on the valve timing. This proportional control is defined:

$$P_{pu_{n+1}} = \frac{SV_{lv,\,modelled}}{SV_{measured}} \cdot P_{pu_n} \tag{4.20}$$

$$P_{vc_{n+1}} = \frac{SV_{rv,\,modelled}}{SV_{measured}} \cdot P_{vc_n} \tag{4.21}$$

4.4.7 Parameter bounds

To make the identification process more robust and physiologically meaningful, each parameter was constrained within bounds appropriate for that parameter. This constraining of values increases the stability of the model edge cases, and also ensures that the identified parameters have physiological relevance. These parameter bounds are listed in Table 4.2.

4.5 Time-varying elastance (TVE)

The time-varying elastance is a central part of the six-chamber model that is presented in Chapter 3 and identified in the current chapter. Physiologically, the time-varying elastance represents the activation of the myocardial muscle, and is intrinsically linked with the energetics of the heart (Suga, 1990b). In both the model and physiological context, the time-varying elastance is a key component of much of the cardiovascular dynamics, in value, timing and shape. This function is what drives the model. Therefore,

TABLE 4.2: The allowable range of values for the parameters of the six-chamber model. Each parameter is restricted in the identification to be within this range, to insure the parameters are physiologically meaningful.

Parameter	Allowed parameter range
R_{mt}	0.005 – 0.5
R_{sys}	0.1 – 10
E_{ao}	0.1 – 10
R_{av}	0.005 – 0.5
R_{tc}	0.005 – 0.5
R_{pul}	0.05 – 10
E_{pa}	0.1 – 10
R_{pv}	0.005 – 0.5
$E_{es,lvf}$	0.1 – 10
$E_{es,rvf}$	0.1 – 10
P_{vc}	0.1 – minimum of 15 and $(\min(P_{ao,measured}) - 2)$
P_{pu}	1 – minimum of 15 and $\left(\min\left(P_{pa,measured}\right) - 2\right)$

it is critical to get an accurate representation of the time-varying elastance to get meaningful results from the model and the identified parameters. More detail and physiological context about the time-varying elastance is given in Chapter 5.

There are two important effects of time-varying elastance on the six-chamber model, which occur in simulation and identification. As already stated, simulation of the model requires accurate time-varying elastances. However, the identification process also relies heavily on these functions. In every step, except the identification of the contractility, the model (or a simplified version of the model) is simulated. This use of simulation only compounds the sensitivity of the model to the time-varying elastance, as the parameters along with the model simulation are functions of the time-varying elastance.

The interactions between the time-varying elastance and the modelled outputs for any simulation are too complex to attempt to quantify. This issue becomes more problematic when the identification process is included. However, what can be shown is that the

time-varying elastance is important. This importance is most clearly demonstrated through visually comparing the results of simulations with different time-varying elastances. From these results the impact on the identification process can be inferred.

4.5.1 The input waveforms

To show the sensitivity of the model simulation to the time-varying simulation, six different waveforms were used as inputs to the model, with varied shapes to give a range of model responses. These waveforms are shown in Figure 4.6. For simplicity, only the left ventricle time-varying elastances are shown.

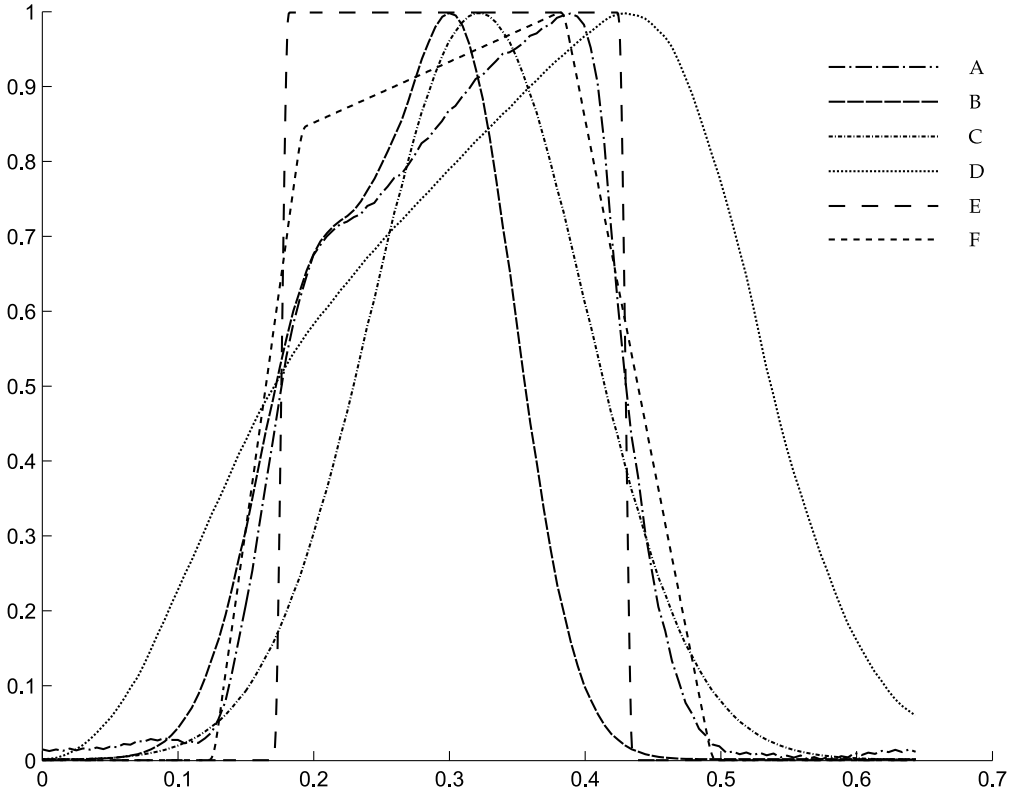

FIGURE 4.6: Six different time-varying elastances. **A**: The measured time-varying elastance, **B**: the time-varying elastance constructed as a sum of Gaussian terms (Chung et al., 1997; Starfinger, 2008), **C**: the time-varying elastance used in the original implementation of the model (Smith, 2004), **D**: a 'universal' time-varying elastance (Suga et al., 1973), **E**: square wave, with smoothed corners, **F**: a piecewise linear, five-segment representation of the time-varying elastance, also with smoothed corners.

4.5.1.1 Waveform A — measured

The first of these waveforms is simply the time-varying elastance computed from the measured data, which is used as the baseline standard for output comparison. This waveform should, by definition, give the best output results. This waveform is defined:

$$e(t) = \frac{\frac{P_v}{V_v}}{\max\left(\frac{P_v}{V_v}\right)} \tag{4.22}$$

4.5.1.2 Waveform B — previous CVS model

This waveform is implemented as a sum of Gaussian terms (Chung et al., 1997), and was used as the best global time-varying elastance before a patient-specific time-varying elastance could be estimated (Starfinger, 2008). This waveform mimics the shape of the measured time-varying elastance, but differs significantly in timing. The equation is defined:

$$e(t) = \sum_{i=1}^{3} A_i \cdot e^{-B_i(t-C_i)^2} \tag{4.23}$$

where the parameters are listed in Table 4.3.

TABLE 4.3: The parameters used for Equation (4.23).

Parameter	$i = 1$	$i = 2$	$i = 3$
A_i	0.9556	0.6249	0.018
B_i	255.4	225.3	4225.0
C_i	0.3060	0.2026	0.2491

4.5.1.3 Waveform C — original CVS model

This waveform is the time-varying elastance used in the origin model definition (Smith, 2004) as a global waveform for both ventricles. This function is a horizontally symmetrical exponential waveform and is defined:

$$e(t) = e^{-80\cdot\left(t-\frac{period}{2}\right)^2} \tag{4.24}$$

4.5.1.4 Waveform D — universal

When the time-varying elastance was initially conceived, it was thought that every time-varying elastance had the same normalised shape (Suga et al., 1973). This shape, as published by Suga et al. (1973), is waveform **D**.

4.5.1.5 Waveform E — square

This waveform is included, not as a realistic time-varying elastance, but as a test of the limitations of the model to extreme time-varying elastance slopes. This waveform is implemented by rounding the measured time-varying elastance to 1 or 0, and smoothing the corners to avoid discontinuities.

4.5.1.6 Waveform F — linear piecewise

This waveform is a simple linear piecewise representation of the time-varying elastance mimicking the basic shape. The waveform was lightly smoothed to avoid discontinuities at the corners.

4.5.2 Model responses to different TVE waveforms

To see the sensitivity of the model to the time-varying elastance, three outputs of the model are shown, the left ventricle pressure, P_{lv}, the aortic pressure, P_{ao} and the pulmonary vein pressure, P_{pu}.

Figure 4.7 shows the left ventricle pressure for each of the time-varying elastances in Figure 4.6. It is clear from the aortic pressure of the model that the time-varying elastance plays a significant role in many aspects of the aortic pressure waveform, including the shape, height and timing. It should be noted, that no other time-varying elastance comes close to matching the output from the measured time-varying elastance of waveform A. The universal time-varying elastance (Suga et al., 1973) significantly underestimates the peak pressure of the left ventricle, where the square wave significantly overestimates it. The key difference here is the slope of the rising

edge of the time-varying elastance. Note also that the shape and timing of the left ventricle pressure closely follow that of the time-varying elastance.

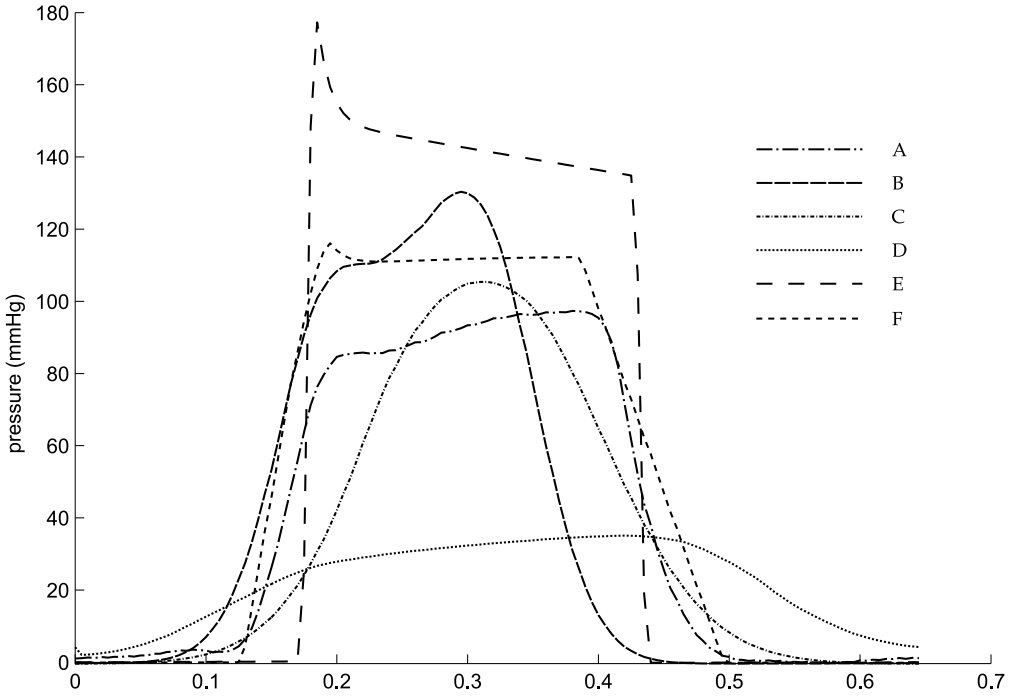

FIGURE 4.7: The left ventricle pressure output of the model using the six different time-varying elastances of Figure 4.6.

Figure 4.8 shows the aortic pressure output of the model. Similar to the left ventricle pressure shown in Figure 4.7, the aortic pressure is sensitive to height, shape and timing of the time-varying elastance.

The pulmonary vein pressure, shown in Figure 4.9, shows some sensitivity to the different time-varying elastances. However, in this case the percentage change in the output of the model is much smaller than either the left ventricle pressure or the aortic pressure.

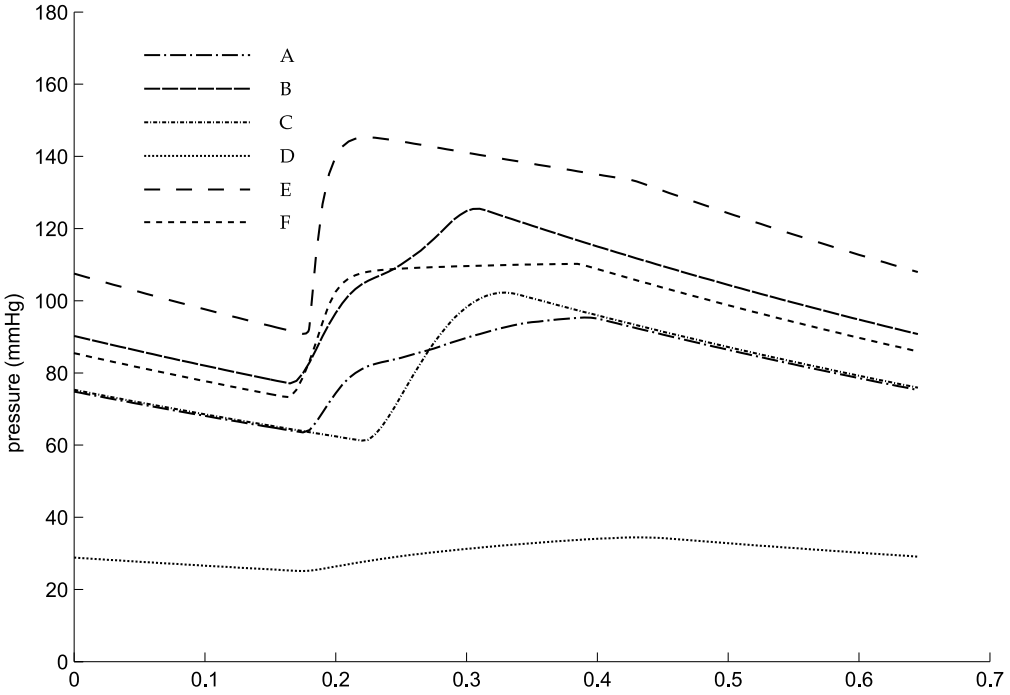

FIGURE 4.8: The aortic pressure output of the model using the six different time-varying elastances of Figure 4.6.

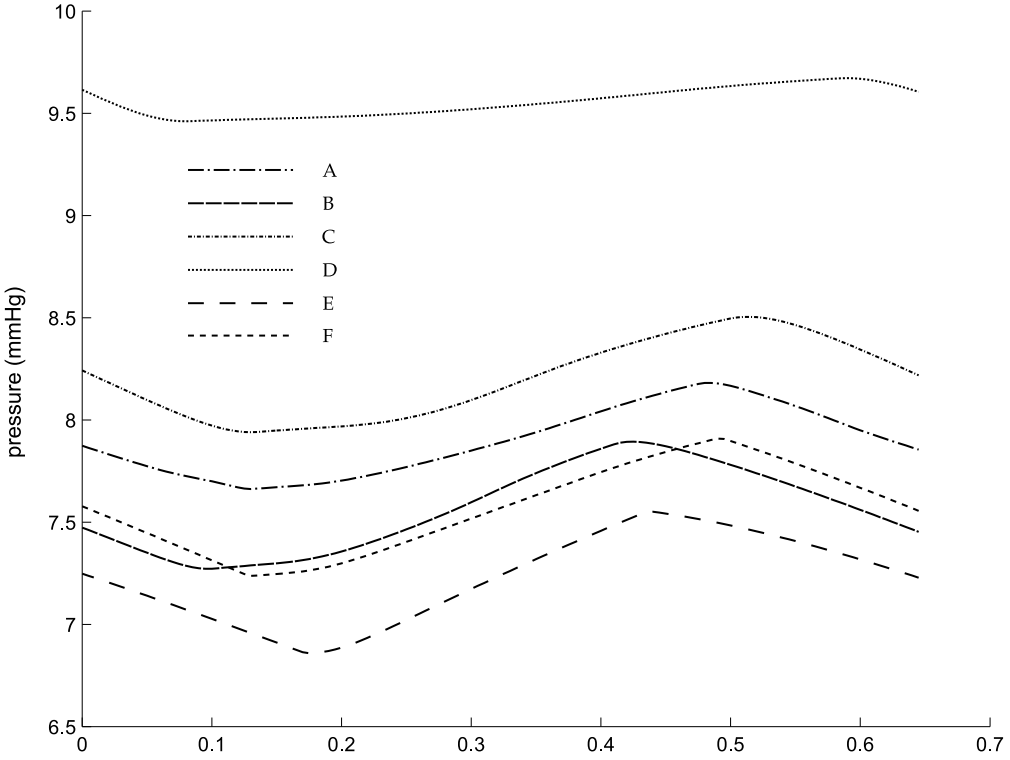

FIGURE 4.9: The pulmonary vein pressure output of the model using the six different time-varying elastances of Figure 4.9.

4.6 Discussion

4.6.1 Parameter identification limitations

A significant limitation on the identification algorithm outlined in this chapter is its reliance on the pulmonary artery pressure, P_{pa} which, when measured, is usually done with a pulmonary artery catheter (PAC). The use of a PAC is not as common as formerly (Johnston et al., 2008; Wiener and Welch, 2007), perhaps due to the questionable or negative effects its use has had on mortality rates (Binanay et al., 2005; Shah et al., 2005). However, it is most likely that the value of the PAC has more to do with the interpretation of the resulting waveforms than the presence of the catheter itself (Shah et al., 2005). Any catheterisation comes with added risk. However, the additional risks of a PAC are regarded as small (Berenholtz et al., 2004; Johnston et al., 2008; Mermel, 1991; Ramritu et al., 2008; Safdar et al., 2002; Weil, 1998). Therefore, with the correct understanding of the data acquired from a PAC, the clinical advantages can be realised. There are many features of the pulmonary artery pressure waveform that can be of clinical use if extracted correctly from the waveform. These metrics include, ventricular contractility, preload, vascular stiffness and resistance. Therefore there is a strong case for the use of a PAC when combined with modelling techniques such as those outlined by the model presented here.

It should also be noted that the identification method could be reformulated to use measurements from echocardiography to eliminate the use of a PAC. However, this approach would significantly reduce the frequency of identification and thus the use of the model, and increase the financial cost. Specifically, echocardiography is not real-time and involves significant clinical effort.

One more limitation of the identification algorithm is the assumption that $V_{d,lvf} = V_{d,rvf} = 0$. In most cases the true values would be non-zero, but are currently unrealistic to measure or identify. The result of this assumption is a slightly different definition of the ventricular contractility from the accepted gold standard (Suga et al., 1973; Sagawa et al., 1977). Thus, the absolute values of $E_{es,lvf}$ and $E_{es,rvf}$ as identified by the model will not match this gold standard. However, due to the lumped parameter nature of the model, and given that physiological values of the dead space volume stay relatively constant, the identified trends in the contractility will track those of the originally

defined gold standard contractility. Hence, the original assumption does not impact on the clinical use.

4.6.2 Sensitivity to the time-varying elastance

It has been shown that the correct time-varying elastance waveform is of critical importance to the simulation of the model in Figures 4.7–4.9, and thus also, the identification, as both rely heavily on model simulation involving the time-varying elastance. Even though it is not realistic to fully quantify the exact sensitivity of the model to the time-varying elastance, or attempt to state, in any meaningful way, the interaction between the model outputs and the time-varying elastance, the simulations with different time-varying elastance in Figures 4.7–4.9 give clear visual illustrations of the sensitivity.

Ultimately, the best result for the model and its identification would be to measure the patient-specific time-varying elastance. Currently, this measurement is not achievable in a clinical setting due to the invasiveness of the procedures required. However, a patient-specific estimation of the time-varying elastance is possible and is presented and discussed in Chapters 6 and 7, as a main outcome of this thesis.

4.7 Summary

This chapter has presented an algorithm for identifying the parameters of the six-chamber model described in Chapter 3. The method uses only measurements that are commonly available in an ICU setting, and provides a robust way to obtain a model that accurately mimics the major haemodynamics of a patient. It has also been demonstrated that an accurate time-varying elastance is required for the simulation of the model and thus, in addition, its identification.

Chapter 5

Time-Varying Elastance

This chapter outlines the development of the time-varying elastance concept, from its initial conception to its current usage and implications. Three major aspects of the time-varying elastance model are discussed, namely the index of contractility, the total mechanical energy of the contracting ventricles, and its usage in lumped parameter models of the cardiovascular system.

5.1 Introduction

The time-varying elastance concept is an elegant and simple approach to representing the contraction of the myocardium. The time-varying elastance model is a high level approach to mathematically represent the dynamics of a ventricle. As such, it does not directly account for the mechanics of contraction. However, it has had much success in several areas (Cooper, 1990; Suga, 1990b), including the derivation of the total mechanical energy of the heart, which to some is a surprising result that seems to go deeper into the mechanics of the ventricle than the conceptual model would allow (Cooper, 1990).

Certain aspects of time-varying elastance concept have had much debate in the literature. These include the linearity and load-independence of the end-systole pressure-volume relationship (Burkhoff et al., 1987; Kass et al., 1989; Baan and Velde, 1988; Burkhoff et al., 1993; Oommen et al., 2003; Mirsky et al., 1987; Su and Crozatier, 1989; Velde et al., 1991; Noda et al., 1993; Kameyama et al., 1998; Lee et al., 1998), along with the universality of

the height and time-to-end-systole normalised time-varying elastance waveform (Jegger et al., 2007; Palmer et al., 2004; Kjorstad et al., 2002). Much of this debate focuses on what is within physiological range, and what can be deemed an appropriate approximation for the context of the model under question. What appears to be generally accepted is the success of the conceptual model both in providing information regarding ventricular energetics and as an input to larger lumped parameter models of the cardiovascular system. As such, the model has taken a firm hold in the physiological understanding of the cardiovascular system.

5.2 Historic context

Metabolic cost of contraction has been studied for many years, with initial studies in the mid 19^{th} century linking chemical change and heat production to muscle contraction (Helmholtz, 1845, 1848). This understanding was further formalised, and a relation was recognised between tension generation and oxygen consumption (Evans and Matsuoka, 1915; Rohde, 1912), with developed tension shown to be a major determinant of left ventricular oxygen consumption (McDonald et al., 1966; Neely et al., 1967; Rodbard et al., 1964; Sarnoff et al., 1958; Weber and Janicki, 1977). The understanding that the metabolic cost of the cardiac contraction can be described in terms of oxygen consumption (Challoner, 1968) was a major step forward in the understanding of the energetic cost of contraction. From this background, Sonnenblick (1962) established a widely used index of contractility, V_{max}, representing the maximum unloaded shortening velocity of the myocardium (Karliner et al., 1971).

A parallel movement to conceptualise the energetics of the heart focused on the fluid dynamic aspects of cardiac function. This line of study was pioneered by the German physiologist Otto Frank who characterised ventricular contraction in a pressure-volume diagram (Frank, 1899; Sagawa et al., 1990). The British physiologist Ernest Starling, extended the work done by Frank on frog hearts, to canine preparations, and developed a relationship between cardiac output and filling pressure, known as Starling's law of the heart (Starling, 1918). Sarnoff and Berglund (1954) later modified Starling's curve to develop a ventricular function curve (Sarnoff and Berglund, 1954) which, together, were used to visualise inotropism and contractility changes.

Discontented with Sonnenblick's concept of a contractility index, V_{max}, Suga et al. (1973), established the long standing (and still current) index of contractility based on a model of the elastance of the ventricular muscle, namely, E_{max} (Suga et al., 1973). Suga and Sagawa (1974) then followed with a wealth of publications embedding E_{max} in clinical usage, and formalising the time-varying elastance model of cardiac dynamics (Warner, 1959; Suga and Sagawa, 1974). Further works linked the fluid dynamic concept of the pressure-volume construction to the metabolic cost represented by oxygen consumption (Suga, 1969b, 1970).

5.3 Maximal elastance, time-varying elastance and the pressure-volume diagram

The time-varying elastance model is a broad concept that has been used in many ways. The most prominent include the index of contractility, E_{max}, the measure of total mechanical energy as the area inside the pressure-volume diagram, and as part of lumped parameter cardiovascular models. The first of these, E_{max} – the line connecting the points of end-systole on the pressure-volume diagram – was suggested to be essentially linear and proportional to contractility (Suga, 1970, 1969a,b, 1971a,b). Suga and Sagawa (1972) concluded that the left ventricle performance could be characterised by a time-varying elastance, $E(t)$ (Suga and Sagawa, 1972), and showed that when normalised to height and time-to-end-systole, the time-varying elastance was independent of loading conditions (Suga et al., 1973; Suga and Sagawa, 1974). These key findings have stayed central to the understanding of cardiac energetics both in cardiovascular research and clinical practice (Hall and Guyton, 2011; Westerhof et al., 2010; Burkhoff, 2009; Campbell et al., 2008).

5.3.1 Maximal elastance, E_{max}

The concept of using E_{max} as a measure of contractility came from empirical studies done by Suga et al. in the late 1960s and early 1970s. These studies showed a remarkably linear relationship between end-systolic pressure and volume, with the slope being insensitive to loading conditions and type of contraction, as well as being sensitive to

the contractile state (Suga et al., 1973; Suga and Sagawa, 1974). Figure 5.1 illustrates the general concept of E_{max} and how it changes with a change in the contractile state.

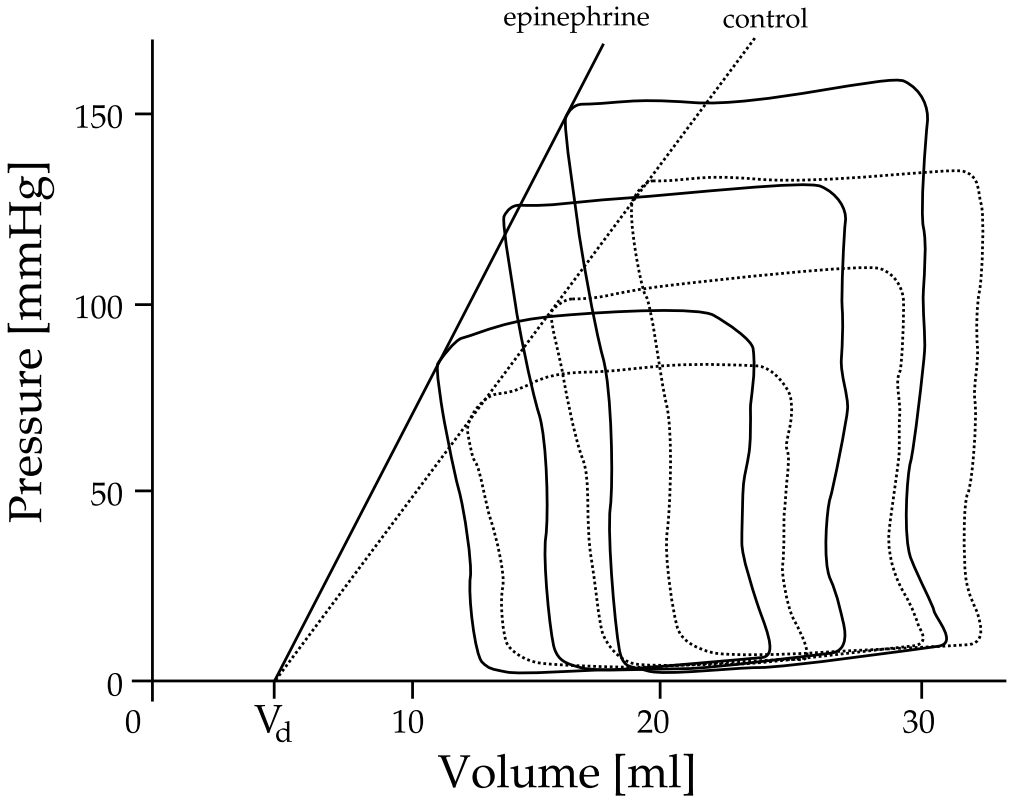

FIGURE 5.1: Left ventricular pressure-volume loops of a denervated heart, adapted from (Suga et al., 1973). The arterial pressure was fixed at three different levels, for each of a control state and an enhanced contractile state.

Despite the controversy about the load-independence and linearity of E_{max} (Burkhoff et al., 1987; Kass et al., 1989; Baan and Velde, 1988; Burkhoff et al., 1993; Oommen et al., 2003; Mirsky et al., 1987; Su and Crozatier, 1989; Velde et al., 1991; Noda et al., 1993; Kameyama et al., 1998; Lee et al., 1998), it is generally acknowledged to be basically linear and load-independent within the physiological range (Kind et al., 2009; Noda et al., 1993; Brinke et al., 2010). This acceptance is evidenced by its extensive use, which, in most cases, depends on its linearity and load-independence. Although it has gained widespread acceptance as being a good measure of contractility (Sagawa, 1981; Kass, 1992; Takaoka et al., 1993; Senzaki et al., 1996; Shishido et al., 2000), E_{max} has had limited uptake in clinical environments due to the relative difficulty of measuring it in a clinical setting (Shishido et al., 2000; Brinke et al., 2010).

The most common and reliable way to measure E_{max} is by recording multiple cardiac pressure-volume loops over a range of volumes, usually through reducing preload via an inferior vena cava occlusion (Kass, 1992). Although feasible, this method is invasive and therefore inappropriate for patients with advanced heart failure. Many attempts have been made to estimate E_{max}, and, in so doing, give more accessibility to the index in a clinical setting. The majority of attempts have focused on reducing the need for the vena cava occlusion manoeuvre, by requiring only a single PV loop (Klotz et al., 2006; Takeuchi et al., 1991; Senzaki et al., 1996; Shih et al., 1997; Shishido et al., 2000; Kjorstad et al., 2002).

E_{max} fits into a bigger modelling picture as the maximum elastance of the time-varying elastance concept. However, E_{max} as a measure of contractility, can be derived, as originally, from the end-systolic pressure-volume relationship. E_{max} is the most sought-after metric from the time-varying elastance concept, due to its clinical significance. Thus, it is used extensively in animal research and increasingly as a clinical tool to gauge cardiac pump function (Westerhof et al., 2010).

Another extension of the E_{max} concept is the value of the dead space volume V_d (Suga et al., 1973), which is the volume intercept of ESPVR. It is generally assumed that ESPVR is linear, and thus V_d is found as an extrapolation of ESPVR. However, ESPVR is non-linear (Claessens et al., 2006), and the non-linearity depends on the contractility (Sato et al., 1998). Therefore, for higher contractilities, V_d will be underestimated, often significantly (Westerhof et al., 2010) using a linear assumption. For this reason, an accurate V_d can be very hard to obtain in a clinical setting, not to mention the invasive nature of the required measurements.

5.3.2 Time-varying elastance (TVE)

Although the use of compliance, or its inverse, elastance, was not new (Warner, 1959), Suga et al. (1973) formalised the concept of a time-varying elastance to characterise the fluid dynamics of the left ventricle. This resulted from the observation that the relationship between pressure and volume in the left ventricle could be accurately approximated by (Suga et al., 1973):

$$P(t) = E(t) \cdot (V(t) - V_d) \tag{5.1}$$

where $P(t)$ is the instantaneous intraventricular pressure, $E(t)$ is the time-varying slope coefficient of the regression line of pressure and volume, $V(t)$ is the instantaneous intraventricular volume, and V_d is the volume at zero pressure (dead space volume), defined, at the time, as the fixed correction volume.

From this observation the pressure-volume regression line $E(t)$ can be constructed in its own right, and given the name time-varying elastance. The dead space volume was assumed constant, although in reality its value decreases with time in the early phase of systole (Sagawa, 1978), remaining virtually constant from around 80 ms onwards. Thus, the value of V_d was typically taken as constant with the end-systolic value (Sagawa, 1978).

Figure 5.2 shows a pressure-volume diagram with isochrone regression lines at specific points all connected to the dead space volume, V_d, with these time points also shown on the time-varying elastance curve. The slopes of these lines, when continuously connected around the entire PV loop, construct $E(t)$.

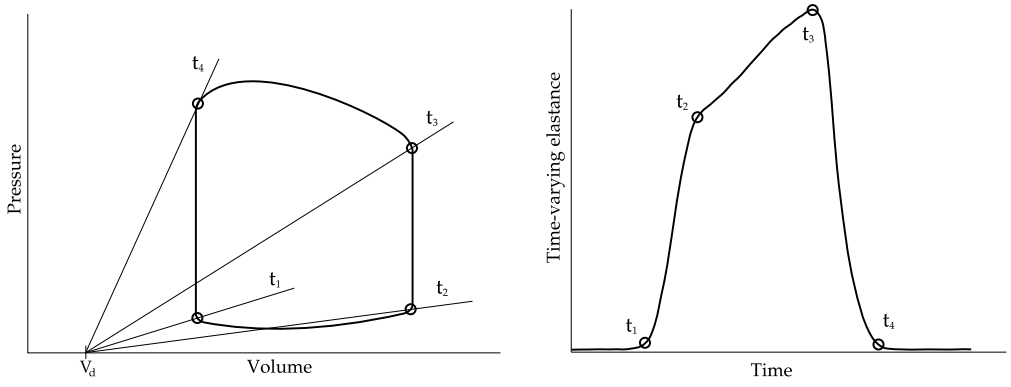

FIGURE 5.2: Isochrone regression lines at times, t_0, t_1, t_2 and t_4, all connected to the dead space volume, V_d (left), and the equivalent time points on the time-varying elastance curve (right).

The curve $E(t)$ that Suga et al. (1973) produced, was a by-product of the goal to conceptualise and visualise the contractility and energetics of the heart. The concept of E_{max}, which was developed first, was extended to cover the entire systolic phase, and, eventually the entire cardiac cycle, even though the authors noted that the equation for $E(t)$ – Equation (5.1) rearranged for $E(t)$ – was not valid for diastole (Sagawa, 1978). Therefore, E_{max} and the total mechanical energy concept of pressure-volume area (PVA) were the main focus of most of their research (Suga, 1990b). The concept of the

time-varying elastance was thus left as a foundation for properties such as E_{max} and PVA. As a result the intrinsic properties of the time-varying elastance, as a waveform, for diagnostic and clinical potential were largely neglected.

Comparison of time and value normalised $E(t)$ curves, $E^n(t^n)$, obtained under different contractile conditions, showed similar shapes. This result led Suga et al. (1973) to the conclusion that E_{max}, the maximum value of $E(t)$, and T_{max}, the time to E_{max}, could be considered the characteristic parameters of the instantaneous pressure-volume ratio curve (Suga et al., 1973). In other words, the time-varying elastance was largely independent of loading conditions and mode of contraction, at least during systole.

The model represented by Equation (5.1) is a one-element time-varying elastance model, equivalent to a circuit consisting of a single variable capacitor connected to a load, as shown in Figure 5.3. Other models exist, such as a two- and three-element model, that attempt to account for additional pressure loss and a constant portion of elastance (Zhong et al., 2005). However, the two- and three-element models have not received as much attention in the literature, likely due to added complexity and limited quality data to justify them.

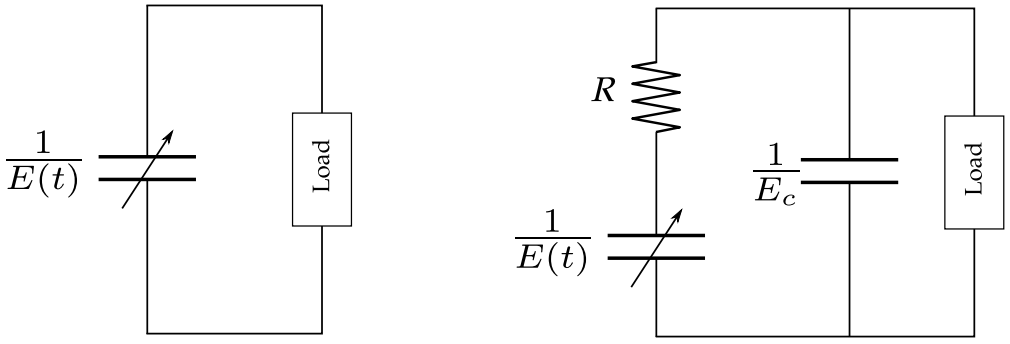

FIGURE 5.3: A one (left) and three (right) element time-varying elastance model. The load, when applied to the cardiovascular context, is the arterial load.

Since the initial conception of the one element model, there have been many attempts to improve the model, primarily in recognition that the left ventricular pressure is dependant on flow and thus the loading conditions (Hunter et al., 1979, 1983; Shroff et al., 1985; Templeton et al., 1972; Vaartjes and Boom, 1987). This issue is especially valid during ejection and relaxation (Campbell et al., 2008). In fact, the first such

model improvement came from the original authors (Suga et al., 1980), extending the one-element model to a three-element model shown in Figure 5.3.

Shroff et al. (1983) developed a more involved model, containing elastance, resistance and inductance, all three of which depend on time, pressure, volume, flow and flow acceleration (Shroff et al., 1983). Inertia was found to be negligible, while the resistance helped adjust for the known pressure errors in the previous one-element model (Suga et al., 1980). Viscous and passive elastic elements have also been added to the original time-varying elastance concept (Hunter et al., 1983). Wijkstra and Boom (1991) revamped the three element model (Suga et al., 1980), with a similar motivation leading to the introduction of flow dependence into the model (Wijkstra and Boom, 1991). Finally, the addition of a second, stiffer series elastance was shown to better predict lag in the ventricle pressure drop after a stepwise increase in ejection flow (Covell et al., 1975; Schiereck and Boom, 1978; Templeton et al., 1972; Vaartjes and Boom, 1987; Yasumura et al., 1989b).

Models are still being developed with similar attention to flow and load dependence. Zhong et al. (2005) uses a passive and active elastance model (Zhong et al., 2005) to account for a filling resistance, while Kind et al. (2009) showed a load-dependence on the time course of contraction and cardiac timing (Kind et al., 2009). This load dependence was based on observations in rats (Lee et al., 1998), mice (Claessens et al., 2006), and dogs (Burkhoff et al., 1987; Kass et al., 1989; Velde et al., 1991) that isochrones and the ESPVR are generally non-linear and that their non-linearity depends on the contractile state of the heart (Sato et al., 1998). The solution that Kind et al. (2009) developed involved a time-normalisation of the four cardiac phases and the use of isophase lines instead of the isochrones that are generally used (Kind et al., 2009). Hence, significant advances in models and understanding have been made from the original load independent models and assumptions.

Along with the assumption of load-independence, many studies have shown that $E^n(t^n)$ has a similar shape irrespective of loading, disease state and species, leading to the conclusion of a universal time-varying elastance shape (Suga et al., 1973; Senzaki et al., 1996; Georgakopoulos et al., 1998). Senzaki et al. (1996) showed that the normalised time-varying elastance was independent of different cardiac pathologies, contractility, preload and afterload (Senzaki et al., 1996), and the same group followed

with results showing the shape of the normalised time-varying elastance was identical in different animal species (Georgakopoulos et al., 1998). From these results Senzaki et al. (1996) assumed the universality of the time-varying elastance, and proposed a method to estimate the time-varying elastance from a single pressure-volume loop which had important clinical implications (Senzaki et al., 1996). Several other groups have attempted similar things (Hayashi et al., 2000; Lee et al., 2002; McKay et al., 1986). However, there is no consensus in the literature that in fact the normalised time-varying elastance is universal (Jegger et al., 2007). $E^n(t^n)$ has been found to be inaccurate or not applicable to the single-beat methodology (Kjorstad et al., 2002), and in fact, the results of Senzaki et al. (1996) are not all that compelling to support the assumption of a universal time-varying elastance (Jegger et al., 2007; Senzaki et al., 1996).

The overall simplified model of the time-varying elastance as first proposed (Suga et al., 1973), and most widely used today, has its limitations in the curve-linearity of ESPVR, afterload dependence of $E(t)$ and the variability of the dead space volume V_d (Little and Freeman, 1987; Sato et al., 1998; Shishido et al., 2000). However, it has been widely used to great success, especially as the input to lumped parameter models. These models range in their intended purpose, from specific to quite general, and vary in the amount of the circulation they attempt to simulate. Single chamber models exist for the left ventricle, which use the time-varying elastance concept as an input (Avanzolini et al., 1985), along with full-system models intended to study the ventricles and their interaction (Santamore and Burkhoff, 1991; Amoore et al., 1992). More generalised full-system models based on the underlying time-varying elastance concept range from a minimalistic approach (Starfinger et al., 2007; Burkhoff and Tyberg, 1993; Olansen et al., 2000) to the very complex (Liang and Liu, 2005; Sun et al., 1997; Kappel et al., 2007).

The range of model size and complexity that utilises the concept of the time-varying elastance gives credibility to the use of such an assumption, as well as the reliability and physiological relevance of the model, despite the concern by some researchers that time-varying elastance is purely a phenomenological assertion (Loiselle et al., 2008; Cooper, 1990; Landesberg et al., 1993; Claessens et al., 2006; Campbell et al., 2008).

5.3.3 Pressure-volume area

Following on from the work to understand E_{max} and $E(t)$, Suga (1979b) theorised that the total mechanical energy of a contraction could be deduced from the $E(t)$ model (Suga, 1979b). This idea comes from the physics of the time-varying elastance model relating to mechanical energy, and is validated by correlations with oxygen consumption. Given that the heart relies almost exclusively on oxidative metabolism for energy generation, this approach thus assumes that the rate of oxygen consumption can provide an adequate measure of the total energy utilization (Suga, 1979b; Braunwald, 1976). This conceptual framework not only validates the total mechanical energy derivation, but gives more weight to the physiological significance of the time-varying model itself.

The pressure-volume diagram and time-varying elastance are linked concepts, although they can be used independently. The PV diagram is a trace of the time-varying elastance on a different set of coordinates, namely pressure and volume. Although the correlation for oxygen consumption and mechanical work comes from the PV diagram, it is the underlying model of mechanical elasticity, the time-varying elastance model, that allows an analytical formulation of mechanical energy giving physiological backing to the correlation (Suga, 1979b).

For an ideal elastic material, the potential energy at a stretch length x_s, can be calculated:

$$PE = \int_0^{x_s} f(x)dx \tag{5.2}$$

where $f(x)$ is a length-dependant force function (Suga, 1979b). For a linear material, this equation becomes $PE = \frac{1}{2} \cdot kx^2$ where k is the slope of the linear force-length relation. For any function f, the potential energy is the area under f.

The time-varying elastance concept is that of a special elastic material, whose spring constant changes with time, although at any one instant its force-length relation is still linear. A major difference between this approach, and a normal elastic material, is that potential energy can be generated without any additional stretch by increasing the stiffness of the material. In both cases, the potential energy at any instant in time is independent of the stretch history. This approach thus implies that the potential energy remaining in the ventricle at the end of systole is the area of the triangle below

the ESPVR line, between the volume axis and the point of end-systole, as shown in Figure 5.4.

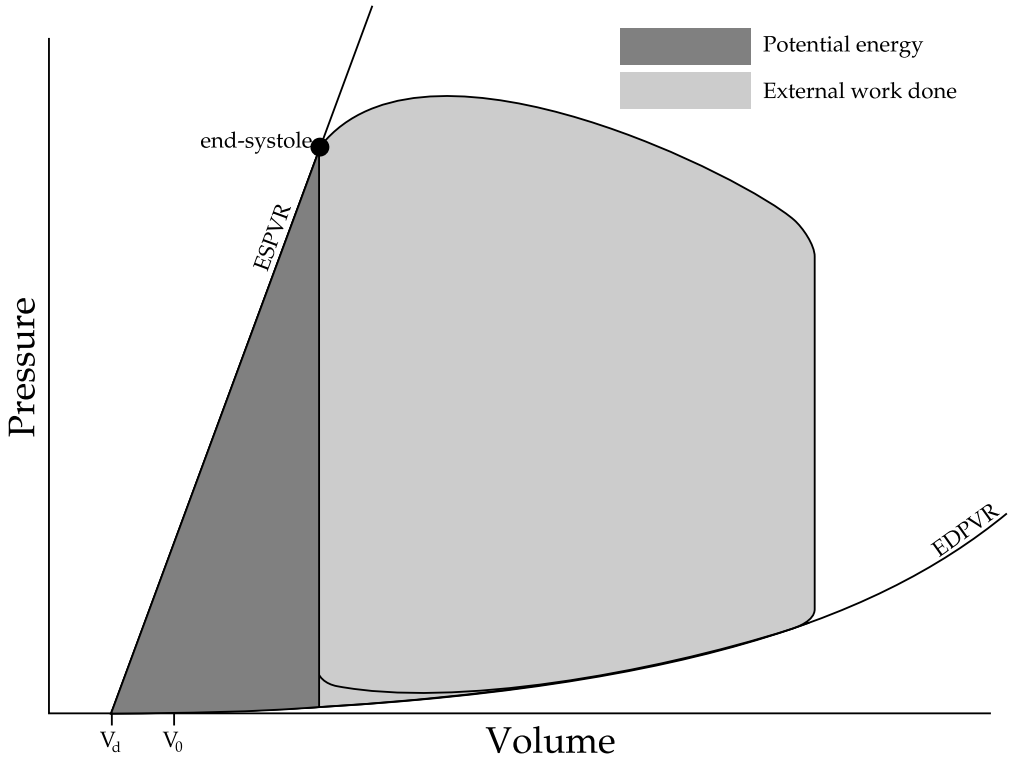

FIGURE 5.4: The total mechanical energy for a contracting ventricle as represented by the sum of the work done by the ventricle (light grey area) and the potential energy remaining in the muscle at the end of systole (dark grey area).

The second part of the energetic analysis of the ventricle contraction is the actual work done during contraction. In a similar fashion to the potential energy, the work done is the integral of the line traced during systole on the PV diagram, shown in Figure 5.4. Therefore, the total energy required for a contraction equates to the work done during the contraction, plus the potential energy remaining in the material at the end of systole. Note that the area, or energy, under the end-diastolic pressure-volume curve is left out of this mechanical energy formulation, as this energy does not appear to be actively supplied (Monroe and French, 1960; Suga, 1979b).

It is this formulation of total mechanical energy (work done plus potential energy) that correlated linearly with oxygen consumption under various preload and afterload conditions (Suga, 1990b; Loiselle et al., 2008), validating it as a useful metric of cardiac energetics (Suga, 1990b, 1979b). A further implication of this energetic concept and

formulation is that it allows the myocardial contractile efficiency to be determined directly (Suga et al., 1986, 1984).

The pressure-volume-area approach to mechanical cardiac performance has some major advantages over methods that use contractile parameters, such as force and shortening velocity (Kass and Maughan, 1988; Katz, 1988). However, two short-comings of the PVA approach as compared to load and heat have been outlined (Suga, 1990b). First, the fraction of myocardial oxygen consumption cannot generally be isolated from that of contractile events (Suga et al., 1983; Yasumura et al., 1989a). Second, the fractions for initial heat cannot be separated from that of recovery heat (Gibbs and Chapman, 1985; Suga et al., 1986). Despite these minor drawbacks, this approach has had much attention in both literature and physiological textbooks.

5.4 Discussion

The concept of the time-varying elastance is well established and successful in animal research, but has made only minor advances into the clinical environment, beyond that of a purely academic understanding of the heart. The concept of maximal elastance is firmly grounded as the gold standard for measurement of ventricular contractility despite the clinical difficulties of measuring it. To this end, many researchers, with varying degrees of success, have tried to find less invasive means to obtain a measure of E_{max} (Senzaki et al., 1996; Guarini et al., 1998; Swamy et al., 2009; Shishido et al., 2000; Brinke et al., 2010).

Although much is understood about the time-varying elastance concept, there are two areas which remain controversial. These are the load-independence, and universality of the time-varying elastance shape. The initial concept (Suga et al., 1973) suggested this load-independence and universality, and it seems to have moved from a general rule to a physiological law, despite the range of publications suggesting otherwise. Perhaps this is because of the success of the contractile index that partially relies on such a load-independence. However, this index of contractility is only one aspect of the overall time-varying elastance concept. It should be clear that at a fundamental level, the time-varying elastance is dependent on loading conditions, simply by the number of attempts to improve the one-element model by including load dependent

variables such as flow (Hunter et al., 1979, 1983; Shroff et al., 1985; Templeton et al., 1972; Vaartjes and Boom, 1987). There is also no underlying necessity for the model to be load-independent, rather this property was inferred from empirical measurements, not from the conception of the model or the underlying physiology (Suga et al., 1973). In fact, to some, the model deviates from physiology far enough for it to be considered surprising that the time-varying elastance concept is as successful as it has been in describing the state of the ventricles (Cooper, 1990).

The universality of the normalised time-varying elastance has seen less attention and controversy in the literature, perhaps because this assumption is required by fewer models and clinical implications and thus has been less important. However, this is a growing area, with estimations of the E_{max} relying on the universality of the time-varying elastance, as well as other estimations relying on the opposite assumption, see Chapter 8.

Lumped parameter models of the cardiovascular system have long relied on the time-varying elastance of the ventricles as an input function. As such, the time-varying elastance becomes a driver for the model, and is thus usually validated based on the success of the overall cardiovascular model, rather than of the physiological meaning and accuracy of the time-varying elastance itself. In fact, most of the attempts to estimate and model the time-varying elastance are based on this indirect form of validation (Senzaki et al., 1996; Guarini et al., 1998; Swamy et al., 2009; Shishido et al., 2000; Brinke et al., 2010). There is nothing wrong with using an indirect form of validation, provided the context stays within the bounds of the validation. However, due to the physiological nature of the time-varying elastance model, its success in describing the contractile state, and the total mechanical energy of the heart, it would be reasonable to expect that an estimation of the time-varying elastance could be validated on its own merits (Stevenson et al., 2012b).

5.5 Summary

This chapter has presented the evolution of the time-varying elastance concept, and implications arising from aspects of the model such as the contractile index, E_{max}, and the total mechanical energy of the heart. The overall model has remained a central part

of the understanding of the cardiovascular system in research, textbooks and clinical application, although direct clinical application has yet to see major advances due to the invasiveness of the procedures required to obtain measurements of the waveforms. There is also controversy in the literature on specific assumptions that can be made surrounding the time-varying elastance concept, specifically the load-independence and universality of the time and value normalised shape of the waveform. Despite this controversy, the overall concept is well accepted in many areas, most notably as an index of contractility and as an input to lumped parameter models of the cardiovascular system.

Chapter 6

Processing the aortic and pulmonary artery pressure waveforms

This chapter presents the first half of the process of estimating the ventricular time-varying elastance. Specifically, the processing of the aortic and pulmonary artery pressure waveforms to extract the required data. Specific points on these two waveforms are required by the algorithms developed in Chapter 7 to estimate the time-varying elastance. To estimate the time-varying elastance algorithmically at the bedside, the required points on the pressure waveforms must be able to be automatically extracted in a reliable and accurate way.

6.1 Introduction

There is much data available in an ICU setting. However, much of that data is effectively lost due to it being hidden deep in the waveforms displayed to the clinician. To extract that information, complex models are needed to process the waveforms and give clinical and physiological meaning to the numerical data. This approach creates a physiological picture from complex dynamics embedded in the waveform, acting to clarify the data presented into a clinical context.

There are also waveforms that cannot be measured in an ICU setting, such as the time-varying elastance, due to the invasive nature of the required procedure. In the literature to date, this particular waveform has not had much attention in a clinical context, as it

is not considered practical to measure in humans. However, the time-varying elastance has much to offer the clinician in the way of diagnostic potential, as the measurement is so closely linked to the energetics of the heart, and thus the state of the heart's function. The only way to access the information content of the time-varying elastance is to estimate this waveform from other data and waveforms that are practical to measure.

A second motivation to obtain the time-varying elastance waveform is to provide a required input for the cardiovascular system model, discussed in Chapter 3. This input provides the driving force behind the model, and is often referred to as the driver function. Previously, a global approximation has been used as the input, which, by nature, does not take into account any patient-specific deviation from this less-than-ideal approximation. As was shown in Chapter 4, the time-varying elastance has significant influence on the model outputs. A patient's specific function would thus offer significant clinical potential beyond its direct value.

The general approach to approximate the time-varying elastance can be divided into two halves. First, specific points need to be extracted from the pressure waveforms. Second, using predetermined correlations, these points are correlated to specific points on the time-varying elastance waveform. From these general correlations a curve can be drawn forming the final approximated waveform. The measured pressure waveforms of the aortic and pulmonary artery pressures can be noisy and/or biased in such a way as to make extracting the required points non trivial. Hence, initial signal processing is required, which is the focus of this chapter.

6.2 Methods

A high-level view of this approach is presented in Figure 6.1, which shows the formation and use of the correlations to generate estimated time-varying elastance waveforms. This chapter is focused on the left half of Figure 6.1, that of extracting data from the pressure waveforms for later use.

The overall method described here, and in Chapter 7, is shown in Figure 6.2. However, this approach is useful if and only if it is possible to automate the detection of the required points, defined in Equation (6.1), on the aortic pressure, P_{ao}, and pulmonary artery pressure, P_{pa}, waveforms, which are shown in Figures 6.3 and 6.4.

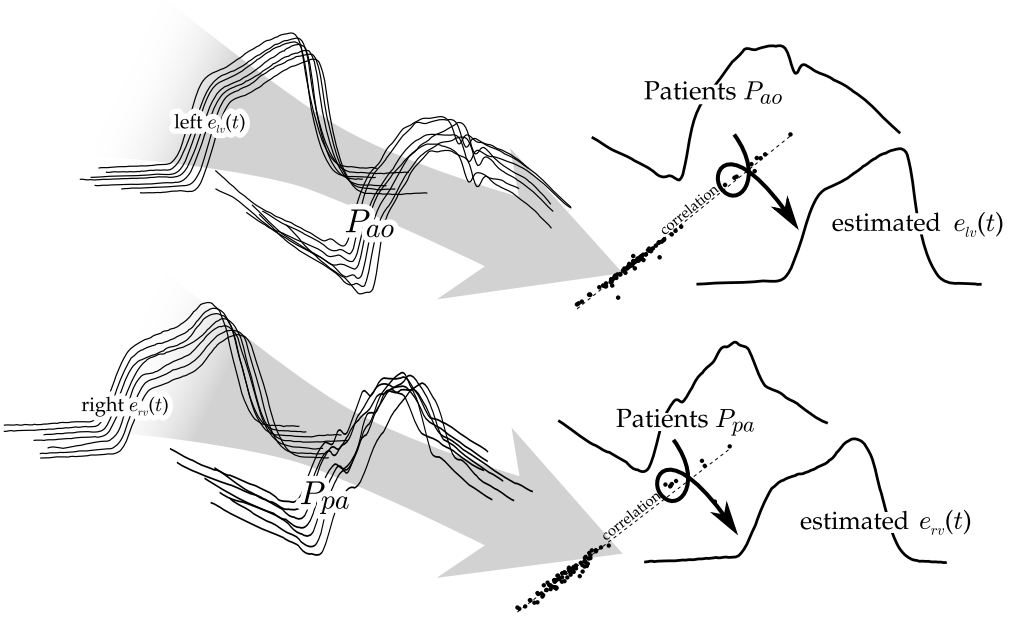

FIGURE 6.1: The figure shows a conceptualised overview of the process described in this chapter and Chapter 7, and further implications. From the many measured left ventricular time-varying elastance waveforms, $e_{lv}(t)$, along with many aortic pressure waveforms, P_{ao}, correlations are derived — the information flow is shown through the large grey arrow. Once these correlations are known, they can be used along with the aortic pressure waveform (from a specific patient), to arrive at an estimation of their time-varying elastance waveform. The equivalent for the right side is also shown.

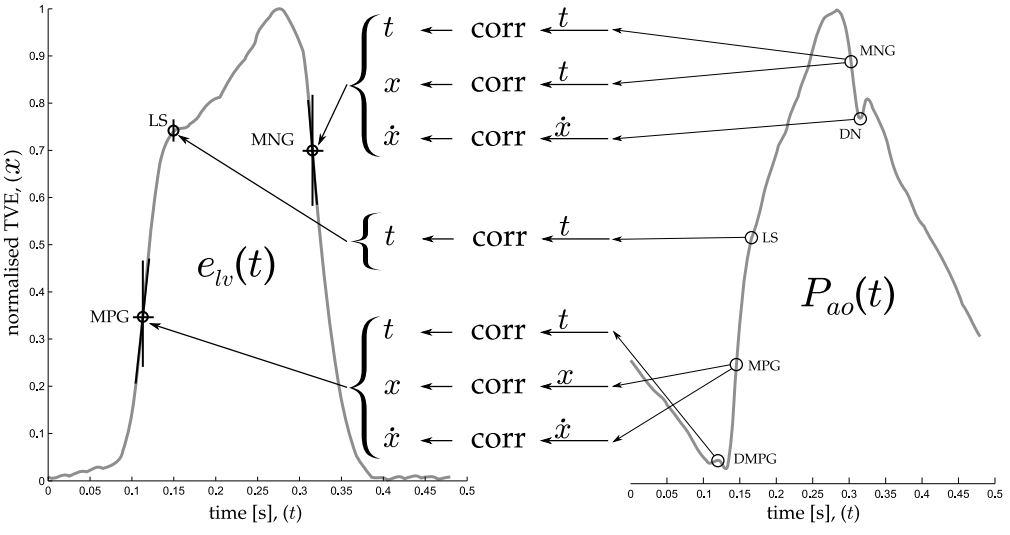

FIGURE 6.2: To illustrate what can be done with the identified points on the aortic pressure, an example of the formation of the estimated time-varying elastance elastance is shown here, while the terms are defined in Equation (6.1).

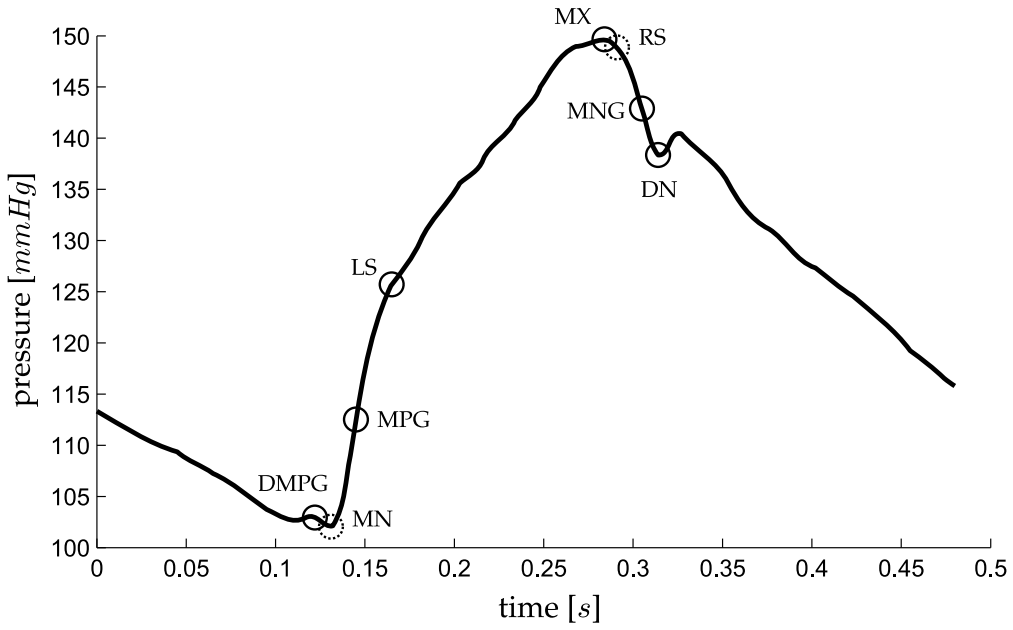

FIGURE 6.3: A representative aortic pressure waveform over one heart beat with relevant points, defined in Equation (6.1), marked on it. The two dashed circles, *MN* and *RS* are used only in locating other points.

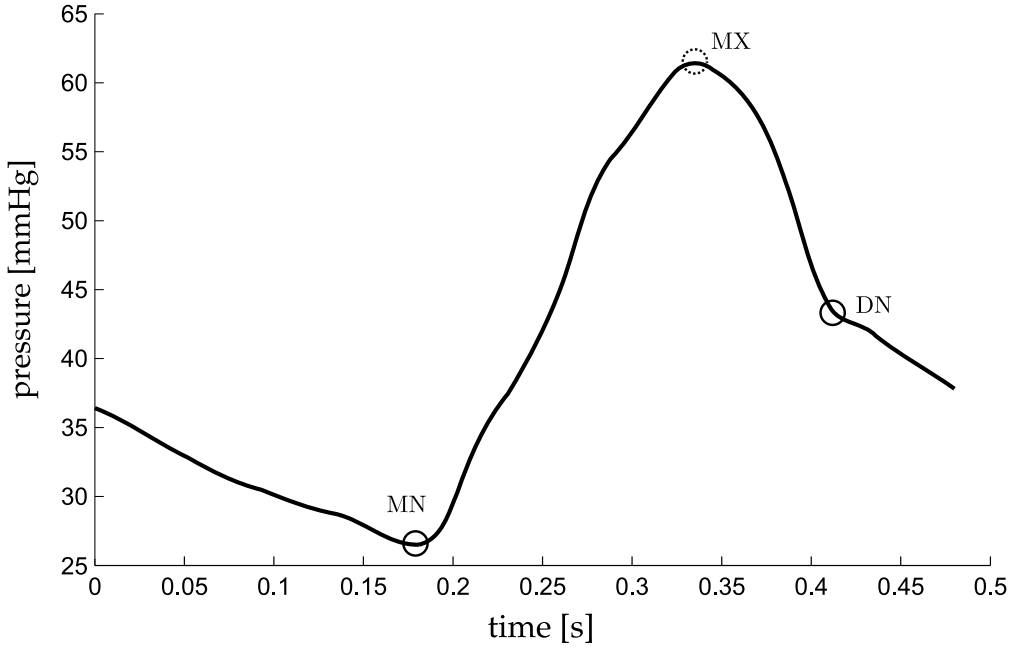

FIGURE 6.4: A representative pulmonary artery pressure waveform over one heart beat with relevant points, defined in Equation (6.1), marked on it. The dashed circle, *MX* is used only to help find other points.

To begin, a naming convention is defined:

$$\begin{aligned} e(t) &\equiv \text{ventricular time varying elastance} \\ P_{ao} &\equiv \text{aortic pressure} \\ P_{pa} &\equiv \text{pulmonary artery pressure} \\ DMPG &\equiv \text{driver maximum positive gradient} \\ MN &\equiv \text{minimum point} \\ MPG &\equiv \text{maximum positive gradient} \\ LS &\equiv \text{left shoulder} \\ MX &\equiv \text{maximum} \\ RS &\equiv \text{right shoulder} \\ MNG &\equiv \text{maximum negative gradient} \\ DN &\equiv \text{dicrotic notch} \end{aligned} \tag{6.1}$$

6.3 Shear Transform

A shear transform is defined to aid feature extraction from the measured P_{ao} and P_{pa} waveforms. This transform is defined:

$$\mathcal{S} \equiv (t, X(t)) \rightarrow (t, \phi_{shear}(X(t))) \tag{6.2}$$

where:

$$\phi_{shear}\left(X(t)\right) = X(t) + mt + c, \quad t_0 < t < t_{end} \tag{6.3}$$

$$X(t) \equiv \text{discrete, time valued data} \tag{6.4}$$

and the parameters t_0 and t_{end} are set depending on the region or period of interest. The parameters m and c are chosen such that:

$$\phi_{shear}(X(t_0)) = X(t_0) = \phi_{shear}(X(t_{end})) \tag{6.5}$$

Equation (6.5) leads to:

$$\begin{aligned} X(t_0) + m \cdot t_0 + c &= X(t_0) \\ X(t_{end}) + m \cdot t_{end} + c &= X(t_0) \end{aligned} \tag{6.6}$$

Solving Equation (6.6), for m and c yields:

$$\begin{aligned} m &= \frac{X(t_0) - X(t_{end})}{t_{end} - t_0} \\ c &= -m \cdot t_0 \end{aligned} \tag{6.7}$$

To better understand how this transformation operates, a line can be visualised from **A** to **C** in Figure 6.5, representing a portion of the waveform in Figure 6.3. The waveform is then rotated about **A** so the line **A**–**C** becomes horizontal, while time remains unchanged. Hence, it is a rotation and contraction that projects the line onto a horizontal axis.

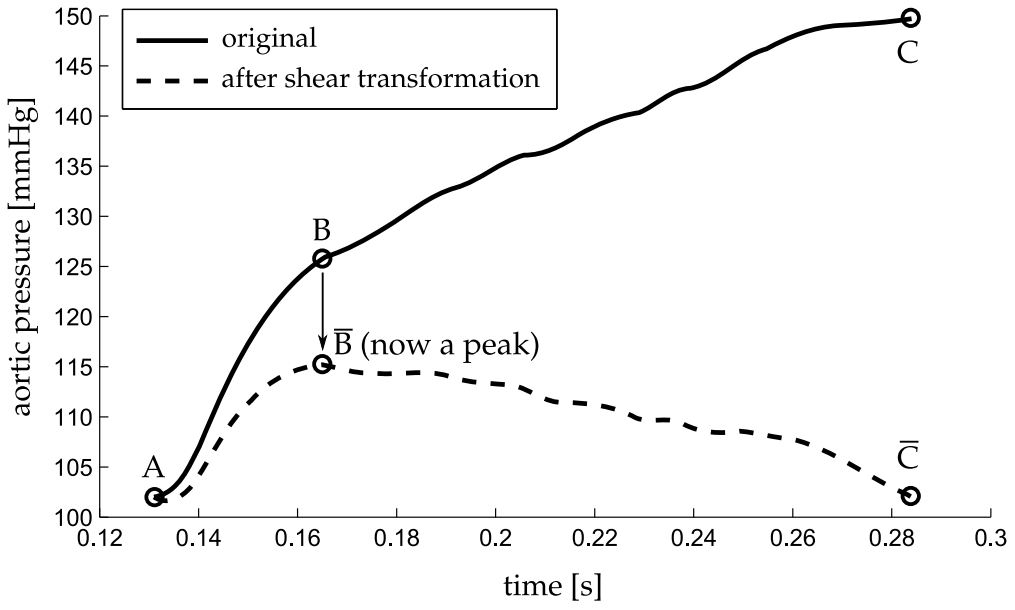

FIGURE 6.5: An illustration of the shear transformation of Equation (6.2), turning a hard to locate "shoulder", **B**, into an easily found maximum point $\overline{\mathbf{B}}$.

The effect of this transformation is to transform the difficult-to-find "shoulder" point **B** into an easily found peak of a curve, or for the reflection of **A**→**B** in x, a minimum of the curve. A "shoulder" is defined as a point at which two near linear lines with different slopes meet, such as the point *LS* in Figure 6.3. Thus, the use of this transformation

makes it far easier to algorithmically locate aspects of the waveforms which can be otherwise difficult to find.

The transform, $\mathcal{S}$, is used in two ways. First, it is used to locate a point of interest based on the maximum or minimum point of $\mathcal{S}$. This use is demonstrated in Figure 6.5. Hence, a desired point P is defined:

$$P = \mathcal{S}_{max} \text{ or } \mathcal{S}_{min} \tag{6.8}$$

Both local maximum, $\mathcal{S}_{max(local)}$, and minimum, $\mathcal{S}_{min(local)}$, are also required. $\mathcal{S}_{max(local)}$ exists and is the maximum point of $\mathcal{S}$, if and only if, there exists a maximum stationary point that does not fall at the temporal boundary of $\mathcal{S}$, and similarly for $\mathcal{S}_{min(local)}$.

The second way the shear transform of Equation (6.2) is used relates to the verification of a particular point given an initial estimation. For example, the first estimation of the point MN, in Figure 6.3, is the global minimum of the waveform, after which this point is verified using the shear transform, resulting in confirmation of the point, or the finding of a new point to use in its place. This approach works by locating the minimum point of the shear transform, P_2, over a given range, t, near the first estimation, P_1, and also defining a threshold time, D. If the point P_2 lies temporally within $t_{P_1} \pm D$, then the correct point is the initial estimation P_1, otherwise the correct point is P_2.

The choice of $\mathcal{S}_{max}$ or $\mathcal{S}_{min}$, range of time, t, and the threshold time, D, are defined for the type of point under consideration. The specific values, listed in Section 6.4, are chosen empirically, based on which features appear close to the point of interest, and the temporal variation that has been observed in these features.

These two situations are graphically shown in Figure 6.6 and Figure 6.7 for positive values of D. However, the same applies for negative values, for which the real point lies before the point P_1, instead of after it. The complete process is defined:

$$P = \begin{cases} P_1 & \text{if } t_{P_2} \text{ lies within } t_{P_1} \pm D \\ P_2 & \text{otherwise} \end{cases} \tag{6.9}$$

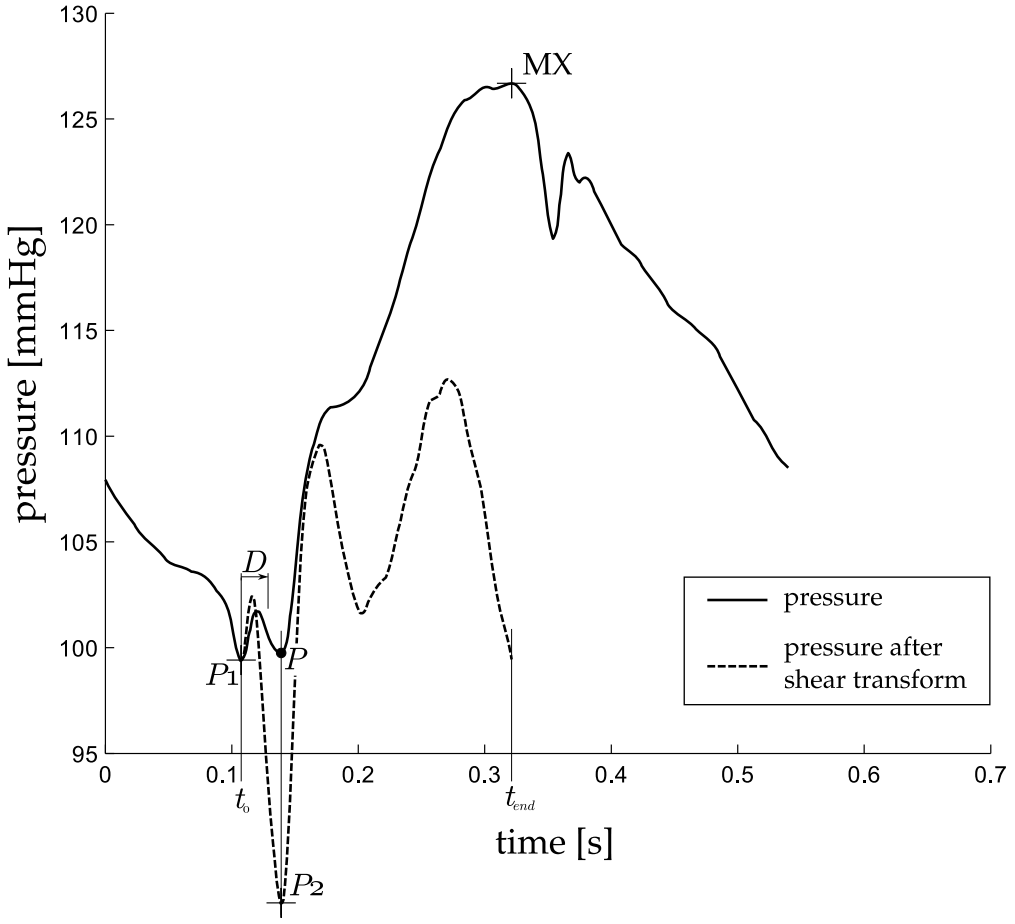

FIGURE 6.6: The desired point for MN is P. However, in this example the global minimum of the waveform is P_1, which is the initial estimation for MN. A shear transform of the pressure waveform between P_1 and MX reveals a minimum (P_2) outside the range of D, thus P_2 is taken as the time of MN.

where:

$$\begin{aligned} P_1 &\equiv \text{initial point to be checked} \\ P_2 &\equiv \mathcal{S}_{max} \text{ or } \mathcal{S}_{min} \text{ (chosen separately)} \\ D &\equiv \text{threshold time} \\ t &\in \{t : t_0 < t < t_{end}\} \end{aligned} \tag{6.10}$$

Combined, these two methods of use, shown in Figures 6.5–6.7, create a robust and computationally fast method for locating certain hard-to-find points on a waveform.

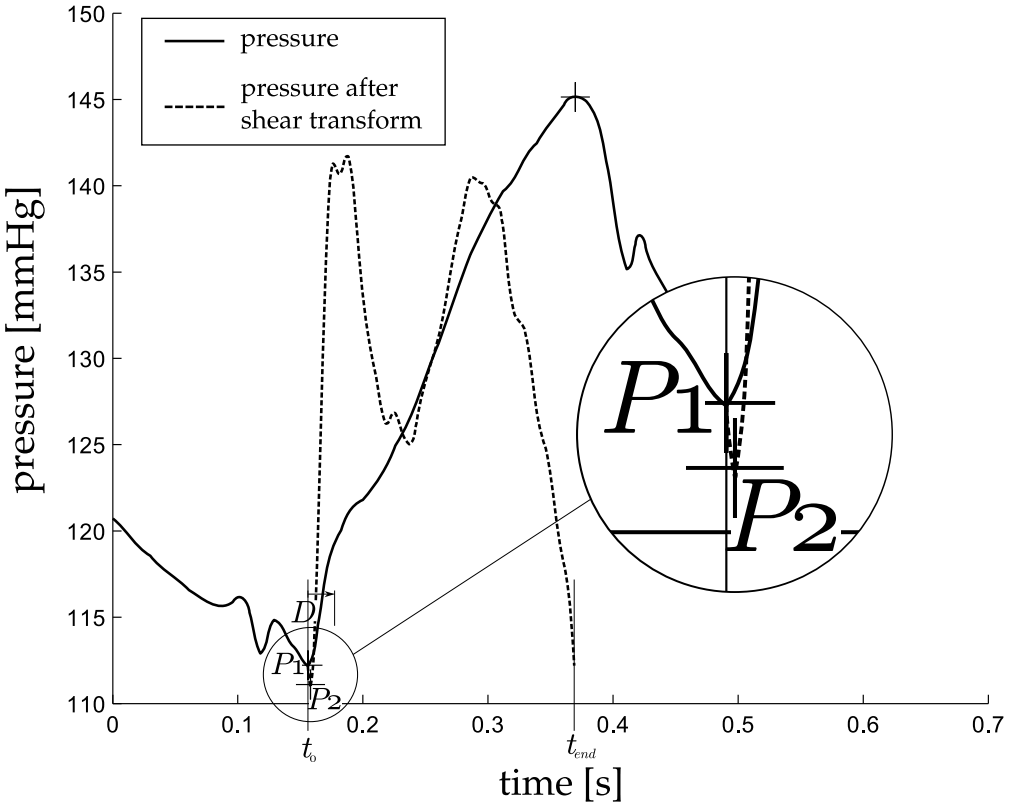

FIGURE 6.7: This example is the other situation in the process of finding MN to Figure 6.6, i.e. the initial estimation of the global minimum for MN is correct. Here, the minimum of the shear transform from P_1 to MX falls within the range of D, thus the P_1 is taken as MN.

6.4 Point location method

The method for finding the points is described in Table 6.1, along with Sections 6.4.1 and 6.4.2. Table 6.1 gives the full method, except for the points $DMPG$ and DN, which are described in the next two sections, along with a graphical illustration. The graphical illustrations are the out-working of the method for a representative waveform, and are intended only to aid the reader in their understanding of the method, and not to formally describe the method itself. Due to the complexity of the method for the points $DMPG$ and DN, these two have been described in Table 6.1 only for the simplest, and most common case, with the full method described in separate sections with relevant figures.

TABLE 6.1: The step by step method for finding the points on P_{ao} and P_{pa}, as labelled on the right. The graphics beside each step are for illustration only and are not meant to be part of the definition of the method, rather they are to demonstrate the method in operation on a representative P_{ao} waveform. Note that the methods described here for $DMPG$ and DN are not complete as these require a more complex method. Refer to Sections 6.4.1 and 6.4.2 for the complete method for these two points.

Step	Description	Example	Relevance
Step 1	Find the global maximum	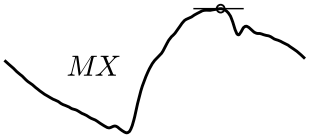	P_{pa} & P_{ao}
Step 2	Find the global minimum, and check this point with Equation (6.7), where $D = 0.025$, $t_0 = t_{P_1}$, $t_{end} = t_{MX}$ and $P_2 = \mathcal{S}_{max}$		P_{pa} & P_{ao}
Step 3	For the simplest case, find $\mathcal{S}_{max}$ between $\frac{3}{4} \cdot t_{MN}$ and t_{MN}, for the complete method see Section 6.4.1	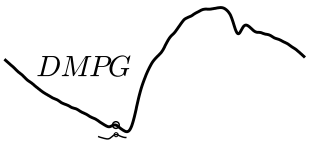	P_{ao}
Step 4	Find $\mathcal{S}_{max}$ between MN and MX, and check with Equation (6.9) where $D = -0.05 \cdot period$, $t_0 = t_{MN}$, and $t_{end} = t_{P_1}$	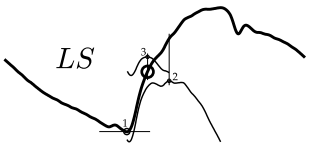	P_{ao}
Step 5	Find the maximum positive gradient between MN and LS	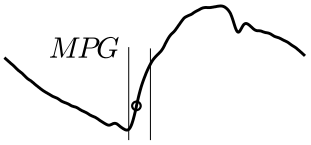	P_{ao}
Step 6	The most basic method is to find $\mathcal{S}_{min}$ between t_{MX} and t_{end}, which is shown to the right. For the complete method see Section 6.4.2		P_{pa} & P_{ao}
Step 7	Find $\mathcal{S}_{max}$ between MX_2 and DN. MX_2 is defined in Equation (6.14)	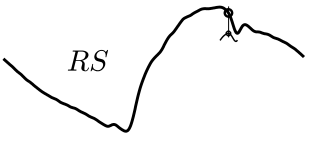	P_{ao}

Table 6.1 — *(continued)*

Step	Description	Example	Relevance
Step 8	Find the maximum negative gradient between RS and DN		P_{ao}

6.4.1 Finding $DMPG$

There are some cases where $DMPG$ is equivalent to MN, see Figure 6.3. These cases occur when:

$$(t_{MX} - t_{MN}) < period \cdot 0.25 \tag{6.11}$$

When Equation (6.11) is not true, $DMPG$ is found as the $\mathcal{S}_{max(local)}$ from $\frac{3}{4} \cdot t_{MN}$ to MN, see Figure 6.8. However, there are a few cases, for both sepsis and pulmonary embolism, in which a local maximum of $\mathcal{S}$ does not exist except at the boundaries of the region, which is not acceptable if an automated detection method is desired. In such cases, a point P_2, is defined as the $\mathcal{S}_{min}$ from $\frac{3}{4} \cdot t_{MN}$ to MN. If $\mathcal{S}_{max(local)}$ from P_2 to MN exists, this is taken as $DMPG$, see Figure 6.9, otherwise $DMPG$ is defined as $\mathcal{S}_{max(local)}$ from $\frac{3}{4} \cdot t_{MN}$ to P_2, see Figure 6.10. If this final local maximum does not exist, $DMPG$ is defined as $\frac{3}{4} \cdot t_{MN}$. These specific cases occur due to noise, variability and dysfunction, and are part of what makes robust algorithmic or automated processing difficult.

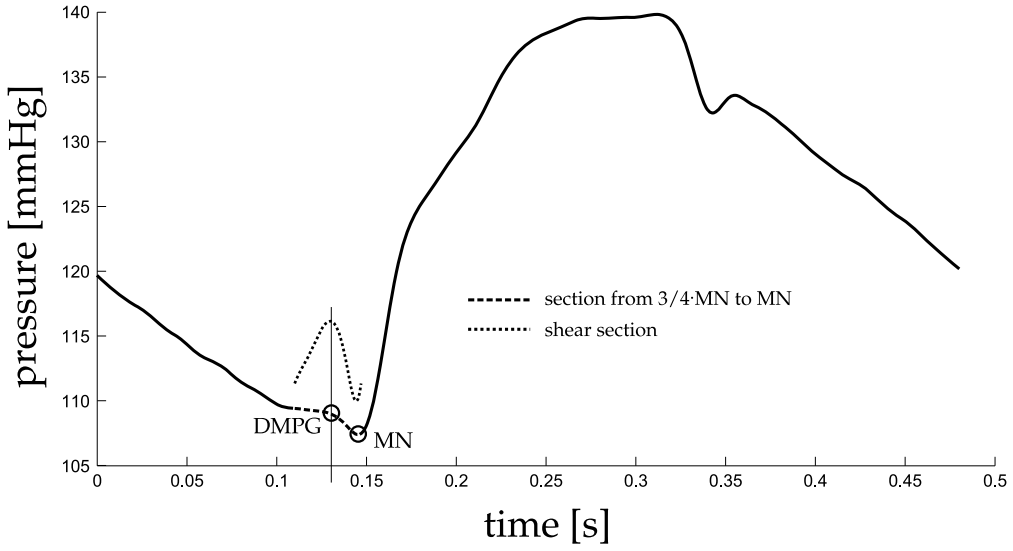

FIGURE 6.8: A straight forward case for finding $DMPG$, where P_1 of Equation (6.13) exists, thus $DMPG \equiv P_1$.

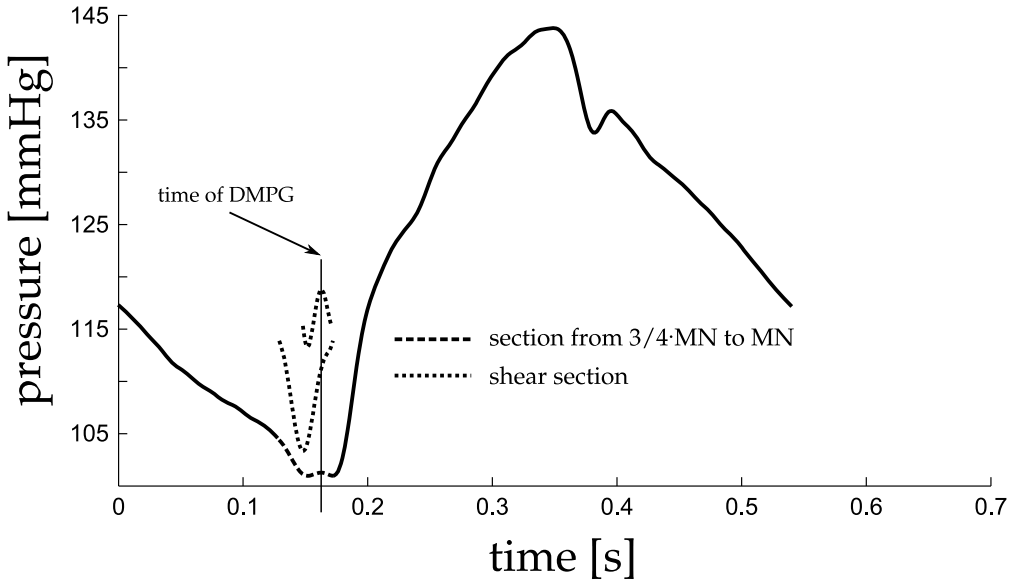

FIGURE 6.9: A less common case for finding $DMPG$, where P_1 of Equation (6.13) does not exist, but P_3 does, thus $DMPG \equiv P_3$.

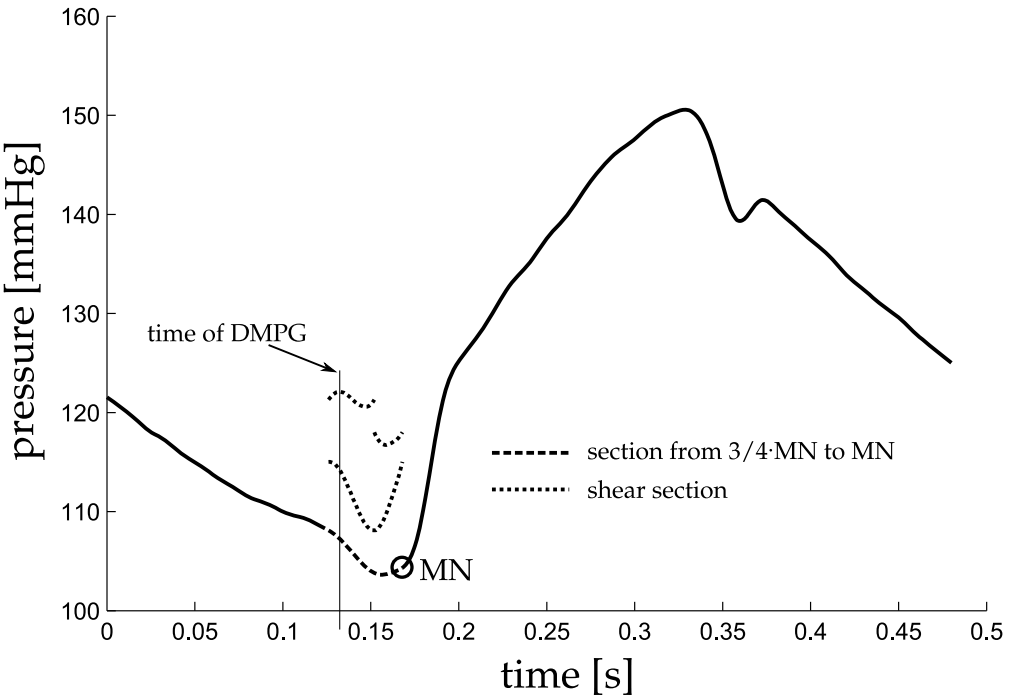

FIGURE 6.10: A less common case for finding $DMPG$, where P_1, and P_3 of Equation (6.13) do not exist, but P_4 does, thus $DMPG \equiv P_4$.

This process is defined:

$$P = \begin{cases} P_1 & \text{if } \exists\ P_1 \\ P_3 & \text{if } \exists\ P_3 \\ P_4 & \text{if } \exists\ P_4 \\ \frac{3}{4} \cdot t_{MN} & \text{otherwise} \end{cases} \tag{6.12}$$

where:

$$\begin{aligned} P_1 &\equiv \mathcal{S}_{max(local)},\ t \in \{t : \frac{3}{4} \cdot t_{MN} < t < t_{MN}\} \\ P_2 &\equiv \mathcal{S}_{min(local)},\ t \in \{t : \frac{3}{4} \cdot t_{MN} < t < t_{MN}\} \\ P_3 &\equiv \mathcal{S}_{max(local)},\ t \in \{t : t_{P_2} < t < t_{MN}\} \\ P_4 &\equiv \mathcal{S}_{max(local)},\ t \in \{t : \frac{3}{4} \cdot t_{MN} < t < t_{P_2}\} \end{aligned} \tag{6.13}$$

6.4.2 Finding DN

The general approach to find the point DN in Figure 6.3 is to find $\mathcal{S}_{min}$ between t_{MX} and t_{end} (end of the waveform). However, in a number of cases this approach fails due to oscillations towards the end of the waveform, as shown in Figure 6.11. In addition, using only the first local minimum, as would work in Figure 6.11, works in only a few cases and is therefore not a robust solution. Hence, a more specific algorithm is required.

Hence, a second maximum point is defined:

$$\begin{aligned} MX_2 \equiv &\text{ max point of } P_{ao}(t), \\ &t \in \{t : t_{MN} + \frac{period}{5} < t < period\} \end{aligned} \tag{6.14}$$

Next, two more intermediate points are defined:

$$DN_1 \equiv \text{(lowest) } \mathcal{S}_{min(local)}, t \in \{t : t_{MX_2} < t < period\} \tag{6.15}$$

$$DN_2 \equiv \text{first } \mathcal{S}_{min(local)}, t \in \{t : t_{MX_2} < t < period\} \tag{6.16}$$

From DN_1 and DN_2, the real DN is chosen, defined:

$$DN = \begin{cases} DN_1 & \text{if } (C_A \wedge C_B) \vee (C_C \wedge C_D) \\ DN_2 & \text{otherwise} \end{cases} \tag{6.17}$$

where the logical conditions are defined:

$$\begin{aligned} C_A &\equiv DN_2 > MX_2 \\ C_B &\equiv (t_{DN_2} - t_{MX_2}) < 0.15 \cdot period \\ C_C &\equiv \frac{DN_2 - DN_1}{P_{ao}(t_{MX})} > 0.02 \\ C_D &\equiv (t_{DN_2} - t_{MX_2}) < 0.11 \cdot period \end{aligned} \tag{6.18}$$

When using a measured P_{pa} waveform, DN is defined:

$$DN = DN_1 \tag{6.19}$$

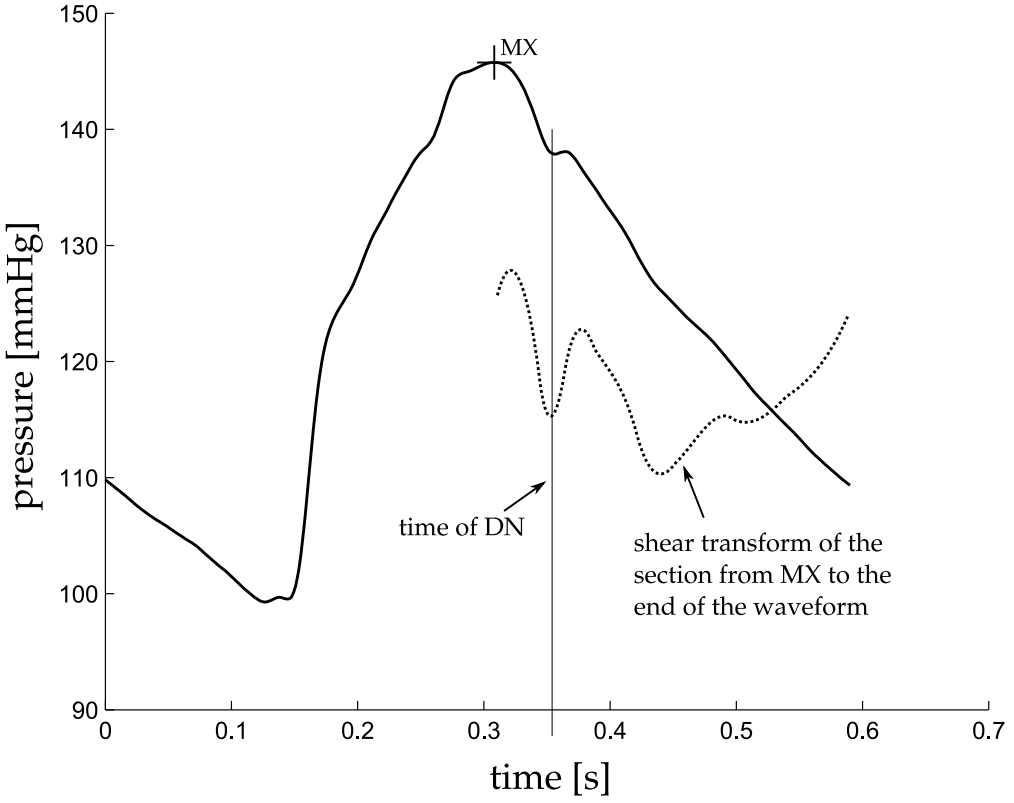

FIGURE 6.11: An example of where the first local minimum of the shear transform is the correct time for the point DN.

6.4.3 Validation Test

The method presented was developed on a set of data from five pigs (51 waveforms) in which pulmonary embolism was induced (Desaive et al., 2005; Ghuysen et al., 2008). The method was then independently tested on a further five pigs (37 waveforms) in which septic shock was induced, and treated with haemofiltration (Lambermont et al., 2003, 2006). These data sets are therefore effectively development and validation tests.

The points on all waveforms (see Figures 6.3 and 6.4) were identified or checked individually by eye. The two gradients (MPG and MNG) were first located through simple computation, and then individually checked by eye and corrected where necessary. Due to the nature and location of these points (maximum gradient of a sigmoidal function), they are the two easiest and most reliable to find algorithmically, and, in fact, the algorithmic approach is more accurate than hand selection. The two "shoulders" (LS and RS) were first located through an algorithm developed prior to that which

is described in this chapter, after which each point was individually checked and corrected. Because there is no formal definition for the location of these "shoulder" points, it was left to an algorithmic definition. For a validation test this definition is self fulfilling. However, as *LS* (*RS* is used only to aid in finding *MNG*, and is thus not included in the validation results) is found as an intermediate step to the estimation of the time-varying elastance, its full and more formal validation would be the results of the time-varying estimation, which is not in the scope of this chapter, (see Chapter 7). All the remaining points were hand selected.

The automated method was applied to the waveforms and the identified points assessed against the known points for accuracy in time. The use of separate data with different cardiac dysfunction to design and test the method ensures the robustness of the validation method.

6.5 Results

For the points *MN* and *DN* required when using P_{pa} (Figure 6.4), the method located both points in 87 of the 88 waveforms to within the sampling frequency of 200Hz (0.005 sec), missing *DN*, from one waveform. This missed point is in a waveform at the start of the third pig of the sepsis cohort and is unique to the data set, both in the measured time-varying elastance and P_{pa}, as shown in Figure 6.12, compared to the more typical P_{pa} waveform in Figure 6.4. The failure is due to the unusual second peak of P_{pa}, and the early decay of the time-varying elastance.

For each P_{ao} waveform, the method locates eight points, *MX*, *MN*, *DMPG*, *LS*, *MPG*, *DN*, *RS*, *MNG*. However, *RS* and *MN* are used only to aid the location of other points. These two points were both located with sufficient accuracy to enable the method to progress in all 88 waveforms. Results for the other six points are shown in Table 6.2. Of 528 total points, 519 were found temporally within 1 %, four within 5 %, four within 10 % and one within 20 %.

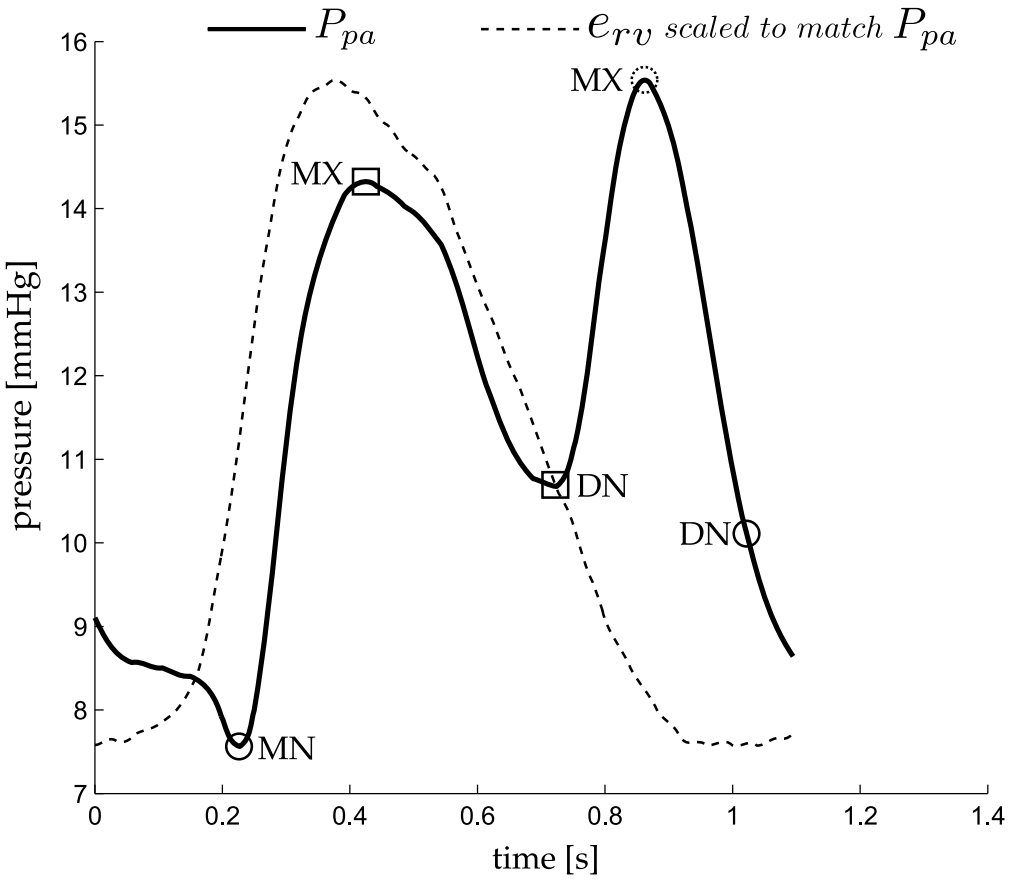

FIGURE 6.12: P_{pa} alongside the matching time-varying elastance. The automatic or algorithmic method failed to capture the correct *DN* point, locating a point too late in the waveform (circle), the real *DN* and associated *MX* are marked by squares.

TABLE 6.2: Accuracy of the method: number of points grouped by absolute error (of 88 total points). * note that the validation of *LS* here is partially self fulfilling and is included here only for completeness.

	$< 1\,\%$	1–5 %	5–10 %	10–20 %
DMPG	84	1	3	0
MPG	88	0	0	0
*LS**	86	1	1	0
MX	88	0	0	0
MNG	87	0	0	1
DN	86	2	0	0
TOTAL	519	4	4	1

6.6 Discussion

The automated, algorithmic method presented, enables the mapping between aortic pressure, P_{ao}, pulmonary artery pressure, P_{pa}, and the ventricular time-varying elastance, $e_{rv}(t)$ and $e_{lv}(t)$, by accurately processing the P_{ao} and P_{pa} waveforms to identify specific points. Once combined, they provide a useful tool for clinicians to obtain accurate time-varying elastance waveforms without further invasive or risky sensors or procedures.

There are other ways to locate the points on the pressure waveforms, most notably a derivative and second derivative method. However, this derivative-based approach becomes problematic in practice due the noise inherent in the waveforms. The method that has been developed in this chapter was designed to work with the level of noise that is typically seen on these measurements, and is therefore more involved than a simple derivative-based method.

The method presented was robust to the typical and significant variation and noise in P_{ao} and P_{pa} waveforms. The method was developed on five pigs in which pulmonary embolism was induced, and then tested independently with data from another set of five pigs in which septic shock was induced. The results give confidence that this method will generalize to a wider set of disease states and to human data.

However, while the results were very good, this research needs further validation on a wider cohort of pigs and types of dysfunction to further quantify its limits and accuracy. Direct validation on humans is the ultimate goal. However, the results appear robust, and justify and enable a wide range of further more in-depth validation studies of both the method and its potential uses when reconstructing the time-varying elastance for monitoring and diagnosis.

Clinically, it must be noted that for this method to work, a Swan-Ganz catheter is assumed. If radial artery pressure was measured instead, there would be more oscillations in the waveform, potentially requiring modifications. Swan-Ganz catheters are still used, and this method presented would add value to their use, which is otherwise sometimes contested (Frazier and Skinner, 2008; Chatterjee, 2009; Cooper and Doig, 1996).

The method developed in this chapter shows promise for gaining clinical insight and improving diagnosis. It can enable clinicians to get more information about the patient's current state, without the use of more invasive procedures, as well as beat-to-beat tracking of this information. This level of detail is far more than is currently available, does not add addition risk as it requires no further procedures or sensors, and could potentially lead to better and earlier diagnosis of dysfunction, as well as better knowledge of treatment responses.

6.7 Summary

This chapter has presented a robust, and potentially dysfunction-independent method to find the waveform points necessary to use proven methods to non-invasively and automatically estimate the otherwise unavailable left and right ventricular time-varying elastances, with accuracy well within measurement error. This capability is enabled using standard measurements that are already commonly used in an intensive care setting, thus involving no additional risk to the patient. The results thus justify prospective validation and extension of these results towards clinical application.

Chapter 7

Estimating ventricular time-varying elastance

In Chapter 6, points were extracted from the aortic and pulmonary artery pressure waveforms, P_{ao} and P_{pa}, respectively. The primary purpose is to facilitate the estimation of the time-varying elastance on a patient-specific basis. This chapter presents the method of estimating this time-varying elastance using these points. The combination of Chapters 6 and 7 results in a method to estimate the time-varying elastance waveforms from measured pressure waveform data that is readily available in an intensive care setting.

7.1 Introduction

Detailed cardiac energetics are too invasive to measure in an ICU setting. In particular, such a measurement requires ventricle pressure and volume (Suga, 1971a), and is therefore not done in practice. However, if the relevant energetics could be captured using data from a nearby catheter, the clinical potential of such measurements could be realised. To date, no such method achieves this aim.

This chapter presents a model for estimating the time-varying elastance from observed ventricular pressure-volume behaviour, to be used in the modelling of broader cardiovascular system (Smith, 2004; Starfinger et al., 2008a; Chung et al., 1997; Revie et al., 2011a,b). This elastance is required by the cardiovascular model of Chapter 3 to deliver

the pressure-volume measurements observed, and thus implicitly contains preload and afterload information.

Time-varying elastance (TVE) is defined as (Suga and Sagawa, 1974):

$$e(t) = \frac{P_v(t)}{V_v(t) - V_d} \tag{7.1}$$

where, V_d is the intercept of the end-systolic pressure-volume relation with the volume axis (Sagawa, 1981) and $V_d = 0$ is assumed for simplicity, $P_v(t)$ is the ventricle pressure and $V_v(t)$ is the ventricle volume. The waveform $e(t)$ is typically normalised to a value of 1.0 (Suga et al., 1973). As stated in Chapter 5, the model of time-varying elastance is load-dependent, and does not have a universal shape, even when normalised with respect to time and value as some have suggested (Suga et al., 1973). More detail and discussion regarding the TVE see Chapter 5.

Load conditions are diagnostic and thus the model for TVE presented monitors these changes as the time varying ability of the heart to pump blood. It thus provides a measure of heart function and energetics (Suga et al., 1973; Senzaki et al., 1996; Sunagawa et al., 1984).

There have been several attempts to estimate TVE (Guarini et al., 1998; Swamy et al., 2009; Shishido et al., 2000; Senzaki et al., 1996; Brinke et al., 2010). Most studies present a method using the TVE to estimate a specific parameter, most commonly end-systolic elastance (Shishido et al., 2000; Brinke et al., 2010; Senzaki et al., 1996) and ejection fraction (Swamy et al., 2009). However, their validation is based on these metrics, not on the resulting TVE waveform, which contains unique clinical information.

This chapter is focused not on the absolute values of the elastance, such as end-systolic elastance. Rather, the focus is on the shape, and change of shape of the time-varying waveform within a specific patient as dysfunction occurs and the patient's state changes. This intra-patient variability is reflected in the (relative) shape as it evolves over time. Thus, the patient is their own comparator in this use.

It is unclear how much specific clinical information can be obtained from the TVE waveform, other than the highly sought-after end-systolic elastance (Burkhoff, 2009), and a measure of cardiac work (the area under the TVE waveform is analogous to work done by the ventricle). The absolute value of the work done is lost with the

normalisation of the waveform, but the relative changes to work over time remain. This point holds true for a constant inotropic state, as the end-systolic elastance will remain the same. For a varying end-systolic elastance, the relative change in cardiac power will still be visible to the TVE through the altered shape from an increased heart rate.

Beyond cardiac work, a number of TVE features have been highly correlated to clinically relevant parameters in a previously developed circulatory model (Starfinger et al., 2007). Equally, it contains similar information to that of the pressure-volume (PV) loops, which are known to contain information on cardiac function (Sagawa, 1978) including cardiac work (Suga, 1990b; Burkhoff and Sagawa, 1986), contractility (Broscheit et al., 2006; Suga et al., 1973), O_2 consumption (Burkhoff and Sagawa, 1986; Suga, 1979a), and all the states of filling, contraction, ejection and relaxation (Hall and Guyton, 2011). Overall, the TVE reflects cardiac state, cardiac output or blood volume, and net preload and afterload, all of which change with different cardiac dysfunction. Hence, the ability to directly measure TVE, which does not currently exist without significantly invasive additional testing, should yield clinically useful insight and diagnostically valuable information. For a more in-depth discussion of the TVE see Chapter 5.

This research is unique in that the end goal is to produce the TVE function in its own right, validating the TVE waveform on its own accuracy compared to the invasively and directly measured waveform. This waveform identification is done through the use of only commonly available metrics in an ICU setting, and thus by being non-invasive, it is meant that it is no more invasive than traditional care and requires no further invasive sensors or procedures.

7.2 Methods

7.2.1 Concept

Ventricular time-varying elastance cannot be directly measured without invasive procedures. However, the information contained within the time-varying elastance waveform can be seen in other parts of the closely intertwined cardiovascular system. Therefore, with the right knowledge and transformations, that information can be collected

and translated into an estimation of a metric (time-varying elastance) that would not normally be possible to obtain.

The best accessible source of indirect information about time-varying elastance is directly down-stream of the ventricles, at the aorta and the pulmonary artery. This location is the first to 'see' any results of a change in elastance during systole. Thus, the aortic and pulmonary artery pressure waveforms (P_{ao} and P_{pa}, respectively) are key sources of information, which contain surrounding load conditions, to reconstruct time-varying elastances. It can be assumed, and seen from the data presented in this chapter, that the shape of the time-varying elastance is load dependent. For further discussion on the time-varying elastance's load dependence, see Chapter 5.

Figure 7.1 shows the overall method of this chapter. Known points on the aortic pressure waveform are correlated with points on the left ventricle TVE (described in Section 7.2.4), giving equations that enable estimations of these left ventricle points from the aortic pressure alone. A function is then used to draw a smooth line through these estimated points (described in Section 7.2.3) giving a continuous approximation of the left ventricle TVE. The right ventricle is estimated in a similar way. Known points from the estimated left ventricle TVE, time values taken from the pulmonary artery pressure, and the global end-diastolic volume (GEDV) are correlated with points from the right ventricle TVE, again creating equations used to estimated a continuous right ventricle TVE. This overview is shown graphically in Figure 7.1.

A total of eight pieces of information, within the four labelled points on time-varying elastance waveforms, are needed to draw a smooth curve for the estimated time-varying elastance. These points (MNG, LS, MPG and MX) are shown on the TVE waveforms in Figure 7.1 and, beside the respective TVE (with the exception of MX as this is always 1) the breakdown and origin of their values are shown. The points on the pressure waveform required in this method, from Equation (6.1), are shown on the aortic and pulmonary artery pressure waveforms. The large hollow arrows show the overall flow of information within the method, while the smaller arrows show the more fine-grained flow of information.

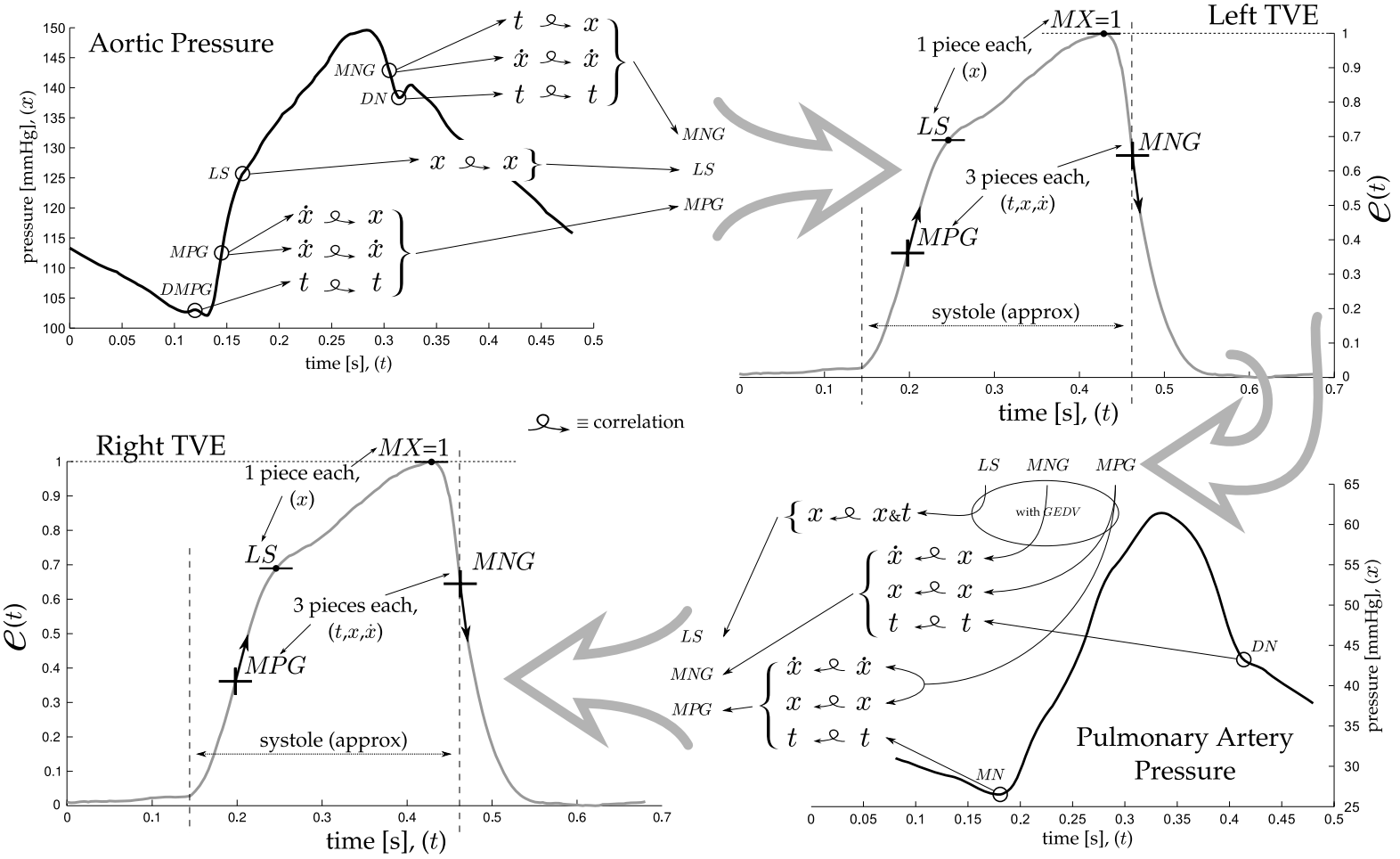

FIGURE 7.1: An overall description of the method presented in this chapter, showing the left and right TVE waveforms with the four points required to reconstruct them, along with the origin of these values on the pressure waveforms. The large hollow arrows show the general flow of information, while the smaller arrows show more fine-grained flow.

A simpler model is shown in Figure 7.2, which visually shows the difference between the academic side described in this chapter and the potential clinical use of this research.

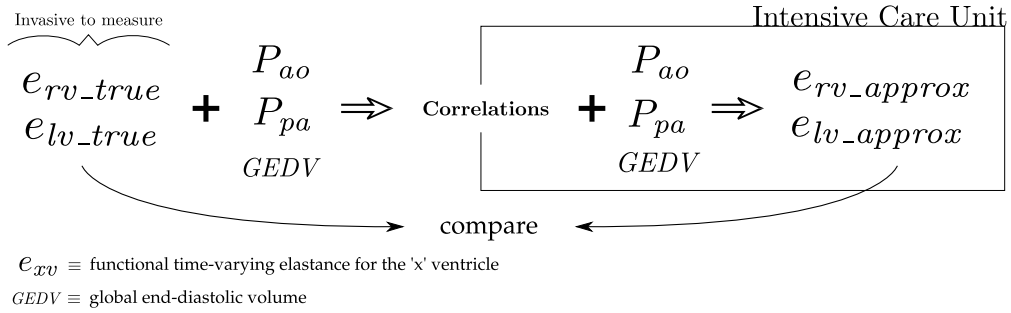

FIGURE 7.2: A simple high-level overview of the method within this chapter. It can be divided into two parts, the first involves the preparation of the correlations from invasively measured metrics, the second, a clinical method for use in an intensive care setting.

It should be noted that the two catheter locations (aorta and pulmonary artery) can 'see' the ventricles only during systole, inferring that information about the time-varying elastance can be known only during systole. However, this limitation is not clinically significant, as time-varying elastance is primarily defined by what happens during systole, where it is most active. In addition, systole is the period in which blood is pumped, which is the primary outcome of the time-varying elastance in terms of clinical relevance. Changes in cardiac elastance due to dysfunction would change this time-varying elastance, but the clinical significance would be seen in the altered blood flow.

7.2.2 Animal Data

The method presented was developed on a cohort of nine porcine subjects divided into two groups. The first group (five subjects) in which pulmonary embolism was induced (Desaive et al., 2005; Ghuysen et al., 2008). The second group (four subjects) in which septic shock was induced (Lambermont et al., 2003). Both trials were under the control of the ethics committee of the medical faculty of Liege, Belgium.

Measurements were taken every 30 minutes. In total, the first group had 51 sets of measurements across the five pigs, while the septic shock cohort had 34 over four pigs. For each pig, the following relevant measurements were taken: P_{ao}, P_{pa}, left and

right ventricle volume (V_{lv}, V_{rv}), left and right ventricle pressure (P_{lv}, P_{rv}). Aortic and pulmonary artery pressure were measured using catheters, while right and left ventricle pressures and volumes were directly measured using 7F, 12 electrodes conductance micro manometer tipped catheters.

Left and right time-varying elastances were calculated directly with the respective pressure and volume waveforms via Equation (7.1), while setting the dead space volume to zero. GEDV was calculated as the sum of the individual maximum volumes of the left and right ventricles.

The data contains varying degrees of cardiac dysfunction from healthy to the fully developed disease state. It thus provides a good test of the presented methods. The use of two dysfunction states is designed to illustrate the method's potential robustness, as well as its potential clinical use.

7.2.3 Waveform construction

The general shape of the time-varying elastance has three main sections: an exponential rise (A), a shoulder section (B) and an exponential decay (C), as shown in Figure 7.3. An invasive vena cava occlusion manoeuvre is assumed to be not available and thus $V_d = 0$ in Equation (7.1). The time-varying elastance is normalized to 1.0 (Suga et al., 1973).

The shape of the time-varying elastance waveform is formed from three known locations on the waveform; time, slope and height of the maximum rising gradient (t_1, $\dot{x}_1$,x_1) and maximum falling gradient (t_3, $\dot{x}_3$,x_3), (analogous to MPG and MNG respectively in Figure 7.1), and the height of the waveform's left shoulder, x_2, (analogous to LS, in Figure 7.1). These are seven of the eight values needed to reproduce the waveforms. The eighth is the height of the right shoulder (MX, in Figure 7.1) which is always unity. The seven variable values are found with correlations from points on the P_{ao} and P_{pa} waveforms, as described in Section 7.2.4.

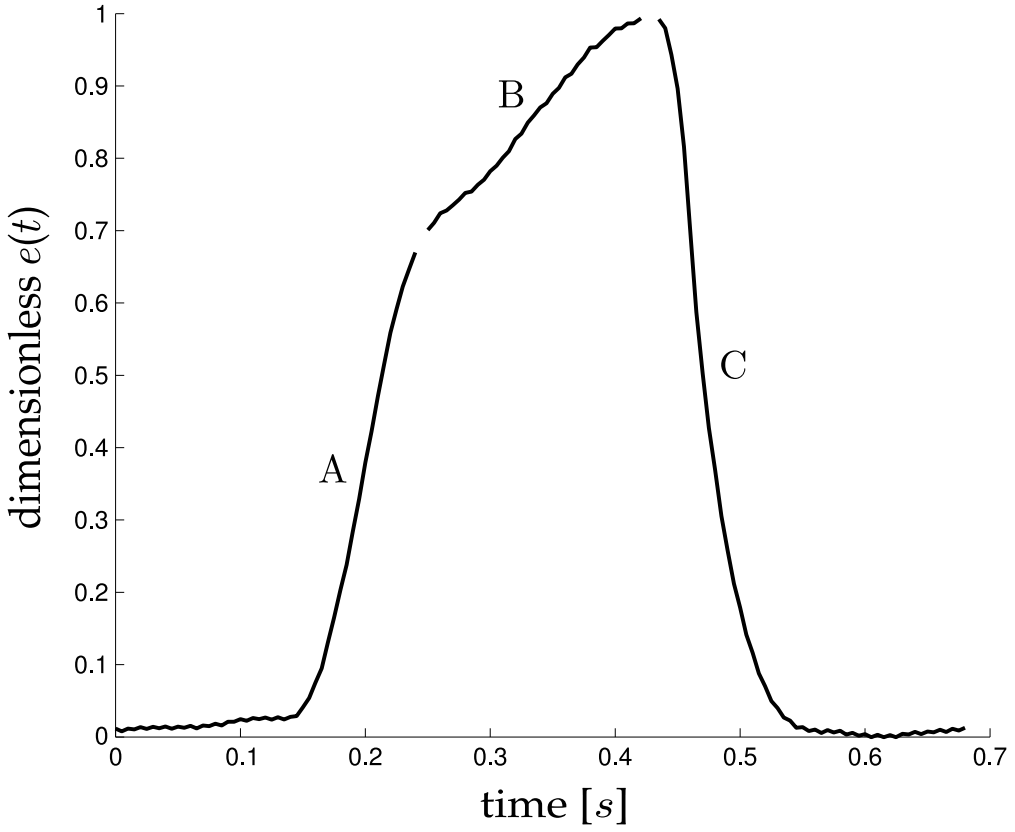

FIGURE 7.3: An example of a typical time-varying elastance broken into its main sections, an exponential rise (A), decay (C) and a near linear section in between (B).

The TVE waveform is assumed to closely fit two exponential functions (one rise and one decay) joined by a straight line and $e(t)$ is thus defined:

$$e(t) = \begin{cases} F_\alpha(t) & 0 < t < c_\alpha \\ \frac{(1-x_2)(t-c_\alpha)}{c_\beta - c_\alpha} + x_2 & c_\alpha < t < c_\beta \\ F_\beta(t) & c_\beta < t < period \end{cases} \tag{7.2}$$

where:

$$F_i = a_i \cdot e^{-b_i(t-c_i)^2} \tag{7.3}$$

and the coefficients of Equation (7.3), also seen in Equation (7.2), are fitted for a specific waveform, and are defined:

$$\begin{aligned} a_\alpha &= x_2 \\ b_\alpha &= -\frac{log(x_1/x_2)}{exp(log(-log(x_1/x_2)\cdot 2\cdot (x_1/\dot{x}_1))\cdot 2)} \\ c_\alpha &= -\frac{log(x_1/x_2)\cdot 2\cdot x_1 - \dot{x}_1\cdot t_1}{\dot{x}_1} \end{aligned} \tag{7.4}$$

where a_β, b_β and c_β are similarly defined by replacing subscript one with three and setting $x_2 = 1$.

This waveform model was chosen for its simplicity and shape, requiring a minimal amount of data to fit the model, while providing a model flexible enough to represent the real waveform. Due to the nature of the cardiovascular model that uses this function as an input, see Chapter 3, it is important that this waveform is continuously differentiable. A comparison of different TVE model shapes can be found in Section 4.5. From Section 4.5 it can be seen that the cardiovascular model is sensitive to the first derivative of the TVE model, making any straight line piecewise model less optimal than the chosen model.

7.2.4 Cardiac Elastance Correlations

The right and left ventricle elastances are constructed using Equations (7.2)–(7.4). However, the eight values that identify the separate elastances are found in different ways.

Table 7.1 shows three different types of correlations, the first of which (α) is the standard correlation used in most statistical analysis. The second two types, β and γ, are extensions to two and three variables, respectively.

TABLE 7.1: Reconstruction formulae for the three different types of correlations used to estimate the time-varying elastance.

Key	Re-construction Formula
α	$y = mx + c$
β	$y = m_1x_1 + m_2x_2 + c$
γ	$y = m_1x_1 + m_2x_2 + m_3x_3 + c$

The left time-varying elastance values are relatively straightforward to find, and all use the standard correlations, α, from Table 7.1. The right time-varying elastance is slightly harder to estimate, in part because there is no direct downstream access to the right ventricle similar to that of the left ventricle. This difficulty occurs because only timing information is taken from P_{pa}, which can be replaced with electrocardiography (ECG) and central venous pressure (CVP), as the P_{pa} waveform is not as commonly measured in an ICU. This self-imposed limitation makes the method more clinically applicable.

This limitation necessitates other means to estimate the required values on the right side, which is mostly done through the use of multi-variable correlations involving GEDV, and the estimated left time-varying elastance. GEDV is closely connected to the average volume in the right ventricle, and thus serves to add additional scaling. The specific correlations found between the left and right elastances are shown in Section 7.3.

7.2.5 Error calculations

The errors of the estimated time-varying elastance waveforms are defined using a distance metric between the true e_{true} and estimated e_{est} waveforms, after both waveforms have been normalised to the heart rate (producing a waveform confined to a 1x1 box). This normalisation allows the error metric to be consistent in all directions. This error metric is chosen over a more standard root mean square error (RMSE), to more accurately reflect the error between the waveforms. Due to the shape of these waveforms, a RMSE would over emphasise the error due to any slight timing mismatch

in the steep sections of the waveform. The error at each point on the approximated waveform is thus defined:

$$\delta_i = \min_{t \in [0,1]} \left\{ \sqrt{(t_i - t)^2 + (e_{est}(t_i) - e_{true}(t))^2} \right\}, \quad i = 1, \dots N \tag{7.5}$$

where N is the number of discrete points on the approximated waveform. The error of the estimated waveforms is represented by a median and a 90^{th} percentile of the values of δ_i in Equation (7.5), for both single waveforms and whole cohort errors. Where multiple waveforms are involved in a single error metric (such as those of the whole cohort), the δ_i values are concatenated into a single vector before the median and percentile errors are calculated. The values of δ_i in Equation (7.5), geometrically correspond to the distance from the point $(t_i, e_{est}(t_i))$ to the closest point in the curve $\{(t, e_{true}(t)), t \in [0,1]\}$, as illustrated in Figure 7.4. For practicality of computation, the real waveform is discretised, such that the number of points is greater than N. Due to this discretisation the error is over estimated, as the line between the two points is not the exact normal line of the point on the estimated waveform. This approximation is chosen over the exact calculation due to the fact that for a given point on the estimated waveform there is no guarantee that a point exists on the real waveform that is exactly normal to it.

7.2.6 Analyses

The time-varying elastances were estimated for every measurement taken at 30-minute intervals during the onset of the porcine cohort's cardiac dysfunction, in two different ways. First, using the correlations created with the entire cohort of nine pigs (both dysfunctions). Second, using the correlations determined from only the five (or four) pigs from the alternative dysfunction (pulmonary embolism or septic shock). These estimations were then evaluated against the true time-varying elastance to determine the error, as defined in Equation (7.5), which is then presented in summary statistics.

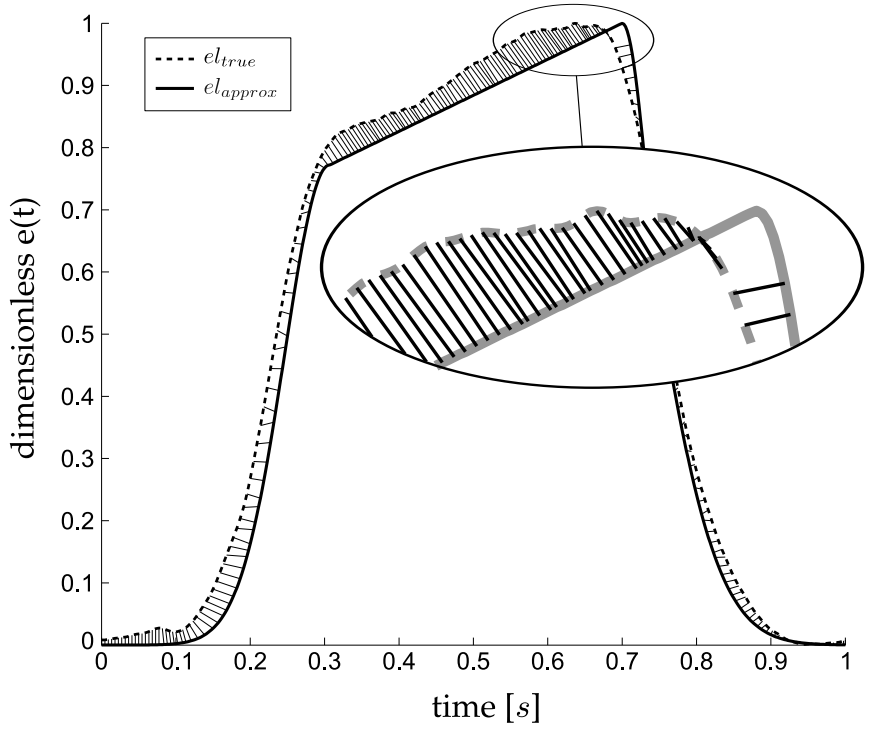

FIGURE 7.4: An example of the calculation of the error metric. At each point on the true waveform, the nearest point on the estimated waveform is located, and the distance between these two points is calculated (draw as solid lines). This is an approximation of the normal distance between the two waveforms. From this series of error values along the waveform, median and 90th percentile errors are calculated.

7.3 Results

7.3.1 Correlations

The correlations on both left and right sides, as defined in Figure 7.1, were good. The R values can be found in Tables 7.2 and 7.3 for the left and right, respectively. The best, median and worst correlations by R value are visualised in Figure 7.5 to show the best, the central tendency and the worst case range. The left side correlations are very strong, especially those estimating time. The right side correlations are weaker than the left, due to the approximations made by not using P_{pa} values, which increases clinical applicability. However, they are still strong enough to produce very accurate overall estimations of the continuous right time-varying elastance.

TABLE 7.2: Correlations for points on the left ventricle elastance. All points use correlation α defined in Table 7.1.

Estimate	Correlated to	R value	Coefficients
MPG_x (x_1)	$\frac{P_{ao}(MPG)_{\dot{x}}}{HR}$	0.71	$m = 2.521 \times 10^{-5}$ $c = 3.732 \times 10^{-1}$
MPG_t (t_1)	$P_{ao}(DMPG)_t$	0.99	$m = 1.007$ $c = 1.615 \times 10^{-3}$
$\dot{MPG}$ $(\dot{x}_1)$	$\frac{P_{ao}(MPG)_{\dot{x}}}{HR}$	0.94	$m = 4.126 \times 10^{-3}$ $c = 8.665$
MNG_x (x_3)	$P_{ao}(MNG)_t$	0.56	$m = 3.370 \times 10^{-1}$ $c = 4.886 \times 10^{-1}$
MNG_t (t_3)	$P_{ao}(DN)_t$	0.99	$m = 1.028$ $c = -9.148 \times 10^{-3}$
$\dot{MNG}$ $(\dot{x}_3)$	$log(\frac{P_{ao}(MNG)_{\dot{x}}}{HR})$	-0.77	$m = -5.510$ $c = 1.871 \times 10^{+1}$
LS_x (x_2)	$\frac{Pao(LS)_x}{HR \cdot MX_x}$	0.74	$m = 9.627 \times 10^{-2}$ $c = 5.867 \times 10^{-1}$

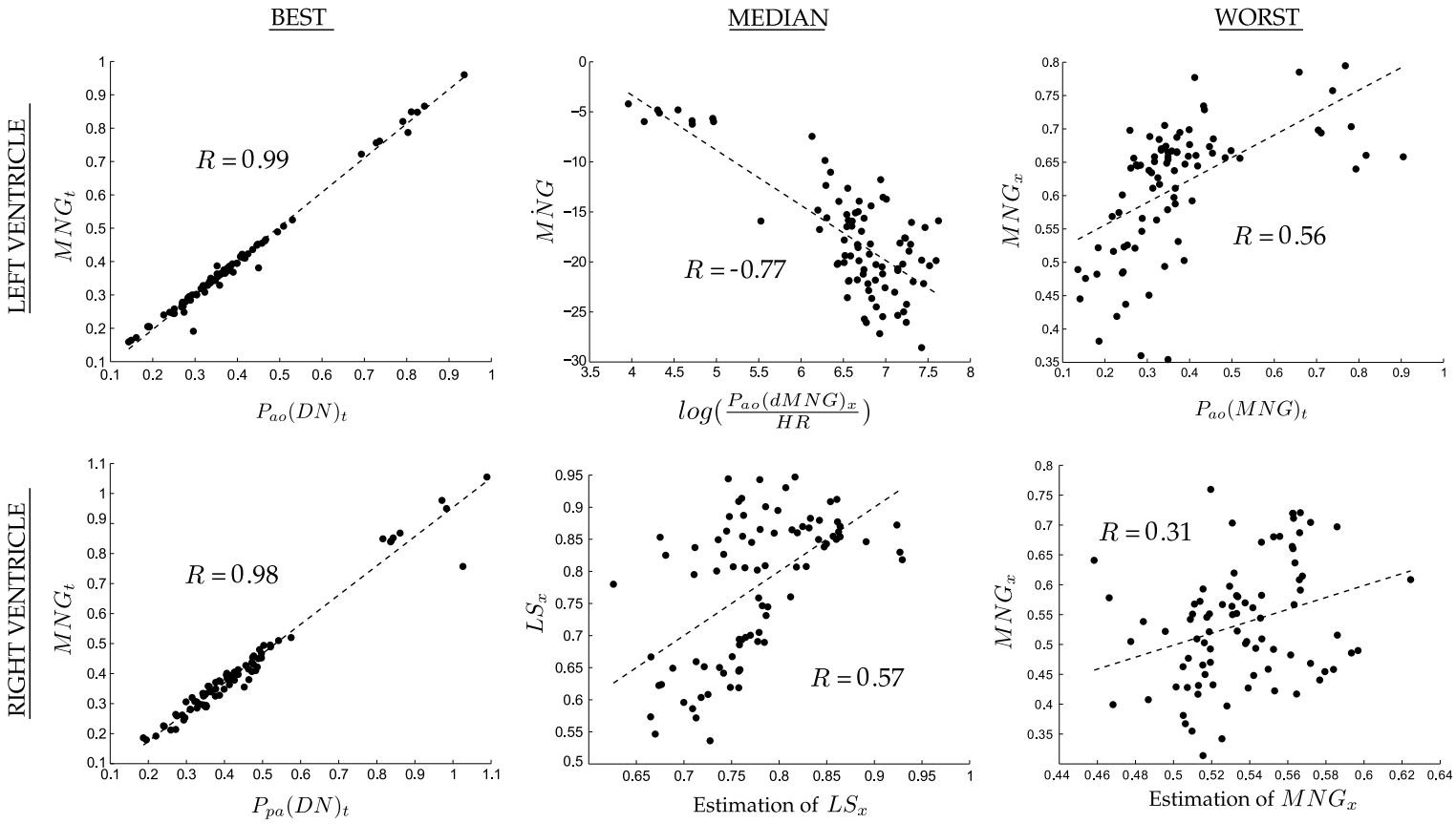

FIGURE 7.5: Three correlations are shown for each of the left (top row), and the right time-varying elastance (bottom row). These three represent the best (left), median (middle) and worst (right) correlations by R value. The median and worst case for the right time-varying elastance are multi-variable correlations, and therefore only a visualisation, so they cannot be used to read off data in the way a single variable correlations graph can.

TABLE 7.3: Correlations for points on the right ventricle elastance. The different formulae, for the column 'Type', are defined in Table 7.1.

Estimate	Correlated to	R	Type	Coefficients
MPG_x (x_1)	$GEDV$, $e_{lv}(MPG)_x$	0.42	β	$m_1 = -1.137 \times 10^{-3}$ $m_2 = 3.521 \times 10^{-1}$ $c = 4.524 \times 10^{-1}$
MPG_t (t_1)	$P_{pa}(MN)_t$	0.97	α	$m = 1.023$ $c = -4.102 \times 10^{-3}$
$M\dot{P}G$ ($\dot{x}_1$)	$GEDV$, $e_{lv}(MPG)_{\dot{x}}$	0.80	β	$m_1 = -1.286 \times 10^{-2}$ $m_2 = 6.446 \times 10^{-1}$ $c = 6.910$
MNG_x (x_3)	$GEDV$, $e_{lv}(MNG)_x$	0.31	β	$m_1 = 1.233 \times 10^{-3}$ $m_2 = 1.824 \times 10^{-1}$ $c = 2.348 \times 10^{-1}$
MNG_t (t_3)	$P_{pa}(DN)_t$	0.98	α	$m = 9.751 \times 10^{-1}$ $c = -2.081 \times 10^{-2}$
$M\dot{N}G$ ($\dot{x}_3$)	$GEDV$, $e_{lv}(MPG)_x$	0.37	β	$m_1 = -6.096 \times 10^{-2}$ $m_2 = 1.446$ $c = -4.331$
LS_x (x_2)	$GEDV$, $e_{lv}(LS)_x$, $e_{lv}(LS)_t$	0.57	γ	$m_1 = -2.054 \times 10^{-3}$ $m_2 = 3.209 \times 10^{-1}$ $m_3 = -3.538 \times 10^{-1}$ $c = 9.045 \times 10^{-1}$

7.3.2 Cardiac Elastances

The cross validation (described in Section 7.2.6) ensures robustness and independent validation. The results comparing directly measured $e(t)$ to estimated waveforms are listed in Tables 7.4 and 7.5 for both the correlations using all data, and for the independent cross validation using only correlations from the alternative dysfunction. The estimated waveforms are illustrated in Figure 7.6, with the 10^{th}, 50^{th} and 90^{th} percentile (by percentage error) estimated results. Table 7.4 shows the errors for the same estimated waveforms for pulmonary embolism and septic shock, in terms of the percentage error between clinically measured and estimated time-varying elastance.

TABLE 7.4: Percentage errors in the reconstructed driver functions, for pulmonary embolism and septic shock, using correlations derived from the whole cohort of 85 datasets.

	Pulmonary embolism		Septic shock	
	left	right	left	right
median	1.10%	2.10%	2.03%	2.87%
90^{th} percentile	3.35%	6.53%	5.62%	8.65%

Table 7.5 shows the errors using the correlations derived from one dysfunction to approximate the time-varying elastance of the alternative dysfunction. This last assessment cancels out any inherent dependence of the method, outlined in this chapter, on the dysfunction itself. Thus, it is a very rigorous and robust test.

TABLE 7.5: Percentage errors in the reconstructed driver functions, for pulmonary embolism and septic shock, for the independent cross validation using correlations derived from the alternative trial of cardiac dysfunction.

	Pulmonary embolism (based on septic shock)		Septic shock (based on PE)	
	left	right	left	right
median	1.26%	2.51%	2.54%	2.90%
90^{th} percentile	4.87%	7.07%	8.25%	9.30%

The results, in this case, show the method is independent of dysfunction, which is an extremely important result. For a method to reliably give insight into a specific patient's cardiac dysfunction, it must not rely on the patient having a specific cardiac dysfunction. It is also another validation of the accuracy and potential of this method, which gives further confidence that the method will generalise over a wider set of dysfunctions.

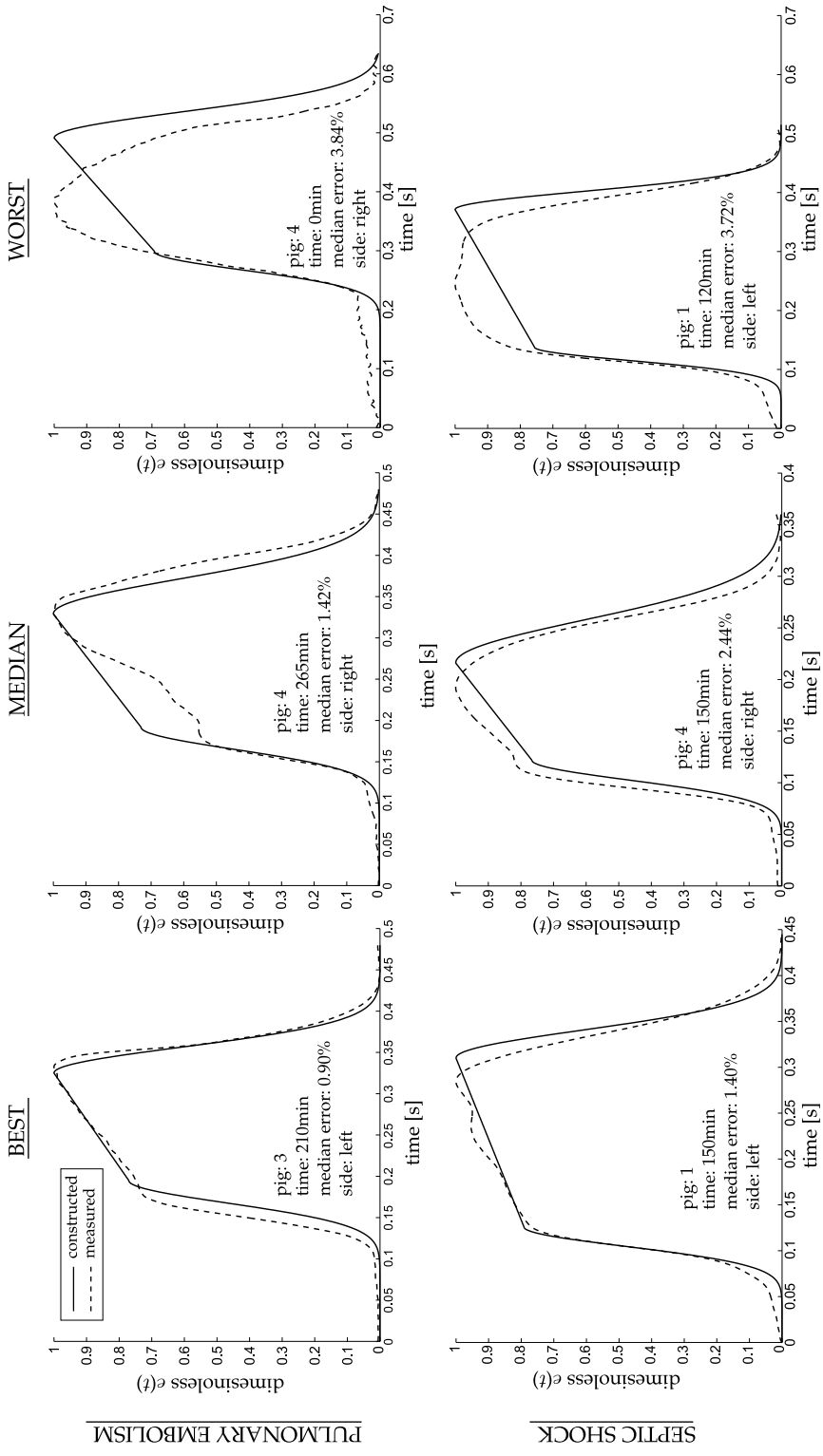

FIGURE 7.6: Results of the estimation of the time-varying elastance alongside the corresponding measured elastance, for both pulmonary embolism (top row) and septic shock (bottom row). For both conditions, the 10^{th}, 50^{th} and 90^{th} percentile cases, by median error, are shown in positions left, middle and right respectively.

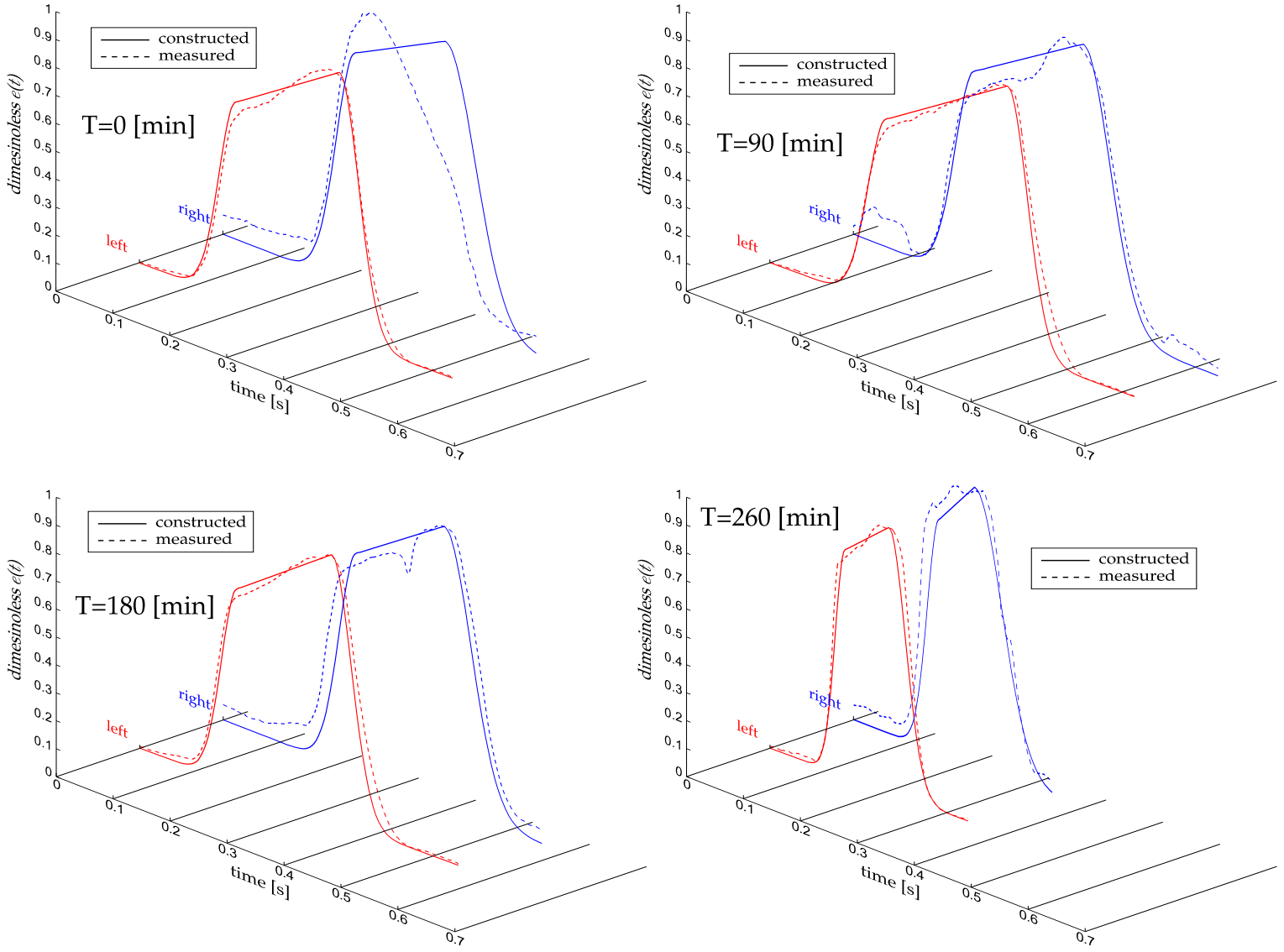

FIGURE 7.7: Four reconstructions of the left and right time-varying elastance, from the same pig, as the pulmonary embolism progresses from healthy at $t = 0$ to the end of trial at $t = 260$.

Figure 7.7 shows four reconstructed time-varying elastances versus the directly measured time-varying elastances, for pig number 4, at four different times during the onset of pulmonary embolism. In particular, the dramatic decrease in period at $t = 260$ min, is captured very well. Overall, the trends and basic shape are captured very well for the left and reasonably well for the right.

7.4 Discussion

A method for identifying time varying elastance of the left and right ventricles, was developed that does not require an occlusion manoeuvre to find V_d, and avoids invasive procedures to measure the left and right ventricle volumes and pressure. These time varying elastance functions can be used as the input driver function into a lumped parameter cardiovascular model. The method tracks the main, clinically important time features on the driver functions, such as the start and end of ejection. This method was validated on two sets of porcine data, which included multiple measurements of five pigs in which pulmonary embolism was induced, and four pigs in which septic shock was induced.

All models are approximations to capture observed physics, and thus all models offer advantages in understanding these observations as well as the limitations of any necessary assumptions made.

The approach taken to choose the mapping from the known metrics to the time-varying elastance, was based both on physiology and accuracy of the resulting time-varying elastance waveform. Thus, some mappings may not be the most obvious choice based on purely physiological reasoning. In particular, some of these mappings may appear to be counterintuitive. For example, although MPG and MNG appear to have symmetry of meaning in the aortic pressure waveform, this does not transfer into symmetrical meaning for cardiac energetics, and therefore they do not have symmetry in the chosen mappings.

The correlations that were used in the reconstructions presented in this chapter are generally strong. The time-based correlations are especially strong, as seen in, for example, the two left hand plots (”BEST“) in Figure 7.5, and lead to very good estimations of the waveform timing. There are also some rather poor correlations, the

worst of which predicts the value of the right ventricle TVE at the point MNG. This correlation has $R = 0.31$, and a correlation plot that barely shows any correlation at all. However, the final estimations of the waveform are not very sensitive to this value, and therefore can produce reasonably accurate waveform estimations from values of MNG_x that are error prone. However, it is important to note that the main results for this chapter are the errors of the reconstructed waveforms, rather than the presence of correlations, and these errors were generally small.

There is also a marked difference in the correlation's R values between the left and right sides. This is mostly due to not having direct access to the right side of the heart, since all but the timing of the P_{pa} waveforms have been neglected. Information about the right side of the heart is inferred from the left side. Although this results in significantly lower R-valued correlations (compared to the left), the waveform reconstructions are still good, with the errors averaging only 5 % higher than the left side for the cross dysfunction validation.

As would be expected from the correlations in Table 7.2, the timings of the reconstructed waveforms were very good, capturing the ascending and descending exponential sections very closely across a large change in cardiac condition, including an approximate doubling in heart rate. The biggest difference in the real and reconstructed waveforms usually appeared in the flat section (B of Figure 7.3). This error could be reduced by using a higher order polynomial or model. However, simulation has shown that this error is not of significant importance to the existing cardiovascular model (Starfinger et al., 2008a).

The specific waveform for TVE was chosen as a balance between accuracy and complexity. A model (waveform shape) was needed that provided enough information to capture the necessary cardiac dynamics, while remaining as simple as possible. The simplest waveform shape, that could approximate the time-varying elastance, is that of three, non-zero, straight lines. To fit this model, four points would be required. Equivalently, two points with associated gradients and two heights — points with free 'x' coordinate — which is the currently used data, see Figure 7.1. However, for the same amount of information and no additional computational complexity, a model of two exponential curves and one straight line (the chosen model) can be fitted. Furthermore, this model is continuously differentiable, which can be computationally advantageous

in numerical simulation. This more complex shape provides more accurate results, without adding complexity to the process of fitting. Beyond this model structure, more complex models would require additional information to be found from the pressure waveforms.

Finally, it is worth noting that the overall philosophy and approach of this research is to add complexity only as required to capture and predict clinical data, and thus to keep the model as simple as possible. The straight line approach would also have the benefit of simplifying any semi-analytical solution to speeding up the simulations. However, until such a semi-analytical approach is developed, the current exponential formulation is used as it provides more accuracy for non additional cost.

For simplicity of the model, V_d was set to zero, which is a limitation of the current approach. However, even with this discarded parameter, the model is still able to capture the necessary dynamics, and provide useful additional information to an ICU clinician based on the trends observed in TVE shape relative to this assumption. Having an accurate V_d value in addition would add useful information, but is not identifiable from the data available without added invasive sensors.

Another limitation of the chapter is the small number ($N = 9$) of porcine subjects, although there were a large number ($N = 85$) of data sets used, and only two dysfunctions. However, this chapter serves as a proof of concept. In particular, the results are intended to justify the methods and thus a larger, complete prospective validation.

Although this study used the pulmonary artery pressure, the points found in the pulmonary artery pressure waveform could be estimated using the central venous pressure and ECG. Thus, there is the potential to construct the driver functions without any knowledge of the right side of the heart. This option would avoid using pulmonary artery pressure measurements, which are less commonly available in an ICU than aortic pressure measurements. This study did not have access to CVP and ECG data for the porcine cohort so used pulmonary artery pressure instead. Future work will investigate these clinically relevant extensions to minimise invasiveness, including the application of the methods within an ICU setting.

7.5 Summary

This chapter describes a method that has huge clinical potential. Currently, disease states like pulmonary embolism and septic shock are difficult to diagnose accurately and reliably due to the lack of useful information accessible to the clinician. With access to the left and right ventricular time-varying elastance waveforms, more information can be processed in a meaningful and productive way, resulting in better diagnostic and treatment decisions. This is achieved through a method that uses only currently available metrics in the ICU, and thus is no more invasive (no additional risk) than standard clinical practice.

Chapter 8

Clinical diagnostics

This chapter looks at the time-varying elastance and pressure waveforms for their intrinsic clinical value outside of their use in the cardiovascular model. Three metrics are estimated that have clinical relevance for the cardiac dysfunctions of pulmonary embolism and septic shock.

8.1 Introduction

Acute cardiovascular dysfunctions, like pulmonary embolism (PE) and septic shock, severely alter cardiovascular system (CVS) haemodynamics. These changes can be seen — through measurements made by catheters placed around the heart — as changes in pressure and flow, and reflect the dynamic changes in the balance of preload and afterload, indicating an altered cardiac energetic state (Weber and Janicki, 1979; Ross, 1976). However, to access much of this information, the waveforms from the catheters need to be processed or modelled in ways beyond what is currently available. Through such processing, energetic metrics can be obtained that would be far too invasive to measure directly, offering insight beyond what is normally available.

If more of the cardiac energetic metrics could be captured from the data typically obtained from catheters already present in an ICU setting. Such an approach would enable the currently unrealised clinical potential of these catheters to be realised, adding significant new insight. This chapter presents a method to estimate three of

these metrics: afterload, systemic vascular resistance (R_{sys}), and pulmonary vascular resistance (R_{pul}).

These three metrics are useful in the diagnosis of pulmonary embolism, in which R_{pul} increases (Goldhaber and Elliott, 2003; Elliott, 1992), and for septic shock where R_{sys} commonly decreases (Parrillo et al., 1990; Annane et al., 2005), and is linked, by definition, to a decrease in afterload. The ability to track these three metrics in real time, at the bedside, would give valuable non-additionally-invasive information to the clinician, compared to what is currently available, and potentially decrease the time taken to reach a diagnosis, increase the reliability of that diagnosis, and ultimately improve patient outcomes through better management.

8.2 Methods

The overall approach in this study was to gather as much information as possible, from a proven ventricular time-varying elastance approximations (Stevenson et al., 2012b) and the aortic pressure waveform, that would yield more information about the current cardiac dysfunction of the patient. The study was conducted on experimental data taken from a cohort of nine porcine subjects. These nine subjects were divided into two groups with five pigs in which pulmonary embolism was induced (Desaive et al., 2005; Ghuysen et al., 2008). Septic shock was induced in the remaining four pigs, these were treated with haemofiltration starting at two hours (Lambermont et al., 2003). Both studies were under the control of the Ethics Committee of the Medical Faculty of Liege, Belgium.

In all subjects except one, measurements were taken every 30 minutes for the duration of the trial. The exception was a 60-minute interval for one pig in the septic shock cohort. For each signal, 10 consecutive heartbeats were recorded and averaged, to a single heartbeat, and stored as a representative of that waveform, at that time. In total, 51 heartbeats for the pulmonary embolism group, and 34 for the septic shock group, were saved. In each case, the following relevant measurements were taken: aortic pressure (P_{ao}), pulmonary artery pressure (P_{pa}), left and right ventricle volume (V_{lv}, V_{rv}), and left and right ventricle pressure (P_{lv}, P_{rv}). Both the aortic and pulmonary

artery pressure were measured using catheters, along with direct measurements of the right and left ventricle pressure and volume.

The captured data includes the whole range of each dysfunction from healthy to the fully developed disease state. Thus, this dataset provides good observation of the progression of the disease state. For full experimental details see (Desaive et al., 2005; Ghuysen et al., 2008; Lambermont et al., 2003).

8.2.1 Time-varying elastance

From the data gathered, an approximation of the time-varying elastance, e_{lv}, was calculated and presented in detail in Chapter 7. The pressure waveforms were processed to find the location of specific features (Stevenson et al., 2012a), as detailed in Chapter 6. Once these locations are known, a continuous time-varying elastance can be constructed that very closely approximates invasively measured ventricular elastance. This approximation is achieved through correlations that map the points on the pressure waveforms to points on the cardiac elastance waveform, through which a continuous curve can be drawn. The points on the aortic pressure waveform and a high-level view of this method is shown in Figure 8.1. Again, details are presented in Chapters 6 and 7.

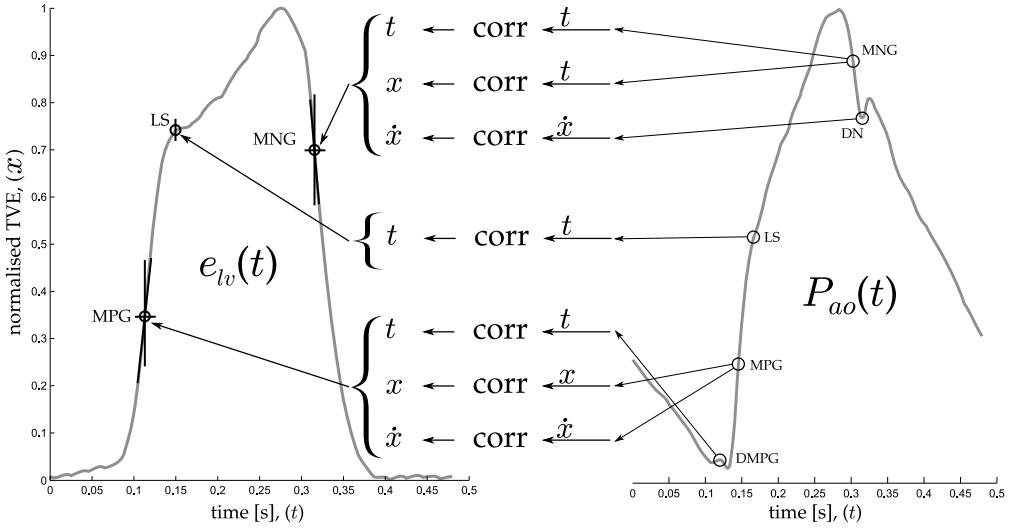

FIGURE 8.1: The left time-varying elastance, e_{lv}, and P_{ao} showing the relationship between them and specific points on both waveforms.

8.2.2 Dysfunction markers

The three properties, afterload (AL), systemic vascular resistance (R_{sys}) and pulmonary artery resistance (R_{pul}), change with both septic shock and pulmonary embolism. However, none of these metrics are known, or directly and easily measurable, in an intensive care setting. The true values for these metrics were calculated from the pressure waveforms.

In particular, the true value of afterload (AL) was determined as the slope on the pressure-volume (PV) loop from the point of end-diastole (mapped vertically down to the abscissa) to the point of end-systole, as shown in Figure 8.2. Both end-diastole and end-systole were located from the crossing points of the measured left ventricle and aortic pressure waveforms.

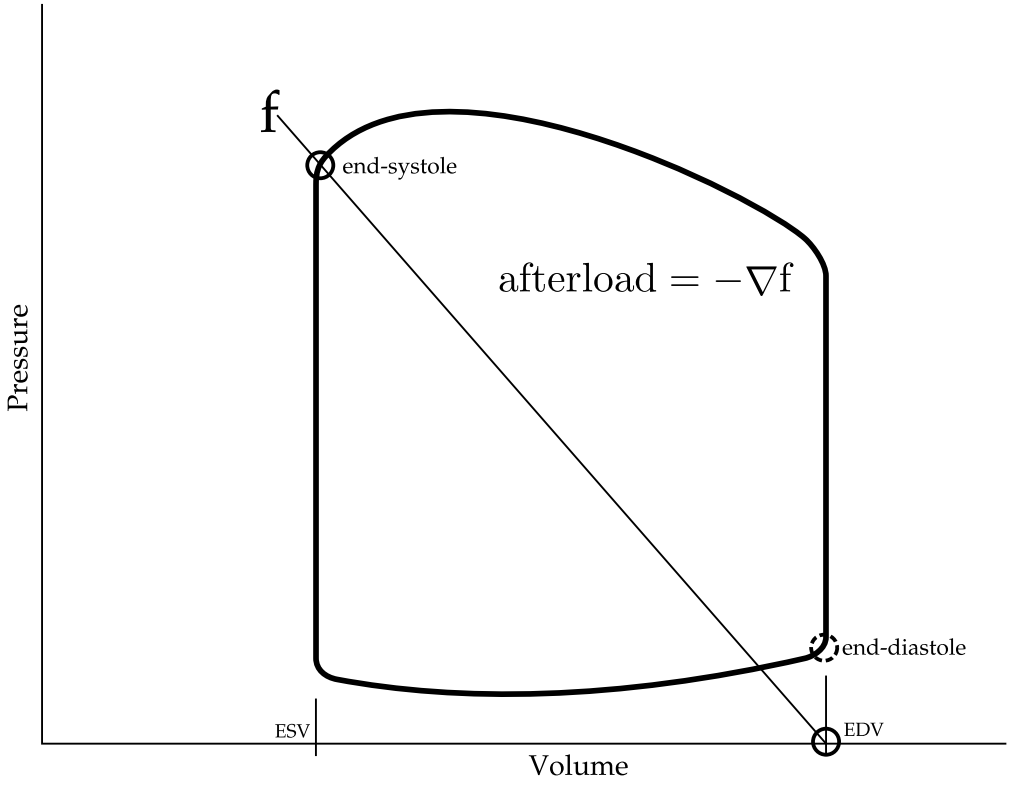

FIGURE 8.2: Method for directly measuring a value for afterload on the left ventricle pressure-volume loop.

The value for R_{pul} is defined using a model-based measure (Starfinger et al., 2008a):

$$R_{pul} = \int_{t=0}^{period} \frac{P_{pa} - P_{pu}}{Q_{pul}} \mathrm{d}t \tag{8.1}$$

where, P_{pu} is the pressure in the pulmonary vein, Q_{pul} is the flow through the pulmonary artery, and thus the integral of Q_{pul} over one heartbeat is the right stroke volume (RSV). The pulmonary vein pressure was not measured in the porcine cohort, and as an approximation has been set to 0. Thus R_{pul} becomes:

$$R_{pul} = \frac{1}{RSV} \cdot \int_{t=0}^{period} P_{pa}(t)\ \mathrm{d}t \tag{8.2}$$

This approximation should capture all necessary trends for this analysis.

R_{sys} is defined in a similar way to R_{pul} (Starfinger et al., 2008a):

$$R_{sys} = \int_{t=0}^{period} \frac{P_{ao} - P_{vc}}{Q_{sys}} \mathrm{d}t \tag{8.3}$$

where, P_{vc} is the pressure in the vena cava, Q_{sys} is the flow through the aorta, and thus the integral of Q_{sys} over one heartbeat is the left ventricle stroke volume (LSV). The vena cava pressure is calculated as the pressure in the right ventricle at the time of end-systole. Thus, R_{sys} becomes:

$$R_{sys} = \frac{1}{LSV} \cdot \int_{t=0}^{period} P_{ao}(t) - P_{rv}(\text{end-systole})\ \mathrm{d}t \tag{8.4}$$

8.2.3 Analysis

To find the correlations for the three metrics under consideration, a grid search was performed computing all correlations between these three metrics and data that can be typically obtained in an ICU setting. The data from the ICU includes: the aortic pressure waveform, processed as outlined in (Stevenson et al., 2012a); and the estimated time-varying elastance (Stevenson et al., 2012b). From the resulting correlations, one was chosen for each to the three metrics, R_{pul}, R_{sys} and afterload that best matched the following criteria:

1. high correlation using data from the related dysfunction
2. good correlation using data from the other dysfunction
3. the correlation produces estimations which track important characterises of both dysfunctions

4. the correlation does not erroneously confuse characteristics of the two dysfunctions
5. the correlation equation is physiologically justifiable

8.3 Results

8.3.1 Correlation for Afterload (AL)

From the grid search results for afterload, the following metrics show very good accuracy in tracking afterload in the septic shock cohort:

$$AL \quad \propto \quad GEDV \cdot \frac{\int_{t=0}^{period} P_{ao}\, \mathrm{d}t}{LSV \cdot \text{end-systole}_t} \tag{8.5}$$

where $GEDV$ is the global end-diastolic volume, calculated as the sum of the maximum left and right ventricle volumes. This correlation yielded $R^2 = 0.72$ for the combined pulmonary embolism and septic shock cohorts.

Afterload is thus approximated:

$$AL_{approx} = m \cdot GEDV \cdot \frac{\int_{t=0}^{period} P_{ao}\, \mathrm{d}t}{LSV \cdot \text{end-systole}_t} + C \tag{8.6}$$

where C and m are the coefficients of the correlation, where $C = -1.08$ and $m = 8.43 \times 10^{-3}$ from the data in this analysis.

Figures 8.3 and 8.4 show the correlations and their straight line estimators for the pulmonary embolism and septic shock cohort, respectively. The estimations for afterload are shown in Figure 8.5.

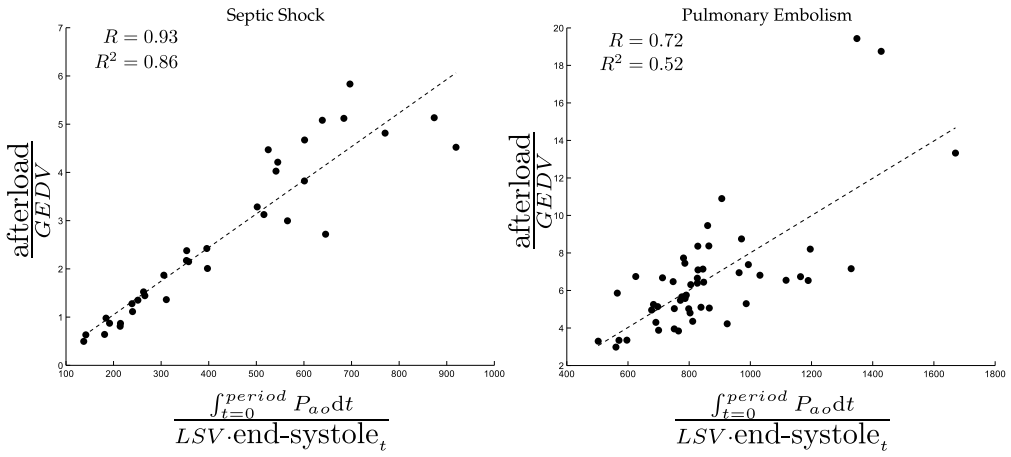

FIGURE 8.3: The correlation for estimating afterload, in the septic shock and pulmonary embolism cohorts separately.

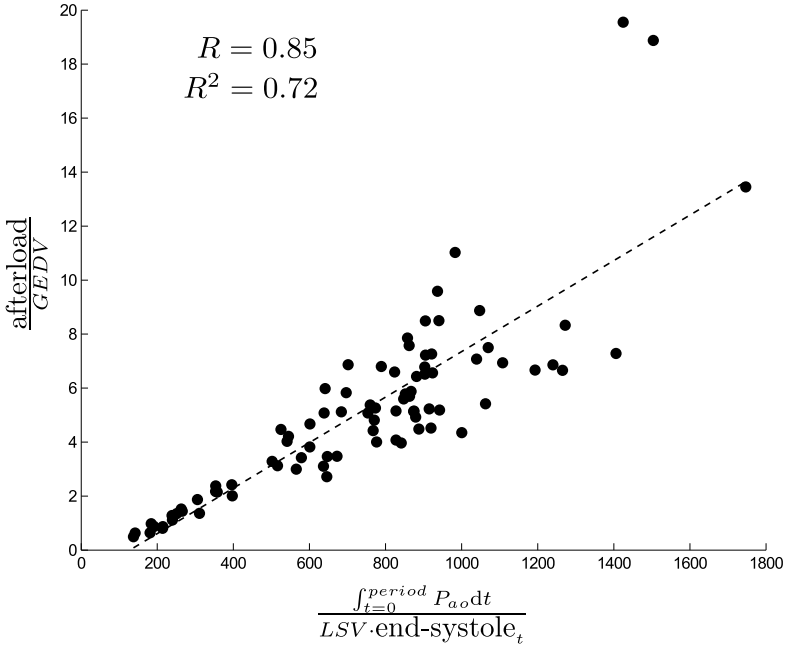

FIGURE 8.4: The correlation for estimating afterload in the combined septic shock and pulmonary embolism cohorts.

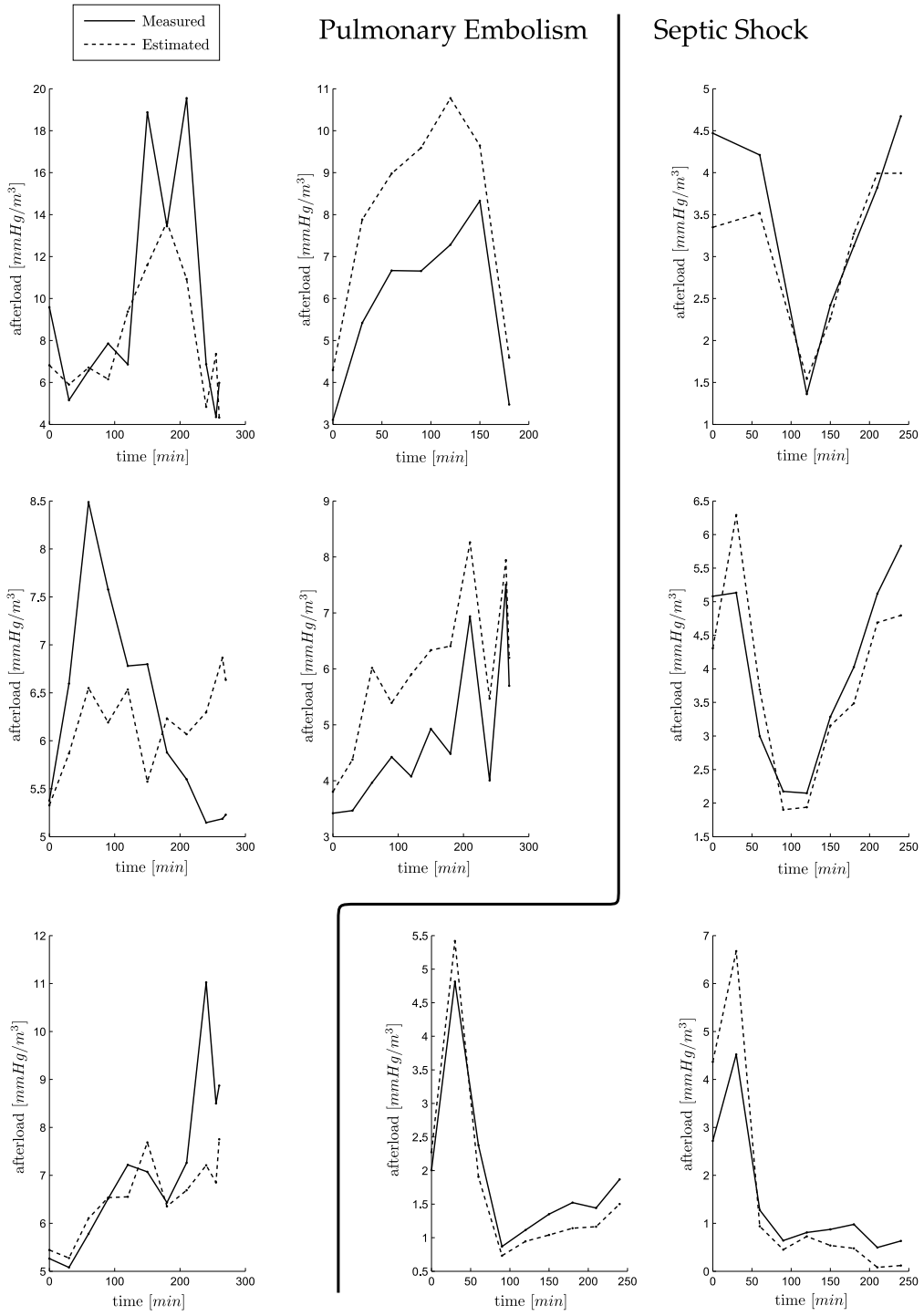

FIGURE 8.5: Estimating afterload on the pulmonary embolism and septic shock cohorts, based on estimators created on the combined cohort, of Figure 8.4.

8.3.2 Correlation for systemic resistance (R_{sys})

The correlation that produced the best results for R_{sys} was:

$$R_{sys} \quad \propto \quad period \cdot \frac{P_{ao}(DMPG)}{LSV} \tag{8.7}$$

where $DMPG$ is defined in Figure 8.1, where $R^2 = 0.84$ for the combined pulmonary embolism and septic shock cohorts.

The approximation of R_{sys} is thus defined:

$$R_{sys,approx} = m \cdot period \cdot \frac{P_{ao}(DMPG)}{LSV} + C \tag{8.8}$$

where C and m are the coefficients of the correlation, where $C = -0.0522$ and $m = 0.916$ for these cohorts.

Figures 8.6 and 8.7 show the correlations and their straight line estimators for the pulmonary embolism and septic shock cohort, respectively. The estimations for R_{sys} are shown in Figure 8.9.

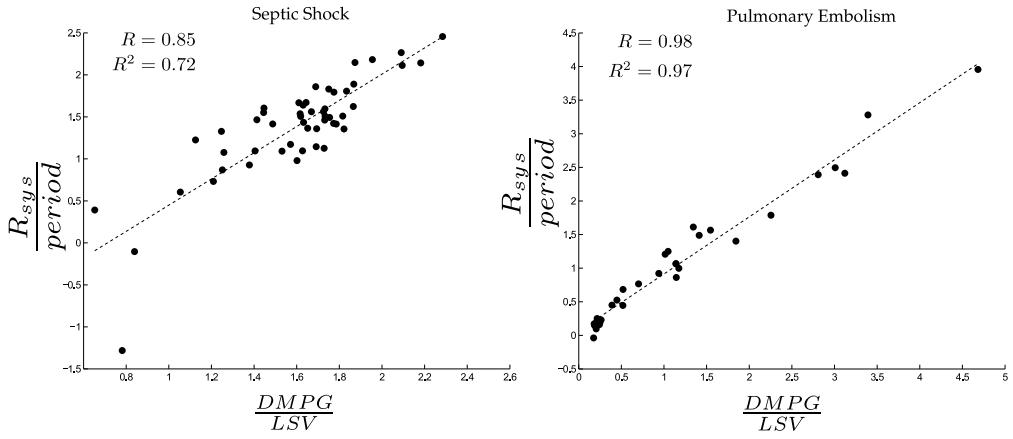

FIGURE 8.6: The correlation for estimating R_{sys}, in the septic shock and pulmonary embolism cohorts separately.

This estimator, for R_{sys}, can be justified from the CVS model, outlined in Chapter 3. Equation (8.4) can be further simplified to:

$$R_{sys} = \frac{t}{LSV} \cdot (\overline{P_{ao}} - P_{rv}(\text{end-systole})) \tag{8.9}$$

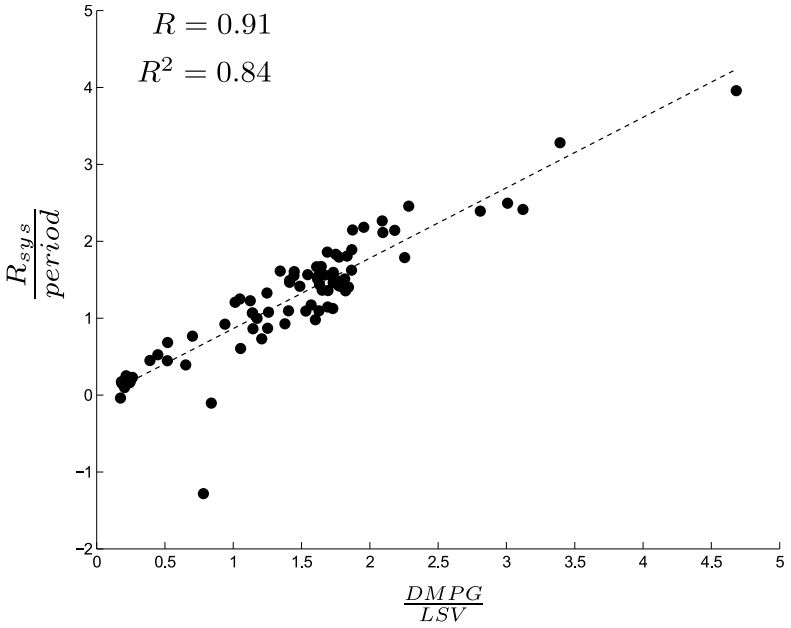

FIGURE 8.7: The correlation for estimating R_{sys} in the combined septic shock and pulmonary embolism cohorts.

where the over-bar represents a mean value of P_{ao}. Equation (8.9) closely resembles the form of the correlation in Equation (8.8), especially since there is an extremely strong correlation between the mean aortic pressure, $\overline{P_{ao}}$, and the point $P_{ao}(DMPG)$, which is shown in Figure 8.8.

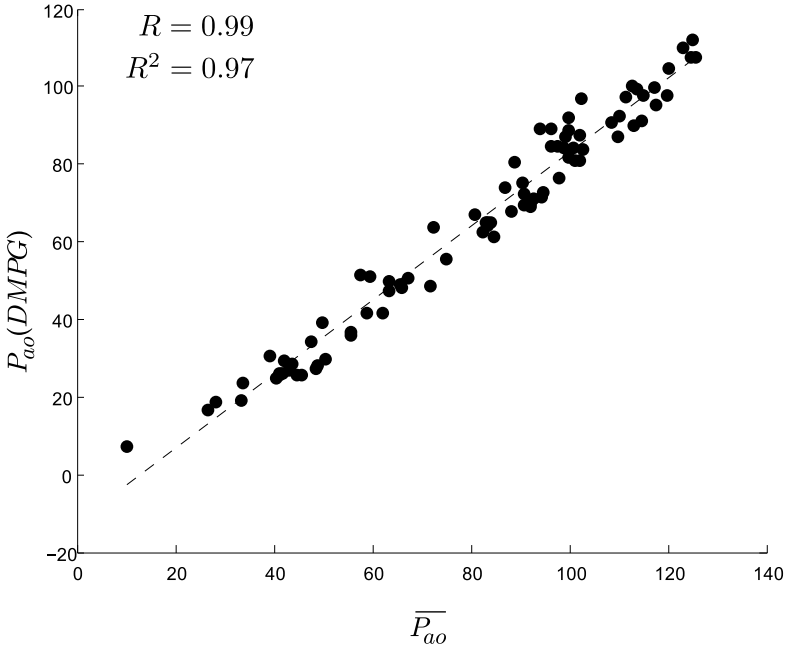

FIGURE 8.8: The correlation between the mean aortic pressure and the point $P_{ao}(DMPG)$, with a correlation coefficient of $R = 0.985$.

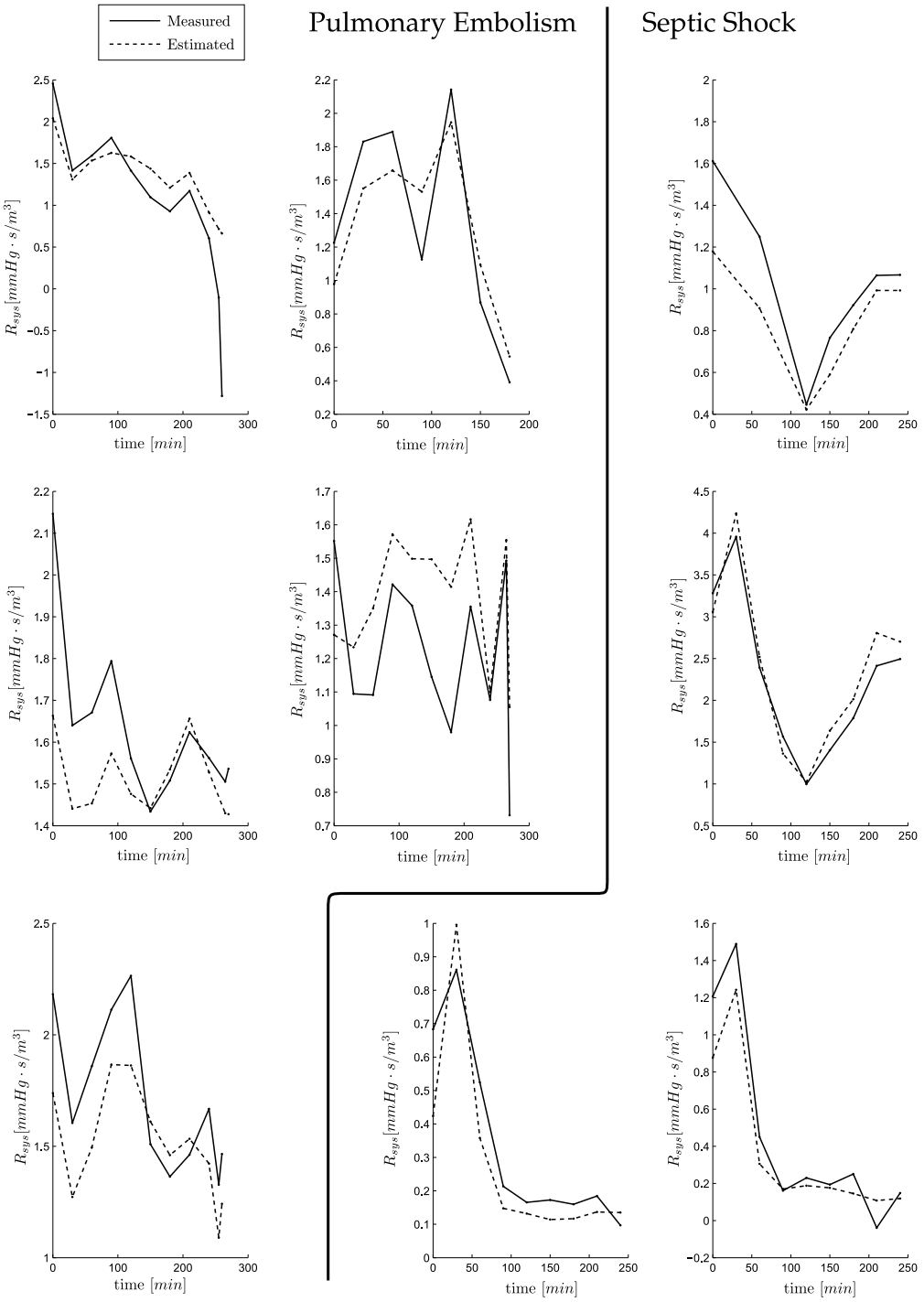

FIGURE 8.9: Estimating R_{sys} on the pulmonary embolism and septic shock cohorts, based on estimators created on the combined cohort, of Figure 8.7.

8.3.3 Correlation for pulmonary resistance (R_{pul})

The correlation that produced the best results for R_{pul} was:

$$\frac{R_{pul}}{period^2} \propto \frac{e_{lv}(MPG)}{RSV \cdot period} \tag{8.10}$$

where MPG is defined in Figure 8.1, where $R^2 = 0.536$. Thus, the approximation of R_{pul} is defined:

$$R_{pul,approx} = C_1 + C_2 \cdot \frac{e_{lv}(MPG)}{RSV \cdot period} \tag{8.11}$$

where:

$$\begin{aligned} C_1 &= period^2 \cdot C \\ C_2 &= period^2 \cdot m \end{aligned} \tag{8.12}$$

and C and m are the coefficients of the correlation, where $C = 0.29$ and $m = 44.2$ for these cohorts.

Figures 8.10 and 8.11 show the correlations and their straight-line estimators for the pulmonary embolism and septic shock cohort respectively. The estimations for R_{pul} are shown in Figure 8.12.

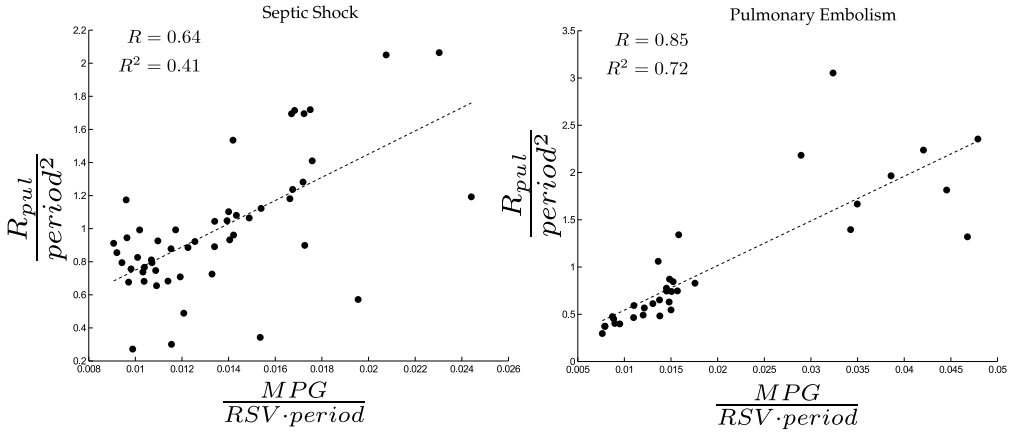

FIGURE 8.10: The correlation for estimating R_{pul} in the septic shock and pulmonary embolism cohorts, separately.

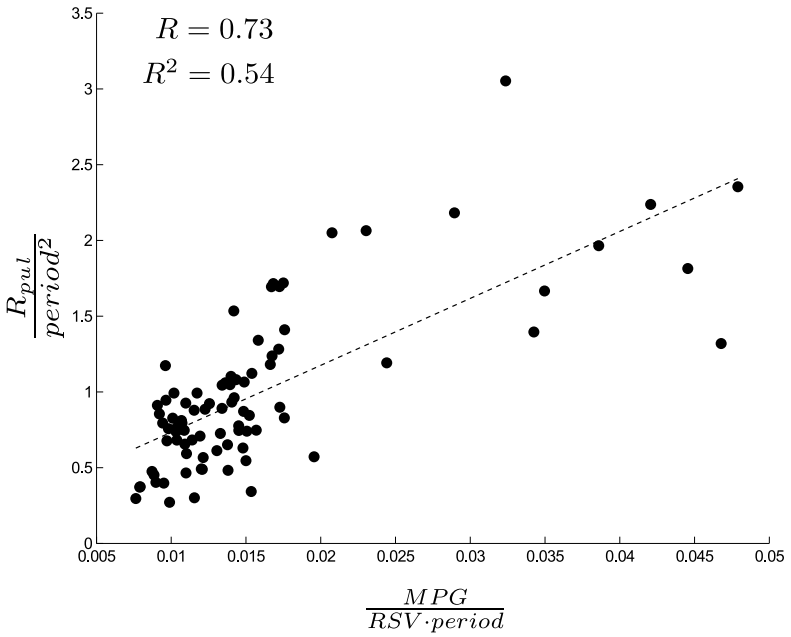

FIGURE 8.11: The correlation for estimating R_{pul} in the combined septic shock and pulmonary embolism cohorts.

This estimator, for R_{pul}, can be justified from the CVS model, outlined in Chapter 3. Equation (8.1) can be alternatively simplified to:

$$R_{pul} = \frac{t}{RSV} \cdot (\overline{P_{pa}} - \overline{P_{pu}}) \tag{8.13}$$

where the over-bar represents a mean of P_{pa} and P_{pu}. This equation and the correlation shown in Equation (8.10), are linked by the assumption that $e_{lv}(MPG)$ is proportional to the difference in mean aortic and pulmonary vein pressure.

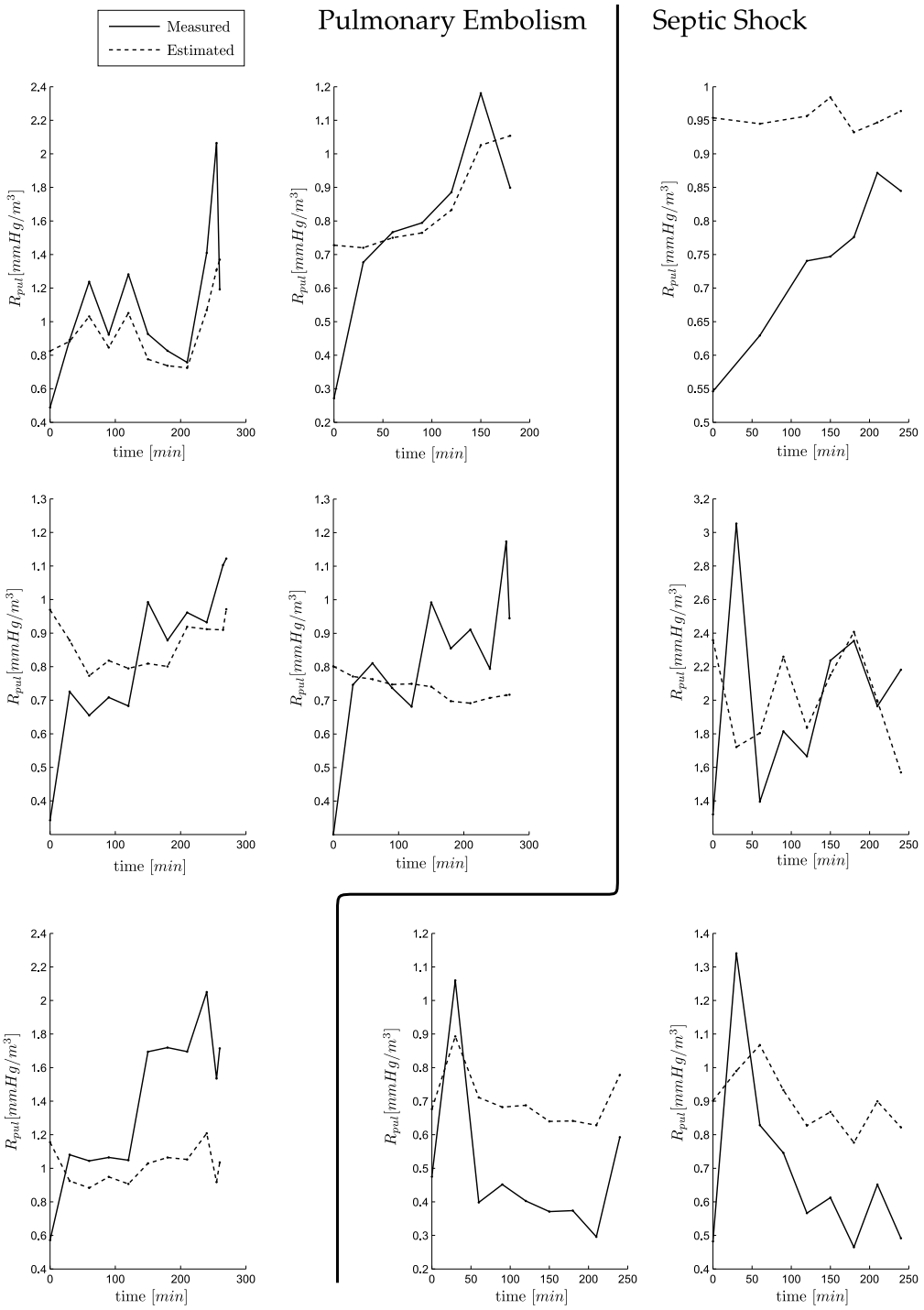

FIGURE 8.12: Estimating R_{pul} on the pulmonary embolism and septic shock cohorts, based on estimators created on the combined cohort, of Figure 8.11.

8.4 Discussion

The results presented in this chapter, provide good, but not perfect, estimations of afterload, R_{sys} and R_{pul} over a wide range of disease states and their evolution. The correlations are based on readily available measurements (aortic pressure, stroke volume and GEDV) and estimates of elastance (e_{lv}). They are also generic and applicable across both cohorts with their different presentation. Thus, errors in the resulting estimates are acceptable, given overall good results of $R^2 = 0.72$, 0.84 and 0.54, because these values are not at all available otherwise.

It should be noted that all three correlations require an estimate or measurement of stroke volume for each side of the heart (RSV and LSV). In most cases, the left and right stroke volume should be the same or very similar, in which case RSV and LSV could be replaced with the more generic stroke volume that is often available in the ICU from PiCCO and similar approaches. However, the subjects in this trial showed significant differences between the two stroke volumes and thus, for this presentation, they have been kept separate.

The correlations presented in this chapter were chosen as those that best matched the most critical dysfunction, while still being able to match the trends for the other dysfunction. However, there is justification from the clinically validated CVS model of Chapter 3 as well. In particular, the correlations for R_{pul} and R_{sys} can be partially derived from the model itself.

A distinction can be made between the two disease states from the estimations shown in Figures 8.5, 8.9 and 8.12. A sharp drop is clearly visible in all the septic shock subjects in both afterload and R_{sys}, but importantly, it occurs in none of the pulmonary embolism subjects. It could therefore be assumed, that if this sharp drop is seen, the subject has a higher probability of having septic shock, despite potentially similar outward presentation in terms of reduced cardiac output and stroke volume.

Similarly, for the pulmonary embolism cohort, a steady but significant increase in the estimated R_{pul} is observed, while for the septic shock cohort, R_{pul} averages out to be steady with a slight decline. These results can be seen in Figure 8.12.

The three parameter estimations presented in this chapter are all very useful metrics to have access to as a clinician, for both diagnosis and management. For example, if R_{sys} is tracked in real time, it would enable accurate determination of when vasopressor therapy should begin, and based on responsiveness to that therapy, R_{sys} could help optimise dosage. Importantly, none of these metrics are available currently, without extensive additional invasive procedures, so this approach would be a major step forward.

The main effect of these metrics is their relative change over time, and this behaviour is captured very well in almost all cases. The two exceptions were for the third and fourth subjects in the pulmonary embolism cohort. For the third subject for afterload, shown in Figure 8.5 (column 1, row 2), although the estimation in this specific case does not follow the trend, the estimation will not be confused with sepsis, as afterload does not fall sharply. Hence, in combination the three metrics are effective and specific in monitoring and diagnosis. For the fourth subject for R_{pul}, shown in Figure 8.12 (column 2, row 2), the exception is more troubling. This subject presents in a similar way to those with septic shock, thus an additional factor must be called upon to distinguish between pulmonary embolism and septic shock, in this case.

The diagnostic value of this information is seen when comparing the two cardiac dysfunctions, and the relative trend lines for both parameters. In pulmonary embolism, R_{pul} will increase due to the obstruction in the pulmonary artery. However, R_{pul} also increases in septic shock, usually at a slower rate. Given the results in this chapter, R_{pul} does increase more for pulmonary embolism, but not by a significant margin. It is only when R_{pul} is combined with afterload and R_{sys}, that the distinction can be clearly made between the two cardiac dysfunctions.

Similarly for the septic shock subjects, both afterload and R_{sys} show rapid decreases in the early stages, after which they level off. This recovery is most likely due to the effects of haemofiltration (Revie et al., 2013; Lambermont et al., 2006). Compared to this initial drop in afterload and R_{sys} for septic shock, the metrics for pulmonary embolism show a gradual but distinct rise, but, most notably, they do not show the initial drop as seen in septic shock.

A larger cohort would be needed to fully validate this study. However, the results presented demonstrate the use of non-additionally-invasive procedures to extract useful

information that would otherwise be unknown to an intensive care clinician. They may thus increase the value of any catheters that may be present, which are currently increasingly out of favour as the data they provide cannot be effectively applied.

As discussed earlier, this approach is not without limitations. The differences between the two dysfunctions studied, namely pulmonary embolism and septic shock, are distinct in most instances but not all. This lack of global clarity calls for additional information and characterisations to fully differentiate between the two dysfunctions, and to achieve potentially more accurate correlations. However, even with perfect correlations, the resulting data is only as good as the estimations of the CVS model, which, itself cannot fully distinguish between the two dysfunctions with these metrics alone.

8.5 Summary

This chapter has presented a method to estimate afterload, systemic vascular resistance and pulmonary vascular resistance, using measurements that are commonly available in an intensive care setting without any additional invasive procedures. These estimations are accurate in their relative trends, and can distinguish between these two common dysfunctions despite similar initial presentation. Hence, they can, in combination, provide useful addition information to the diagnosis and management of pulmonary embolism and septic shock.

In essence, although the presented correlations cannot be relied upon in isolation, they provide additional information to a clinician. They thus add effective information to develop an evolving picture of statistical probability for a final diagnosis of cardiac dysfunction.

Chapter 9

Conclusions

This chapter draws together the research presented in this dissertation, including the motivation and main achievements.

9.1 Background and motivation

The ICU treats the most critically ill patients in the hospital and deals with a diverse set of cardiovascular and other physiological dysfunctions. The nature of the ICU means that decisions on diagnosis and treatment are time critical, and often their accuracy is the difference between life and death. Therefore, it is of utmost importance that the clinical staff are presented with a full and clear picture of the state of their patients, including the cardiovascular state, which is troubled by complex interactions and reflex responses that can mask dysfunction. One method of simplifying the wealth of information available through monitoring, is to create a computer model of the patient's cardiovascular state. Such a model is presented in this research that accurately represents a specific patient's cardiovascular state, giving the clinician clear and more understandable information.

The main thrust of this research is to provide this model with a necessary input waveform, the time-varying elastance, that would be too invasive to actually measure in an intensive care unit. The success of the estimation of this waveform resulted in the use of the time-varying elastance on its own, separate from the cardiovascular model, to give clinically relevant information. Therefore, this research has achieved two major

goals: increasing the accuracy of the cardiovascular model through a patient-specific time-varying elastance waveform, and providing an accurate estimation of the time-varying elastance for use directly in understanding and tracking the state of a patient's heart.

9.2 Main achievements

A small but significant result of this research is the approach developed to process the noisy and variable measured waveforms for use in the estimation of the time-varying elastance. Without this method, a real-time estimation of the time-varying elastance would not have been possible. The method is described in detail in Section 6.3, and involves a shear transformation of specific sections of the waveform in question, resulting in the required point becoming a global maximum or minimum of the transformed shape. In other words, a hard-to-find "shoulder" is transformed into an easy-to-locate maximum or minimum. This method, along with the other details mentioned in Chapter 6, allowed for the automation of the accurate location of the required points. This outcome paved the way to estimate the time-varying elastance in a real-time algorithmic manner, giving easy access to a valuable source of information, and an input function to the lumped parameter model of Chapter 3.

The most significant result of this research is the ability to estimate the time-varying elastance of a specific patient with only the data commonly available in an ICU setting. This outcome results in additional information relating directly to the energetics of the heart, with no additional risk beyond standard care practices. There have been prior attempts to estimate the time-varying elastance, but none have achieved validation based on the measured time-varying elastance, such as was done in Chapter 7. Although the estimated waveform is a value-normalised time-varying elastance, it has been shown that the shape of this waveform is dependant on loading conditions, and is thus clinically relevant in assessing diagnosis and treatments response, despite the controversy surrounding this concept.

The implications of having an easily accessible estimation of the time-varying elastance waveform are numerous. Most significantly, it enables a more accurate simulation and identification of the patient-specific cardiovascular model presented in Chapters 3

and 4, along with the intrinsic clinical relevance of the waveform shape itself. It was demonstrated in Chapter 4 that the time-varying elastance input function to the cardiovascular model and identification process is important. Previous research on this model has used population waveforms, which inherently neglect patient-specific energetic information. Using a waveform that accurately resembles the patient's true time-varying elastance results in a more accurate identification of the model parameters, as well as more accurate simulations. Accurately identified parameters are crucial to using the model to diagnose and track disease state, and thus, having the right time-varying elastance input allows for more reliable parameters to influence clinicians on diagnosis and treatment paths, ultimately leading to better patient care and outcomes.

Aside from the cardiovascular model and the implications of a better patient representation within the model, the time-varying elastance has clinical potential on its own. This clinical potential was demonstrated in Chapter 8, although more work could be done to utilise the full depth of information in this waveform. Due to the proximity and centrality of the time-varying elastance waveform to the cardiovascular system, and its dependence on loading conditions, it provides a good source of information of the health of the heart. This information just needs to be unlocked from the waveform and presented in an understandable and easily accessible way. Chapter 8 started this process, and clearly shows the potential for much of the information gained from the full cardiovascular model to be extracted directly from the time-varying elastance waveform and measured pressure waveforms. This direct extraction bypasses the computation cost of identifying and simulating the full cardiovascular model, and thus yields a novel model-based diagnostic tool, useful in its own right.

9.3 Summary

The central premise of this research is the ability to estimate the time-varying elastance of the left and right ventricles in a patient-specific manner in an ICU environment. This goal was achieved with very good accuracy, with no additional risk to the patient beyond standard care practices. It also raises, and at least partially answers, a question about the importance and relevance of the time-varying elastance itself in the clinical setting. For the first time, there is now an easily accessible method for estimating the time-varying elastance in an ICU environment, which should be able to give valuable

additional information, apart from the cardiovascular model. In this manner, some variables have been demonstrated to be accessible from this waveform, yielding several potential new pathways for diagnosis and treatment.

Chapter 10

Future Work

This chapter outlines the next steps in this line of research, from further validation and clinical trials to improved estimation and modelling techniques.

10.1 Further validation

Validation is key to any model or estimation method, and is thus central to the progression of the research. Specifically, clinical validation, both from animal trials and, ultimately, human trials.

10.1.1 Trials

A critical step in the future of this research is further validation of all aspects of the time-varying elastance estimation. The best form of validation requires the measurement of the true time-varying elastance, and thus must be done through animal trials where the left and right ventricular pressure and volume are measured. Current data is from porcine subjects, and further porcine trials over a range of cardiac dysfunctions would allow for fine tuning of the estimation parameters, and better confidence in the resulting estimation method.

Furthermore, similar trials on other animals such as goats or dogs would be helpful to extend the applicability of the model beyond just porcine subjects, resulting in a more generalised algorithm in the preparation for its use in humans. Direct validation

of the time-varying elastance in humans is currently an unrealisable goal due to the invasiveness of the required procedures. It is foreseeable that this could change with improvements in non-invasive procedures for collecting ventricular data, or new technology. However, until such a time, the only validation that is practically achievable is indirectly through the performance of models driven by the estimated time-varying elastance, such as the six-chamber cardiovascular model presented in this research. Such indirect validation can be achieved on both animals and humans, thus linking the invasive and direct validation with indirect model performance. Therefore a future step is to perform human trials, recording the measurements typically taken in the ICU, over a range of subjects, conditions and condition severities. Due to the nature of human trials, gathering the number of subjects is a lengthy process but one which would be hugely beneficial to the overall strengthening of this research.

Humans trials, such as those just mentioned, would not only help to validate the time-varying elastance, but be instrumental in the further development and validation of the cardiovascular model as a whole, and thus serve a wider goal and body of research. Such cardiovascular model validation would help to progress the model towards clinical usage, which is an overall goal of the research group.

10.1.2 Clinical diagnostics

So far there has not been much attention in the literature to the clinical diagnostic capability of the time-varying elastance waveform. This is perhaps due to the lack of availability of such a waveform in a clinical environment, or the controversy over the universality, or otherwise, of the shape of the normalised time-varying elastance. However, from this research it is clear that the time-varying elastance is not universal in its shape, and there exists useful information in the waveform. It just remains to further develop what has been shown in this research, extracting more information from the time-varying elastance with better accuracy, and demonstrating and proving its worth in a clinical setting.

To achieve this, the aforementioned trials would be a prerequisite. This would enable a large body of data, across various dysfunctions and dysfunction severities, to be analysed.

10.2 Dead space volume

The current model, as presented in the research, assumes that the dead space volume of the ventricles V_d, is zero. This is not generally the case, and thus will lead to some inaccuracy in the model. Given the equation for the time-varying elastance, the dead space volume adjusts the shape of the time-varying elastance, most notably by altering the height of the left shoulder. This implies that, given sufficient accuracy of the estimated time-varying elastance, the real dead space volume may, at least in part, be embedded into the shape of the waveform, and thus could be extracted. This would lead to greater direct insight into the cardiovascular state of the patient, along with an improved cardiovascular system model.

10.3 Modelled estimation

10.3.1 CVP and ECG

The porcine data used in this research did not have central venous pressure (CVP) or ECG recorded. Instead, only timing was used from the pulmonary artery waveform, P_{pa}, to future proof the method for an ICU setting, as P_{pa} is not as commonly available as other metrics. The timing taken from P_{pa} can be found on the CVP and ECG waveforms, and thus the pulmonary artery pressure should not be needed at all, provided CVP and ECG are known, which are both commonly measured in an ICU. However, because cohort data with all of these three measurements was not available during this study, the validation and actual correlations required for this to happen is left as future work.

10.3.2 Time-varying elastance model

At the core of the time-varying elastance concept is an altered Windkessel model, similar to those used in the passive elastic chambers of the cardiovascular model. Therefore, direct mathematical models of the time-varying elastance come naturally to the concept. It would thus seem likely that given the right configuration of a type of Windkessel model, a more robust time-varying elastance model should be achievable.

There are methods in the literature(Aguado-Sierra et al., 2008), which allow for the estimation of the flow rate, given the aortic pressure. This adds another extremely rich piece of information to the time-varying elastance model. Flow is also inherently dependant on loading conditions, thus giving greater insight into the cardiovascular state. Adding flow to the estimation of time-varying elastance could prove beneficial in terms of both the accuracy and range of diagnostics capabilities of the final waveform.

10.3.3 Maximal elastance

Currently the estimated time-varying elastance is value-normalised, and thus the maximal elastance E_{max} is not known. However, it has been shown that E_{max} is a useful predictor of flow-generating capacity of the ventricle (Suga and Sagawa, 1974), and thus it is conceivable that the reverse could also be possible. Therefore, given the flow, E_{max} could be extracted, resulting in the full raw waveform of the time-varying elastance, along with the much sought-after maximal elastance as a measure of contractility.

Similar to flow and maximal elastance, Suga and Sagawa (1974) showed that stroke volume is a function of preload, afterload and maximal elastance. Therefore a similar reversal could take place enhancing an estimation of the maximal elastance as a function of loading conditions and stroke volume.

10.4 Clinical integration

The final stage of such future research would see relevant methods and information being taken into clinical settings. Due to the time-sensitive and life-critical decisions that are made on a daily basis, clinical staff in an ICU setting need all the help they can get. Therefore, the ultimate goal of the overarching body of research is to integrate the patient-specific cardiovascular model and time-varying elastance waveforms into clinical practice. To reach this goal, further validation and trials must be performed to cement the accuracy, robustness and clinical relevance of the these methods.

Bibliography

Abramson, N. S.; Wald, K. S.; Grenvik, A. N.; Robinson, D.; and Snyder, J. V. (1980). "Adverse occurrences in intensive care units". *JAMA : the journal of the American Medical Association*, 244(14), pp. 1582–4.

Agnelli, G.; Becattini, C.; and Kirschstein, T. (2002). "Thrombolysis vs heparin in the treatment of pulmonary embolism: a clinical outcome-based meta-analysis". *Archives of internal medicine*, 162(22), pp. 2537–41.

Aguado-Sierra, J.; Alastruey, J.; Wang, J.-J.; Hadjiloizou, N.; Davies, J.; and Parker, K. H. (2008). "Separation of the reservoir and wave pressure and velocity from measurements at an arbitrary location in arteries". *Proceedings of the Institution of Mechanical Engineers. Part H, Journal of engineering in medicine*, 222(4), pp. 403–16.

Al Otair, H.; Chaudhry, M.; Shaikh, S.; and BaHammam, A. (2009). "Outcome of patients with pulmonary embolism admitted to the intensive care unit". *Annals of Thoracic Medicine*, 4(1), pp. 13.

Alberti, C.; Brun-Buisson, C.; Burchardi, H.; Martin, C.; Goodman, S.; Artigas, A.; Sicignano, A.; Palazzo, M.; Moreno, R.; Boulmé, R.; Lepage, E.; and Le Gall, R. (2002). "Epidemiology of sepsis and infection in ICU patients from an international multicentre cohort study". *Intensive care medicine*, 28(2), pp. 108–21.

Amoore, J. N.; Santamore, W. P.; Corin, W. J.; and George, D. T. (1992). "Computer simulation of the effects of ventricular interdependence on indices of left ventricular systolic function". *Journal of biomedical engineering*, 14(3), pp. 257–62.

Anderson, D. R. (2007). "Computed Tomographic Pulmonary Angiography vs Ventilation-Perfusion Lung Scanning in Patients With Suspected Pulmonary Embolism". *JAMA: The Journal of the American Medical Association*, 298(23), pp. 2743.

Angus, D. C.; Linde-Zwirble, W. T.; Lidicker, J.; Clermont, G.; Carcillo, J.; and Pinsky, M. R. (2001). "Epidemiology of severe sepsis in the United States: analysis of incidence, outcome, and associated costs of care". *Critical Care Medicine*, 29(7), pp. 1303–10.

Annane, D.; Aegerter, P.; Jars-Guincestre, M. C.; and Guidet, B. (2003). "Current epidemiology of septic shock: the CUB-Réa Network". *American journal of respiratory and critical care medicine*, 168(2), pp. 165–172.

Annane, D.; Bellissant, E.; and Cavaillon, J.-M. (2005). "Septic shock". *The Lancet*, 365(9453), pp. 63–78.

Annane, D.; Trabold, F.; Sharshar, T.; Jarrin, I.; Blanc, A. S.; Raphael, J. C.; and Gajdos, P. (1999). "Inappropriate sympathetic activation at onset of septic shock: a spectral analysis approach". *American journal of respiratory and critical care medicine*, 160(2), pp. 458–465.

Anrep, G. (1912). "On the part played by the suprarenals in the normal vascular reactions of the body". *The Journal of physiology*, 45(5), pp. 307–17.

Antonini-Canterin, F.; Faggiano, P.; Zanuttini, D.; and Ribichini, F. (1999). "Is aortic valve resistance more clinically meaningful than valve area in aortic stenosis?". *Heart*, 82(1), pp. 9–10.

Artero, A.; Zaragoza, R.; and Nogueira, J. M. (2012). "Epidemiology of Severe Sepsis and Septic Shock". In Fernandez, R., editor, *Severe Sepsis and Septic Shock - Understanding a Serious Killer*. InTech.

Avanzolini, G.; Barbini, P.; Cappello, A.; and Cevese, A. (1985). "Time-varying mechanical properties of the left ventricle–a computer simulation". *IEEE transactions on bio-medical engineering*, 32(10), pp. 756–63.

Baan, J. and Velde, E. T. (1988). "Sensitivity of left ventricular end-systolic pressure-volume relation to type of loading intervention in dogs". *Circulation Research*, 62, pp. 1247–58.

Bahloul, M.; Chaari, A.; Kallel, H.; Abid, L.; Hamida, C. B.; Dammak, H.; Rekik, N.; Mnif, J.; Chelly, H.; and Bouaziz, M. (2010). "Pulmonary embolism in intensive

care unit: Predictive factors, clinical manifestations and outcome". *Annals of Thoracic Medicine*, 5(2), pp. 97.

Batzel, J. J. and Bachar, M. (2010). "Modeling the cardiovascular-respiratory control system: data, model analysis, and parameter estimation". *Acta biotheoretica*, 58(4), pp. 369–80.

Berenholtz, S. M.; Pronovost, P. J.; Lipsett, P. A.; Hobson, D.; Earsing, K.; Farley, J. E.; Milanovich, S.; Garrett-Mayer, E.; Winters, B. D.; Rubin, H. R.; Dorman, T.; and Perl, T. M. (2004). "Eliminating catheter-related bloodstream infections in the intensive care unit". *Critical care medicine*, 32(10), pp. 2014–20.

Bermejo, J.; García-Fernández, M. A.; Torrecilla, E. G.; Bueno, H.; Moreno, M. M.; San Román, D.; and Delcán, J. L. (1996). "Effects of dobutamine on Doppler echocardiographic indexes of aortic stenosis". *Journal of the American College of Cardiology*, 28(5), pp. 1206–13.

Beyar, R.; Hausknecht, M. J.; Halperin, H. R.; Yin, F. C.; and Weisfeldt, M. L. (1987). "Interaction between cardiac chambers and thoracic pressure in intact circulation". *American Journal of Physiology*, 253(5 Pt 2), pp. H1240–H1252.

Binanay, C.; Califf, R. M.; Hasselblad, V.; O'Connor, C. M.; Shah, M. R.; Sopko, G.; Stevenson, L. W.; Francis, G. S.; Leier, C. V.; and Miller, L. W. (2005). "Evaluation study of congestive heart failure and pulmonary artery catheterization effectiveness: the ESCAPE trial". *JAMA : the journal of the American Medical Association*, 294(13), pp. 1625–33.

Blais, C.; Pibarot, P.; Dumesnil, J. G.; Garcia, D.; Chen, D.; and Durand, L. G. (2001). "Comparison of valve resistance with effective orifice area regarding flow dependence". *The American journal of cardiology*, 88(1), pp. 45–52.

Blitz, L. R. and Herrmann, H. C. (1996). "Hemodynamic assessment of patients with low-flow, low-gradient valvular aortic stenosis". *The American journal of cardiology*, 78(6), pp. 657–61.

Bone, R. C.; Balk, R. A.; Cerra, F. B.; Dellinger, R. P.; Fein, A. M.; Knaus, W. A.; Schein, R. M.; and Sibbald, W. J. (1992). "Definitions for sepsis and organ failure and guidelines for the use of innovative therapies in sepsis. The ACCP/SCCM Consensus

Conference Committee. American College of Chest Physicians/Society of Critical Care Medicine". *Chest*, 101(6), pp. 1644–55.

Bouman, C. (2007). "High-Volume Hemofiltration as Adjunctive Therapy for Sepsis and Systemic Inflammatory Response Syndrome: Background, Definition and a Descriptive Analysis of Animal and Human Studies". *Advances in Sepsis*, 6(2), pp. 47–57.

Braunwald, E. (1976). *Mechanisms of contraction of the normal and failing heart*. Little, Brown, Boston, 2nd editio edition.

Brinke, E. A.; Klautz, R. J.; Verwey, H. F.; Wall, E. E.; Dion, R. A.; and Steendijk, P. (2010). "Single-beat estimation of the left ventricular end-systolic pressure-volume relationship in patients with heart failure". *Acta Physiologica (Oxf)*, 198(1), pp. 37–46.

Broscheit, J. A.; Weidemann, F.; Strotmann, J.; Steendijk, P.; Karle, H.; Roewer, N.; and Greim, C. A. (2006). "Time-varying elastance concept applied to the relation of carotid arterial flow velocity and ventricular area". *Journal af Cardiothoracic and Vascular Anesthesia*, 20(3), pp. 340–6.

Burkhoff, D. (2002). *Mechanical properties of the heart and its interaction with the vascular system*. Course Material, Columbia University, New York, USA.

Burkhoff, D. (2009). "Chasing the Elusive Pressure-Volume Relationship". *Journal of the American College of Cardiology. Cardiovascular Imaging*, 2, pp. 1282–4.

Burkhoff, D.; De Tombe, P. P.; and Hunter, W. C. (1993). "Impact of ejection on magnitude and time course of ventricular pressure-generating capacity". *The American journal of physiology*, 265(3 Pt 2), pp. H899–909.

Burkhoff, D.; Mirsky, I.; and Suga, H. (2005). "Assessment of systolic and diastolic ventricular properties via pressure-volume analysis: a guide for clinical, translational, and basic researchers". *American journal of physiology. Heart and circulatory physiology*, 289(2), pp. H501–12.

Burkhoff, D. and Sagawa, K. (1986). "Ventricular efficiency predicted by an analytical model". *American Journal of Physiology*, 250(6 Pt 2), pp. R1021–7.

Burkhoff, D.; Sugiura, S.; Yue, D. T.; and Sagawa, K. (1987). "Contractility-dependent curvilinearity of end-systolic pressure-volume relations". *American Journal of Physiology*, 252(6 Pt 2), pp. H1218–27.

Burkhoff, D. and Tyberg, J. V. (1993). "Why does pulmonary venous pressure rise after onset of LV dysfunction: a theoretical analysis". *The American journal of physiology*, 265(5 Pt 2), pp. H1819–28.

Calvin, J. E.; Driedger, A. A.; and Sibbald, W. J. (1981). "An assessment of myocardial function in human sepsis utilizing ECG gated cardiac scintigraphy". *Chest*, 80(5), pp. 579–86.

Campbell, K. B.; Simpson, A. M.; Campbell, S. G.; Granzier, H. L.; and Slinker, B. K. (2008). "Dynamic left ventricular elastance: a model for integrating cardiac muscle contraction into ventricular pressure-volume relationships". *Journal of applied physiology (Bethesda, Md. : 1985)*, 104(4), pp. 958–75.

Casale, P. N.; Palacios, I. F.; Abascal, V. M.; Harrell, L.; Davidoff, R.; Weyman, A. E.; and Fifer, M. A. (1992). "Effects of dobutamine on Gorlin and continuity equation valve areas and valve resistance in valvular aortic stenosis". *The American journal of cardiology*, 70(13), pp. 1175–9.

Challoner, D. R. (1968). "Respiration in myocardium". *Nature*, 217(5123), pp. 78–9.

Chase, J. G.; Shaw, G.; Le Compte, A.; Lonergan, T.; Willacy, M.; Wong, X.-W.; Lin, J.; Lotz, T.; Lee, D.; and Hann, C. (2008). "Implementation and evaluation of the SPRINT protocol for tight glycaemic control in critically ill patients: a clinical practice change". *Critical care (London, England)*, 12(2), pp. R49.

Chatterjee, K. (2009). "The Swan-Ganz Catheters: Past, Present, and Future". *Circulation*, 119, pp. 147–152.

Chen, C. H.; Nevo, E.; Fetics, B.; Pak, P. H.; Yin, F. C.; Maughan, W. L.; and Kass, D. A. (1997). "Estimation of central aortic pressure waveform by mathematical transformation of radial tonometry pressure. Validation of generalized transfer function". *Circulation*, 95(7), pp. 1827–36.

Chung, D. C.; Niranjan, S. C.; Clark, J.; Bidani, A.; Johnston, W. E.; Zwischenberger, J. B.; and Traber, D. L. (1997). "A dynamic model of ventricular interaction and pericardial influence". *American Journal of Physiology*, 272(6 Pt 2), pp. H2942–62.

Claessens, T. E.; Georgakopoulos, D.; Afanasyeva, M.; Vermeersch, S. J.; Millar, H. D.; Stergiopulos, N.; Westerhof, N.; Verdonck, P. R.; and Segers, P. (2006). "Nonlinear isochrones in murine left ventricular pressure-volume loops: how well does the time-varying elastance concept hold?". *American journal of physiology. Heart and circulatory physiology*, 290(4), pp. H1474–83.

Cloud, G. C.; Rajkumar, C.; Kooner, J.; Cooke, J.; and Bulpitt, C. J. (2003). "Estimation of central aortic pressure by SphygmoCor requires intra-arterial peripheral pressures". *Clinical science (London, England : 1979)*, 105(2), pp. 219–25.

Cole, L.; Bellomo, R.; Journois, D.; Davenport, P.; Baldwin, I.; and Tipping, P. (2001). "High-volume haemofiltration in human septic shock". *Intensive care medicine*, 27(6), pp. 978–86.

Cooper, A. B. and Doig, G. S. S. (1996). "Pulmonary artery catheters in the critically ill". *Critical Care Medicine*, 12, pp. 777–94.

Cooper, G. (1990). "Load and length regulation of cardiac energetics". *Annual review of physiology*, 52, pp. 505–22.

Cornejo, R.; Downey, P.; Castro, R.; Romero, C.; Regueira, T.; Vega, J.; Castillo, L.; Andresen, M.; Dougnac, A.; Bugedo, G.; and Hernandez, G. (2006). "High-volume hemofiltration as salvage therapy in severe hyperdynamic septic shock". *Intensive care medicine*, 32(5), pp. 713–722.

Corrigan, J. J. J.; Ray, W. L.; and May, N. (1968). "Changes in the blood coagulation system associated with septicemia". *The New England journal of medicine*, 279(16), pp. 851–856.

Covell, J. W.; Taylor, R. R.; Sonnenblick, E. H.; and Ross, J. (1975). "Series elasticity in the intact heart. Evidence for the application of the Hill model for muscle to the intact left ventricle". *Pflügers Archiv : European journal of physiology*, 357(3-4), pp. 225–36.

De Backer, D.; Creteur, J.; Preiser, J.-C.; Dubois, M.-J.; and Vincent, J.-L. (2002). "Microvascular blood flow is altered in patients with sepsis". *American journal of respiratory and critical care medicine*, 166(1), pp. 98–104.

Dellinger, R. P.; Levy, M. M.; Carlet, J. M.; Bion, J.; Parker, M. M.; Jaeschke, R.; Reinhart, K.; Angus, D. C.; Brun-Buisson, C.; Beale, R.; Calandra, T.; Dhainaut, J.-F.; Gerlach, H.; Harvey, M.; Marini, J. J.; Marshall, J.; Ranieri, M.; Ramsay, G.; Sevransky, J.; Thompson, B. T.; Townsend, S.; Vender, J. S.; Zimmerman, J. L.; and Vincent, J.-L. (2008). "Surviving Sepsis Campaign: international guidelines for management of severe sepsis and septic shock: 2008". *Intensive care medicine*, 34(1), pp. 17–60.

Desaive, T.; Dutron, S.; Lambermont, B.; Kolh, P.; Hann, C. E.; Chase, J. G.; Dauby, P. C.; and Ghuysen, A. (2005). "Close-loop model of the cardiovascular system including ventricular interaction and valve dynamics: application to pulmonary embolism". *12th Intl Conference on Biomedical Engineering (ICBME)*.

Desaive, T.; Ghuysen, A.; Lambermont, B.; Kolh, P.; Dauby, P. C.; Starfinger, C.; Hann, C. E.; Chase, J. G.; and Shaw, G. M. (2008). "Cardiovascular Modelling and Identification in Septic Shock - Experimental validation". In *Proceedings of the 17th IFAC World Congress*, Seoul, Korea.

Di Nisio, M.; Squizzato, A.; Rutjes, A. W. S.; Büller, H. R.; Zwinderman, A. H.; and Bossuyt, P. M. M. (2007). "Diagnostic accuracy of D-dimer test for exclusion of venous thromboembolism: a systematic review". *Journal of thrombosis and haemostasis: JTH*, 5(2), pp. 296–304.

Dombrovskiy, V. Y.; Martin, A. A.; Sunderram, J.; and Paz, H. L. (2007). "Rapid increase in hospitalization and mortality rates for severe sepsis in the United States: a trend analysis from 1993 to 2003". *Critical care medicine*, 35(5), pp. 1244–50.

Donchin, Y.; Gopher, D.; Olin, M.; Badihi, Y.; Biesky, M.; Sprung, C. L.; Pizov, R.; and Cotev, S. (1995). "A look into the nature and causes of human errors in the intensive care unit". *Critical care medicine*, 23(2), pp. 294–300.

Douketis, J. D. (2001). "Prognosis in pulmonary embolism". *Current opinion in pulmonary medicine*, 7(5), pp. 354–9.

Elliott, C. G. (1992). "Pulmonary physiology during pulmonary embolism". *Chest*, 101(4 Suppl), pp. 163S–71S.

Evans, A.; Shaw, G. M.; Le Compte, A.; Tan, C.-S.; Ward, L.; Steel, J.; Pretty, C. G.; Pfeifer, L.; Penning, S.; Suhaimi, F.; Signal, M.; Desaive, T.; and Chase, J. G. (2011). "Pilot proof of concept clinical trials of Stochastic Targeted (STAR) glycemic control". *Annals of intensive care*, 1, pp. 38.

Evans, C. L. and Matsuoka, Y. (1915). "The effect of various mechanical conditions on the gaseous metabolism and efficiency of the mammalian heart". *The Journal of physiology*, 49(5), pp. 378–405.

Fogel, M. A.; Weinberg, P. M.; Gupta, K. B.; Rychik, J.; Hubbard, A.; Hoffman, E. A.; and Haselgrove, J. (1998). "Mechanics of the single left ventricle: a study in ventricular-ventricular interaction II". *Circulation*, 98(4), pp. 330–8.

Fogliardi, R.; Di Donfrancesco, M.; and Burattini, R. (1996). "Comparison of linear and nonlinear formulations of the three-element windkessel model". *The American journal of physiology*, 271(6 Pt 2), pp. H2661–8.

Ford, L. E.; Feldman, T.; and Carroll, J. D. (1994). "Valve resistance". *Circulation*, 89(2), pp. 893–5.

Ford, L. E.; Feldman, T.; Chiu, Y. C.; and Carroll, J. D. (1990). "Hemodynamic resistance as a measure of functional impairment in aortic valvular stenosis". *Circulation research*, 66(1), pp. 1–7.

Frank, O. (1895). *Zur Dynamik des Herzmuskels.*. Druck v. R. Oldenbourg.

Frank, O. (1899). "Die grundform des arteriellen pulses, Erste Abhandlung, Mathematische Analyse". *Z Biol*, 37, pp. 483–526.

Frazier, S. K. and Skinner, G. J. (2008). "Pulmonary artery catheters: state of the controversy". *Journal of Cardiovascular Nursing*, 23, pp. 113–21.

Fung, Y. C. (1993). *Biomechanics: Mechanical Properties of Living Tissues, Second Edition*. Springer.

Gan, C. T.; Lankhaar, J. W.; Marcus, J. T.; Westerhof, N.; Marques, K. M.; Bronzwaer, J. G.; Boonstra, A.; Postmus, P. E.; and Vonk-Noordegraaf, A. (2006). "Impaired left ventricular filling due to right-to-left ventricular interaction in patients with pulmonary arterial hypertension". *American Journal of Physiology. Heart and Circulatory Physiology*, 290(4), pp. H1528–33.

Ganz, W.; Donoso, R.; Marcus, H. S.; Forrester, J. S.; and Swan, H. J. (1971). "A new technique for measurement of cardiac output by thermodilution in man". *The American journal of cardiology*, 27(4), pp. 392–6.

Georgakopoulos, D.; Mitzner, W. A.; Chen, C. H.; Byrne, B. J.; Millar, H. D.; Hare, J. M.; and Kass, D. A. (1998). "In vivo murine left ventricular pressure-volume relations by miniaturized conductance micromanometry". *The American journal of physiology*, 274(4 Pt 2), pp. H1416–22.

Ghuysen, A.; Lambermont, B.; Kolh, P.; Tchana-Sato, V.; Magis, D.; Gerard, P.; Mommens, V.; Janssen, N.; Desaive, T.; and D'Orio, V. (2008). "Alteration of right ventricular-pulmonary vascular coupling in a porcine model of progressive pressure overloading". *Shock*, 29(2), pp. 197–204.

Gibbs, C. L. and Chapman, J. B. (1985). "Cardiac mechanics and energetics: chemomechanical transduction in cardiac muscle". *The American journal of physiology*, 249(2 Pt 2), pp. H199–206.

Goldhaber, S. Z. (2002). "Echocardiography in the management of pulmonary embolism". *Annals of internal medicine*, 136(9), pp. 691–700.

Goldhaber, S. Z. and Elliott, C. G. (2003). "Acute pulmonary embolism: part I: epidemiology, pathophysiology, and diagnosis". *Circulation*, 108(22), pp. 2726–9.

Goldhaber, S. Z.; Visani, L.; and De Rosa, M. (1999). "Acute pulmonary embolism: clinical outcomes in the International Cooperative Pulmonary Embolism Registry (ICOPER)". *Lancet*, 353(9162), pp. 1386–9.

Greenberg, S. B.; Murphy, G. S.; and Vender, J. S. (2009). "Current use of the pulmonary artery catheter". *Current opinion in critical care*, 15(3), pp. 249–53.

Grenvik, A.; Ayres, S. M.; and Holbrook, P. R. (1989). *Textbook of Critical Care*. W.B. Saunders Company, Philadelphia, 2nd edition.

Groot, M. R.; van Marwijk Kooy, M.; Pouwels, J. G.; Engelage, A. H.; Kuipers, B. F.; and Büller, H. R. (1999). "The use of a rapid D-dimer blood test in the diagnostic work-up for pulmonary embolism: a management study". *Thrombosis and haemostasis*, 82(6), pp. 1588–92.

Guarini, M.; Urzúa, J.; Cipriano, A.; and González, W. (1998). "Estimation of caridac function from computer analysis of the arterial pressure waveform". *IEEE Transactions on Biomedical Engineering*, 45(12), pp. 1420–8.

Hall, J. E. and Guyton, A. C. (2011). *Guyton and Hall Textbook of Medical Physiology*. Elsevier Health Sciences.

Hann, C. E.; Chase, J. G.; and Shaw, G. M. (2005). "Efficient implementation of non-linear valve law and ventricular interaction dynamics in the minimal cardiac model". *Computer Methods and Programs in Biomedicine*, 80(1), pp. 65–74.

Hayashi, K.; Shigemi, K.; Shishido, T.; Sugimachi, M.; and Sunagawa, K. (2000). "Single-beat estimation of ventricular end-systolic elastance-effective arterial elastance as an index of ventricular mechanoenergetic performance". *Anesthesiology*, 92(6), pp. 1769–76.

Heidenreich, P. A.; Trogdon, J. G.; Khavjou, O. A.; Butler, J.; Dracup, K.; Ezekowitz, M. D.; Finkelstein, E. A.; Hong, Y.; Johnston, S. C.; Khera, A.; Lloyd-Jones, D. M.; Nelson, S. A.; Nichol, G.; Orenstein, D.; Wilson, P. W. F.; and Woo, Y. J. (2011). "Forecasting the Future of Cardiovascular Disease in the United States A Policy Statement From the American Heart Association". *Circulation*, 123(8), pp. 933–44.

Helmholtz, H. (1845). "Ueber den Stoffverbrauch bei der Muskelaktion". *Mueller's Arch Anal Phyiol*, pages 72–83.

Helmholtz, H. (1848). "Ueber die warmeentwicklung der muskelaction". *Mueller's Arch Anal Phyiol*, pages 144–64.

Hope, S. A.; Tay, D. B.; Meredith, I. T.; and Cameron, J. D. (2004). "Use of arterial transfer functions for the derivation of central aortic waveform characteristics in subjects with type 2 diabetes and cardiovascular disease". *Diabetes care*, 27(3), pp. 746–51.

Hosepud, J. D. and Greenberg, B. H. (2007). *Congestive Heart Failure*. Lippincott Williams & Wilkins, Philadelphia.

Hunter, W. C.; Janicki, J. S.; Weber, K. T.; and Noordergraaf, A. (1979). "Flow-pulse response: a new method for the characterization of ventricular mechanics". *The American journal of physiology*, 237(3), pp. H282–92.

Hunter, W. C.; Janicki, J. S.; Weber, K. T.; and Noordergraaf, A. (1983). "Systolic mechanical properties of the left ventricle. Effects of volume and contractile state". *Circulation research*, 52(3), pp. 319–27.

Investigators, T. C. (1997). "Low-Molecular-Weight Heparin in the Treatment of Patients with Venous Thromboembolism". *New England Journal of Medicine*, 337(10), pp. 657–62.

Jacob, R. and Kissling, G. (1989). "Ventricular pressure-volume relations as the primary basis for evaluation of cardiac mechanics. Return to Frank's diagram". *Basic research in cardiology*, 84(3), pp. 227–46.

Jardin, F.; Dubourg, O.; and Bourdarias, J. P. (1997). "Echocardiographic pattern of acute cor pulmonale". *Chest*, 111(1), pp. 209–17.

Jegger, D.; Mallik, A. S.; Nasratullah, M.; Jeanrenaud, X.; Silva, R.; Tevaearai, H.; Segesser, L. K.; and Stergiopulos, N. (2007). "The effect of a myocardial infarction on the normalized time-varying elastance curve". *Journal of applied physiology (Bethesda, Md. : 1985)*, 102(3), pp. 1123–9.

Johnston, I. G.; Fraser, J. F.; Sabapathy, S.; and Kruger, P. S. (2008). "The pulmonary artery catheter in Australasia: a survey investigating intensive care physicians' knowledge and perception of future trends in use". *Anaesthesia and intensive care*, 36(1), pp. 84–9.

Kameyama, T.; Chen, Z.; Bell, S. P.; Fabian, J.; and LeWinter, M. M. (1998). "Mechanoenergetic studies in isolated mouse hearts". *The American journal of physiology*, 274(1 Pt 2), pp. H366–74.

Kappel, F.; Fink, M.; and Batzel, J. J. (2007). "Aspects of control of the cardiovascular-respiratory system during orthostatic stress induced by lower body negative pressure". *Mathematical biosciences*, 206(2), pp. 273–308.

Karliner, J. S.; Gault, J. H.; Eckberg, D.; Mullins, C. B.; and Ross, J. (1971). "Mean velocity of fiber shortening. A simplified measure of left ventricular myocardial contractility". *Circulation*, 44(3), pp. 323–33.

Karlsson, S.; Varpula, M.; Ruokonen, E.; Pettilä, V.; Parviainen, I.; Ala-Kokko, T. I.; Kolho, E.; and Rintala, E. M. (2007). "Incidence, treatment, and outcome of severe

sepsis in ICU-treated adults in Finland: the Finnsepsis study". *Intensive care medicine*, 33(3), pp. 435–43.

Kasper, W.; Konstantinides, S.; Geibel, A.; Olschewski, M.; Heinrich, F.; Grosser, K. D.; Rauber, K.; Iversen, S.; Redecker, M.; and Kienast, J. (1997). "Management strategies and determinants of outcome in acute major pulmonary embolism: results of a multicenter registry". *Journal of the American College of Cardiology*, 30(5), pp. 1165–71.

Kass, D. A. (1992). "Clinical evaluation of left heart function by conductance catheter technique". *European Heart Journal*, 13 Suppl E, pp. 57–64.

Kass, D. A.; Baughman, K. L.; Pak, P. H.; Cho, P. W.; Levin, H. R.; Gardner, T. J.; Halperin, H. R.; Tsitlik, J. E.; and Acker, M. A. (1995). "Reverse remodeling from cardiomyoplasty in human heart failure. External constraint versus active assist". *Circulation*, 91(9), pp. 2314–8.

Kass, D. A.; Beyar, R.; Lankford, E.; Heard, M.; Maughan, W. L.; and Sagawa, K. (1989). "Influence of contractile state on curvilinearity of in situ end-systolic pressure-volume relations". *Circulation*, 79(1), pp. 167–78.

Kass, D. A. and Maughan, W. L. (1988). "From 'Emax' to pressure-volume relations: a broader view". *Circulation*, 77(6), pp. 1203–12.

Katz, A. M. (1988). "Influence of altered inotropy and lusitropy on ventricular pressure-volume loops". *Journal of the American College of Cardiology*, 11(2), pp. 438–45.

Kearon, C. (2003). "Diagnosis of pulmonary embolism". *CMAJ*, 168(2), pp. 183–94.

Kennedy, P. J.; Leathley, C. M.; and Hughes, C. F. (2010). "Clinical practice variation". *The Medical journal of Australia*, 193(8 Suppl), pp. S97–9.

Kind, T.; Westerhof, N.; Faes, T. J.; Lankhaar, J. W.; Steendijk, P.; and Vonk-Noordegraaf, A. (2009). "Cardiac phase-dependent time normalization reduces load dependence of time-varying elastance". *American Journal of Physiology. Heart and Circulatory Physiology*, 296(2), pp. H342–9.

Kjorstad, K. E.; Korvald, C.; and Myrmel, T. (2002). "Pressure-volume-based single-beat estimations cannot predict left ventricular contractility in vivo". *American journal of physiology. Heart and circulatory physiology*, 282(5), pp. H1739–50.

Klabunde, R. E. (2011). *Cardiovascular Physiology Concepts*. Lippincott Williams & Wilkins, second edition.

Klotz, S.; Dickstein, M. L.; and Burkhoff, D. (2007). "A computational method of prediction of the end-diastolic pressure-volume relationship by single beat". *Nature Protocols*, 2(9), pp. 2152–8.

Klotz, S.; Foronjy, R. F.; Dickstein, M. L.; Gu, A.; Garrelds, I. M.; Danser, A. H. J.; Oz, M. C.; D'Armiento, J.; and Burkhoff, D. (2005). "Mechanical unloading during left ventricular assist device support increases left ventricular collagen cross-linking and myocardial stiffness". *Circulation*, 112(3), pp. 364–74.

Klotz, S.; Hay, I.; Dickstein, M. L.; Yi, G.-H. H.; Wang, J.; Maurer, M. S.; Kass, D. a.; and Burkhoff, D. (2006). "Single-beat estimation of end-diastolic pressure-volume relationship: a novel method with potential for noninvasive application". *American Journal of Physiology. Heart and Circulatory Physiology*, 291(1), pp. H403–12.

Knowlton, F. P. and Starling, E. H. (1912). "The influence of variations in temperature and blood-pressure on the performance of the isolated mammalian heart". *The Journal of physiology*, 44(3), pp. 206–19.

Konstam, M. A.; Cohen, S. R.; Salem, D. N.; Conlon, T. P.; Isner, J. M.; Das, D.; Zile, M. R.; Levine, H. J.; and Kahn, P. C. (1985). "Comparison of left and right ventricular end-systolic pressure-volume relations in congestive heart failure". *Journal of the American College of Cardiology*, 5(6), pp. 1326–34.

Konstantinides, S.; Geibel, A.; Olschewski, M.; Heinrich, F.; Grosser, K.; Rauber, K.; Iversen, S.; Redecker, M.; Kienast, J.; Just, H.; and Kasper, W. (1997). "Association Between Thrombolytic Treatment and the Prognosis of Hemodynamically Stable Patients With Major Pulmonary Embolism Results of a Multicenter Registry". *Circulation*, 96(3), pp. 882–8.

Kramer, P.; Wigger, W.; Rieger, J.; Matthaei, D.; and Scheler, F. (1977). "Arteriovenous haemofiltration: a new and simple method for treatment of over-hydrated patients resistant to diuretics". *Klinische Wochenschrift*, 55(22), pp. 1121–2.

Krosl, P. and Abel, F. L. (1998). "Problems with use of the end systolic pressure-volume slope as an indicator of left ventricular contractility: an alternate method". *Shock*, 10(4), pp. 285–91.

Kruip, M. J. H. A.; Leclercq, M. G. L.; Heul, C.; Prins, M. H.; and Büller, H. R. (2003). "Diagnostic Strategies for Excluding Pulmonary Embolism in Clinical Outcome Studies: A Systematic Review". *Annals of Internal Medicine*, 138(12), pp. 941–51.

Lambermont, B.; Delanaye, P.; Dogne, J. M.; Ghuysen, A.; Janssen, N.; Dubois, B.; Desaive, T.; Kolh, P.; D'Orio, V.; and Krzesinski, J. M. (2006). "Large-pore membrane hemofiltration increases cytokine clearance and improves right ventricular-vascular coupling during endotoxic shock in pigs". *Artificial Organs*, 30(7), pp. 560–4.

Lambermont, B.; Ghuysen, A.; Kolh, P.; Tchana-Sato, V.; Segers, P.; Gerard, P.; Morimont, P.; Magis, D.; Dogne, J. M.; Masereel, B.; and D'Orio, V. (2003). "Effects of endotoxic shock on right ventricular systolic function and mechanical efficiency". *Cardiovascular Research*, 59(2), pp. 412–8.

Landesberg, A.; Beyar, R.; and Sideman, S. (1993). "Time varying elastance and cardiac muscle energetics based on calcium kinetics and crossbridges cycling". In *Proceedings of Computers in Cardiology Conference*, pages 373–376. IEEE Comput. Soc. Press.

Lang, R. M.; Borow, K. M.; Neumann, A.; and Janzen, D. (1986). "Systemic vascular resistance: an unreliable index of left ventricular afterload". *Circulation*, 74(5), pp. 1114–23.

Le Compte, A.; Chase, J. G.; Lynn, A.; Hann, C.; Shaw, G.; Wong, X.-W.; and Lin, J. (2009). "Blood glucose controller for neonatal intensive care: virtual trials development and first clinical trials". *Journal of diabetes science and technology*, 3(5), pp. 1066–81.

Le Gal, G.; Righini, M.; Roy, P.-M.; Sanchez, O.; Aujesky, D.; Bounameaux, H.; and Perrier, A. (2006). "Prediction of pulmonary embolism in the emergency department: the revised Geneva score". *Annals of internal medicine*, 144(3), pp. 165–171.

Lee, S.; Ohga, Y.; Tachibana, H.; Syuu, Y.; Ito, H.; Harada, M.; Suga, H.; and Takaki, M. (1998). "Effects of myosin isozyme shift on curvilinearity of the left ventricular end-systolic pressure-volume relation of In situ rat hearts". *The Japanese journal of physiology*, 48(6), pp. 445–55.

Lee, W. S.; Nakayama, M.; Huang, W. P.; Chiou, K. R.; Wu, C. C.; Nevo, E.; Fetics, B.; Kass, D. A.; Ding, P. Y.; and Chen, C. H. (2002). "Assessment of left ventricular end-systolic elastance from aortic pressure-left ventricular volume relations". *Heart Vessels*, 16(3), pp. 99–104.

Li, J. K.; Cui, T.; and Drzewiecki, G. M. (1990). "A nonlinear model of the arterial system incorporating a pressure-dependent compliance". *IEEE transactions on bio-medical engineering*, 37(7), pp. 673–8.

Liang, F. and Liu, H. (2005). "A Closed-Loop Lumped Parameter Computational Model for Human Cardiovascular System". *JSME International Journal Series C*, 48(4), pp. 484–493.

Little, W. C. and Freeman, G. L. (1987). "Description of LV pressure-volume relations by time-varying elastance and source resistance". *The American journal of physiology*, 253(1 Pt 2), pp. H83–90.

Loiselle, D. S.; Crampin, E. J.; Niederer, S. A.; Smith, N. P.; and Barclay, C. J. (2008). "Energetic consequences of mechanical loads". *Progress in biophysics and molecular biology*, 97(2-3), pp. 348–66.

Martin, G. S.; Mannino, D. M.; Eaton, S.; and Moss, M. (2003). "The Epidemiology of Sepsis in the United States from 1979 through 2000". *New England Journal of Medicine*, 348(16), pp. 1546–54.

Martini, F. H.; Nath, J. L.; and Bartholomew, E. F. (2011). *Fundamentals of Anatomy & Physiology*. Benjamin Cummings, ninth edition.

Mascherbauer, J.; Schima, H.; Rosenhek, R.; Czerny, M.; Maurer, G.; and Baumgartner, H. (2004). "Value and limitations of aortic valve resistance with particular consideration of low flow-low gradient aortic stenosis: an in vitro study". *European heart journal*, 25(9), pp. 787–93.

McDonald, R. H.; Taylor, R. R.; and Cingolani, H. E. (1966). "Measurement of myocardial developed tension and its relation to oxygen consumption". *The American journal of physiology*, 211(3), pp. 667–73.

McGill, H. C. J.; McMahan, C. A.; and Gidding, S. S. (2008). "Preventing heart disease in the 21st century: implications of the Pathobiological Determinants of Atherosclerosis in Youth (PDAY) study". *Circulation*, 117(9), pp. 1216–27.

McIntyre, K. M. and Sasahara, A. A. (1971). "The hemodynamic response to pulmonary embolism in patients without prior cardiopulmonary disease". *The American journal of cardiology*, 28(3), pp. 288–94.

McKay, R. G.; Aroesty, J. M.; Heller, G. V.; Royal, H. D.; Warren, S. E.; and Grossman, W. (1986). "Assessment of the end-systolic pressure-volume relationship in human beings with the use of a time-varying elastance model". *Circulation*, 74(1), pp. 97–104.

Melchior, F. M.; Srinivasan, R. S.; and Charles, J. B. (1992). "Mathematical modeling of human cardiovascular system for simulation of orthostatic response". *American Journal of Physiology*, 262(6 Pt 2), pp. H1920–33.

Mendis, S.; Puska, P.; and Norrving, B. (2011). *Global Atlas on cardiovascular disease prevention and control*. World Health Organization.

Mermel, L. (1991). "The pathogenesis and epidemiology of catheter-related infection with pulmonary artery Swan-Ganz catheters: A prospective study utilizing molecular subtyping". *The American Journal of Medicine*, 91(3), pp. S197–S205.

Michard, F.; Alaya, S.; Zarka, V.; Bahloul, M.; Richard, C.; and Teboul, J. L. (2003). "Global End-Diastolic Volume as an Indicator of Cardiac Preload in Patients With Septic Shock". *Chest*, 124(5), pp. 1900–8.

Milnor, W. R. (1975). "Arterial impedance as ventricular afterload". *Circulation Research*, 36(5), pp. 565–70.

Miron, M. J.; Perrier, A.; Bounameaux, H.; Moerloose, P.; Slosman, D. O.; Didier, D.; and Junod, A. (1999). "Contribution of noninvasive evaluation to the diagnosis of pulmonary embolism in hospitalized patients". *The European respiratory journal: official journal of the European Society for Clinical Respiratory Physiology*, 13(6), pp. 1365–70.

Mirsky, I.; Tajimi, T.; and Peterson, K. L. (1987). "The development of the entire end-systolic pressure-volume and ejection fraction-afterload relations: a new concept of systolic myocardial stiffness". *Circulation*, 76(2), pp. 343–56.

Monroe, R. G. and French, G. (1960). "Ventricular pressure-volume relationships and oxygen consumption in fibrillation and arrest". *Circulation research*, 8, pp. 260–6.

Monye, De, W. and Pattynama, P. M. (2001). "Contrast-enhanced spiral computed tomography of the pulmonary arteries: an overview". *Seminars in thrombosis and hemostasis*, 27(1), pp. 33–9.

Moreno, R.; Matos, R.; and Fevereiro, T. (2002). "Organ Failure". In Vincent, J.-L.; Carlet, J.; and Opal, S. M., editors, *The Sepsis Text*, pages 29–46. Springer US.

Morris, A. H. (2001). "Rational use of computerized protocols in the intensive care unit". *Critical care (London, England)*, 5(5), pp. 249–54.

Moscato, F.; Vollkron, M.; Bergmeister, H.; Wieselthaler, G.; Leonard, E.; and Schima, H. (2007). "Left ventricular pressure-volume loop analysis during continuous cardiac assist in acute animal trials". *Artificial Organs*, 31(5), pp. 369–76.

Moser, K. M.; Fedullo, P. F.; LitteJohn, J. K.; and Crawford, R. (1994). "Frequent asymptomatic pulmonary embolism in patients with deep venous thrombosis". *JAMA: the journal of the American Medical Association*, 271(3), pp. 223–5.

Munt, B.; Jue, J.; Gin, K.; Fenwick, J.; and Tweeddale, M. (1998). "Diastolic filling in human severe sepsis: an echocardiographic study". *Critical care medicine*, 26(11), pp. 1829–1833.

Musset, D.; Parent, F.; Meyer, G.; Maître, S.; Girard, P.; Leroyer, C.; Revel, M.-P.; Carette, M.-F.; Laurent, M.; Charbonnier, B.; Laurent, F.; Mal, H.; Nonent, M.; Lancar, R.; Grenier, P.; and Simonneau, G. (2002). "Diagnostic strategy for patients with suspected pulmonary embolism: a prospective multicentre outcome study". *Lancet*, 360(9349), pp. 1914–20.

Mutoh, T.; Kazumata, K.; Ajiki, M.; Ushikoshi, S.; and Terasaka, S. (2007). "Goal-directed fluid management by bedside transpulmonary hemodynamic monitoring after subarachnoid hemorrhage". *Stroke; a journal of cerebral circulation*, 38(12), pp. 3218–24.

Naess, I. A.; Christiansen, S. C.; Romundstad, P.; Cannegieter, S. C.; Rosendaal, F. R.; and m, J. (2007). "Incidence and mortality of venous thrombosis: a population-based study". *Journal of thrombosis and haemostasis*, 5(4), pp. 692–9.

Nahouraii, R. A. and Rowell, S. E. (2010). "Static Measures of Preload Assessment". *Critical Care Clinics*, 26(2), pp. 295–305.

Nduka, O. O. and Parrillo, J. E. (2009). "The pathophysiology of septic shock". *Critical care clinics*, 25(4), pp. 677–702, vii.

Neely, J. R.; Liebermeister, H.; Battersby, E. J.; and Morgan, H. E. (1967). "Effect of pressure development on oxygen consumption by isolated rat heart". *The American journal of physiology*, 212(4), pp. 804–14.

Nichols, W. W. and Pepine, C. J. (1982). "Left ventricular afterload and aortic input impedance: implications of pulsatile blood flow". *Progress in cardiovascular diseases*, 24(4), pp. 293–306.

Noda, T.; Cheng, C. P.; De Tombe, P. P.; and Little, W. C. (1993). "Curvilinearity of LV end-systolic pressure-volume and dP/dtmax-end-diastolic volume relations". *American Journal of Physiology*, 265(3 Pt 2), pp. H910–7.

Norton, J. M. (2001). "Toward Consistent Definitions for Preload and Afterload". *Advances in Physiology Education*, 25(1), pp. 53–61.

Olansen, J. B.; Clark, J. W.; Khoury, D.; Ghorbel, F.; and Bidani, A. (2000). "A closed-loop model of the canine cardiovascular system that includes ventricular interaction". *Computers and biomedical research, an international journal*, 33(4), pp. 260–95.

Oommen, B.; Karamanoglu, M.; and Kovacs, S. J. (2003). "Modeling time varying elastance: the meaning of 'load-independence"'. *Cardiovascular Engineering*, 3(4), pp. 123–30.

O'Rourke, M. F. (1982). "Vascular impedance in studies of arterial and cardiac function". *Physiological reviews*, 62(2), pp. 570–623.

O'Rourke, M. F. (2004). "Estimation of central aortic pressure by SphygmoCor requires accurate peripheral pressure measurement". *Clinical science (London, England : 1979)*, 106(4), pp. 434–5; author reply 436–7.

Ottesen, J. T.; Olufsen, M. S.; and Larsen, J. K. (2004). *Applied Mathematical Models in Human Physiology*. Society for Industrial and Applied Mathematics.

Pacher, P.; Nagayama, T.; Mukhopadhyay, P.; Bátkai, S.; and Kass, D. (2008). "Measurement of cardiac function using pressure-volume conductance catheter technique in mice and rats". *Nature protocols*, 3, pp. 1422–34.

Paeme, S.; Moorhead, K. T.; Chase, J. G.; Lambermont, B.; Kolh, P.; D'orio, V.; Pierard, L.; Moonen, M.; Lancellotti, P.; Dauby, P. C.; and Desaive, T. (2011). "Mathematical

multi-scale model of the cardiovascular system including mitral valve dynamics. Application to ischemic mitral insufficiency". *Biomedical engineering online*, 10(1), pp. 86.

Palmer, B. M.; Noguchi, T.; Wang, Y.; Heim, J. R.; Alpert, N. R.; Burgon, P. G.; Seidman, C. E.; Seidman, J. G.; Maughan, D. W.; and LeWinter, M. M. (2004). "Effect of cardiac myosin binding protein-C on mechanoenergetics in mouse myocardium". *Circulation research*, 94(12), pp. 1615–22.

Parker, M. M.; McCarthy, K. E.; Ognibene, F. P.; and Parrillo, J. E. (1990). "Right ventricular dysfunction and dilatation, similar to left ventricular changes, characterize the cardiac depression of septic shock in humans". *Chest*, 97(1), pp. 126–31.

Parrillo, J. E.; Parker, M. M.; Natanson, C.; Suffredini, A. F.; Danner, R. L.; Cunnion, R. E.; and Ognibene, F. P. (1990). "Septic shock in humans. Advances in the understanding of pathogenesis, cardiovascular dysfunction, and therapy". *Annals of internal medicine*, 113(3), pp. 227–42.

Pauca, A. L.; O'Rourke, M. F.; and Kon, N. D. (2001). "Prospective Evaluation of a Method for Estimating Ascending Aortic Pressure From the Radial Artery Pressure Waveform". *Hypertension*, 38(4), pp. 932–7.

Perrier, A.; Desmarais, S.; Miron, M. J.; Moerloose, P.; Lepage, R.; Slosman, D.; Didier, D.; Unger, P. F.; Patenaude, J. V.; and Bounameaux, H. (1999). "Non-invasive diagnosis of venous thromboembolism in outpatients". *Lancet*, 353(9148), pp. 190–5.

Perrier, A.; Howarth, N.; Didier, D.; Loubeyre, P.; Unger, P. F.; Moerloose, P.; Slosman, D.; Junod, A.; and Bounameaux, H. (2001). "Performance of helical computed tomography in unselected outpatients with suspected pulmonary embolism". *Annals of internal medicine*, 135(2), pp. 88–97.

Perrier, A.; Miron, M. J.; Desmarais, S.; Moerloose, P.; Slosman, D.; Didier, D.; Unger, P. F.; Junod, A.; Patenaude, J. V.; and Bounameaux, H. (2000). "Using clinical evaluation and lung scan to rule out suspected pulmonary embolism: Is it a valid option in patients with normal results of lower-limb venous compression ultrasonography?". *Archives of internal medicine*, 160(4), pp. 512–6.

Pineda, L. A.; S, H. V.; and Grant, B. J. B. (2001). "Clinical Suspicion of Fatal Pulmonary Embolism". *Chest*, 120(3), pp. 791–5.

Pinsky, M. R. (2003). "Rationale for cardiovascular monitoring". *Current opinion in critical care*, 9(3), pp. 222–4.

Pinsky, M. R. (2007). "Hemodynamic evaluation and monitoring in the ICU". *Chest*, 132(6), pp. 2020–9.

Pironet, A. (2011). *Méthodes d'identification des paramètres dans un modèle du système cardiovasculaire*. Masters, Université de Liège.

Pironet, A.; Revie, J.; Paeme, S.; Dauby, P.; Chase, J. G.; and Desaive, T. (2012). "Development and Identification of a Closed-Loop Model of the Cardiovascular System Including the Atria". In *Proceedings of the 8th IFAC Symposium on Biological and Medical Systems*, Budapest, Hungary.

Poelaert, J.; Declerck, C.; Vogelaers, D.; Colardyn, F.; and Visser, C. A. (1997). "Left ventricular systolic and diastolic function in septic shock". *Intensive care medicine*, 23(5), pp. 553–60.

Pouleur, H.; Rousseau, M. F.; Eyll, C.; Stoleru, L.; Hayashida, W.; Udelson, J. A.; Dolan, N.; Kinan, D.; Gallagher, P.; and Ahn, S. (1993). "Effects of long-term enalapril therapy on left ventricular diastolic properties in patients with depressed ejection fraction. SOLVD Investigators". *Circulation*, 88(2), pp. 481–91.

Puchalski, M. D.; Williams, R. V.; Askovich, B.; Minich, L. L.; Mart, C.; and Tani, L. Y. (2007). "Assessment of right ventricular size and function: echo versus magnetic resonance imaging". *Congenital heart disease*, 2(1), pp. 27–31.

Ramritu, P.; Halton, K.; Cook, D.; Whitby, M.; and Graves, N. (2008). "Catheter-related bloodstream infections in intensive care units: a systematic review with meta-analysis". *Journal of advanced nursing*, 62(1), pp. 3–21.

Rapaport, S. I.; Tatter, D.; Coeur-Barron, N.; and Hjort, P. F. (1964). "Pseudomonas septicemia with intravascular clotting leading to the generalized shwartzman reaction". *The New England journal of medicine*, 271, pp. 80–4.

Remick, D. G. (2007). "Pathophysiology of Sepsis". *The American Journal of Pathology*, 170(5), pp. 1435–44.

Revie, J.; Stevenson, D.; Chase, G.; Hann, C. E.; Lambermont, B.; Ghuysen, A.; Kolh, P.; Morimont, P.; Shaw, G. M.; and Desaive, T. (2011a). "Clinical detection and

monitoring of acute pulmonary embolism: proof of concept of a computer-based method". *Annals of Intensive Care*, 1, pp. 33.

Revie, J.; Stevenson, D.; Chase, J. G.; Hann, C. E.; Lambermont, B.; Ghuysen, A.; Kolh, P.; Shaw, G. M.; Heldmann, S.; and Desaive, T. (2011b). "Validation of subject-specific cardiovascular system models from porcine measurements". *Computer Methods and Programs in Biomedicine*, 109(2), pp. 197–210.

Revie, J. A.; Stevenson, D.; Chase, J. G.; Pretty, C. J.; Lambermont, B. C.; Ghuysen, A.; Kolh, P.; Shaw, G. M.; and Desaive, T. (2013). "Evaluation of a model-based hemodynamic monitoring method in a porcine study of septic shock". *Computational and mathematical methods in medicine*, 2013.

Rivers, E.; Nguyen, B.; Havstad, S.; Ressler, J.; Muzzin, A.; Knoblich, B.; Peterson, E.; and Tomlanovich, M. (2001). "Early Goal-Directed Therapy in the Treatment of Severe Sepsis and Septic Shock". *New England Journal of Medicine*, 345(19), pp. 1368–77.

Rodbard, S.; Williams, C. B.; Rodbard, D.; and Berglund, E. (1964). "Myocardial Tension and Oxygen Uptake". *Circulation Research*, 14(2), pp. 139–49.

Roger, V. L.; Go, A. S.; Lloyd-Jones, D. M.; Adams, R. J.; Berry, J. D.; Brown, T. M.; Carnethon, M. R.; Dai, S.; Simone, G.; Ford, E. S.; Fox, C. S.; Fullerton, H. J.; Gillespie, C.; Greenlund, K. J.; Hailpern, S. M.; Heit, J. A.; Ho, P. M.; Howard, V. J.; Kissela, B. M.; Kittner, S. J.; Lackland, D. T.; Lichtman, J. H.; Lisabeth, L. D.; Makuc, D. M.; Marcus, G. M.; Marelli, A.; Matchar, D. B.; McDermott, M. M.; Meigs, J. B.; Moy, C. S.; Mozaffarian, D.; Mussolino, M. E.; Nichol, G.; Paynter, N. P.; Rosamond, W. D.; Sorlie, P. D.; Stafford, R. S.; Turan, T. N.; Turner, M. B.; Wong, N. D.; and Wylie-Rosett, J. (2011). "Heart Disease and Stroke Statistics 2011 Update". *Circulation*, 123(4), pp. e18–e209.

Roger, V. L.; Go, A. S.; Lloyd-Jones, D. M.; Benjamin, E. J.; Berry, J. D.; Borden, W. B.; Bravata, D. M.; Dai, S.; Ford, E. S.; Fox, C. S.; Fullerton, H. J.; Gillespie, C.; Hailpern, S. M.; Heit, J. A.; Howard, V. J.; Kissela, B. M.; Kittner, S. J.; Lackland, D. T.; Lichtman, J. H.; Lisabeth, L. D.; Makuc, D. M.; Marcus, G. M.; Marelli, A.; Matchar, D. B.; Moy, C. S.; Mozaffarian, D.; Mussolino, M. E.; Nichol, G.; Paynter, N. P.; Soliman, E. Z.; Sorlie, P. D.; Sotoodehnia, N.; Turan, T. N.; Virani, S. S.; Wong, N. D.; Woo, D.; and

Turner, M. B. (2012). "Heart Disease and Stroke Statistics 2012 Update A Report From the American Heart Association". *Circulation*, 125(1), pp. e2–e220.

Rogiers, P. (2005). "High-volume hemofiltration in septic shock". *Critical Care*, 9(4), pp. 329–30.

Rohde, E. (1912). "Über den Einflußder mechanischen Bedingungen auf die Tätigkeit und den Sauerstoffverbrauch des Warmblüterherzens". *Archiv für Experimentelle Pathologie und Pharmakologie*, 68(6), pp. 401–34.

Ross, J. J. (1976). "Afterload mismatch and preload reserve: a conceptual framework for the analysis of ventricular function". *Progress in Cardiovascular Diseases*, 18, pp. 255–64.

Roy, P.-M.; Meyer, G.; Vielle, B.; Gall, C. L.; Verschuren, F.; Carpentier, F.; Leveau, P.; and Furber, A. (2006). "Appropriateness of Diagnostic Management and Outcomes of Suspected Pulmonary Embolism". *Annals of Internal Medicine*, 144(3), pp. 157–64.

Royse, C. F. and Royse, A. G. (2005). "The myocardial and vascular effects of bupivacaine, levobupivacaine, and ropivacaine using pressure volume loops". *Anesthesia and analgesia*, 101(3), pp. 679–87, table of contents.

Safdar, N.; Kluger, D. M.; and Maki, D. G. (2002). "A review of risk factors for catheter-related bloodstream infection caused by percutaneously inserted, noncuffed central venous catheters: implications for preventive strategies". *Medicine*, 81(6), pp. 466–79.

Sagawa, K. (1978). "The ventricular pressure-volume diagram revisited". *Circulation Research*, 43(5), pp. 677–87.

Sagawa, K. (1981). "The end-systolic pressure-volume relation of the ventricle: definition, modifications and clinical use". *Circulation*, 63(6), pp. 1223–7.

Sagawa, K.; Lie, R. K.; and Schaefer, J. (1990). "Translation of Otto Frank's paper "Die Grundform des Arteriellen Pulses" Zeitschrift fur Biologie 37: 483-526 (1899)". *J Mol Cell Cardiol*, 22(3), pp. 253–77.

Sagawa, K.; Muaghan, L.; and Sunagawa, K. (1988). *Cardiac Contraction and the Pressure-Volume Relationship*. Oxford University Press, New-York.

Sagawa, K.; Suga, H.; Shoukas, A. A.; and Bakalar, K. M. (1977). "End-systolic pressure/volume ratio: A new index of ventricular contractility". *The American Journal of Cardiology*, 40(5), pp. 748–53.

Sakka, S. G.; Rühl, C. C.; Pfeiffer, U. J.; Beale, R.; McLuckie, A.; Reinhart, K.; and Meier-Hellmann, A. (2000). "Assessment of cardiac preload and extravascular lung water by single transpulmonary thermodilution". *Intensive care medicine*, 26(2), pp. 180–7.

Salvo, I.; Cian, W.; Musicco, M.; Langer, M.; Piadena, R.; Wolfler, A.; Montani, C.; and Magni, E. (1995). "The Italian SEPSIS study: preliminary results on the incidence and evolution of SIRS, sepsis, severe sepsis and septic shock". *Intensive care medicine*, 21 Suppl 2, pp. S244–9.

Sandler, D. A. and Martin, J. F. (1989). "Autopsy proven pulmonary embolism in hospital patients: are we detecting enough deep vein thrombosis?". *Journal of the Royal Society of Medicine*, 82(4), pp. 203–5.

Santamore, W. P. and Burkhoff, D. (1991). "Hemodynamic consequences of ventricular interaction as assessed by model analysis". *American Journal of Physiology*, 260(1 Pt 2), pp. H146–57.

Sarnoff, S. J. and Berglund, E. (1954). "Ventricular Function: I. Starling's Law of the Heart Studied by Means of Simultaneous Right and Left Ventricular Function Curves in the Dog". *Circulation*, 9(5), pp. 706–718.

Sarnoff, S. J.; Braunwald, E.; Welch, G. H.; Case, R. B.; Stainsby, W. N.; and Macruz, R. (1958). "Hemodynamic determinants of oxygen consumption of the heart with special reference to the tension-time index". *The American journal of physiology*, 192(1), pp. 148–56.

Sarnoff, S. J. and Mitchell, J. H. (1961). "The regulation of the performance of the heart". *The American journal of medicine*, 30, pp. 747–71.

Sato, T.; Shishido, T.; Kawada, T.; Miyano, H.; Miyashita, H.; Inagaki, M.; Sugimachi, M.; and Sunagawa, K. (1998). "ESPVR of in situ rat left ventricle shows contractility-dependent curvilinearity". *The American journal of physiology*, 274(5 Pt 2), pp. H1429–34.

Schiereck, P. and Boom, H. B. (1978). "Left ventricular active stiffness: dependency on time and inotropic state". *Pflügers Archiv : European journal of physiology*, 374(2), pp. 135–43.

Senzaki, H.; Chen, C. H.; and Kass, D. A. (1996). "Single-beat estimation of end-systolic pressure-volume relation in humans. A new method with the potential for noninvasive application". *Circulation*, 94(10), pp. 2497–506.

Sevitt, S. and Gallagher, N. (1961). "Venous thrombosis and pulmonary embolism. A clinico-pathological study in injured and burned patients". *British Journal of Surgery*, 48(211), pp. 475–89.

Shah, M. R.; Hasselblad, V.; Stevenson, L. W.; Binanay, C.; O'Connor, C. M.; Sopko, G.; and Califf, R. M. (2005). "Impact of the pulmonary artery catheter in critically ill patients: meta-analysis of randomized clinical trials". *JAMA : the journal of the American Medical Association*, 294(13), pp. 1664–70.

Shih, H.; Hillel, Z.; Declerck, C.; Anagnostopoulos, C.; Kuroda, M.; and Thys, D. (1997). "An algorithm for real-time, continuous evaluation of left ventricular mechanics by single-beat estimation of arterial and ventricular elastance". *Journal of clinical monitoring*, 13(3), pp. 157–70.

Shishido, T.; Hayashi, K.; Shigemi, K.; Sato, T.; Sugimachi, M.; and Sunagawa, K. (2000). "Single-beat estimation of end-systolic elastance using bilinearly approximated time-varying elastance curve". *Circulation*, 102(16), pp. 1983–9.

Shoucri, R. (2006). "The end-systolic pressure-volume relation and its application to the study of the contractility of the cardiac muscle". In *Computers in cardiology*, pages 297 –300, Valencia. IEEE.

Shroff, S. G.; Janicki, J. S.; and Weber, K. T. (1983). "Left ventricular systolic dynamics in terms of its chamber mechanical properties". *The American journal of physiology*, 245(1), pp. H110–24.

Shroff, S. G.; Janicki, J. S.; and Weber, K. T. (1985). "Evidence and quantitation of left ventricular systolic resistance". *The American journal of physiology*, 249(2 Pt 2), pp. H358–70.

Smith, B. W. (2004). *Minimal haemodynamic modelling of the heart & circulation for clinical application*. Phd, University of Canterbury.

Smith, B. W.; Andreassen, S.; Shaw, G. M.; Jensen, P. L.; Rees, S. E.; and Chase, J. G. (2007). "Simulation of cardiovascular system diseases by including the autonomic nervous system into a minimal model". *Computer methods and programs in biomedicine*, 86(2), pp. 153–60.

Smith, B. W.; Chase, J. G.; Nokes, R. I.; Shaw, G. M.; and David, T. (2003). "Velocity profile method for time varying resistance in minimal cardiovascular system models". *Physics in Medicine and Biology*, 48(20), pp. 3375–87.

Smith, B. W.; Chase, J. G.; Nokes, R. I.; Shaw, G. M.; and Wake, G. (2004). "Minimal haemodynamic system model including ventricular interaction and valve dynamics". *Medical Engineering & Physics*, 26(2), pp. 131–9.

Smith, B. W.; Chase, J. G.; Shaw, G. M.; and Nokes, R. I. (2005). "Experimentally verified minimal cardiovascular system model for rapid diagnostic assistance". *Control Engineering Practice*, 13, pp. 1183–93.

Smith, B. W.; Chase, J. G.; Shaw, G. M.; and Nokes, R. I. (2006). "Simulating transient ventricular interaction using a minimal cardiovascular system model". *Physiological Measurement*, 27(2), pp. 165–79.

Sonnenblick, E. H. (1962). "Force-velocity relations in mammalian heart muscle". *American Journal of Physiology. Legacy Content*, 202(5), pp. 931–9.

Spronk, P. E.; Ince, C.; Gardien, M. J.; Mathura, K. R.; Straaten, H. M. O.-v.; and Zandstra, D. F. (2002). "Nitroglycerin in septic shock after intravascular volume resuscitation". *The Lancet*, 360(9343), pp. 1395–6.

Starfinger, C. (2008). *Patient-Specific Modelling of the Cardiovascular System for Diagnosis and Therapy Assistance in Critical Care*. Phd, University of Canterbury.

Starfinger, C.; Chase, J. G.; Hann, C. E.; Shaw, G. M.; Lambermont, B.; Ghuysen, A.; Kolh, P.; Dauby, P. C.; and Desaive, T. (2008a). "Model-based identification and diagnosis of a porcine model of induced endotoxic shock with hemofiltration". *Mathematical Biosciences*, 216(2), pp. 132–9.

Starfinger, C.; Chase, J. G.; Hann, C. E.; Shaw, G. M.; Lambert, P.; Smith, B. W.; Sloth, E.; Larsson, A.; Andreassen, S.; and Rees, S. (2008b). "Model-based identification of PEEP titrations during different volemic levels". *Computer methods and programs in biomedicine*, 91(2), pp. 135–44.

Starfinger, C.; Hann, C. E.; Chase, J. G.; Desaive, T.; Ghuysen, A.; and Shaw, G. M. (2007). "Model-based cardiac diagnosis of pulmonary embolism". *Computer methods and programs in biomedicine*, 87(1), pp. 46–60.

Starling, E. H. (1918). *The Linacre lecture on the law of the heart*. Longmans, Green, & Company.

Stein, P. D.; Athanasoulis, C.; Alavi, A.; Greenspan, R. H.; Hales, C. A.; Saltzman, H. A.; Vreim, C. E.; Terrin, M. L.; and Weg, J. G. (1992). "Complications and validity of pulmonary angiography in acute pulmonary embolism". *Circulation*, 85(2), pp. 462–8.

Stein, P. D.; Hull, R. D.; Patel, K. C.; Olson, R. E.; Ghali, W. A.; Brant, R.; Biel, R. K.; Bharadia, V.; and Kalra, N. K. (2004). "D-dimer for the exclusion of acute venous thrombosis and pulmonary embolism: a systematic review". *Annals of internal medicine*, 140(8), pp. 589–602.

Stetz, C. W.; Miller, R. G.; Kelly, G. E.; and Raffin, T. A. (1982). "Reliability of the thermodilution method in the determination of cardiac output in clinical practice". *The American review of respiratory disease*, 126(6), pp. 1001–4.

Stevenson, D.; Revie, J.; Chase, J. G.; Hann, C. E.; Shaw, G. M.; Lambermont, B.; Ghuysen, A.; Kolh, P.; and Desaive, T. (2012a). "Algorithmic Processing of the Pressure Waveforms to Facilitate Estimation of Cardiac Elastance". *BioMedical Engineering OnLine*, 11, pp. 28.

Stevenson, D.; Revie, J.; Chase, J. G.; Hann, C. E.; Shaw, G. M.; Lambermont, B.; Ghuysen, A.; Kolh, P.; and Desaive, T. (2012b). "Beat-to-beat estimation of the continuous left and right cardiac elastance from metrics commonly available in clinical settings". *BioMedical Engineering OnLine*, 11, pp. 73.

Su, J. B. and Crozatier, B. (1989). "Preload-induced curvilinearity of left ventricular end-systolic pressure-volume relations. Effects on derived indexes in closed-chest dogs". *Circulation*, 79(2), pp. 431–40.

Suga, H. (1969a). "Analysis of left ventricular pumping by its pressure-volume coefficient (in Japanese with an English abstact)". *Jpn J Med Biol Eng*, 7, pp. 406–15.

Suga, H. (1969b). "Time course of left ventricular pressure-volume relationship under various enddiastolic volume". *Japanese Heart Journal*, 10(6), pp. 509–15.

Suga, H. (1970). "Time course of left ventricular pressure-volume relationship under various extents of aortic occlusion". *Japanese Heart Journal*, 11(4), pp. 373–8.

Suga, H. (1971a). "Left ventricular time-varying pressure-volume ratio in systole as an index of myocardial inotropism". *Japanese Heart Journal*, 12(2), pp. 153–60.

Suga, H. (1971b). "Theoretical analysis of a left-ventricular pumping model based on the systolic time-varying pressure-volume ratio". *IEEE Transactions on Biomedical Engineering*, 18(1), pp. 47–55.

Suga, H. (1979a). "Total internal mechanical work of ventricle assessed from quick release pressure-volume curve". *Japanese Journal of Physiology*, 29(3), pp. 227–37.

Suga, H. (1979b). "Total mechanical energy of a ventricle model and cardiac oxygen consumption". *American Journal of Physiology. Heart and Circulatory Physiology*, 236(3), pp. H498–5.

Suga, H. (1990a). "Cardiac mechanics and energetics - from Emax to PVA". *Front Med Biol Eng*, 2(1), pp. 3–22.

Suga, H. (1990b). "Ventricular energetics". *Physiological Reviews*, 70(2), pp. 247–77.

Suga, H.; Hisano, R.; Goto, Y.; Yamada, O.; and Igarashi, Y. (1983). "Effect of positive inotropic agents on the relation between oxygen consumption and systolic pressure volume area in canine left ventricle". *Circulation research*, 53(3), pp. 306–18.

Suga, H.; Igarashi, Y.; Yamada, O.; and Goto, Y. (1986). "Cardiac oxygen consumption and systolic pressure volume area". *Basic research in cardiology*, 81 Suppl 1, pp. 39–50.

Suga, H. and Sagawa, K. (1972). "Mathematical interrelationship between instantaneous ventricular pressure-volume ratio and myocardial force-velocity relation". *Annals of biomedical engineering*, 1(2), pp. 160–81.

Suga, H. and Sagawa, K. (1974). "Instantaneous pressure-volume relationships and their ratio in the excised, supported canine left ventricle". *Circulation Research*, 35(1), pp. 117–26.

Suga, H.; Sagawa, K.; and Demer, L. (1980). "Determinants of instantaneous pressure in canine left ventricle. Time and volume specification". *Circulation Research*, 46(2), pp. 256–63.

Suga, H.; Sagawa, K.; and Shoukas, A. A. (1973). "Load independence of the instantaneous pressure-volume ratio of the canine left ventricle and effects of epinephrine and heart rate on the ratio". *Circulation Research*, 32(3), pp. 314–22.

Suga, H.; Yamada, O.; and Goto, Y. (1984). "Energetics of ventricular contraction as traced in the pressure-volume diagram". *Federation proceedings*, 43(9), pp. 2411–3.

Sun, Y.; Beshara, M.; Lucariello, R. J.; and Chiaramida, S. A. (1997). "A comprehensive model for right-left heart interaction under the influence of pericardium and baroreflex". *American Journal of Physiology. Heart and Circulatory Physiology*, 272(3), pp. H1499–1515.

Sunagawa, K.; Sagawa, K.; and Maughan, W. L. (1984). "Ventricular interaction with the loading system". *Annals of Biomedical Engineering*, 12(2), pp. 163–89.

Suresh, G.; Horbar, J. D.; Plsek, P.; Gray, J.; Edwards, W. H.; Shiono, P. H.; Ursprung, R.; Nickerson, J.; Lucey, J. F.; and Goldmann, D. (2004). "Voluntary anonymous reporting of medical errors for neonatal intensive care". *Pediatrics*, 113(6), pp. 1609–18.

Swamy, G.; Kuiper, J.; Gudur, M. S. R.; Bari Oliver, N.; and Mukkamala, R. (2009). "Continuous Left Ventricular Ejection Fraction Monitoring by Aortic Pressure Waveform Analysis". *Annals of Biomedical Engineering*, 37(6), pp. 1055–68.

Takaoka, H.; Takeuchi, M.; Odake, M.; Hayashi, Y.; Hata, K.; Mori, M.; and Yokoyama, M. (1993). "Comparison of hemodynamic determinants for myocardial oxygen consumption under different contractile states in human ventricle". *Circulation*, 87(1), pp. 59–69.

Takeuchi, M.; Igarashi, Y.; Tomimoto, S.; Odake, M.; Hayashi, T.; Tsukamoto, T.; Hata, K.; Takaoka, H.; and Fukuzaki, H. (1991). "Single-beat estimation of the slope of the

end-systolic pressure-volume relation in the human left ventricle". *Circulation*, 83(1), pp. 202–12.

Tapson, V. F. (2007). "Venous thromboembolism prophylaxis in acutely ill hospitalized medical patients: findings from the International Medical Prevention Registry on Venous Thromboembolism". *CHEST Journal*, 132(3), pp. 936–45.

Tapson, V. F. (2008). "Acute Pulmonary Embolism". *New England Journal of Medicine*, 358(10), pp. 1037–52.

Templeton, G. H.; Ecker, R. R.; and Mitchell, J. H. (1972). "Left ventricular stiffness during diastole and systole: the influence of changes in volume and inotropic state". *Cardiovascular Research*, 6(1), pp. 95–100.

Ten Wolde, M.; Hagen, P. J.; Macgillavry, M. R.; Pollen, I. J.; Mairuhu, A. T. A.; Koopman, M. M. W.; Prins, M. H.; Hoekstra, O. S.; Brandjes, D. P. M.; Postmus, P. E.; and Büller, H. R. (2004). "Non-invasive diagnostic work-up of patients with clinically suspected pulmonary embolism; results of a management study". *Journal of thrombosis and haemostasis: JTH*, 2(7), pp. 1110–1117.

Torbicki, A.; Perrier, A.; Konstantinides, S.; Agnelli, G.; Galiè, N.; Pruszczyk, P.; Bengel, F.; Brady, A. J. B.; Ferreira, D.; Janssens, U.; Klepetko, W.; Mayer, E.; Remy-Jardin, M.; and Bassand, J.-P. (2008). "Guidelines on the diagnosis and management of acute pulmonary embolism: the Task Force for the Diagnosis and Management of Acute Pulmonary Embolism of the European Society of Cardiology (ESC)". *European heart journal*, 29(18), pp. 2276–2315.

Tortora, G. J. and Derrickson, B. H. (2011). *Principles of Anatomy and Physiology*. Wiley, 13 edition.

Tsitlik, J. E.; Halperin, H. R.; Popel, A. S.; Shoukas, A. A.; Yin, F. C.; and Westerhof, N. (1992). "Modeling the circulation with three-terminal electrical networks containing special nonlinear capacitors". *Annals of biomedical engineering*, 20(6), pp. 595–616.

Ursino, M. (1999). "A mathematical model of the carotid baroregulation in pulsating conditions". *IEEE transactions on bio-medical engineering*, 46(4), pp. 382–92.

Vaartjes, S. R. and Boom, H. B. (1987). "Left ventricular internal resistance and unloaded ejection flow assessed from pressure-flow relations: a flow-clamp study on isolated rabbit hearts". *Circulation research*, 60(5), pp. 727–37.

Van Strijen, M. J. L.; De Monye, W.; Kieft, G. J.; Pattynama, P. M. T.; Prins, M. H.; and Huisman, M. V. (2005). "Accuracy of single-detector spiral CT in the diagnosis of pulmonary embolism: a prospective multicenter cohort study of consecutive patients with abnormal perfusion scintigraphy". *Journal of thrombosis and haemostasis*, 3(1), pp. 17–25.

Velde, E. T.; Burkhoff, D.; Steendijk, P.; Karsdon, J.; Sagawa, K.; and Baan, J. (1991). "Nonlinearity and load sensitivity of end-systolic pressure-volume relation of canine left ventricle in vivo". *Circulation*, 83(1), pp. 315–27.

Vieillard-Baron, A.; Prin, S.; Chergui, K.; Dubourg, O.; and Jardin, F. (2003). "Hemodynamic Instability in Sepsis Bedside Assessment by Doppler Echocardiography". *American Journal of Respiratory and Critical Care Medicine*, 168(11), pp. 1270–1276.

Wan, S.; Quinlan, D. J.; Agnelli, G.; and Eikelboom, J. W. (2004). "Thrombolysis compared with heparin for the initial treatment of pulmonary embolism: a meta-analysis of the randomized controlled trials". *Circulation*, 110(6), pp. 744–9.

Wang, J.-J.; O'Brien, A. B.; Shrive, N. G.; Parker, K. H.; and Tyberg, J. V. (2003). "Time-domain representation of ventricular-arterial coupling as a windkessel and wave system". *American Journal of Physiology. Heart and Circulatory Physiology*, 284(4), pp. H1358–68.

Warner, H. (1959). "The Use of an Analog Computer for Analysis of Control Mechanisms in the Circulation". *Proceedings of the IRE*, 47(11), pp. 1913–6.

Watson, R. S.; Carcillo, J. A.; Linde-Zwirble, W. T.; Clermont, G.; Lidicker, J.; and Angus, D. C. (2003). "The Epidemiology of Severe Sepsis in Children in the United States". *American Journal of Respiratory and Critical Care Medicine*, 167(5), pp. 695–701.

Weber, K. T. and Janicki, J. S. (1977). "Myocardial oxygen consumption: the role of wall force and shortening". *The American journal of physiology*, 233(4), pp. H421–30.

Weber, K. T. and Janicki, J. S. (1979). "The heart as a muscle-pump system and the concept of heart-failure". *American Heart Journal*, 98(3), pp. 371–84.

Weber, K. T.; Janicki, J. S.; Hunter, W. C.; Shroff, S.; Pearlman, E. S.; and Fishman, A. P. (1982). "The contractile behavior of the heart and its functional coupling to the circulation". *Progress in cardiovascular diseases*, 24(5), pp. 375–400.

Weil, M. H. (1998). "The assault on the Swan-Ganz catheter: a case history of constrained technology, constrained bedside clinicians, and constrained monetary expenditures". *Chest*, 113(5), pp. 1379–86.

Weisfeldt, M.; Shoukas, A.; Weiss, J.; Dashkoff, N.; Come, P.; Griffith, L.; ASHUFF, S.; Ducci, H.; and Sagawa, K. (1976). "Emax as a new contractility index in man (abstr)". *Circulation*, 54(suppl II), pp. 31.

Wells, P. S.; Anderson, D. R.; Rodger, M.; Ginsberg, J. S.; Kearon, C.; Gent, M.; Turpie, A. G.; Bormanis, J.; Weitz, J.; Chamberlain, M.; Bowie, D.; Barnes, D.; and Hirsh, J. (2000). "Derivation of a simple clinical model to categorize patients probability of pulmonary embolism: increasing the models utility with the SimpliRED D-dimer". *Thrombosis and haemostasis*, 83(3), pp. 416–420.

Wells, P. S.; Ginsberg, J. S.; Anderson, D. R.; Kearon, C.; Gent, M.; Turpie, A. G.; Bormanis, J.; Weitz, J.; Chamberlain, M.; Bowie, D.; Barnes, D.; and Hirsh, J. (1998). "Use of a Clinical Model for Safe Management of Patients with Suspected Pulmonary Embolism". *Annals of Internal Medicine*, 129(12), pp. 997–1005.

Wennberg, J. E. (2002). "Unwarranted variations in healthcare delivery: implications for academic medical centres". *British Medical Journal (Clinical research ed.)*, 325(7370), pp. 961–4.

Westerhof, B. E.; Guelen, I.; Stok, W. J.; Lasance, H. A. J.; Ascoop, C. A. P. L.; Wesseling, K. H.; Westerhof, N.; Bos, W. J. W.; Stergiopulos, N.; and Spaan, J. A. E. (2008). "Individualization of transfer function in estimation of central aortic pressure from the peripheral pulse is not required in patients at rest". *Journal of applied physiology (Bethesda, Md. : 1985)*, 105(6), pp. 1858–63.

Westerhof, N.; Lankhaar, J.-W.; and Westerhof, B. E. (2009). "The arterial Windkessel". *Medical & biological engineering & computing*, 47(2), pp. 131–41.

Westerhof, W.; Stergiopulos, N.; and Noble, M. (2010). *Snapshots of hemodynamics*. Springer, second edition.

White, F. M. (1991). *Viscous Fluid Flow*. McGraw-Hill, Inc, USA.

Wicki, J.; Perneger, T. V.; Junod, A. F.; Bounameaux, H.; and Perrier, A. (2001). "Assessing clinical probability of pulmonary embolism in the emergency ward: a simple score". *Archives of internal medicine*, 161(1), pp. 92–7.

Wiener, R. S. and Welch, H. G. (2007). "Trends in the use of the pulmonary artery catheter in the United States, 1993-2004". *JAMA : the journal of the American Medical Association*, 298(4), pp. 423–9.

Wigfull, J. (2005). "Critical assessment of haemodynamic data". *Continuing Education in Anaesthesia, Critical Care & Pain*, 5(3), pp. 84–88.

Wijkstra, H. and Boom, H. B. (1991). "Left-ventricular dynamic model based on constant ejection flow periods". *IEEE transactions on bio-medical engineering*, 38(12), pp. 1204–12.

Wood, K. E. (2002). "Major pulmonary embolism: review of a pathophysiologic approach to the golden hour of hemodynamically significant pulmonary embolism". *Chest*, 121(3), pp. 877–905.

Yasumura, Y.; Nozawa, T.; Futaki, S.; Tanaka, N.; and Suga, H. (1989a). "Minor preload dependence of O2 consumption of unloaded contraction in dog heart". *The American journal of physiology*, 256(5 Pt 2), pp. H1289–94.

Yasumura, Y.; Nozawa, T.; Futaki, S.; Tanaka, N.; and Suga, H. (1989b). "Time-invariant oxygen cost of mechanical energy in dog left ventricle: consistency and inconsistency of time-varying elastance model with myocardial energetics". *Circulation research*, 64(4), pp. 764–78.

Zhong, L.; Ghista, D. N.; Ng, E. Y. K.; and Lim, S. T. (2005). "Passive and active ventricular elastances of the left ventricle". *Biomedical engineering online*, 4(1), pp. 10.